SESSION I

GENERAL MATRIX METHODS I

Session Chairman:

Richard F. Hoener

Assistant for Research and Technology, Structures Division, Air Force Flight Dynamics Laboratory, Wright-Patterson Air Force Base, Ohio

CONTINUA AND DISCONTINUA *

An Apercu of Recent Developments of the Matrix Displacement Methods

J.H. Argyris **

University of London, England
and University of Stuttgart, Germany

The paper attempts to give a broad survey of some of the developments in the field of matrix methods of structural analysis achieved at the Institut für Statik und Dynamik in Stuttgart and at Imperial College, London, since 1963. Practically all the material presented, but for a limited number of applications and illustrations, has not been published externally and only made available to The Boeing Company, Aircraft Division, in research reports. In view of the very extensive nature of the investigations covering linear and non-linear phenomena in the static and dynamic fields, it has proved necessary to restrict considerably our apercu. This is regrettable, especially for a main address, but inevitable, in view of the limited space available. At the same time, the author did not consider it fair to the reader to present a vast amount of material just in the form of final results, but preferred to select some typical investigations and to cover them in such a manner that they could be immediately applied by the specialist. In view of this policy, it was decided to concentrate on unpublished developments of the Matrix Displacement method but even here a number of important topics have had to be omitted. In particular, our applications on visco-elastic and other time-dependent effects on structures are not covered, although the technique is essentially included in sections on the analysis on elasto-plastic phenomena.

* This research has been sponsored in part by the Air Force Flight Dynamics Laboratory under Contract AF 61(052)-854 through the European Office of Aerospace Research (EOAR), United States Air Force.

** Professor of Aeronautical Structures, Imperial College of Science and Technology, University of London, England; and Director, Institut für Statik und Dynamik der Luft- und Raumfahrtkonstruktionen, University of Stuttgart, Germany.

I. Application of Kinematic Natural Modes to Elements, Linear Theory

I.1 Introduction

The author initiated in 1962[3] a new approach to the formulation of the Matrix Displacement method, which had a considerable influence on its further development and extension. Whilst working over a considerable time on the application of the Displacement method to problems involving large displacements and strains, as well as inelastic behaviour, it became increasingly clear that the standard specification of kinematic modes due to unit nodal displacements in the direction of the axes yields extremely complex and tortuous expressions, which suffer, moreover, from a grave defect, that they do not display in many cases the necessary symmetry with respect to the chosen system of axes. However, a sudden inspiration following many aesthetically abortive attempts led to the basic concepts of geometrical stiffness and in connexion with it to the ideas of natural modes of straining and natural stiffness. Essentially, the natural modes are the pure straining modes which exclude rigid body displacements. Since then, the whole Matrix Displacement method has been remodelled on this basis, first for triangles, flanges, beams and ultimately to the whole list of elements in our programme library[5]. We show in the present Section, after a brief introduction to the linear theory, the application of this new technique to two elements, a parallelogram element with eight nodal points under plane stress, and a tetrahedron element with 10. These elements are chosen out of a wide collection in order to illustrate another refinement in the Matrix Displacement method. One of the chief characteristics of the basic elements of the original displacement analysis, subh as the tetrahedron, triangle and flange, was the assumption of constant strain over the whole element; similar if aot extreme restrictions were imposed on the parallelogram. This inevitably yields considerable discontinuities of stress at the nodal points and serious difficulties in deducing a logical scheme for a physically more conclusive interpretation of the stress distribution. To reduce this uncertainty and improve on the accuracy of the stress predictions the author introduced in a number of Research Reports to The Boeing Company so-called refined elements like tetrahedron, triangular and flange elements to which he assigned no longer a constant strain but a linear variation. Naturally, this more advanced definition of strain requires the insertion of additional nodal points into these elements. We observe that the new flange has three, the triangle six and the tetrahedron ten nodal points respectively. The additional vertices are conveniently taken to lie midway between the original nodal points. In deriving the stiffnesses of these elements the natural mode approach proves its superiority by yielding with a minimum of algebra concise expressions. On the other hand, the previous method of imposing a displacement to each nodal point in turn proves aumbersome and leads to most complex formulae. In two articles to appear shortly the author discusses the new triangle and flange[15, 16]. Here we only indicate briefly how the new triangular element may be used to build-up a kinematically most satisfactory spar web [18], which has the

additional advantage in that it may be unsymmetrical. The detailed investigation of new elements is restricted in the present Chapter to the aforementioned tetrahedron and parallelogram elements on which we impose the linear strain assumption. They both display most markedly the advantages of the new approach. Further illustrations to the natural mode technique appear in the second chapter dealing with plates and shells under bending and in the fifth chapter discussing large displacements and strains. A number of examples illustrate the gain in accuracy in the estimation of stresses and strains achieved, for the same number of unknowns, through the adoption of the new elements.

Another significant advance in the kinematic analysis concerns the evaluation of kinematically consistent lumped masses. This, to the author's knowledge, was first developed independently by Archer[27] and the author[10]. Although the technique is in principle identical to that of the Rayleigh-Ritz method, the new formulation within the framework of the Displacement method allows to dispose of all variational adornments and achieves a more direct and compact matrix expression, which is computationally advantageous. For constant strain elements it proves usually more convenient to use the unit displacement technique, not in conjunction with natural modes, but with unit displacements applied at the nodal points. At the same time much can be gained by introducing co-ordinates natural to the geometry of the element. This is illustrated here for a triangular element in space and the tetrahedron previously derived in Ref.10. For more complex strain assumptions the natural mode technique is again the more successful and is used here on the aforementioned parallelogram element. Further applications are to be found in the next Section.

1.2 A Resumé of the Natural Mode Technique

Consider an element with n nodal points in space. The freedom of choice of the deformation pattern to be adopted, is limited by the $3n$ nodal displacements, which may be imposed in turn at the n nodal points, and by the condition, in general upheld, that all kinematic compatibility conditions are satisfied at the boundary. Now it is clear, that such a definition of the state of deformation also includes rigid body displacements, which do not give rise to straining and hence do not affect, in principle, the stiffness of the element. To describe hence the straining condition of the element we only require $\nu = (3n-6)$ kinematic modes; for plane problems the corresponding figure is $(2n-3)$. For example, the deformation of a triangle with three nodal points at the corners under an assumed constant strain, is fully defined by three modes, the corresponding stiffness being of the same order, whilst the dimensions of the complete elemental stiffness is necessarily (6 x 6). These $(3n-6)$ or $(2n-3)$ modes are denoted by us as natural modes and the corresponding vector, being a measure of their magnitude, carries the symbol ρ_N ; skill in selecting these modes greatly simplifies the matrix formulation and the computations. The associated stiffness matrix k_N , of reduced order $(3n-6)$ or $(2n-3)$, is also designated as a natural or invarient one. The complete description of the displacements of an element requires, of course, information on rigid body motions which is contained in a (6 x 1) or (3 x 1) vector ρ_0 . To fix ideas, all subsequent arguments in this Section are restricted to the three-dimensional case, but the results may immediately be translated into the two-dimensional state.

Following our above argument we have two alternative vectors to describe the deformation. First, the standard nodal displacement which we write here as

$$\rho = \{\rho_1 \quad \rho_2 \quad ------ \rho_n\} \qquad (3n \times 1) \qquad (I,1)$$

where

$$\rho_i = \{u_i \quad v_i \quad w_i\} \qquad (I,1a)$$

and secondly the natural cum rigid body vectors ρ_N and ρ_0 of dimensions $(3n-6)\times 1$ and (6×1) respectively, which we may assemble as the single vector

$$\rho' = \{\rho_N \quad \rho_0\} \qquad (3n \times 1) \qquad (I,2)$$

A different sequential order is sometimes preferable for ρ but this does not affect our basic argument. The selection of the modes ρ_N essentially determines the strain vector ε which, following the method of Ref. 13, is expressed for a cartesian system of axes as

$$\varepsilon = \left\{ \varepsilon_{xx} \quad \varepsilon_{yy} \quad \varepsilon_{zz} \quad \frac{1}{\sqrt{2}}\varepsilon_{xy} \quad \frac{1}{\sqrt{2}}\varepsilon_{yz} \quad \frac{1}{\sqrt{2}}\varepsilon_{zx} \right\} \qquad (I,3)$$

Clearly within the linear small displacement theory a relation of the type

$$\varepsilon = \alpha_N \rho_N \qquad (I,4)$$

must hold. At the same time the natural modes ρ_N must be derivable by a linear transformation from the nodal displacements ρ. In fact,

$$\rho_N = a_N \rho \qquad (I,5)$$

However, for the development of the general theory it is more appropriate to consider the complete transformation relation between ρ' and ρ. Thus, we have

$$\rho' = \{\rho_N \quad \rho_0\} = a_e \rho = \{a_N \quad a_0\}\rho \qquad (I,6)$$

which may be split into Eq. (5) and the rigid body components

$$\rho_0 = a_0 \rho \qquad (I,6a)$$

Having selected the natural modes ρ_N and rigid body modes ρ_0 it is often straightforward to write down the submatrices a_N and a_0 of a_e; see, for example, the analysis of the constant strain triangle and tetrahedron in Refs. 3, 12, 13. On the other hand it is in many instances more convenient to set up first the inverse relation which we write in the form

$$\rho = \begin{bmatrix} A_N & A_0 \end{bmatrix} \{\rho_N \quad \rho_0\} = A_e \rho'$$
$$= A_N \rho_N + A_0 \rho_0 \qquad (I,7)$$

Here A_N and A_o are known matrices expressing the nodal displacements for unit natural modes ρ_N and rigid body modes ρ_o respectively.

Inversion of Eq.(7) is, as a rule, extremely simple and accomplished by suitable linear combinations of the rows of A_e until it is reduced to a unit matrix I_{3n}. Formally, we have

$$a_e = \begin{bmatrix} a_N \\ a_o \end{bmatrix} = A_e^{-1} = \begin{bmatrix} A_N & A_o \end{bmatrix}^{-1} \qquad (1,8)$$

the matrix a_N in particular being given by

$$a_N = \begin{bmatrix} I, & O \end{bmatrix} A_e^{-1} \qquad (1,8a)$$

Associated with the alternative definitions of the deformations ρ and ρ', there are the (generalized)forces P and P' respectively. Thus,

$$P = \{ P_1 \quad P_2 \; ----- P_n \} \qquad (3n \times 1) \qquad (1,9)$$

where

$$P_i = \{ U_i \quad V_i \quad W_i \} \qquad (3 \times 1) \qquad (1,9a)$$

Also

$$P' = \{ P_N \quad P_o \} \qquad (3n \times 1) \qquad (1,10)$$

where P_N is $(3n-1)\times 1$ vector of the self-equilibrating pairs of forces associated with ρ_N and

$$P_o = \{ U_o \quad V_o \quad W_o \} \qquad (3 \times 1) \qquad (1,10a)$$

are the resultants of the body and surface forces acting on the element. Generally we have $P_o = O$ but this may not hold in the presence of inertia loads and similar effects; see also below.

From the invariance of the work expression and application of Eq.(7) we find

$$\tfrac{1}{2} P^t \rho = \tfrac{1}{2} P'^t \rho' = \tfrac{1}{2} P'^t a_e \rho$$

and hence the relation dual to Eq.(6)

$$P = a_e^t P' = a_N^t P_N + a_o^t P_o \qquad (1,11)$$

When no external resultants are acting on the body we obtain

$$P = a_N^t P_N \qquad (1,11a)$$

which is dual to Eq.(5).

In many cases, the strain transformation (4) may be written down directly using the assumed modes, without having first to express the current displacement vector at a point (x, y, z) of the

element

$$W = \{u \quad v \quad w\} \tag{I,12}$$

in terms of ρ_N . This proves, for example, not only possible but advantageous for the tetrahedron with ten nodal points analysed in Section I.A. The same applies indirectly to the triangular element under bending and membrane action considered in II.12 to 14. On the other hand, there are many instances, as for example in the parallelogram element, where it is simpler to start with W in terms of the complete vector ρ' . In such cases , we write

$$W = \omega_e \rho' = [\omega_N \quad \omega_0]\{\rho_N \quad \rho_0\} = \omega_N \rho_N + \omega_0 \rho_0 \tag{I,13}$$

where the matrix ω_e is, of course, a function of (x, y, z) . Using Eq.(6) in (13) we find

$$W = \omega_e a_e \rho = \Pi_e \rho \tag{I,14}$$

where

$$\Pi_e = \omega_e a_e \qquad (3 \times 3n) \tag{I,15}$$

is an important transformation matrix, as we shall see later. If an external force R

$$R = \{U \quad V \quad W\} \tag{I,16}$$

is acting at a point (x, y, z) of an element, the invariance of work leads to the following expression for the kinematically equivalent nodal forces P_e at the nodal points

$$P_e = \Pi_e^t R \tag{I,17}$$

The significance of this relation will become evident in the following Section. When the kinematic analysis is initiated with a relation of the type (13) it is necessary to establish by differentiation the matrix α_N of Eq.(4). We easily confirm that

$$\varepsilon = \vartheta W = \vartheta \omega_N \rho_N \tag{I,18}$$

and hence

$$\alpha_N = \vartheta \omega_N \qquad 3 \times (3n-6) \tag{I,18a}$$

where ϑ is the differential operator

$$\vartheta = \begin{bmatrix} \partial/\partial x & 0 & 0 \\ 0 & \partial/\partial y & 0 \\ 0 & 0 & \partial/\partial z \\ \frac{1}{\sqrt{2}}\partial/\partial y & \frac{1}{\sqrt{2}}\partial/\partial x & 0 \\ 0 & \frac{1}{\sqrt{2}}\partial/\partial z & \frac{1}{\sqrt{2}}\partial/\partial y \\ \frac{1}{\sqrt{2}}\partial/\partial z & 0 & \frac{1}{\sqrt{2}}\partial/\partial x \end{bmatrix} \qquad (I,19)$$

We next derive the natural stiffness associated with the ρ_N modes. To this purpose we require the stress vector σ, which for a cartesian system is defined as

$$\sigma = \{ \sigma_{xx} \quad \sigma_{yy} \quad \sigma_{zz} \quad \sqrt{2}\,\sigma_{xy} \quad \sqrt{2}\,\sigma_{yz} \quad \sqrt{2}\,\sigma_{zx} \} \qquad (I,20)$$

The stress-strain relation is then written as

$$\sigma = E\,\varepsilon \qquad (I,21)$$

where E, a (6 x 6) matrix, may describe an arbitrary anisotropic elastic behaviour[13]. Application of the Unit Displacement method to the strains ε_N due to unit ρ_N in Eq.(4) leads to

$$k_N = \int \varepsilon^t \sigma \, dV = \int a_N^t E\, a_N \, dV \qquad (I,22)$$

To obtain the complete $(3n \times 3n)$ stiffness matrix k corresponding to the vector ρ we apply the dual relations (5) and (11a) to find

$$k = a_N^t k_N a_N \qquad (I,23)$$

We may now proceed to the formation of the stiffness matrix K of the assembled structure and apply the Boolean transformation of Refs.3 and 4 in the form

$$K = a^t k a \qquad (I,24)$$

Denoting by R the vector of the externally applied loads and by J the initial load vector arising from initial strain η due to thermal, plastic and viscous effects, the load displacement relationship becomes

$$R = K r + a^t J \qquad (I,25)$$

which is the fundamental equation of the Matrix Displacement method[1]. Solution of Eq.(25) yields the displacements r and the stresses σ. Since the strains deduced from r are the total strains, the corresponding elastic component necessary for the evaluation of σ via Eq.(21), may be obtained by subtraction of the initial strains η. Alternatively the stresses σ may be formed by deduction of the initial load effects J. The details of this procedure, which, as we shall see in Chapter V, are also

applicable in the presence of plastic and viscous effects, are laid out for the two-dimensional case and for beams in Refs. 1, 3, 16 and for the three-dimensional case in Ref. 13, see also Section 1.4. In many instances it may be preferable to set up initially J_N, the initial load vector associated with the natural displacement vector ρ_N. This is, for example, the case when the material is anisotropic; see Ref. 13. The vector J referred to the basic co-ordinate system $Oxyz$ is then in accordance with Eq.(11a)

$$J = a_N^t J_N \tag{I,26}$$

Note

We conclude this Section by drawing attention to an analogy between the method of generating self-equilibrating and statically equivalent forces in fuselages and wings as proposed in Ref. 2, and the setting up of the matrices a_N and a_o for the natural and rigid body modes in accordance with Eq.(8), see also Eqs.(IV.21,22) of Ref. 2. Let us also consider the forces P_N, P_o and P associated with the vectors ρ' and ρ respectively. Application of the invariant work expression in conjunction with Eq.(7) leads to

$$P_N^t \rho_N + P_o^t \rho_o = P^t \rho = P^t A_N \rho_N + P^t A_o \rho_o \tag{a}$$

Clearly this relation is independent of the selected modes ρ_N and ρ_o. Hence

$$P_N = A_N^t P \qquad (3n-6)\times 1 \quad \text{and} \quad P_o = A_o^t P \qquad (6\times 1) \tag{b}$$

The first transformation defines the natural nodal forces whilst the second yields the resultant vector of the nodal loads P. Substitution of Eqs.(11) in (a) yields

$$a_N^t = \begin{bmatrix} A_o^t \\ A_N^t \end{bmatrix} \begin{bmatrix} 0 & I_{3n-6} \end{bmatrix} \quad \text{and} \quad a_o^t = \begin{bmatrix} A_o^t \\ A_N^t \end{bmatrix} \begin{bmatrix} I_6 & 0 \end{bmatrix} \tag{c}$$

which corresponds exactly to the expressions for b_1 and b_o in Ref. 2.

I.3 Kinematically Consistent Mass Matrix for an Element

Another advance which greatly improved the convenience and accuracy of the Displacement method in the dynamic field is the introduction of nodal lumped masses, which are kinematically consistent with the assumed straining modes ρ_N. They yield for the same number of nodal points a much better prediction of the eigenfrequencies and eigenvectors, which is all the more successful the higher the frequency. Fundamentally this approach may be related to the Rayleigh-Ritz technique, but its modern formulation in terms of the Matrix Displacement method is due to Archer[27] and the writer[10].

There are a number of alternative and equivalent ways of deriving the kinematically consistent lumped mass matrix m. Consider, for example, an infinitesimal volume dV within an element of

a three-dimensional continuum. Its mass is $\delta\, dV$ where δ is the density, and the inertia force

$$d\mathcal{R}_i = -\delta\, dV \ddot{w} = -\delta\, dV \pi_e \ddot{\rho} \qquad (I,27)$$

where the last expression follows from Eq.(14). Assuming harmonic motion we find

$$d\hat{\mathcal{R}}_i = \omega^2 \delta\, dV \pi_e \hat{\rho} \qquad (I,27a)$$

where ω is the circular frequency and $\hat{\mathcal{R}}$, $\hat{\rho}$ ($3n \times 1$) vectors, denote the amplitudes of the components in $\mathcal{R}, \rho$. The kinematically equivalent inertial loads $d\hat{P}_i$ at the nodal points may now be determined from Eq.(17) as

$$d\hat{P}_i = \omega^2 \delta\, dV \pi_e^t \pi_e \hat{\rho} \qquad (I,27b)$$

Integrating over the element we find

$$\hat{P}_i = \omega^2 \left[\int_V \delta \pi_e^t \pi_e\, dV\right] \hat{\rho} \qquad (I,27c)$$

On the other hand by definition of a lumped mass matrix m at the nodal points of an element we have

$$\hat{P}_i = \omega^2 m \hat{\rho} \qquad (I,27d)$$

It follows that the kinematically consistent mass matrix m is

$$m = \int_V \delta \pi_e^t \pi_e\, dV = a_e^t \left[\int_V \delta \varpi_e^t \varpi_e\, dV\right] a_e \qquad (I,28)$$

or for a constant density δ

$$m = \delta \int_V \pi_e^t \pi_e\, dV = \delta a_e^t \left[\int_V \varpi_e^t \varpi_e\, dV\right] a_e \qquad (I,28a)$$

where the second expression proves preferable when operating not directly with the ρ modes but with the combination of the ρ_N and ρ_0 modes.

Alternatively we may confirm Eqs.(28) by proceeding via the kinetic energy expression. By definition the kinetic energy dT of a mass element $dm = \delta\, dV$ oscillating harmonically with a circular frequency ω and amplitude $\hat{w}$ is

$$dT = \omega^2 \delta\, dV \hat{w}^t \hat{w} = \omega^2 \delta\, dV \hat{\rho}^t \pi_e^t \pi_e \hat{\rho} \qquad (I,29)$$

Integrating over the volume of the element we find

$$T = \omega^2 \hat{\rho}^{*t} \left[\int_V \delta \pi_e^t \pi_e \, dV \right] \hat{\rho} = \omega^2 \hat{\rho}^t m \hat{\rho} \qquad (I,29a)$$

where the last expression follows once more from the definition of m . Eq.(29a) yields the same result as Eqs.(28,28a). As a matter of interest, we may also write

$$m = \frac{\partial^2 T}{\partial \hat{\rho}^2} = \int_V \delta \pi_e^t \pi_e \, dV \qquad (I,28b)$$

We have applied Eqs.(28) and (28a) to all current elements in the ASKA library and set up the corresponding kinematically consistent lumped mass matrix m . Rotorblades were successfully analysed in this manner and showed excellent agreement with experimental results up to the highest measured frequencies; the inadequacy of the past empirical lumping approach became thereby particularly striking. For reasons of space we cannot reproduce here these interesting data. However, Section I.8 compares the theoretical predictions with the experimental results obtained for the free-free oscillations of a delta wing type structure. The lumped mass for a parallelogram element with eight nodal points is derived in Section I.6 of the present Chapter. Applications to plates and shells are discussed in Section II.

Having established the lumped mass m for a single element the mass matrix M for the assembled structure is obtained by the congruent Boolean transformation of Eq.(24), viz,

$$M = a^t m a \qquad (I,30)$$

Here, and in the following Section, we illustrate the method on some simple examples, which were originally given in a Boeing Research Report[10] and at a IUTAM Conference on Linear Vibrations in Paris, April 13 - 15, 1965. Consider first a triangle in space with three nodal points idealized by the standard constant strain assumption. The displacements u, v, w must then necessarily vary linearly between nodal points, and since the mass element $m \, dA$ * has no directional preference we observe that there is no inertia coupling between displacements in the orthogonal x, y, z directions. Also the mass matrix m of order (9 x 9) is evidently invariant with the direction of the axes of the cartesian system $O x y z$. For reasons of the aforementioned orthogonality it is preferable to introduce here the alternative sequence

$$\bar{\rho} = \{ u \quad v \quad w \} \qquad (I,31)$$

where

$$u = \{ u_1 \quad u_2 \quad u_3 \} \qquad (3 \times 1) \qquad (I,31a)$$

for the nodal displacements. In accordance with our above argument the mass matrix $\bar{m}_e$ corresponding to $\bar{\rho}$ has the diagonal supermatrix form

* m mass per unit area $= \delta t$ where δ is the mass-density of the material and t thickness of the triangle.

$$\bar{m}_e = \begin{bmatrix} \bar{m} & \bar{m} & \bar{m} \end{bmatrix} \qquad (9 \times 9) \qquad (I,32)$$

To find the submatrix $\bar{m}$ we only require, in accordance with our directional invariance statement, to consider at a point of the triangle a typical in-plane displacement u parallel to an axis Ox, (Fig.I.1). Introducing the natural homogeneous triangular co-ordinates $\zeta_1, \zeta_2, \zeta_3$ for which the relationship

$$\zeta_1 + \zeta_2 + \zeta_3 = 1 \qquad (I,33)$$

holds, we may express the linear variation of u over the area by the simply formula

$$u = \pi_{eu} u = \begin{bmatrix} \zeta_1 & \zeta_2 & \zeta_3 \end{bmatrix} u \qquad (I,34)$$

where u is given by Eq.(31a). In accordance with Eq.(28) the component lumped mass matrix $\bar{m}$ is

$$\bar{m} = \int_V \delta\, \pi_{eu}^t \pi_{eu}\, dV = \int_A \delta t\, \pi_{eu}^t \pi_{eu}\, dA \qquad (I,35)$$

Substitution of Eq.(34) yields for a homogeneous plate of constant thickness t

$$\bar{m} = \frac{\delta V}{12} \begin{bmatrix} 2 & 1 & 1 \\ 1 & 2 & 1 \\ 1 & 1 & 2 \end{bmatrix} \qquad (I,36)$$

where $V = At$ is the volume of the triangle. For the derivation of Eq.(36) we only require the integrals

$$\int_A t\, \zeta_i \zeta_j\, dA = \begin{cases} V/12 & \text{for } i \neq j \\ 2V/12 & \text{for } i = j \end{cases} \qquad (I,37)$$

This solves the problem for the triangle.

Next we analyse the problem of the tetrahedron (Fig.I.2) . The previous argument on the orthogonality and invariance of the mass matrix is here also applicable. Writing the displacement vector $\bar{\rho}$ again in the sequence of Eq.(31) but noting that u etc. are now

$$u = \begin{Bmatrix} u_1 & u_2 & u_3 & u_4 \end{Bmatrix} \qquad (4 \times 1) \qquad (I,31b)$$

the kinematically consistent mass matrix of the tetrahedron is found to be given once more by Eq.(32), but with the submatrices $\bar{m}$ now of order (4 x 4). The imposed linear variation of the displacements is expressed most conveniently by the homogeneous tetrahedron co-ordinates ζ_1 to ζ_4 of Fig.I.2, for which an analogous relation to Eq.(33) is applicable. Thus we have

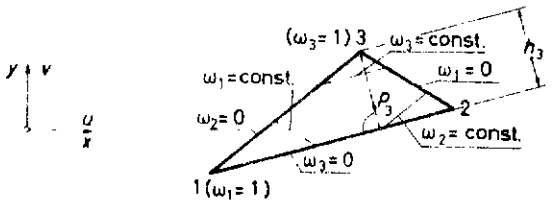

Natural Triangular Co-ordinates for Derivation of Equivalent Lumped Mass Fig. I.1.

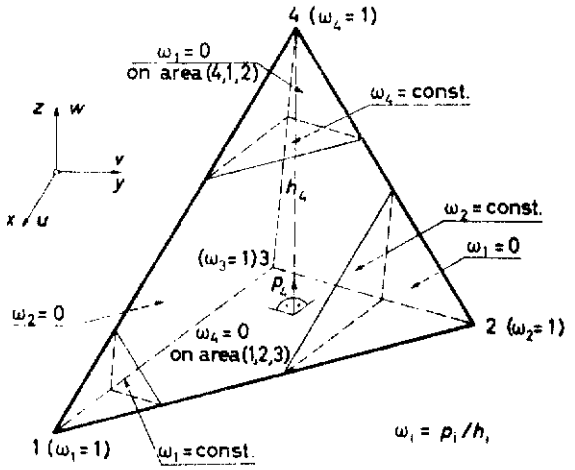

Natural Tetrahedron Co-ordinates for Derivation of Equivalent Lumped Mass Fig. I.2

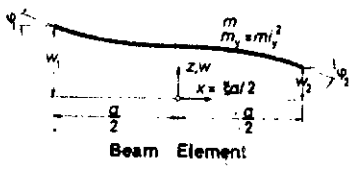

Beam Element

Support \ Mode	f/f exact 1	2	3	4	Eigen-modes	Number of Elements
Free-free	1·20	1·48	-	-	0	1
	1·008	0·97			2	
	1·002	1·15	1·45	1·40	0	2
	1·000	1·01	0·98	0·98	4	
Simple support	1·11	1·27	-	-	0	1
	1·000	1·01			2	
	1·003	1·11	1·23	1·27	0	2
	1·000	1·00	1·01	1·01	4	
Cantilever	1·01	1·58	-	-	0	1
	1·000	1·01	0·95	0·99	2	

Frequencies f for Uniform Beam

Kinematic Idealisation for Inertia of Beam Fig.I.3

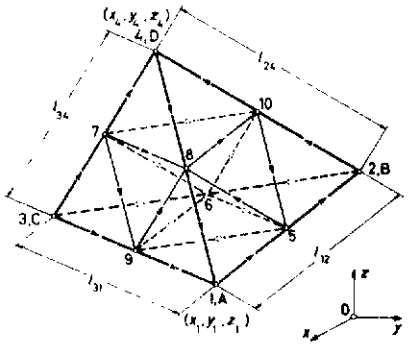

Geometry of Tetrahedron and Positive Directions of Edges Fig. I.4

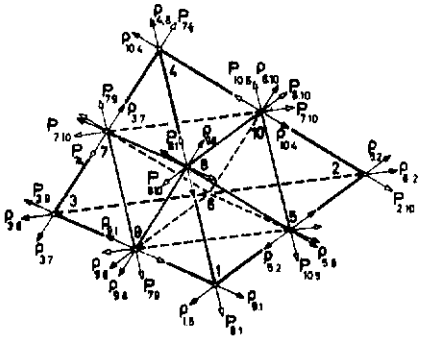

Natural Elongations and Nodal Forces Fig I.5

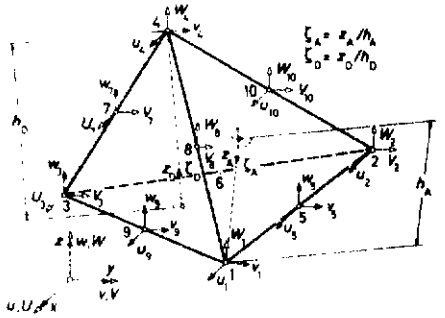

Cartesian Definition of Nodal Displacements and Loads
Homogeneous Tetrahedron Co-ordinates Fig I.6

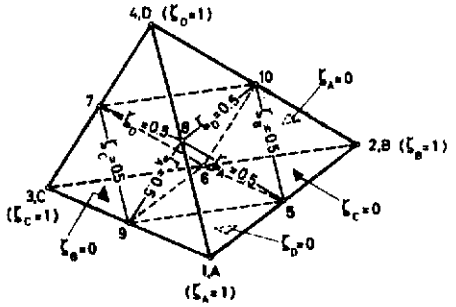

Homogeneous Tetrahedron Co-ordinates Fig I.7

$$u = \pi_{eu} u = [\zeta_1 \quad \zeta_2 \quad \zeta_3 \quad \zeta_4]\, u \tag{I,38}$$

The mass matrix $\bar{m}$ is derived from the first of Eqs.(28) and yields after substitution of Eq.(37)

$$\bar{m} = \frac{\delta V}{20}\begin{bmatrix} 2 & 1 & 1 & 1 \\ 1 & 2 & 1 & 1 \\ 1 & 1 & 2 & 1 \\ 1 & 1 & 1 & 2 \end{bmatrix} \tag{I,39}$$

which is easily established with the standard integrals (for constant δ).

$$\int_V \delta \zeta_i \zeta_j \, dV = \begin{cases} \delta V/20 & \text{for} \quad i \neq j \\ 2\delta V/20 & \text{for} \quad i = j \end{cases} \tag{I,40}$$

This completes the investigation of the new lumped masses of a triangular and tetrahedron element. For more details the reader is referred to the original publication[10].

I.4 Elementary Applications of Kinematically Consistent Lumped Masses to Beams; Refinement with Eigenmodes

We now apply the theory of I.3 to elementary beam examples and indicate also a refinement through the introduction of additional eigenmodes described in Ref. 10. This latter technique was also independently developed by Hurty[28] as the writer was informed at the Paris Conference of the IUTAM, April 1965. In view of the simplicity of the problem we do not use the natural mode approach.

Consider the beam element of Fig.I.3, whose deformation in the zx plane, when ignoring shear strains, is defined by the non-dimensional deflexion

$$\omega = w/\ell \tag{I,41}$$

and the rotation

$$\varphi = -\frac{\partial w}{\partial x} = -2\lambda \frac{\partial \omega}{\partial \xi} \tag{I,42}$$

where

$$\lambda = \ell/a \tag{I,43}$$

The reference length ℓ may be chosen as that of the element itself a, if all nodal points of the beam are equidistant. The vector g of Eq.(1) describing the relevant nodal displacements is here

$$g = \{\omega_1 \quad \omega_2 \quad \varphi_1 \quad \varphi_2\} \tag{I,44}$$

The (2 x 1) deformation vector

$$\mathbf{w} = \begin{Bmatrix} \omega & \varphi \end{Bmatrix} \tag{I,45}$$

of a point may be put in the form

$$\mathbf{w} = \Pi_e \, \mathbf{g} \tag{I,46}$$

where in accordance with E.T.B.

$$\Pi_e = \frac{1}{8} \begin{bmatrix} 2(2-3\xi+\xi^3) & 2(2+3\xi-\xi^3) & \frac{1}{\lambda}(-1+\xi+\xi^2-\xi^3) & \frac{1}{\lambda}(1+\xi-\xi^2-\xi^3) \\ 12\lambda(1-\xi^2) & -12\lambda(1-\xi^2) & 2(1-2\xi+3\xi^2) & 2(-1+2\xi+3\xi^2) \end{bmatrix} \tag{I,47}$$

Note that in the present case, we have explicitly given Π_e and not written it in the form $\mathbf{C}_e \, \mathbf{a}_e$.

The (2 x 2) local inertia matrix, corresponding to the displacement $\mathbf{w}$ of Eq.(45) is

$$\mathbf{m} = m \ell^2 \begin{bmatrix} 1 & \\ & \left(\frac{r_y}{\ell}\right)^2 \end{bmatrix} \tag{I,48}$$

in which m is the mass per unit length of the beam and r_y is the radius of gyration of the cross-section about the centroidal y-axis.

Expression (28) for the lumped mass becomes here the (4 x 4) matrix

$$\mathbf{m} = \frac{\ell}{2\lambda} \int_{-1}^{1} \Pi_e^{\mathrm{T}} \, \mathbf{m} \, \Pi_e \, d\xi \tag{I,49}$$

If m and r_y are constant along the length we find

$$\mathbf{m} = \frac{m\ell^3}{420\lambda^2} \begin{bmatrix} 156\lambda^2 & 54\lambda^2 & -22\lambda & 13\lambda \\ 54\lambda^2 & 156\lambda^2 & 13\lambda & 22\lambda \\ -22\lambda & -13\lambda & 4 & -3 \\ 13\lambda & 22\lambda & -3 & 4 \end{bmatrix} + \frac{m\ell^3}{30\lambda} \left(\frac{r_y}{\ell}\right)^2 \begin{bmatrix} 36\lambda^2 & 36\lambda^2 & -3\lambda & -3\lambda \\ -36\lambda^2 & 36\lambda^2 & 3\lambda & 3\lambda \\ -3\lambda & 3\lambda & 4 & -1 \\ -3\lambda & 3\lambda & -1 & 4 \end{bmatrix} \tag{I,50}$$

In Eq.(50) the lumped inertias have been separated into those arising from the translational inertia and those from the distributed rotational inertia of the beam.

To illustrate the application of these lumped masses we can set up the dynamical equations for a single element. The stiffness matrix for the element, corresponding to the displacement vector of Eq.(44) and based on the modes of Eq.(47), is

$$\mathbf{k} = \frac{2EI\lambda}{\ell}\begin{bmatrix} 6\lambda^2 & -6\lambda^2 & -3\lambda & -3\lambda \\ -6\lambda^2 & 6\lambda^2 & 3\lambda & 3\lambda \\ -3\lambda & 3\lambda & 2 & 1 \\ -3\lambda & 3\lambda & 1 & 2 \end{bmatrix} \qquad (1,51)$$

The above derivation ignores shear deformations. Its inclusion, strictly necessary when considering the higher order effects due to rotational inertia, is straightforward and is most easily accomplished on the basis of two additional shearing modes $\omega_s = w_s/\ell$ — which do not give rise to rotations of the end cross-sections —as shown in some detail for a spar element in Ref.3. The matrices φ and Π_e are then of order (6 x 1) and (3 x 6) respectively and the mass and stiffness matrices $\mathbf{m}$ and $\mathbf{k}$ become of order (6 x 6).

For a simple comparison with known exact solutions, it suffices for the present purpose to ignore the contributions to $\mathbf{m}$ from the distributed rotational inertia and the shear strains. Then for the oscillation of a uniform, free-free beam, idealized as a single element, the standard dynamical equation written here in the form

$$[\omega^2\mathbf{m} - \mathbf{k}]\,\mathbf{r} = 0 \qquad (1,52)$$

yields

$$\left[\Lambda\begin{bmatrix} 156\lambda^2 & 54\lambda^2 & -22\lambda & 13\lambda \\ 54\lambda^2 & 156\lambda^2 & -13\lambda & 22\lambda \\ -22\lambda & -13\lambda & 4 & 3 \\ 13\lambda & 22\lambda & 3 & 4 \end{bmatrix} - \begin{bmatrix} 6\lambda^2 & -6\lambda^2 & -3\lambda & -3\lambda \\ -6\lambda^2 & 6\lambda^2 & 3\lambda & 3\lambda \\ -3\lambda & 3\lambda & 2 & 1 \\ -3\lambda & 3\lambda & 1 & 2 \end{bmatrix}\right]\begin{bmatrix} \omega_1 \\ \omega_2 \\ \varphi_1 \\ \varphi_2 \end{bmatrix} = 0 \qquad (1,53)$$

where

$$\Lambda = \frac{\omega^2 m \ell^4}{840\,EI\,\lambda^4} = \frac{\omega^2 m a^4}{840\,EI} \qquad (1,53a)$$

The first four natural frequencies of the free-free beam, calculated from the eigenvalues Λ of this system, are shown in Fig.1.3 as multiples of the exact result. Further standard cases may also be obtained from Eq.(53) by suitable suppression of rows and columns according to the kinematic boundary conditions to be satisfied.

For the cantilever

$$\omega_1 = \varphi_1 = 0$$

while for the simply supported beam

$$\omega_1 = \omega_4 = 0$$

The simply supported beam with two elements requires merely the substitution of $\ell/2$ for ℓ with the kinematic conditions

$\omega_1 = \varphi_2 = 0$ in symmetric modes

$\omega_1 = \omega_2 = 0$ in antisymmetric modes.

Similarly the kinematic conditions for the free-free beam with two elements are

$\varphi_2 = 0$ in symmetric modes

$\omega_2 = 0$ in antisymmetric modes.

For more complex beam systems we may use the assembly technique of Eqs.(24) and (30). The results shown in Fig.1.3 indicate the degree of accuracy which is achieved by the above method of calculating the lumped inertias with only a single element. It must, however, be pointed out that the scheme is essentially designated for handling the lumped masses of more complicated dynamical systems, which require division into a larger number of elements. The present examples are intended only to give a simple demonstration of the accuracy achieved by the systematic application of the principles of the Matrix Displacement method to dynamic cases. At the same time elementary examples of beams and beam assemblies are well suited to demonstrating the power of the extension of our kinematically consistent technique through the introduction of eigenmodes. This refinement given in more detail in Ref. 10 retains the same number of elements, but assigns to them additional kinematic freedoms by introducing internal nodal points or deformation parameters. These additional or eigenmodes do not couple elastically as their name implies with the previous set of deformation modes. In fact, this elastic orthogonality may be extended by a judicious choice of functions to the eigenmodes themselves. Clearly they must satisfy the condition of zero deflexion, slope and bending moment (also shear to certain extent) at the nodal junction points of the elements. The method appears particularly attractive in the present case, since all static and kinematic compatibility conditions are satisfied by the original basic modes of the beam element. We illustrate the procedure by introducing one symmetrical and one antisymmetrical mode for each element. Denoting for the time being the original Π_e

matrix of Eq.(47) by Π_{ob}, we write

$$\Pi_{\bullet} = \begin{bmatrix} \Pi_{ob} & (1-\xi^2)^4 & -\frac{1}{2\lambda}\xi(1-\xi^2)^4 \\ & 16\lambda\xi(1-\xi^2)^3 & (1-\xi^2)^3(1-3\xi^2) \end{bmatrix} \qquad (1,54)$$

Application of Eq.(49) yields then the extended (6 x 6) mass matrix

$$\mathbf{m} = \frac{m\ell^3}{420\lambda^3} \begin{bmatrix} 156\lambda^2 & 54\lambda^2 & -22\lambda & 13\lambda & \frac{256}{3}\lambda^2 & \frac{768}{143}\lambda \\ 54\lambda^2 & 156\lambda^2 & -13\lambda & 22\lambda & \frac{256}{3}\lambda^2 & -\frac{768}{143}\lambda \\ -22\lambda & -13\lambda & 4 & -3 & -\frac{640}{33}\lambda & -\frac{320}{429}\lambda \\ 13\lambda & 22\lambda & -3 & 4 & \frac{640}{33}\lambda & -\frac{320}{429}\lambda \\ \frac{256}{3}\lambda^2 & \frac{256}{3}\lambda^2 & -\frac{640}{33}\lambda & \frac{640}{33}\lambda & \frac{917504}{7293}\lambda^2 & 0 \\ \frac{768}{143}\lambda & -\frac{768}{143}\lambda & -\frac{320}{429}\lambda & -\frac{320}{429}\lambda & 0 & \frac{229376}{46189} \end{bmatrix} \qquad (1,55)$$

in which the rotational inertia terms are ignored although they can easily be taken into account. Correspondingly the stiffness matrix of Eq.(51)

$$\mathbf{k} = \frac{2EI}{\ell}\lambda \begin{bmatrix} 6\lambda^2 & -6\lambda^2 & -3\lambda & -3\lambda & 0 & 0 \\ -6\lambda^2 & 6\lambda^2 & 3\lambda & 3\lambda & 0 & 0 \\ -3\lambda & 3\lambda & 2 & 1 & 0 & 0 \\ -3\lambda & 3\lambda & 1 & 2 & 0 & 0 \\ 0 & 0 & 0 & 0 & \frac{442368}{5005}\lambda^2 & 0 \\ 0 & 0 & 0 & 0 & 0 & \frac{65536}{5005} \end{bmatrix} \qquad (1,56)$$

The computational results are reproduced in Fig.1.3 and indicate a very remarkable degree of improvement in the accuracy of the quencies. We refer, however, to our discussion on the issue of additional kinematic freedoms in Ref.10 and consider that the best approach to kinematic idealization of complex systems requires further intensive research.

1.5 Tetrahedron Element with Linearly Varying Strain

We now return to the main subject of this Chapter, the application of natural modes in the Displacement method, and discuss in the present and following Sections two characteristic examples previously referred to. The first on tetrahedra with linearly varying strain has proved since its incor-

poration into ASKA[5] a great success in the analysis of complex three-dimensional media. To understand our approach it is useful to consult first the fundamental information on tetrahedra of constant strain and stress and arbitrary anisotropic behaviour investigated in Refs. 12, 13. A cardinal point of the theory underlying these papers is the specification of natural strain, stress and associated stiffness which is in close harmony with the given geometry. We also refer the reader to the corresponding ideas for the constant strain triangle developed in Ref.3. The constant strain tetrahedron has a further marked advantage of allowing an extension of the analysis by a very simple procedure into the domain of large displacements and strains. Applications in the small displacement regime are found in Section I.8, whilst those for large displacements are discussed in Section V.6. At the same time the author mentioned in a recent lecture to the R.Ae.S. certain difficulties arising in the interpretation of the stresses at nodal or other points, which are more severe than for constant strain triangles, the corresponding elements in the two-dimensional case. This was the main reason which led to the creation of the more advanced idealised model of a tetrahedron with linearly varying strain. The analysis is briefly reviewed below. Ten nodal points are now assigned to each tetrahedron, six of which are fixed at the midpoints of the six edges. The basic assumption of linear variation of strain is expressed by a set of homogeneous, so-called tetrahedron co-ordinates, which allow an astonishingly concise derivation of the stiffness matrix and the load vector due to initial strains. It should be pointed out that the assumed strain modes satisfy everywhere the kinematic compatibility conditions. This becomes evident, if we remember that the linear variation of strain implies displacements, which are second order functions in the co-ordinates x, y, z. Their coefficients are uniquely determined by the displacements at the nodal points and ensure complete kinematic matching of adjoining elements. At the same time, the present derivation, being exclusively based on the strain expression, does not require any algebraically complex manipulations for the determination of the coefficients associated with the displacement functions. The reader is advised to consult also Ref.15, which solves the analogous problem for a triangular element under linearly varying strain. An important point in the application of the present theory is the correct distribution of an applied loading at the nodal points of a tetrahedron. For example, if one face is subject to a uniform loading the kinematically equivalent forces at the nodal points should be zero at the vertices and one third of the total load on the three intermediate nodal points.

Following the notation of Fig.I.4, we introduce the supermatrices

$$l_e = \left[l_{12} \quad l_{34} \quad l_{41} \quad l_{32} \quad l_{24} \quad l_{31} \right] \quad (24 \times 24) \qquad (I,57)$$

$$\psi = \left\{ \psi_1 \quad \psi_2 \quad \psi_3 \quad \psi_4 \right\} \quad (24 \times 1) \qquad (I,58)$$

where

$$l_{ij} = l_{ij} I_4 \qquad (4 \times 4) \qquad (I,57a)$$

$$\psi_i = \{ x_i \quad y_i \quad z_i \} \qquad (3 \times 1) \qquad (I,58a)$$

In addition we have the diagonal supermatrix

$$\Sigma_{Te} = \left[\Sigma_{T12} \quad \Sigma_{T34} \quad \Sigma_{T41} \quad \Sigma_{T32} \quad \Sigma_{T24} \quad \Sigma_{T31} \right] \qquad (24 \times 72) \qquad (I,59)$$

where

$$\Sigma_{Tij} = \left[\Sigma_{Tij} \quad \Sigma_{Tij} \quad \Sigma_{Tij} \quad \Sigma_{Tij} \right] \qquad (4 \times 12) \qquad (I,59a)$$

Here Σ_{Tij} is the standard row matrix of the direction cosines of the side l_{ij}

$$\Sigma_{Tij} = \frac{1}{l_{ij}} \psi_{ij}^t = \frac{1}{l_{ij}} \left[\psi_j^t - \psi_i^t \right] \qquad (1 \times 3) \qquad (I,59b)$$

We next define a number of numerical matrices, of which the difference or extended Boolean matrix D is shown in Table I.1, where dots denote zero submatrices O_3 .

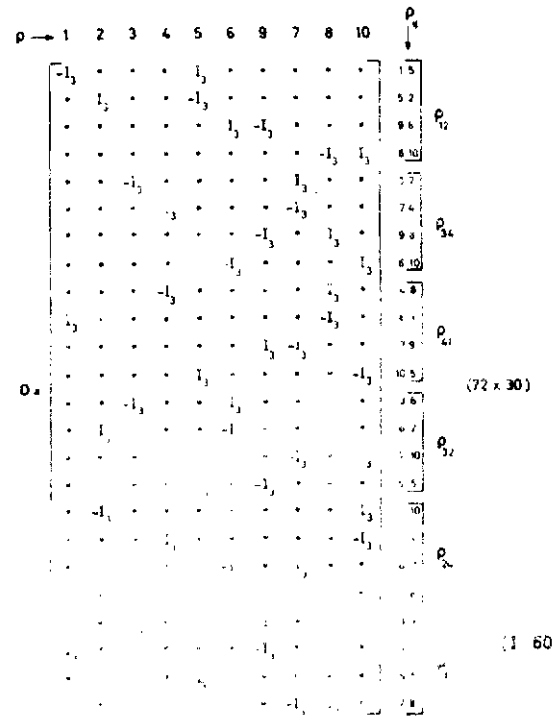

Difference Matrix D for a Tetrahedron
with Linearly Varying Strain

Table I.1

Furthermore

$$b_1 = \begin{bmatrix} 3 & -1 & -1 & -1 \\ & 3 & -1 & -1 \\ & & 8 & -4 \\ \text{Symmetric} & & & 8 \end{bmatrix}, \quad b_2 = \begin{bmatrix} -1 & -1 & 3 & -1 \\ & -1 & -1 & 3 \\ & & 4 & 4 \\ \text{Symmetric} & & & 4 \end{bmatrix}, \quad b_3 = \begin{bmatrix} -1 & -1 & 3 & -1 \\ 3 & -1 & -1 & -1 \\ -1 & 3 & 4 & 4 \\ -1 & -1 & 4 & 8 \end{bmatrix}$$

$$b_4 = \begin{bmatrix} -1 & 3 & -1 & -1 \\ -1 & -1 & -1 & 3 \\ -1 & -1 & 8 & 4 \\ 3 & -1 & 4 & 4 \end{bmatrix}, \quad b_5 = \begin{bmatrix} 3 & -1 & -1 & -1 \\ -1 & -1 & 3 & -1 \\ -1 & -1 & 4 & 8 \\ -1 & 3 & 4 & 4 \end{bmatrix}, \quad b_6 = \begin{bmatrix} -1 & -1 & -1 & 3 \\ -1 & 3 & -1 & -1 \\ 3 & -1 & 4 & 4 \\ -1 & -1 & 8 & 4 \end{bmatrix}$$

$$b_{12} = b_5 = \frac{2}{a} \begin{bmatrix} 3 & 1 & 0 & 0 \\ 1 & 3 & 0 & 0 \\ 1 & 1 & 2 & 0 \\ 1 & 1 & 0 & 2 \end{bmatrix} \qquad (4 \times 4) \qquad (1,61)$$

As in Section 1.2 we define two sets of nodal displacements and forces, the natural and the cartesian. The natural vectors of the elongations and nodal loads ϱ_{ij}, P_{ij} are of dimensions (24 x 1), in accordance with Fig.1.5. We apply the following sequential order and notation

$$\varrho_N = \{ \varrho_{12} \quad \varrho_{34} \quad \varrho_{41} \quad \varrho_{32} \quad \varrho_{24} \quad \varrho_{31} \} \quad (24 \times 1) \quad (1,62)$$

$$P_N = \{ P_{12} \quad P_{34} \quad P_{41} \quad P_{32} \quad P_{24} \quad P_{31} \} \quad (24 \times 1) \quad (1,63)$$

where ϱ_{ij}, P_{ij} are subvectors of order (4 x 1) whose elements are listed on the right hand side of Table 1.1. Their rule of formation is simply that the first two elements correspond to the two natural lengths of an edge —taken in accordance with the adopted positive direction— while the last two appertain to the two grid lines lying on the adjoining faces of the tetrahedron and parallel to the edge in question, the sequence of which is governed by the right-hand screw convention.

For example,

$\varrho_{12} = \{ \varrho_{15} \quad \varrho_{56} \quad \varrho_{68} \quad \varrho_{8,10} \}$, $\varrho_{32} = \{ \varrho_{11} \quad \varrho_{12} \quad \varrho_{13} \quad \varrho_{14} \}$

$P_{24} = \{ P_{29} \quad P_{10,4} \quad P_{67} \quad P_{58} \}$, $P_{31} = \{ P_{9} \quad P_{10} \quad P_{11} \quad P_{12} \}$ (1,64a)

The cartesian set is written in the sequence (listed at the top of Table I,1, see also Fig.I.6).

$$\varrho = \{\varrho_1 \quad \varrho_2 \quad \varrho_3 \quad \varrho_4 \quad \varrho_5 \quad \varrho_6 \quad \varrho_9 \quad \varrho_7 \quad \varrho_8 \quad \varrho_{10}\} \ (30 \times 1) \qquad (I,64)$$

$$P = \{P_1 \quad P_2 \quad P_3 \quad P_4 \quad P_5 \quad P_6 \quad P_9 \quad P_7 \quad P_8 \quad P_{10}\} \ (30 \times 1) \qquad (I,65)$$

where

$$\varrho_i = \{u_i \quad v_i \quad w_i\}, \quad P_i = \{U_i \quad V_i \quad W_i\} \ (3 \times 1) \qquad (I,64a,65a)$$

In accordance with Eqs.(5,11a) we have the dual transformation rules

$$\varrho_N = \mathcal{L}_{Te} D \varrho \quad , \quad P = D^t \mathcal{L}_{Te}^t P_N \qquad (I,66)$$

We conclude the preparatory work with the three-dimensional elastic law connecting the total natural strains ε_N, and component natural stresses σ_N as defined in Refs.12, 13. The specification of these vectors is fixed through the sequence adopted in Eqs.(62) and (63).

$$\varepsilon_N = \{\varepsilon_{12} \quad \varepsilon_{34} \quad \varepsilon_{41} \quad \varepsilon_{32} \quad \varepsilon_{24} \quad \varepsilon_{31}\} \qquad (6 \times 1) \qquad (I,67)$$

$$\sigma_N = \{\sigma_{12} \quad \sigma_{34} \quad \sigma_{41} \quad \sigma_{32} \quad \sigma_{24} \quad \sigma_{31}\} \ (6 \times 1) \qquad (I,68)$$

The reader should note that the arrangement of ε_N and σ_N is different from that used in Ref. 13. We now have

$$\sigma_N = \mathcal{E}_N \varepsilon_N = E \kappa \varepsilon_N \qquad (I,69)$$

where κ is the (6 x 6) matrix of the non-dimensional natural stiffness coefficients of the material

$$\kappa = \begin{bmatrix} \kappa_{11} & \kappa_{12} & \kappa_{13} & \kappa_{14} & \kappa_{15} & \kappa_{16} \\ \kappa_{21} & \kappa_{22} & \kappa_{23} & \kappa_{24} & \kappa_{25} & \kappa_{26} \\ \kappa_{31} & \kappa_{32} & \kappa_{33} & \kappa_{34} & \kappa_{35} & \kappa_{36} \\ \kappa_{41} & \kappa_{42} & \kappa_{43} & \kappa_{44} & \kappa_{45} & \kappa_{46} \\ \kappa_{51} & \kappa_{52} & \kappa_{53} & \kappa_{54} & \kappa_{55} & \kappa_{56} \\ \kappa_{61} & \kappa_{62} & \kappa_{63} & \kappa_{64} & \kappa_{65} & \kappa_{66} \end{bmatrix} \qquad (I,70)$$

a) Material and Cartesian Stiffness Matrices

A concise derivation of the natural stiffness matrix may be achieved by the adoption of the homogeneous tetrahedron coordinates introduced in Section 1.3 for the determination of the lumped mass of a constant strain tetrahedron. Following Figs.1.6,7 we have

$$\zeta_A = z_A/h_A \;,\; \zeta_B = z_B/h_B \;,\; \zeta_C = z_C/h_C \;,\; \zeta_D = z_D/h_D \qquad (1,71)$$

where h_A to h_D are the heights of the tetrahedra and z_A to z_D the distances measured from the feet of the perpendiculars towards the corresponding apices A to D . We adopt here for convenience the temporary notation A, B, C, D for the vertices 1,2,3,4. Any point in space is located by the four co-ordinates ζ_A , ζ_B , ζ_C , ζ_D which satisfy the relation (see also Eq.33)

$$\zeta_A + \zeta_B + \zeta_C + \zeta_D = 1 \qquad (1,72)$$

Correspondingly, an arbitrary linear variation of the strain vector $\tilde{\varepsilon}_N$ at a point $(\zeta_A, \zeta_B, \zeta_C, \zeta_D)$ may be expressed in the symmetrical form (see also Eq.(38)),

$$\tilde{\varepsilon}_N = \zeta_A \varepsilon_{NA} + \zeta_B \varepsilon_{NB} + \zeta_C \varepsilon_{NC} + \zeta_D \varepsilon_{ND} \qquad (6 \times 1) \qquad (1,73)$$

where ε_{NA} etc. are, as yet unknown, (6 x 1) vectors defining the strains at the vertices.

It is now very simple to obtain a matrix relation between any of the vectors ς_{ij} , and the associated four values $\varepsilon_{A,ij}$ to $\varepsilon_{D,ij}$ which we write as the vector

$$e_{ij} = \{ \varepsilon_A \quad \varepsilon_B \quad \varepsilon_C \quad \varepsilon_D \}_{ij} \qquad (4 \times 1) \qquad (1,74)$$

in the form

$$\varsigma_{ij} = \lambda_{ij} b_{ij} e_{ij} \qquad (1,75)$$

For example

$$\varsigma_{12} = \lambda_{12} b_{12} e_{12}$$

where (see Eq.(61))

$$b_{12} = \frac{1}{6} \begin{bmatrix} 3 & 1 & 0 & 0 \\ 1 & 3 & 0 & 0 \\ 1 & 1 & 2 & 0 \\ 1 & 0 & 0 & 2 \end{bmatrix} = b_S \qquad (4 \times 4)$$

All matrices b_{ij} connecting the five other vectors ϱ_{ij} and e_{ij} may be deduced by suitable re-arrangement of the columns of the parent matrix b_5 of Eq.(76). We may invert Eq.(75) to find

$$e_{ij} = d_{ij}\varrho_{ij} \tag{I,77}$$

Thus d_{12} if given by is

$$d_{12} = \frac{1}{l_{12}}\begin{bmatrix} 3 & -1 & 0 & 0 \\ -1 & 3 & 0 & 0 \\ -1 & -1 & 4 & 0 \\ -1 & -1 & 0 & 4 \end{bmatrix} \tag{I,78}$$

Again this matrix may serve as a basis to set up the other d_{ij} by appropriate shifting of the columns. Eq.(77) may be used in conjunction with Eq.(73) to write down any natural strain ε_{ij} in the form

$$\varepsilon_{ij} = \alpha_{ij}\varrho_{ij} \tag{I,79}$$

Taking α_{12} as an example, we find

$$\alpha_{12} = \left[(3\xi_1 - \xi_2 - \xi_3 - \xi_4) \quad (-\xi_1 + 3\xi_2 - \xi_3 - \xi_4) \quad 4\xi_3 \quad 4\xi_4\right] l_{12}^{-1} \quad (1 \times 4) \tag{I,80}$$

in which we revert again to the notation 1, 2, 3, 4 for the vertices of the tetrahedron, and l_{12} is given by Eq.(57a). It is straightforward to obtain the α_{ij} corresponding to all other natural strains ε_{ij}. A perusal of Eq.(80) shows that the characteristic terms $3\xi_1, 3\xi_2$, in the first two elements appertain to the vertices of the edge in question, whilst the last two $4\xi_3, 4\xi_4$ correspond to the remaining two vertices, the order of succession is fixed exactly as in ϱ_{12} by the adopted positive directions of the edges and the right-hand screw convention. As a further example to familiarize the reader with the method of formation, we quote

$$\alpha_{31} = \left[(-\xi_1 - \xi_2 + 3\xi_3 - \xi_4) \quad (3\xi_1 - \xi_2 - \xi_3 - \xi_4) \quad 4\xi_2 \quad 4\xi_4\right] l_{31}^{-1} \tag{I,81}$$

We next assemble the diagonal supermatrix

$$\alpha_{\sim} = \left[\alpha_{12} \quad \alpha_{34} \quad \alpha_{41} \quad \alpha_{32} \quad \alpha_{24} \quad \alpha_{31}\right] \quad (6 \times 24) \tag{I,82}$$

which dictates the transformation

$$\varepsilon_{\sim} = \alpha_{N}\varrho_{N} = \alpha_{N}\Sigma_{re}D\varrho \quad (6 \times 1) \tag{I,83}$$

Application of the unit displacement method gives the natural stiffness k_N ,

$$k_N = \int_V \alpha_N^t \ell_N \alpha_N \, dV \qquad (24 \times 24) \quad (1,84)$$

The integrations may be carried out at a glance once we remember the basic integrals of Eqs.(40), and observe that only four distinct terms emerge. We find

$$k_N = \frac{EV}{5} l_e^{-1} \begin{bmatrix} K_{11}b_1 & K_{12}b_2 & K_{13}b_4 & K_{14}b_6 & K_{15}b_4^t & K_{16}b_3^t \\ & K_{22}b_1 & K_{23}b_3 & K_{24}b_5 & K_{25}b_6^t & K_{26}b_5^t \\ & & K_{33}b_1 & K_{34}b_2 & K_{35}b_4 & K_{36}b_6 \\ & & & K_{44}b_1 & K_{45}b_3 & K_{46}b_5 \\ & \text{symmetric} & & & K_{55}b_1 & K_{56}b_2 \\ & & & & & K_{66}b_1 \end{bmatrix} l_e^{-1} \qquad (1,85)$$

where the (4 x 4) submatrices b_i are defined in Eqs.(61). The cartesian stiffness k of the tetrahedron is obtained by the familiar congruent transformation

$$k = D^t \Sigma_{re}^t k_N \Sigma_{re} D \qquad (30 \times 30) \quad (1,86)$$

The assembly of the complete stiffness matrix K and the determination of the displacements r (and hence $\varepsilon = a\, r$) proceeds as in our previous work.The strains or stresses may then be derived either directly on a cartesian basis, or preferably first via the natural strain and stresses using Eqs. (83) and (69). The determining matrix α_{ij} takes particularly simple forms at the nodal points. For example, $\alpha_{12,1}$, $\alpha_{12,2}$ (where the first two suffices indicate, as before, the direction of the natural strain, and the last, the selected nodal point) are given by

$$\alpha_{12,1} = \begin{bmatrix} 3 & -1 & 0 & 0 \end{bmatrix} l_{12}^{-1} \quad , \quad \alpha_{12,2} = \begin{bmatrix} -1 & 3 & 0 & 0 \end{bmatrix} l_{12}^{-1} \qquad (1,87)$$

Similarly,

$$\alpha_{34,9} = \alpha_{34,6} = \begin{bmatrix} 1 & 1 & 2 & 0 \end{bmatrix} l_{34}^{-1}, \alpha_{34,7} = \alpha_{34,10} = \begin{bmatrix} 1 & 1 & 0 & 2 \end{bmatrix} l_{34}^{-1} \qquad (1,88)$$

Eqs. (87, 88) reproduce all types of matrices appertaining to the vertices and intermediate nodal points of the tetrahedron.

The method developed in this note may incidentally be used to simplify considerably the derivation of the corresponding results in Refs. 15, 16.

b) Effect of Initial Strains.

Using the technique of Eq.(75) and related formulae, it is very simple to establish the effect of

initial strains. Assume for this purpose a linear variation of the (6 x 1) initial strain vector $\tilde{\eta}_N$ at a point (ζ_1, ζ_2, ζ_3, ζ_4) which may be expressed in accordance wirh Eq.(73) as

$$\tilde{\eta}_N = \zeta_1 \eta_{N1} + \zeta_2 \eta_{N2} + \zeta_3 \eta_{N3} + \zeta_4 \eta_{N4} \qquad (6 \times 1) \qquad (1,89)$$

where η_{N1} to η_{N4} are the prescribed (6 x 1) initial strain vectors at the vertices of the tetrahedron. We may now obtain the vector $\varsigma_{N\eta}$, arising from the $\tilde{\eta}_N$ distribution by applying an extended version of Eq.(75) in the form

$$\varsigma_{N\eta} = \mathcal{b}_{se} \mathcal{L}_e \eta_N \qquad (24 \times 1) \qquad (1,90)$$

where

$$\mathcal{b}_{se} = \begin{bmatrix} \mathcal{b}_{12} & \mathcal{b}_{34} & \mathcal{b}_{41} & \mathcal{b}_{32} & \mathcal{b}_{24} & \mathcal{b}_{31} \end{bmatrix} \qquad (24 \times 24) \qquad (1,91)$$

$$\eta_N = \{ h_{12} \quad h_{34} \quad h_{41} \quad h_{32} \quad h_{24} \quad h_{31} \} \qquad (24 \times 1) \qquad (1,92)$$

and

$$\varsigma_{N\eta} = \{ \varsigma_{12,\eta} \quad \varsigma_{34,\eta} \quad \varsigma_{41,\eta} \quad \varsigma_{32,\eta} \quad \varsigma_{24,\eta} \quad \varsigma_{31,\eta} \} \qquad (24 \times 1) \qquad (1,93)$$

The subvectors h_{ij} of η_N follow the pattern of Eq.(74), whilst those of $\varsigma_{N\eta}$ are in line with ς_N of Eq.(62). For example,

$$h_{12} = \{ \eta_A \quad \eta_B \quad \eta_C \quad \eta_D \}_{12}, \quad \varsigma_{32,\eta} = \{ \varsigma_{36} \quad \varsigma_{62} \quad \varsigma_{7,10} \quad \varsigma_{9,5} \}_{\eta} \qquad (4 \times 1) \qquad (1,94)$$

Alternatively, and corresponding more with the method of Ref. 16, we specify a matrix

$$\bar{\mathcal{b}}_{se} = \begin{bmatrix} \mathcal{b}_5 & \mathcal{b}_5 & \mathcal{b}_5 & \mathcal{b}_5 & \mathcal{b}_5 & \mathcal{b}_5 \end{bmatrix} \qquad (24 \times 24) \qquad (1,91a)$$

($\mathcal{b}_5$ being given in Eq.(61)) and write

$$\varsigma_{N\eta} = \bar{\mathcal{b}}_{se} \mathcal{L}_e \bar{\eta}_N \qquad (1,90a)$$

where $\bar{\eta}_N$ is a rearranged vector

$$= \{ \bar{h}_{12} \quad \bar{h}_{34} \quad \bar{h}_{41} \quad \bar{h}_{32} \quad \bar{h}_{24} \quad \bar{h}_{31} \} \qquad (1,92a)$$

and the (4×1) $\bar{h}_{ij}$ vectors are built up in accordance with an order deduced from the corresponding rearrangement of b_{ij} into b_s, which may be derived from η_N of Eq.(92) by Boolean operations. For example, a perusal of b_{24} shows that the vector $\bar{h}_{24}$ is

$$\bar{h}_{24} = \{\eta_B \quad \eta_D \quad \eta_C \quad \eta_A\}_{24} \tag{I,94a}$$

The natural and cartesian initial load vectors J_N and J are now obtained from

$$J_N = -k_N \varrho_{N\eta} \quad , \quad J = -L_{\eta\varepsilon}^t D^t k_N \varrho_{N\eta} \tag{I,95}$$

Having the vector J, the problem may be solved in the presence of thermal effects, plasticity, etc., applying the method of Section III.

Particularly simple forms of J may be set up for an isotropic thermal strain $\bar{\eta}_N$, especially if it be constant within the element, see in this connection Ref.16.

I.6 Parallelogram Element with Linearly Varying Strain

The second element to be discussed is a parallelogram under plane stress to which we seek an arbitrary linear variation of the strains along the edges. To achieve this we introduce eight nodal points, four of which are incorporated at the mid-points of the sides. Complete kinematic compatibility is again ensured with adjoining parallelogram elements of this type. The same is true if the assembly includes flanges with three nodal points. The present parallelogram is more refined than the original model considered in Appendix IV of Ref.3 and rehearsed on a modern basis in Section II, 9,10 of the present publication in conjunction with the development of a bending-cum-membrane theory of shells. The kinematic idealization adopted there is based upon oblique axes parallel to the sides of the parallelogram, see also Fig.I,8. Thus, for a unit nodal displacement in the x (y) direction ε_{xx} (ε_{yy}) is invariant with x (y) but varies linearly with y (x), whilst the opposite is true for the shear strain ε_{xy}. The new procedure for a parallelogram markedly improves the accuracy of the predicted stresses and the convenience of their evaluation.

The approach chosen here for the solution of the problem follows closely the general theory laid down in Section I.2. First we note that with eight nodal points, the total number of kinematic freedoms is $2 \times 8 = 16$. However, since three in-plane rigid body freedoms (two translations and one rotation) may be prescribed, it follows that the number of natural straining modes is $16 - 3 = 13$. These must be chosen in such a manner that they satisfy the basic condition of linear variation of strain. Before proceeding to their description we must refer the reader to the stress and strain conventions adopted for a parallelogram in Section II.4. They are based on an oblique definition in terms of the axes Oxy shown in Table I.2. We assume in what follows knowledge of these concepts and write the two-dimensional oblique stress and strain vectors in the form

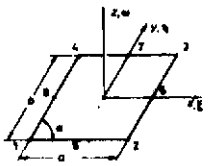

l = Reference Length
λ = l/a $\quad \mu = l/b$
α = $\sin\alpha$
ξ = $2x/a$ $\quad \eta = 2y/b$

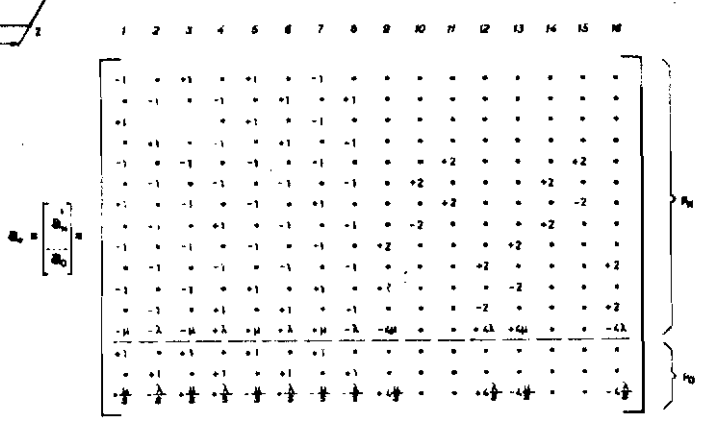

Transformation Matrix a_e for Parallelogram Plate with Eight Nodal Points

Table I,2

$$\sigma = \left\{ \sigma_{xx} \quad \sigma_{yy} \quad \sqrt{2}\,\sigma_{xy} \right\} \tag{I,96}$$

$$\varepsilon = \left\{ \varepsilon_{xx} \quad \varepsilon_{yy} \quad \frac{1}{\sqrt{2}}\,\varepsilon_{xy} \right\} \tag{I,97}$$

The stress-strain relation of arbitrary anisotropic behaviour is expressed as

$$\sigma = E\,\varepsilon = E'\nu\varepsilon \tag{I,98}$$

where

$$\nu = \begin{bmatrix} \nu_{11} & \nu_{12} & \sqrt{2}\,\nu_{13} \\ \nu_{21} & \nu_{22} & \sqrt{2}\,\nu_{23} \\ \sqrt{2}\,\nu_{31} & \sqrt{2}\,\nu_{32} & 2\,\nu_{33} \end{bmatrix} \tag{I,99}$$

E' is a measure of the generalized modulus E and ν_{ij} the non-dimensional coefficients determining the anisotropic behaviour of the material.

The full (16 x 1) vector of the nodal displacements and loads in the oblique sense of Section 11 is written in the non-dimensional form,

$$\rho = \frac{1}{l}\left\{ \rho_1 \quad \rho_2 \quad \rho_3 \quad \rho_4 \quad \rho_5 \quad \rho_6 \quad \rho_7 \quad \rho_8 \right\} \tag{I,100}$$

Correspondingly, the load (or rather moment) vector at the nodal points becomes

$$P = l\left\{ P_1 \quad P_2 \quad P_3 \quad P_4 \quad P_5 \quad P_6 \quad P_7 \quad P_8 \right\} \tag{I,101}$$

where

$$\rho_i = \left\{ u_i \quad v_i \right\} \qquad P_i = \left\{ U_i \quad V_i \right\} \tag{I,102}$$

define the oblique displacements and forces at the nodal points. The natural and rigid body representation is in accordance with Section I, 2, Eqs.(2, 10, 11) described by

$$\rho' = \left\{ \rho_N \quad \rho_0 \right\} = a_e \rho \quad \text{and} \quad \rho_N = a_N \rho \tag{I,103}$$

Also

$$P' = a_e^t P \quad \text{and for an equilibrium state} \quad P_N = a_N^t \rho \tag{I,104}$$

The thirteen selected natural and three rigid body modes are shown in Fig.1.8. The non-dimensional displacement functions may immediately be entered as elements of the relevant (2 x 16) $\alpha_e = [\alpha_N \; \alpha_0]$ matrix. A perusal of the thirteen modes shows that they satisfy the condition of linear variation of strain. It is now possible to derive the matrix a_e, reproduced in Table 1, 2, either directly or by inversion of the A_e matrix which is easier to set up. From the computational point of view it is advantageous to transform it into a generalised Boolean matrix, pre-and postmultiplied with diagonal matrices containing the parameters λ, μ, s . We omit this here for space reasons.

The next task is to set up the matrix α_N of Eq.(4) for which we obtain following the oblique technique of Section II

$$\alpha_N = \begin{bmatrix} 2\lambda & 2\mu & 1/\sqrt{2} \end{bmatrix} \alpha_N \qquad (3 \times 16) \qquad (1,105)$$

where

$$\alpha_N = \begin{bmatrix} 1/4 & 0 & \eta/4 & 0 & 0 & 0 & (1-\eta^2)/4 & 0 & -\xi/2 & 0 & \xi\eta/2 & 0 & 0 \\ 0 & 1/4 & 0 & \xi/4 & 0 & 0 & 0 & (1-\xi^2)/4 & 0 & -\eta/2 & 0 & \xi\eta/2 & 0 \\ 0 & 0 & \mu\xi/2 & \lambda\eta/2 & -\mu\eta & -\lambda\xi & -\mu\xi\eta & -\lambda\xi\eta & 0 & 0 & 0 & 0 & 1/6 \end{bmatrix}$$

(1,106)

The (13 x 13) natural stiffness k_N corresponding to the natural mode vector g_N can be obtained from the following expression

$$k_N = \frac{E' \ell^2 s}{4\lambda\mu} \int_{-1}^{+1}\int_{-1}^{+1} t \alpha_N^t \nu \alpha_N \, d\xi \, d\eta \qquad (13 \times 13) \qquad (1,107)$$

which may easily be verified from the general expression Eq.(22a) and the special formulae for parallelogram plates developed in Chapter II. For a constant thickness t, Table 1.3 reproduces the explicit matrix form for k_N .

The (16 x 16) matrix k associated with the generalized oblique loads $P\ell$ is found from Eq.(23)

$$k = a_N^t k_N a_N \qquad (16 \times 16) \qquad (1,23)$$

where a_N is here given in Table 1.2. It is simple to carry out the congruent transformation and the resultant formula may be equally suitable for machine operations as the direct evaluation of the congruent transformation (23) in the computer. We refer the reader to Ref 30, which gives the relevant formulae and the extension of the theory when the thickness t varies in accordance with the

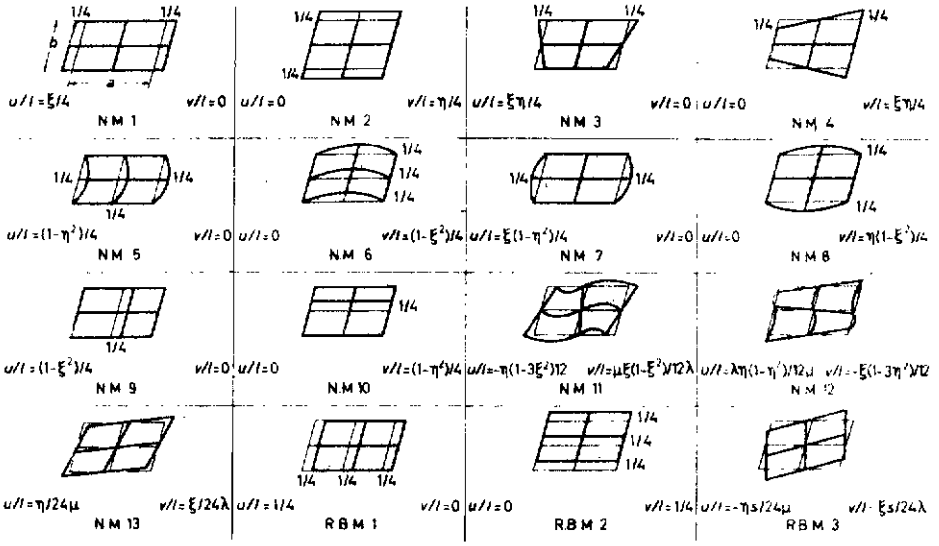

Natural and Rigid Body Modes for a
Parallelogram Membrane Element with Eight Nodal Points Fig.I.8

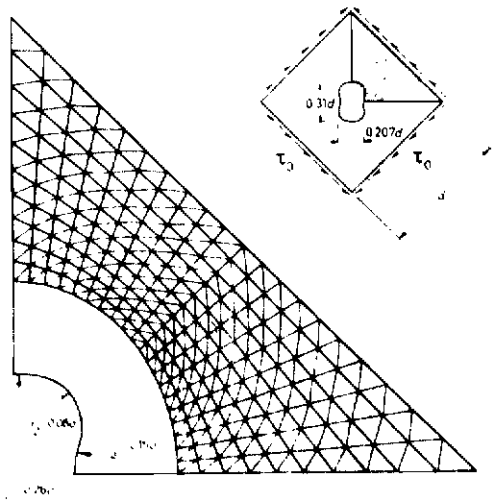

Plate under Shear with Keyhole
TRIM 3 Elements (Outer Grid)

Fig.I.9

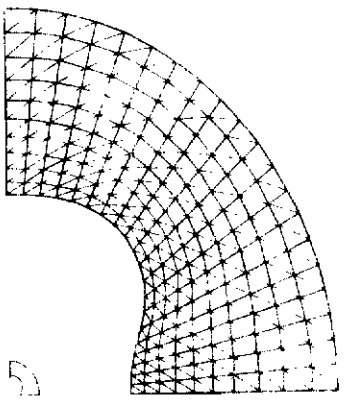

Plate under Shear with Keyhole
TRIM 3 Elements (Inner Grid)

Fig.I.10

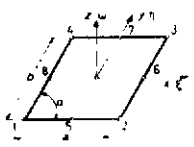

l = Reference Length
$\lambda = l/a \qquad \mu = l/b$
$s = \sin\alpha \qquad c = \cos\alpha$

$$k_N = \frac{Elts}{4}\left[\delta_1 \mathfrak{A}_1 \delta_1 + \delta_2 \mathfrak{A}_2 \delta_2\right]$$

$$\mathfrak{A}_1 = \frac{1}{45}\begin{bmatrix}
45v_{11} & \cdot & \cdot & \cdot & \cdot & \cdot & 30v_{13} & 30v_{12} & \cdot & \cdot & \cdot & 15v_{13} \\
\cdot & \cdot & \cdot & \cdot & \cdot & \cdot & 30v_{12} & 30v_{22} & \cdot & \cdot & \cdot & 15v_{23} \\
\cdot & \cdot & 15v_{11} & 15v_{13} & -30v_{13} & \cdot & \cdot & \cdot & -30v_{12} & \cdot & \cdot & \cdot \\
\cdot & \cdot & 15v_{13} & 15v_{33} & -30v_{33} & \cdot & \cdot & \cdot & -30v_{23} & \cdot & \cdot & \cdot \\
\cdot & \cdot & -30v_{13} & -30v_{33} & \cdot & \cdot & \cdot & \cdot & \cdot & \cdot & \cdot & \cdot \\
30v_{11} & 30v_{12} & \cdot & \cdot & \cdot & 24v_{11} & 20(v_{33}+v_{12}) & \cdot & \cdot & \cdot & \cdot & 10v_{13} \\
30v_{12} & 30v_{22} & \cdot & \cdot & \cdot & 20(v_{33}+v_{12}) & 24v_{22} & 60v_{11} & \cdot & \cdot & \cdot & 10v_{23} \\
\cdot & \cdot & -30v_{13} & -30v_{23} & \cdot & \cdot & \cdot & 60v_{22} & \cdot & \cdot & \cdot & \cdot \\
\cdot & \cdot & \cdot & \cdot & \cdot & \cdot & \cdot & \cdot & \cdot & \cdot & \cdot & \cdot \\
\cdot & \cdot & \cdot & \cdot & \cdot & \cdot & \cdot & \cdot & \cdot & \cdot & \cdot & \cdot \\
15v_{13} & 15v_{23} & \cdot & \cdot & \cdot & 10v_{13} & 10v_{23} & \cdot & \cdot & \cdot & \cdot & \cdot
\end{bmatrix}$$

$$\delta_1 = \sqrt{\frac{\lambda}{\mu}}\left[1\ \frac{\mu}{\lambda}\ 1\ 1\ \frac{\mu}{\lambda}\ 1\ 1\ \frac{\mu}{\lambda}\ 1\ 1\ \frac{1}{\sqrt{\lambda}}\right]$$

$$\mathfrak{A}_2 = \frac{1}{9}\begin{bmatrix}
\cdot & 9v_{11} & \cdot & \cdot & \cdot & \cdot & \cdot & \cdot & \cdot & \cdot & \cdot & \cdot \\
9v_{12} & 9v_{22} & \cdot & \cdot & \cdot & \cdot & \cdot & \cdot & \cdot & \cdot & \cdot & \cdot \\
\cdot & \cdot & 3v_{33} & 3v_{23} & \cdot & -6v_{33} & \cdot & -6v_{13} & \cdot & \cdot & \cdot & \cdot \\
\cdot & \cdot & 3v_{23} & 3v_{22} & \cdot & -6v_{23} & \cdot & -6v_{12} & \cdot & 12v_{11} & \cdot & \cdot \\
\cdot & \cdot & \cdot & \cdot & 12v_{11} & \cdot & \cdot & \cdot & 12v_{11} & \cdot & \cdot & \cdot \\
\cdot & \cdot & -6v_{13} & -6v_{23} & \cdot & 12v_{13} & \cdot & 12v_{13} & \cdot & \cdot & \cdot & \cdot \\
\cdot & \cdot & \cdot & \cdot & \cdot & \cdot & 4v_{11} & \cdot & \cdot & -4v_{13} & -4v_{23} & \cdot \\
\cdot & \cdot & \cdot & \cdot & \cdot & \cdot & \cdot & 4v_{13} & \cdot & -4v_{12} & -4v_{22} & \cdot \\
\cdot & \cdot & -6v_{13} & -6v_{12} & \cdot & 12v_{12} & \cdot & \cdot & \cdot & \cdot & \cdot & \cdot \\
\cdot & \cdot & \cdot & \cdot & 12v_{12} & \cdot & \cdot & \cdot & \cdot & \cdot & \cdot & \cdot \\
\cdot & \cdot & \cdot & \cdot & \cdot & \cdot & -4v_{13} & -4v_{23} & \cdot & \cdot & \cdot & \cdot \\
\cdot & \cdot & \cdot & \cdot & \cdot & \cdot & -4v_{23} & -4v_{22} & \cdot & \cdot & \cdot & \cdot \\
\cdot & \cdot & \cdot & \cdot & \cdot & \cdot & \cdot & \cdot & \cdot & 4v_{12} & 4v_{22} & \cdot \\
\cdot & \cdot & \cdot & \cdot & \cdot & \cdot & \cdot & \cdot & \cdot & \cdot & \cdot & v_{22}
\end{bmatrix}$$

$$\delta_2 = \sqrt{\frac{\mu}{\lambda}}\left[\frac{\lambda}{\mu}\ 1\ 1\ 1\ 1\ \frac{\lambda}{\mu}\ 1\ \frac{\lambda}{\mu}\ \frac{\lambda}{\mu}\ 1\ \frac{\lambda}{\mu}\ 1\ \sqrt{\frac{\lambda}{\mu}}\right]$$

Natural Stiffness Matrix for Parallelogram Membrane Element with Eight Nodal Points — Table I. 3

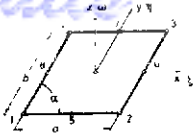

l = Reference Length
$\lambda = l/a \qquad \mu = l/b$
$s = \sin\alpha \qquad c = \cos\alpha$
m = Mass per Unit Area

$$m_{ee} = \frac{md^4}{4s}\left[\delta_1 \mathfrak{B}_1 \delta_1 + \delta_2 \mathfrak{B}_2 \delta_2\right]$$

$$\mathfrak{B}_1 = \begin{bmatrix}
\frac{1}{2} & \cdot & \cdot & \cdot & \cdot & \cdot & \cdot & \cdot & \cdot & \cdot & \cdot & \cdot \\
\cdot & \cdot & \cdot & \cdot & \cdot & \cdot & \cdot & \cdot & \cdot & \cdot & \cdot & \cdot \\
\cdot & \cdot & \frac{1}{36} & \frac{1}{36} & \cdot & \cdot & \cdot & \cdot & \cdot & \cdot & \cdot & \cdot \\
\cdot & \cdot & \frac{1}{36} & \frac{1}{18} & \cdot & \cdot & \cdot & \cdot & \cdot & \cdot & \cdot & \cdot \\
\cdot & \cdot & \cdot & \cdot & \frac{1}{18} & \cdot & \cdot & \cdot & \cdot & \cdot & \cdot & \cdot \\
\frac{1}{18} & \frac{1}{36} & \cdot & \cdot & \cdot & \frac{1}{9} & \frac{1}{45} & \cdot & \cdot & \cdot & \cdot & \frac{1}{108} \\
\frac{1}{36} & \frac{1}{18} & \cdot & \cdot & \cdot & \frac{1}{45} & \frac{1}{9} & \frac{1}{18} & \cdot & \cdot & \cdot & \frac{1}{108} \\
\cdot & \cdot & \cdot & \cdot & \cdot & \cdot & \frac{1}{18} & \frac{1}{9} & \cdot & \cdot & \cdot & \cdot \\
\cdot & \cdot & \cdot & \cdot & \cdot & \cdot & \cdot & \cdot & \cdot & \cdot & \cdot & \cdot \\
\cdot & \cdot & \cdot & \cdot & \cdot & \cdot & \cdot & \cdot & \cdot & \cdot & \cdot & \cdot \\
\frac{1}{72} & \frac{1}{72} & \cdot & \cdot & \cdot & \frac{1}{108} & \frac{1}{108} & \cdot & \cdot & \cdot & \cdot & \frac{1}{432}
\end{bmatrix}$$

$$\delta_3 = \left[1\ c\ 1\ c\ 1\ c\ 1\ c\ 1\ \frac{\lambda}{\mu}\ \frac{1}{\mu}\ 1\ c\ \frac{s}{\mu}\right]$$

$$\mathfrak{B}_2 = \begin{bmatrix}
\frac{1}{2} & \cdot & \cdot & \cdot & \cdot & \cdot & \cdot & \cdot & \cdot & \cdot & \cdot & \cdot \\
\cdot & \cdot & \cdot & \cdot & \cdot & \cdot & \cdot & \cdot & \cdot & \cdot & \cdot & \cdot \\
\cdot & \cdot & \frac{1}{36} & \frac{1}{36} & \cdot & \cdot & \cdot & \cdot & \cdot & \cdot & \cdot & \cdot \\
\cdot & \cdot & \frac{1}{36} & \frac{1}{18} & \cdot & \cdot & \cdot & \cdot & \cdot & \cdot & \cdot & \cdot \\
\cdot & \cdot & \cdot & \cdot & \frac{1}{18} & \cdot & \cdot & \cdot & \cdot & \cdot & \cdot & \cdot \\
\frac{1}{18} & \frac{1}{36} & \cdot & \cdot & \cdot & \frac{1}{9} & \frac{1}{45} & \cdot & \cdot & \cdot & \cdot & \frac{1}{108} \\
\frac{1}{36} & \frac{1}{18} & \cdot & \cdot & \cdot & \frac{1}{45} & \frac{1}{9} & \frac{1}{18} & \cdot & \cdot & \cdot & \frac{1}{108} \\
\cdot & \cdot & \cdot & \cdot & \cdot & \cdot & \frac{1}{18} & \frac{1}{9} & \cdot & \cdot & \cdot & \cdot \\
\cdot & \cdot & \cdot & \cdot & \cdot & \cdot & \cdot & \cdot & \cdot & \cdot & \cdot & \cdot \\
\cdot & \cdot & \cdot & \cdot & \cdot & \cdot & \cdot & \cdot & \cdot & \cdot & \cdot & \cdot \\
\frac{1}{72} & \frac{1}{72} & \cdot & \cdot & \cdot & \frac{1}{108} & \frac{1}{108} & \cdot & \cdot & \cdot & \cdot & \frac{1}{432}
\end{bmatrix}$$

$$\delta_4 = \left[c\ 1\ 1\ 1\ 1\ c\ 1\ 1\ \frac{\mu}{\lambda}\ 1\ c\ \frac{1}{\lambda}\ 1\ c\ \frac{s}{\lambda}\right]$$

Mass Matrix m_{ee} for Parallelogram Membrane Element with Eight Nodal Points — Table I 4

START

01.32 50	SMALL a STARTS	
01 36 09	SMALL a READY	3'19"
01 39.44	SMALL k STARTS	
02 14 00	SMALL k FINISHED AND SAVED	34'16"
02:16 01	BIG K STARTS	
03 02 05	BIG K FINISHED AND SAVED	46'04"
03.05 35	SMALL r STARTS	
09 24 28	SMALL r FINISHED AND SAVED	6h 18'53"
09:25 01	STRESS STARTS	
09 28 59	STRESS FINISHED AND SAVED	3'58"
	TOTAL COMPUTING TIME =	7h 46' 30"

Calculation of Thick-Walled Elliptical Cylinder Computing Times

Table I.5

law

$$t = t_o + t_I \xi + t_{II} \eta + t_{III} \xi \eta \qquad (I,108)$$

We complete this Section by establishing the lumped mass matrix m corresponding to the oblique system Oxy. Application of Eq.(28) and the transformation rules for oblique displacements Eq. (II,40), or direct recourse to Eq.(II, 175) yields the expression

$$m = \frac{\ell^4}{4\lambda\mu s} a_e^t \left[\int_{-1}^{+1}\int_{-1}^{+1} m \varpi_e^t \begin{bmatrix} 1 & -c \\ -c & 1 \end{bmatrix} \varpi_e \, d\xi \, d\eta \right] a_e \qquad (I,109)$$

$$= a_e^t m_{NR} a_e \qquad (I,109a)$$

where m is the mass per unit area

$$s = \sin\alpha \quad , \quad c = \cos\alpha \qquad (I,109b)$$

and

$$m_{NR} = \frac{\ell^4}{4\lambda\mu s} \int_{-1}^{+1}\int_{-1}^{+1} m \varpi_e^t \begin{bmatrix} 1 & -c \\ -c & 1 \end{bmatrix} \varpi_e \, d\xi \, d\eta \quad . \quad (16 \times 16) \qquad (I,110)$$

For a homogeneous plate of constant t the (16 x 16) matrix m_{NR} is reproduced in Table I.4. Very simple formulae may also be esta blished for m itself[30].

The stiffness k and mass matrix m as given above are referred to the oblique system Oxy. In some instances it may be preferable to operate with a cartesian system $Ox'y'$. The necessary transformation rules are established in Section I.2b, Eqs. (30, 31); see also Eq.(II, 160), but note the different sequential order adopted there. To obtain k' and m' based on $Ox'y'$, we use the congruent transformations

$$k' = \mathcal{L}^t k \mathcal{L} \qquad \text{and} \qquad m' = \mathcal{L}^t m \mathcal{L} \qquad (I,111)$$

where $\mathcal{L}$ is the diagonal supermatrix

$$\mathcal{L} = [\, \mathcal{L} \;\; \mathcal{L} \;\; \mathcal{L} \;\; \mathcal{L} \;\; \mathcal{L} \;\; \mathcal{L} \;\; \mathcal{L} \;\; \mathcal{L} \,] \qquad (16 \times 16) \qquad (I,112)$$

each diagonal submatrix $\mathcal{L}$ of which is

$$\mathcal{L} = \begin{bmatrix} 1 & 0 \\ c & s \end{bmatrix} \qquad (2 \times 2) \qquad (1,112a)$$

In Eq.(112a) we assume without loss of generality that the axis Ox' coincides with Ox. The explicit expression for m' is found to be relatively simple. Having established $\mathcal{L}$ and m for a single element, the stiffness and mass matrices K and M for the assembled structure are derived by the standard Boolean operations Eqs. (24, 30).

Ref. 30 presents a generalization of the above method to plane quadrilateral elements.

1.7 Applications to Two- and Three-Dimensional Elastic Media

In this Section we discuss a number of applications of the Matrix Displacement method to two- and three-dimensional problems. They are all essentially concerned with stress concentration phenomena, which present a formidable challenge to any finite element approach. It has already been shown by the author[11] that a good estimate may be achieved by a judicious choice of grid and intelligent inter- and extrapolation of the stress data appertaining to individual elements. These remarks refer specifically to the use of constant strain components like triangles and tetrahedra. For example, in the case of triangles the best results are obtained by taking the average of the cartesian stresses of two adjoining triangles, deriving hence a set of principal stresses and assigning them to the middle point of the common side. The values at the boundary of the assembled system are deduced by extrapolation. If, on the other hand, the averaging process were applied to the nodal points the computed stresses prove unreliable in the neighbourhood of steep stress gradients. Naturally, in fields of smooth stress distribution, the two approaches yield nearly identical results. For tetrahedra in three-dimensional media, the procedure is even more delicate. In general we find the average value of the cartesian stresses of all tetrahedra attached to a nodal point and assign it to the C.G. of the tetrahedra in question. To obtain the values at the boundary double extrapolation and at corners even triple extrapolation proves necessary, which increases the loss of accuracy, this being all the more critical the steeper the stress gradients. In contrast the new triangles and tetrahedra with imposed linear strain variation prove much more amenable to a simple interpretation, since they only require an averaging process of the stresses at the nodal points and no extrapolation. The simplicity of the procedure is striking in comparison with that of their constant strain counterparts. For brevity of reference we use in what follows the labels TRIM3, TETRA4 for the constant strain and TRIM6, TETRA10 for the linear strain elements, these being the headings under which they are entered in the ASKA library; the numeral affixed to the label denotes the number of nodal points of the element in question.

We start with a two-dimensional problem a square plate with a keyhole subject to a pure shear stress distribution at the external boundary. Figs.1.9, 10, 11 show the overall geometry and indicate the alternative grids used in conjunction with TRIM3 and TRIM6 elements. In Fig.1.11 the grid defines only the boundaries of the TRIM6 elements and does not include the intermediate nodal points. As a

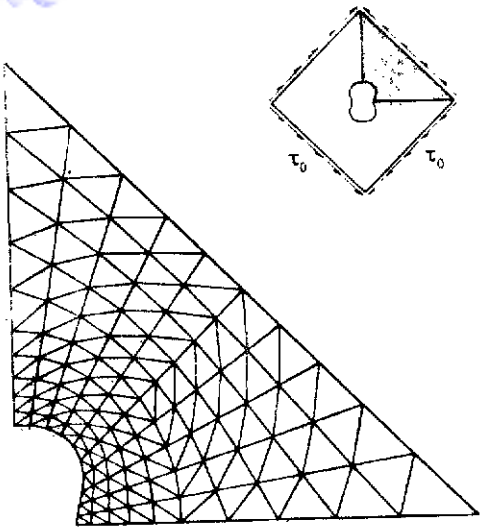

Plate under Shear with Keyhole
TRIM 6 Elements

Fig. I.11

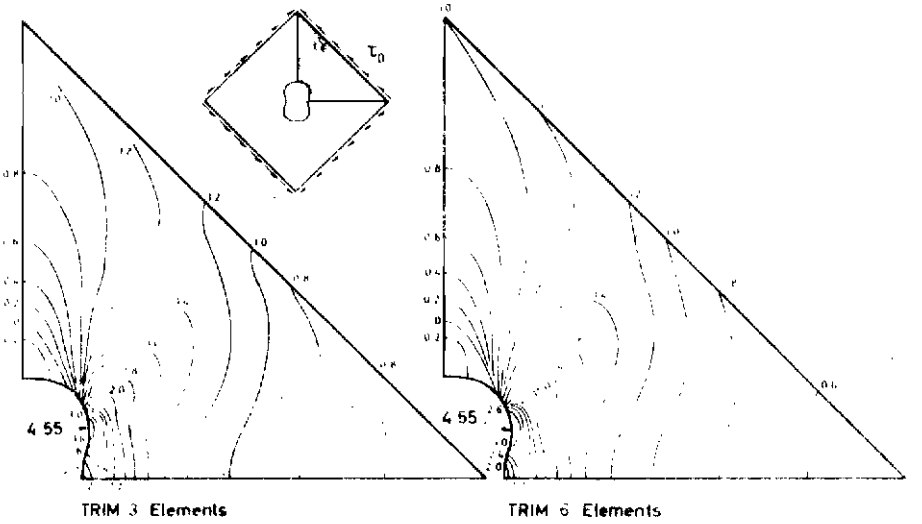

TRIM 3 Elements

TRIM 6 Elements

Plate under Shear with Keyhole
Principal Stress Contours for σ_1/τ_0

Fig. I.12

matter of fact, the total number of nodal points is in both cases identical, which allows a fair comparison between the performance of the two idealisations, moreover the position of the vertices is as nearly the same as geometrical and engineering considerations allow. It is clear that for the same number of nodal points the reproduction of a curved boundary is more accurate by the TRIM3 (and for that matter also by the TETRA4) than by its more refined companion elements. This is the only advantage displayed by the older constant-strain group of components. Due to the symmetry of structure and loading only a quarter of the system need be analysed, the count of considered nodal points and unknowns being for both idealisations 441 and 840 respectively. The total computing time including input of initial data, computation of co-ordinates, averaging process of the stresses, evaluation of the principal stresses and final writing of the results on magnetic tape (but excluding the actual printing was 14m 35s and 14m 2s for the TRIM3 and TRIM6 idealisations. The interpretation of the final results for TRIM6 is straightforward as mentioned above. At the same time some care is necessary when applying a distributed load on the edge of a system idealised with TRIM6 elements. For example, where a uniform loading acts along the side of a triangle, it proves most successful, following also a theoretical argument, to introduce kinematically equivalent concentrated forces, one-sixth of the total load at the vertices bounding the side and two-thirds at the mid-point. This procedure was used in the current example. The results for the non-dimensionalized principal stresses σ_1 / τ_o and σ_2 / τ_o are reproduced in Fig.I,12 and I.13 for TRIM3 and TRIM6; the respective maximum stress concentration factors (S.C.F.) are given as 4.55 and -4.7 respectively. Although the contour lines appear very nearly the same it must be pointed out that whilst those for TRIM6 are obtained immediately, the opposite is true for TRIM3 where significant interpolation effort is required at the steep stress gradients . The coincidence of the values for the S.C.F. is no doubt due to the fact that the engineer responsible for the programming side had the TRIM6 as a guide for the intelligent reading of the TRIM3 output. (A further interpretation of the latter result subsequently appears to lead to a value of 4.6 instead of 4.55). Judging from independent photoelastic results, the accuracy for the S.C.F. appears to be in the region of 5%. We draw the readers attention to the loaded edge where there appear evident deviations from the true stress contours for σ_1 / τ_o and σ_2 / τ_o ; these slight inaccuracies are clearly due to the unavoidable limitation of the finite element approach.

Next we consider a circular plate under an in-plane pair of self-equilibrating radial forces P, for which an exact solution is found in Timoshenko[8]; see Fig.I.14. This example was again analysed with TRIM3 and TRIM6 components for the same number of nodal points. The results for TRIM6 were markedly superior to those for TRIM3, and considering the small number of elements, astonishing accuracy once one moves away from the singular region of the concentrated load. Fig.I.14 displays clearly the good agreement with the continuous solution, at the centre of the circular plate the ratio $\sigma_x / \frac{P}{\pi t}$ was found to be 1.894 as against the exact one of $6/\pi = 1.909$ quoted by Timoshenko. The results for TRIM3 are not reproduced here.

We continue with a group of three-dimensional examples concerning a cube with a spherical or ellipsoidal cavity, subject to a uniform tensile stress σ_{yy} at one face. The solutions to these problems are at the moment all based on TETRA4, but a comparison with TETRA10 is in preparation.

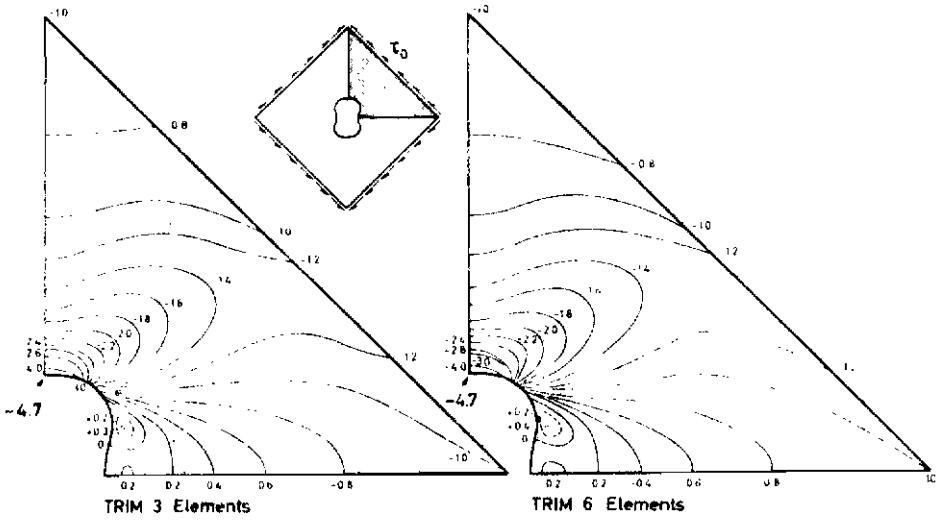

Plate under Shear with Keyhole

Principal Stress Contours for σ_2/τ_0 Fig. I.13

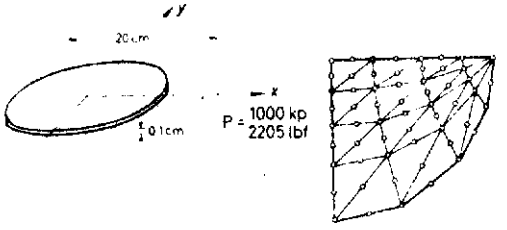

o Exact Result.

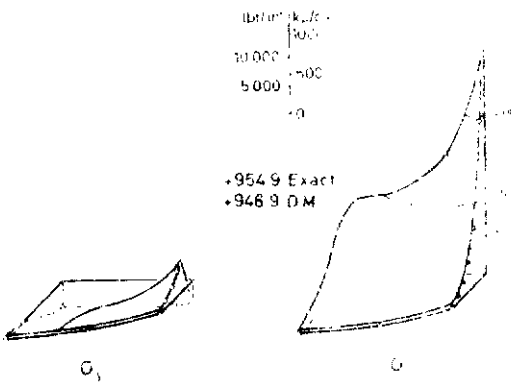

Matrix Displacement Method

Stresses in Circular Plate under End Load

(TRIM 6 Elements)

Fig. I.14

The assembly of the structure is achieved in all cases with a triangular prism itself containing three TETRA elements. Two alternative arrangements 1 and 2 were chosen as shown in Figs. 15 to 18. The stress distribution proves, as a matter of fact, rather sensitive, especially in the neighbourhood of the stress concentration to the arrangement of the tetrahedra as seen by the plotted stress contours. The partitioning 2 of Figs. I.16 and I.18 appears more reliable, judging from the expected correct position of the highest stresses. At the same time the nodal values at the corner points are to be treated with some reserve, due to the triple interpolation process involved. However, the reliability of the inter- and extrapolated values around the cavity appears satisfactory if one remembers that the S.C.F. for an infinite medium with a spherical cavity and a uniform direct stress at infinity is 2.1 and constant at the major circle in a plane perpendicular to the applied stress. The number of tetrahedra, nodal points and unknowns were 1797, 442, 1145 respectively. The accuracy of the S.C.F. results is estimated to lie between 5 and 7%, but a final judgment must be postponed until the TETRA10 results are available. The total computing time including all the aforementioned operations was 120m.

A further three-dimensional example investigated at the Institut für Statik und Dynamik der Luft- und Raumfahrtkonstruktionen, Stuttgart, West Germany, concerns a thick-walled elliptical cylinder subjected to an external uniform transverse pressure $p = 20\ kp/mm^2$ over part of the surface. Figs. I.19 and 20 show the system and the adopted idealisation with TETRA10 elements, note that the basic component is a quadrilateral prism with 5 constituent tetrahedron elements. Since the loading (Fig.I,21) and the structure are symmetrical, only a quarter of it need be analysed and the corresponding numbers of tetrahedra, nodal points, and unknowns are 450, 911, and 2488 respectively. Note that in agreement with our statement on page 28 external nodal forces are only introduced at the midpoints of the relevant edges of the tetrahedra, (Fig.I,21). Table I.5 reproduces the information on the main computational cycles and processing times involved. Of special interest is the fact that the accuracy of the solution of the equation (25) proved highly satisfactory, although only single-precision was used. By our usual checking procedure, the residual loads are obtained by substitution of ς into the right hand side of the expression

$$R = K\tau = a^t k \varsigma \qquad (I,113)$$

and they were found not to exceed by a factor of 10^{-5} the magnitude of the applies individual loads. The transverse stresses σ_{yy} are shown for the cross-sections I, V and IX in Fig.I,22. Fig.I.23 reproduces the transverse displacements. The highest stress is observed to be 78 kp/mm^2, which indicates an S.C.F. of approximately 4. There is little doubt, in view of the nearly perfect continuity of stress at the nodal points, that the stress distribution must be highly accurate.

The final example discussed in the present Section is a square plate of constant thickness with a central square hole and rounded corners with an r/a value of 0.2, subject to a non-uniform temperature distribution as shown in Fig. I.24. The same system, but under uniform shear, is also analysed for the elasto-plastic regime in Section III.6. As idealization we choose an assembly of TRIM6

elements, the numbers of nodal points and unknowns being 309 and 603 respectively; see Figs. III.6, 7. The application of the theory with the initial load vectors $\mathfrak{T}$ is straightforward. The maximum stress ratio $\sigma_1/\sigma_{\sigma\eta\,max}$ is found to be 0.734, $\sigma_{\sigma\eta\,max}$ is the thermal stress arising if all nodal points are blocked and is here -50 kp/mm^2. Further consideration on stress concentration may also be found in Sections III.1 through III.6 dealing with elastoplastic investigations.

I.8 Static and Dynamic Applications to Wing Structures

We present in what follows two particular investigations on wing-type structures using the new elements. In the case of the static solution we also present a comparison with previous data, obtained with TRIM3 covers and the spar elements proposed in Ref.3.

We have to interrupt here our account and refer briefly to a new type of spar web element introduced in conjunction with the TRIM6 idealisation, (see Ref. 18). This approach allows the consideration of unsymmetrical spar webs which need not be even trapezoidal. This proves particularly convenient in connection with some modern supersonic configurations. The new idealisation is constructed by an assembly of four constituent TRIM6 elements as follows. (see Fig.I.25).

Two types of idealisations have to this purpose been investigated, both of which proved equally successful (see Figs. 1, 25, 25a). In the first idealisation we initially slice the spar web thicknesswise into two equal sheets. Each of these is then partitioned into two TRIM6, the common side being in each case one of the diagonals of the original quadrilateral element. The kinematic assembly of four component triangles yields the stiffness and stresses of the web. Eight nodal points are assigned to this element which is denoted in ASKA as SPARTA I. The second idealisation designated as SPARTA II uses once more four TRIM6, these being simply the four component triangles of the quadrilateral, arising when partitioned by its two diagonals (Fig. 1,25a); no difference in accuracy has been recorded between the two idealisations. The quality of the new element may be judged from the comparison of experimental and previous theoretical data for a highly tapered spar shown in Figs. 1.26 to 28; the new computations were actually based on SPARTA I. It is seen that it is at least as good an independent member as the old element carrying the label SPARBS. However, it is much more suitable for wing calculations than SPARBS since it ensures complete kinematic compatibility with FLA3 and TRIM6 elements. The previous spar element idealisation did not allow on the other hand complete kinematic matching with the cover.

We now proceed to a brief review of the static results obtained on the wing structure shown in Fig.I.29. Since this structure was extensively discussed in Ref.3, the construction details need not concern us here. Two computations were performed. In the first one we used the so-called fine grid of Ref.3 in conjunction with TRIM3 and SPARBS. The number of unknowns assuming symmetry with respect to the middle plane of the wing was 494. A parallel investigation was carried out using

TRIM6, FLA3 and SPARTA elements. Two alternative calculations were performed with this idealisation. In the first we ignored the asymmetric nature of the supports and in the second we took account of it, the total number of unknowns rose in the latter instance to 917. Four loading cases were considered but the results of only three are reproduced here, see Fig.1.29. The computational times involved were 5m 11s for 494 unknowns and 36m for 917 unknowns. The rather marked difference in the quoted times arises from the fact that we used for the greater number of unknowns the large capacity storage drum of the UNIVAC 1107 machine, which has, of course, a slower access than the ordinary drums of this computer.

Figs. 1.30 to 39 reproduce the results. They may be commented upon briefly as follows. As far as the deflexions are concerned, there is in all cases much better agreement between the experimental and theoretical values using the new idealisation technique. Similar conclusions may be drawn for the stresses in the flanges, especially in the support triangles and for the loading case A . Much closer agreement was also achieved in the stresses in the cover between spars 1 and 2, this again being all the more marked in the support triangles where the old results were so unsatisfactory that they are not reproduced. Possibly the most striking improvement is that of the shear stresses in the webs, which seem to confirm that the new element is highly suitable for the matrix analysis of wings.

The second theoretical investigation concerns an attempt to verify the finite element and lumped mass approach on the delta wing system shown in Fig.1.40. As seen in the experimental set up, the model is suspended from its nose by a relatively long cable. A very simplified tail unit was also provided as shown in the isometric view of Fig.1.41. The total weight of the structure was approximately 208 lb. Naturally, by this kind of support the system was not strictly in a free-free state. In fact, if considered as a rigid body, the wing was acting as a double pendulum. The two pendulum frequencies were nevertheless so much lower than the basic free-free frequency of the elastic wing that the experimental results on the excited structure may be assumed to reproduce to a high degree of accuracy the free-free state; note that the higher of the two pendulum frequencies is of the order of 5 cps. The main structural details of the wing are indicated in Fig.1.41. More details on the construction and the experiments may be found in the M.Sc.(Eng) Thesis of R.J.J.Taborek (University of London, 1962), Ref.32. This author also performed a rather rough calculation using the Matrix Force method approach in its simplest form. He obtained good agreement on the symmetric modes, especially for the frequencies of the first, second, third and fifth modes. The same applies, but to a lesser extent in the higher modes, to the eigenvectors themselves. A new theoretical investigation carried out at the Institut für Statik und Dynamik applied the grid shown in Fig.1.42 with TRIM6, FLA3 and SPARTA constituent elements. A kinematically equivalent lumped mass was in all cases used in accordance with Eq.(28). The theoretical and experimental results for the frequencies and nodal lines of the first five symmetrical modes are compared in Figs.1.43 and 44. No modes higher than the five symmetric ones were excited so that the reproduction of the computational data is not extended here beyond the fifth mode. As may be seen a highly satisfactory agreement between theory and experiment is achieved. For more details the reader should consult Refs. 10 and 33. Summarizing the reults it appears that the finite element and associated lumped mass matrix analysis yields a reliable tool for the prediction of the dynamic behaviour of complex elastic systems.

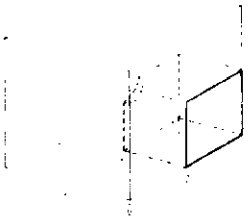

Cube with Spherical Cavity
under Uniform Stress
$\sigma_{yy} = 1\ kp/mm^2$

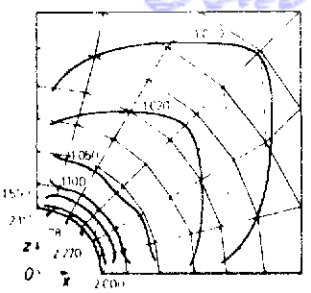

σ_{yy} Contours in *Oxz* Plane

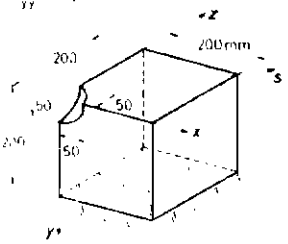

One Eighth of Space of Cube
(Computed Model)

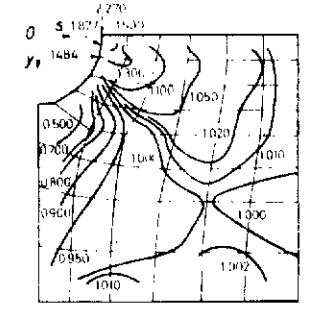

σ_{yy} Contours in *Oys* Plane

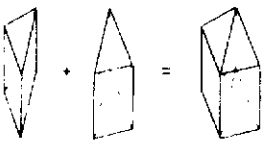

Tetrahedron Components of
Typical Quadrilateral Prisma A

Stress Concentration in a Cube
with Spherical Cavity
(Element Arrangement 1) Fig. I.15

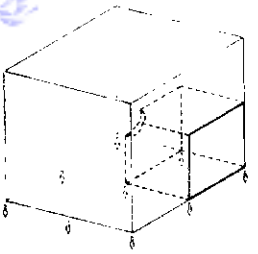

Cube with Spherical Cavity
under Uniform Stress
$\sigma_{yy} = 1\ kp/mm^2$

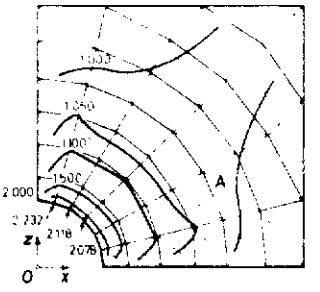

σ_{yy} Contours in *Oxz* Plane

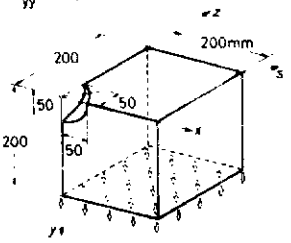

One Eighth of Space of Cube
(Computed Model)

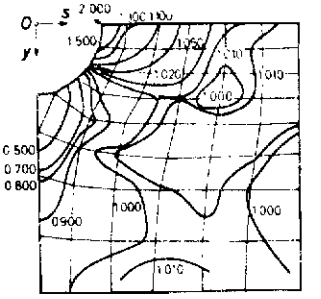

σ_{yy} Contours in *Oys* Plane

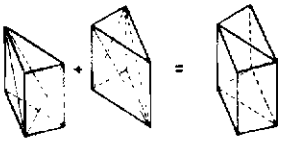

Tetrahedron Components of
Typical Quadrilateral Prisma A

Stress Concentration in a Cube
with Spherical Cavity
(Element Arrangement 2) Fig. I.16

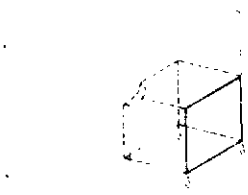

Cube with Ellipsoidal Cavity
under Uniform Stress
$\sigma_{yy} = 1\ kp/mm^2$

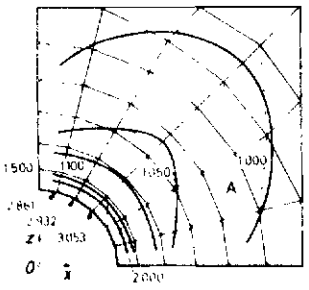

σ_{yy} Contours in *Oxz* Plane

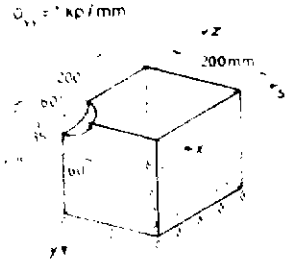

One Eighth of Space of Cube
(Computed Model)

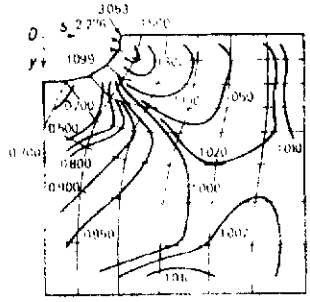

σ_{yy} Contours in *Oys* Plane

Tetrahedron Components of
Typical Quadrilateral Prisma A

Stress Concentration in a Cube
with Ellipsoidal Cavity
(Element Arrangement 1) Fig. I.17

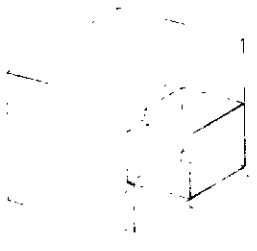

Cube with Ellipsoidal Cavity
under Uniform Stress
$\sigma_{yy} = 1\ kp/mm^2$

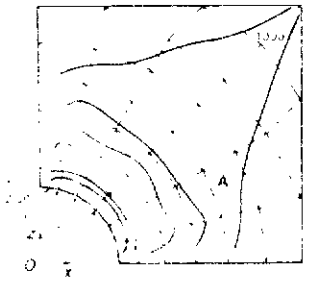

σ_{yy} Contours in *Oxz* Plane

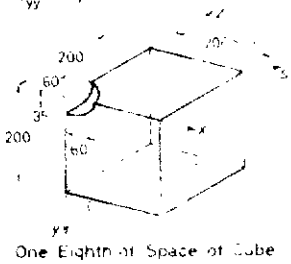

One Eighth of Space of Cube
(Computed Model)

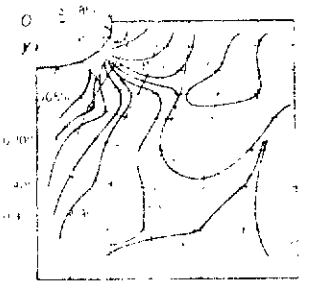

σ_{yy} Contours in *Oys* Plane

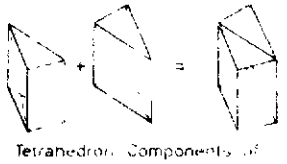

Tetrahedron Components of
Typical Quadrilateral Prisma A

Stress Concentration in a Cube
with Ellipsoidal Cavity
(Element Arrangement 2) Fig. I.18

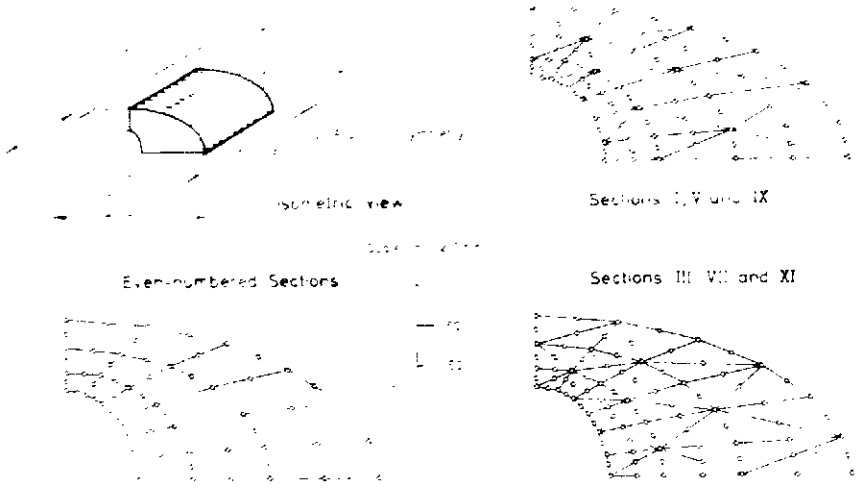

Idealisation of a Thick-Walled Elliptical Cylinder

2488 Unknowns

Fig I 19

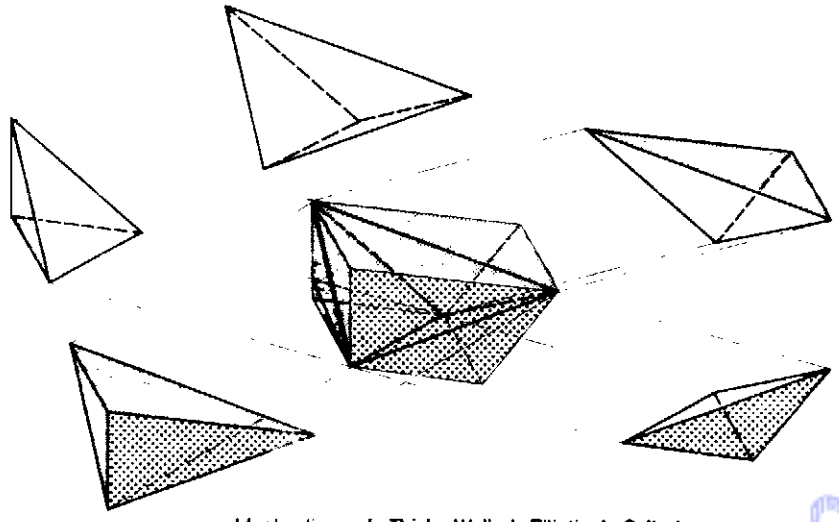

Idealisation of Thick-Walled Elliptical Cylinder

Basic Quadrilateral Prism with Five Constituent Tetrahedra

Fig I 20

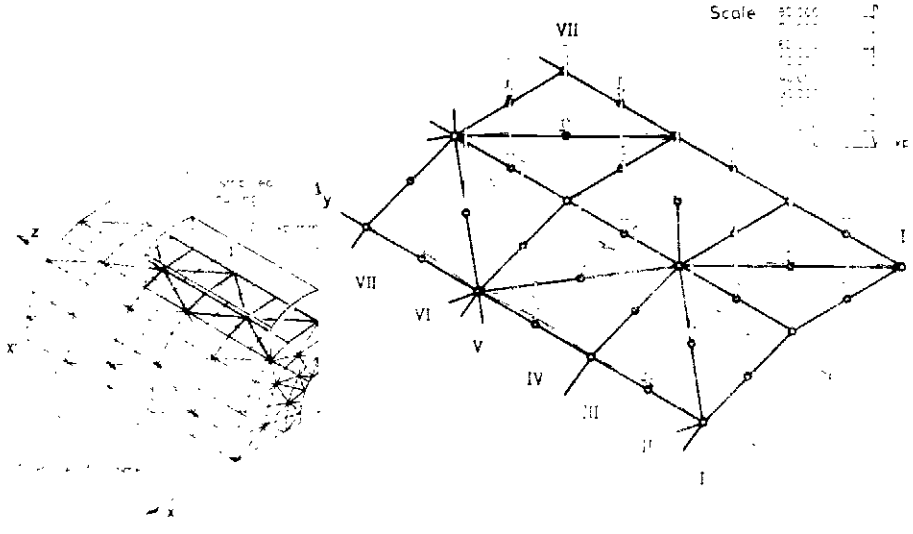

Elliptical Thick-Walled Cylinder under Uniform Transverse Pressure

Representation of Uniform Loading by Nodal Forces

Fig I 21

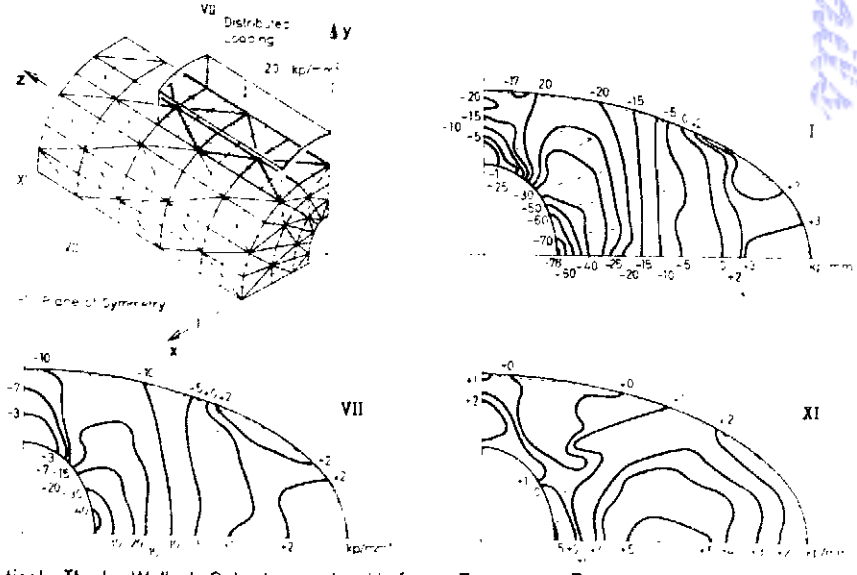

Elliptical Thick-Walled Cylinder under Uniform Transverse Pressure

Contours of σ_{yy} at Sections I, VII, and XI

Fig I 22

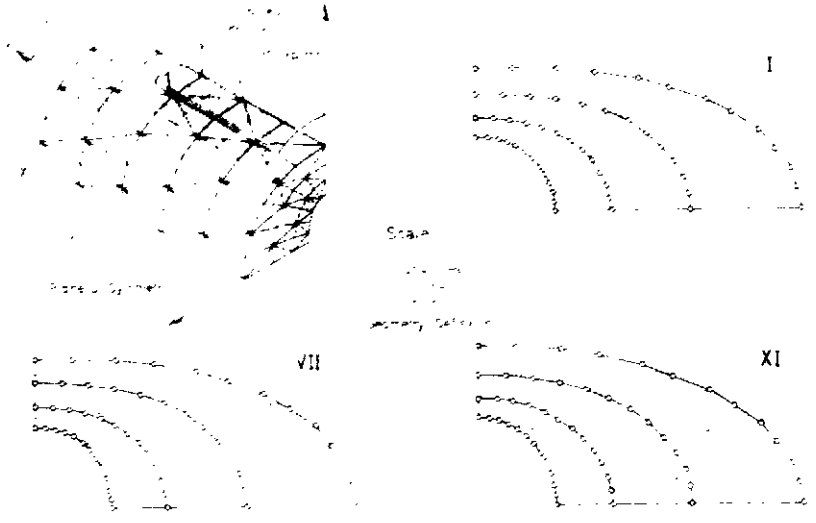

Elliptical Thick-Walled Cylinder under Uniform Transverse Pressure

Transverse Deformation at Sections I, VII and XI

Fig. I. 23

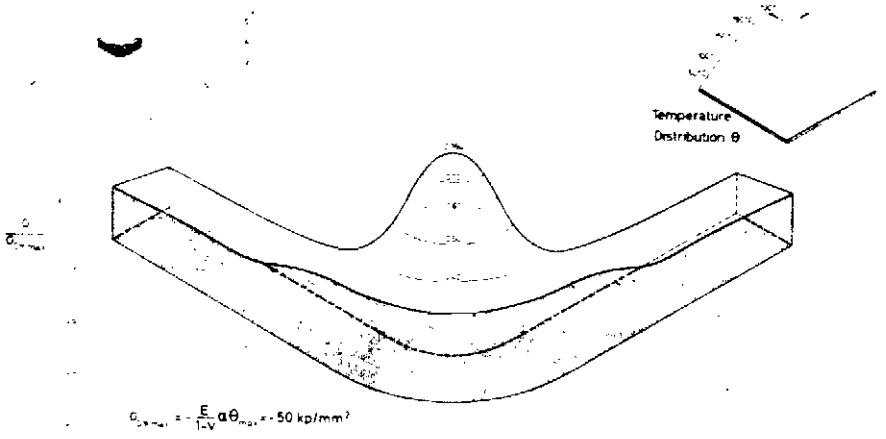

Plate with Central Hole, r/a = 0.2
Applied Non-Uniform Heating
Principal Stress σ_t

Fig. I. 24

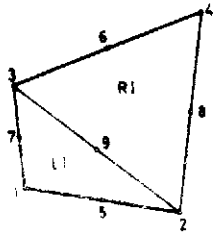

Web Component I
Thickness t/2

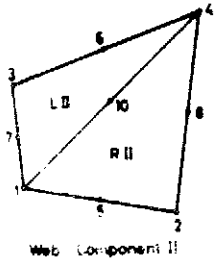

Web Component II
Thickness t/2

SPARTA I Spar Element

Fig I 25

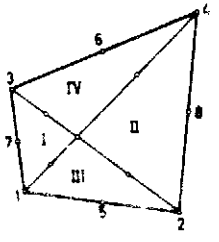

SPARTA II Spar Element

Fig. I. 25a

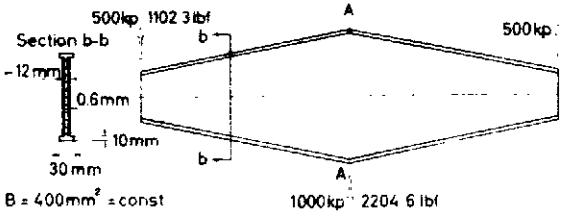

B = 400 mm² = const
Web, sandwich with
paper honeycomb

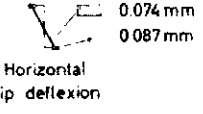

SPARTA, M.D.M.
SPAR, M.D.M.
Experimental
E.T.B. (with shear)

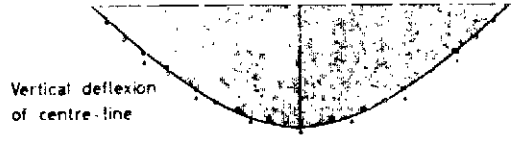

0.78 (0.74) mm
0.76 mm
0.73 mm
0.80 mm

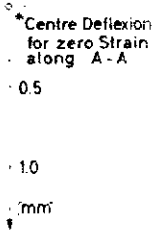

Tapered Beam II
Deflexion

Fig. I. 26

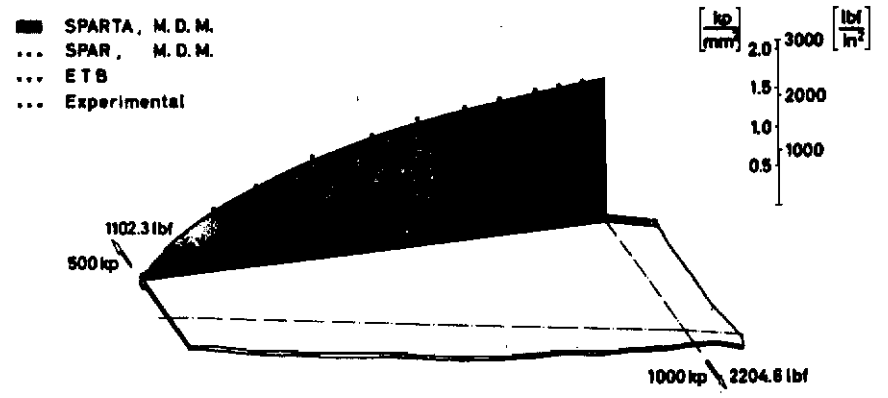

Tapered Beam II
Flange Stress σ_r

Fig.I.27

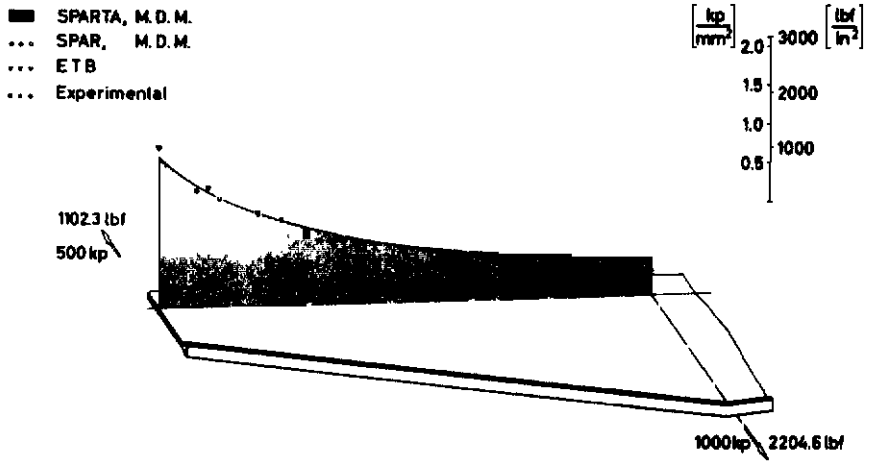

Tapered Beam II
Shear Stress τ_{xy}

Fig.I.28

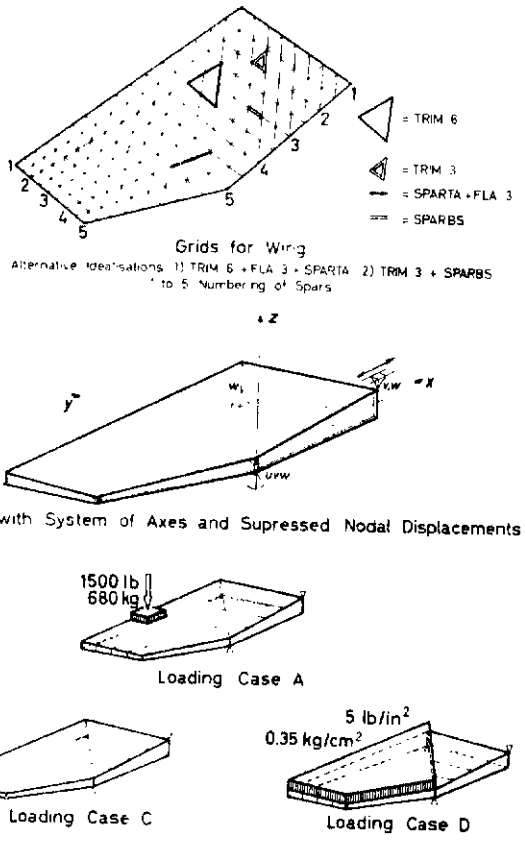

Idealisation and Loading of Wing Fig.I.29

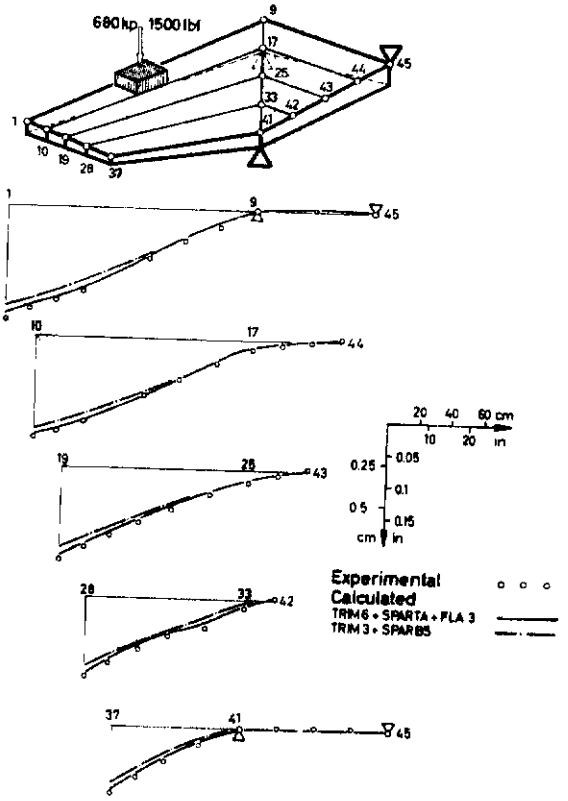

Deflection of Wing – Loading Case A

Fig.I.30

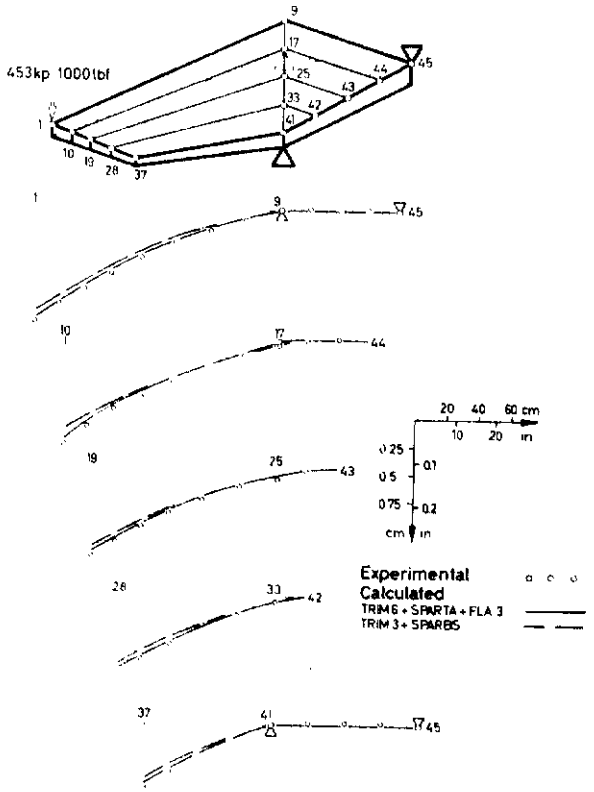

Deflection of Wing – Loading Case C

Fig.I.31

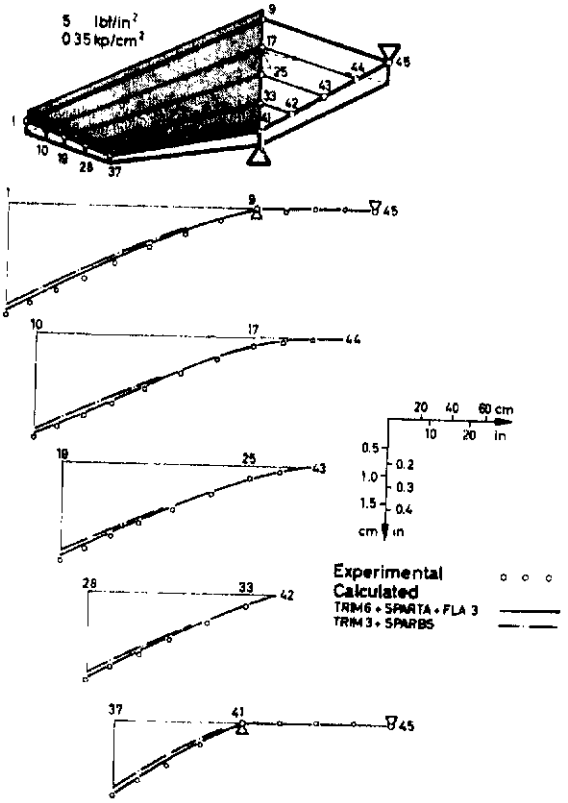

Deflection of Wing – Loading Case D

Fig.I.32

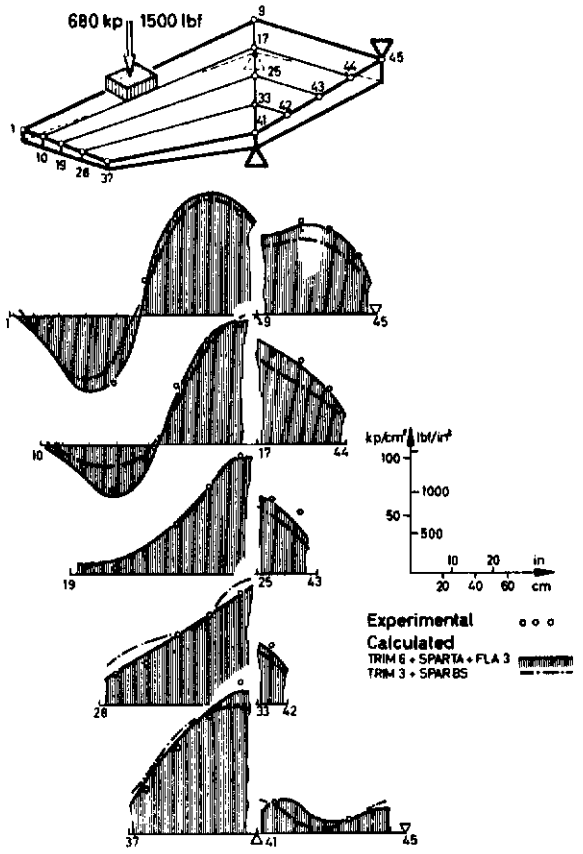

Direct Stresses in Flanges — Loading Case A

Fig.I.33

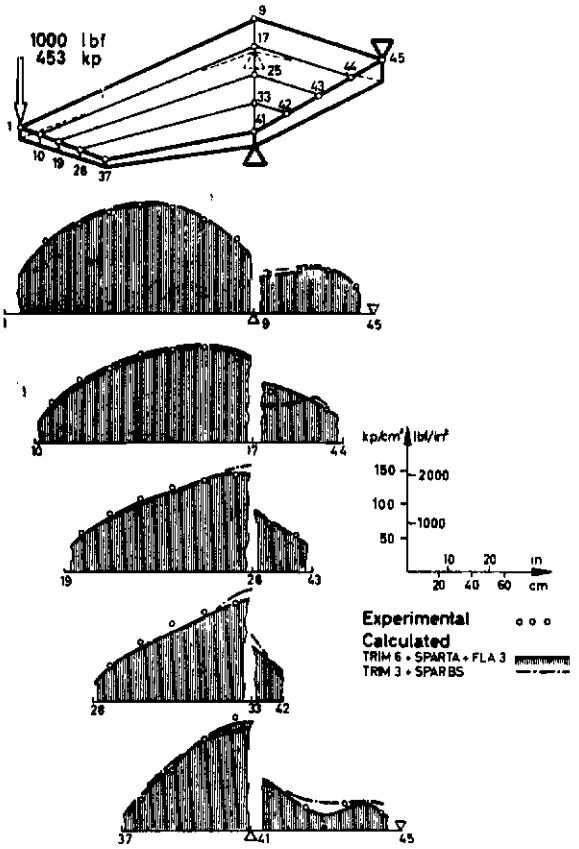

Direct Stresses in Flanges — Loading Case C

Fig.I.34

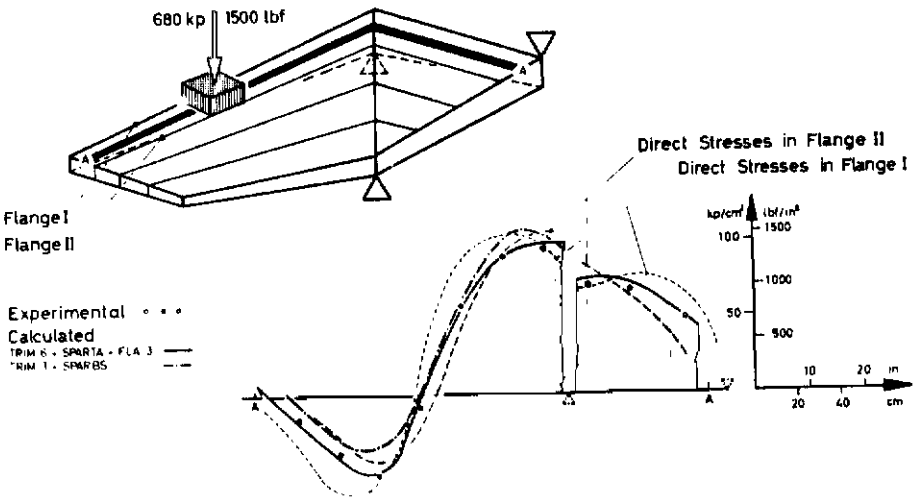

Direct Stresses in Cover — Loading Case A

Fig.I.35

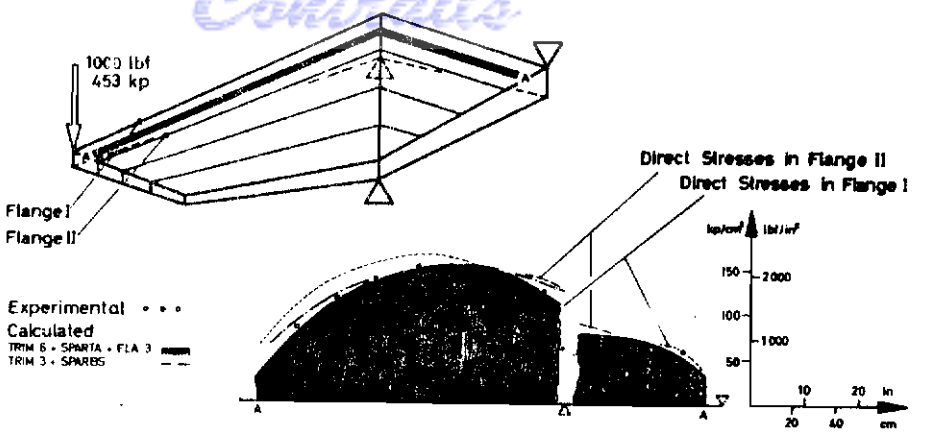

Direct Stresses in Cover — Loading Case C

Fig.I.36

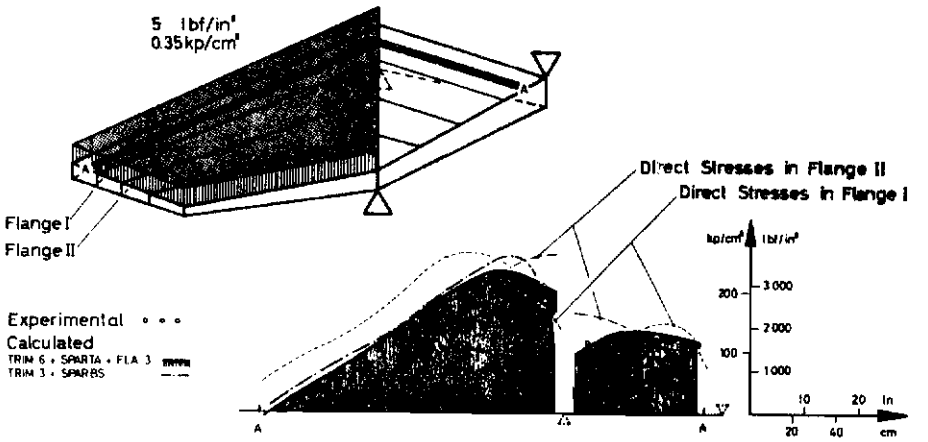

Direct Stresses in Cover — Loading Case D

Fig.I.37

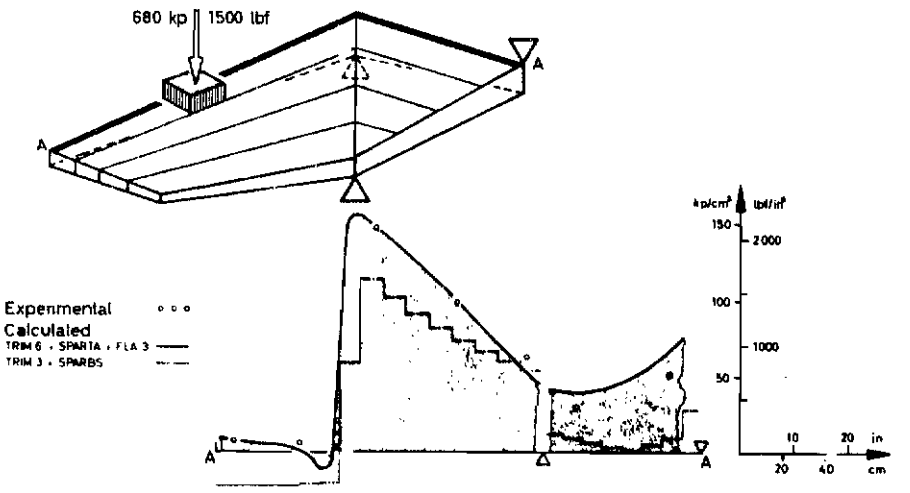

Shear Stresses in Webs — Loading Case A

Fig.I.38

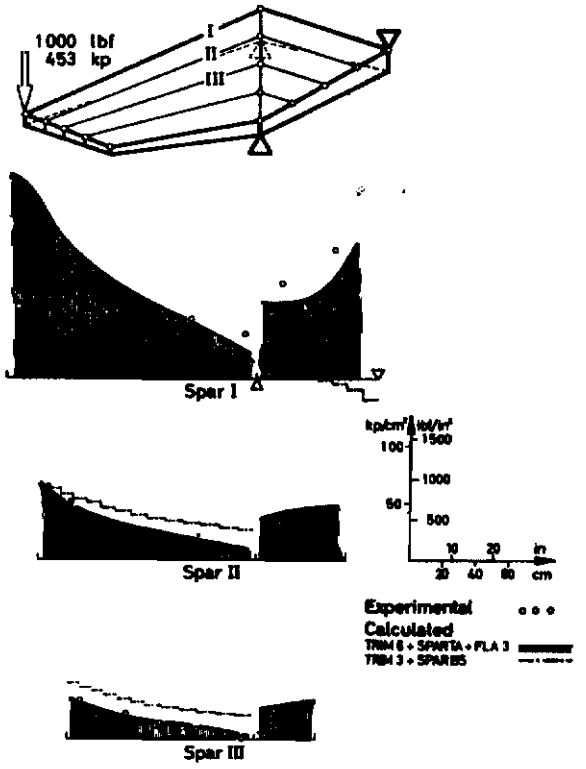

Shear Stresses in Webs Loading Case C

Fig.I.39

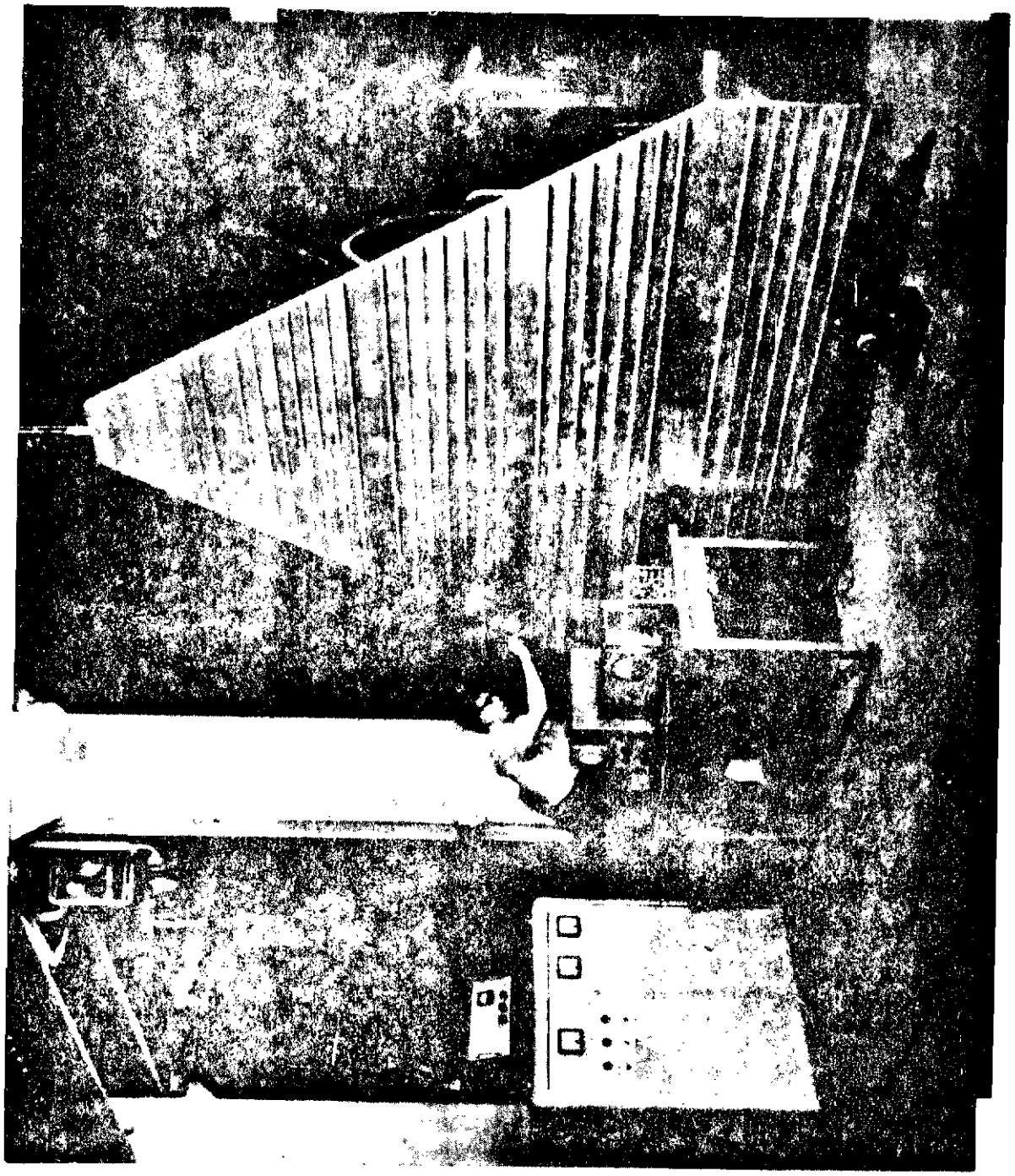

Fig. 1 40

Suspended Delta-Wing

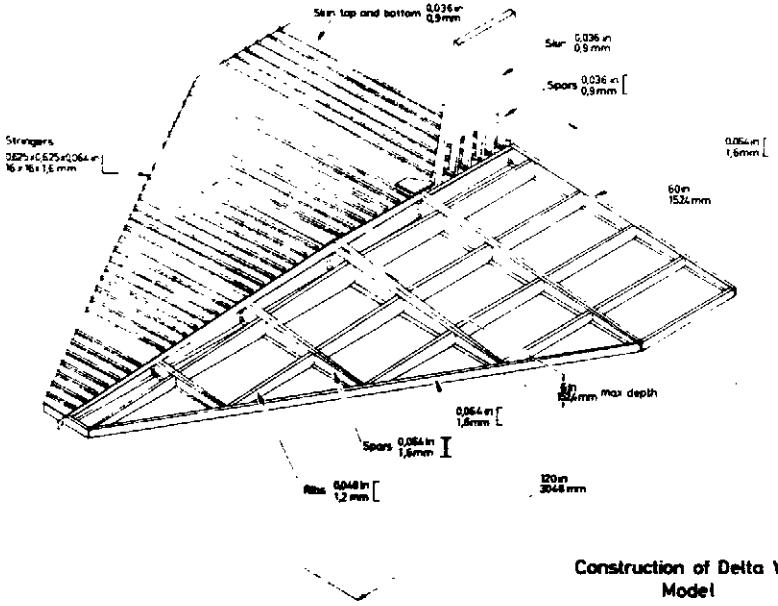

Construction of Delta Wing Model Fig.I.41

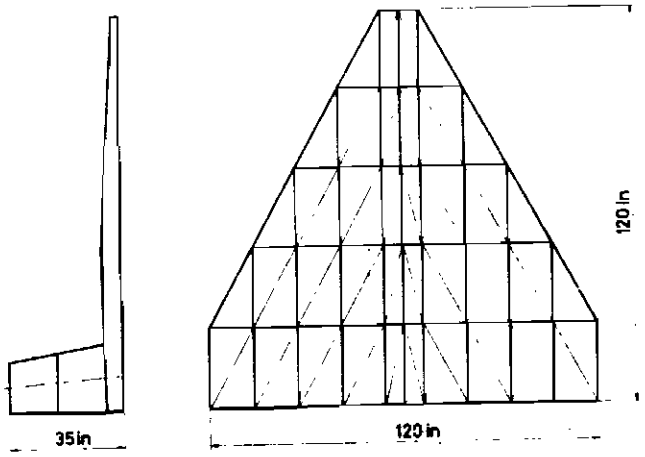

Idealisation of Structure with TRIM 6 + FLA 3 + SPARTA

Fig.I.42

f = (cps) 63.2 Experimental
64.1 Computed

1st Mode

f = (cps) 91.4 Experimental
90.2 Computed

2nd Mode

Symmetrical Modes
Frequencies and Nodal Lines

Fig.I.43

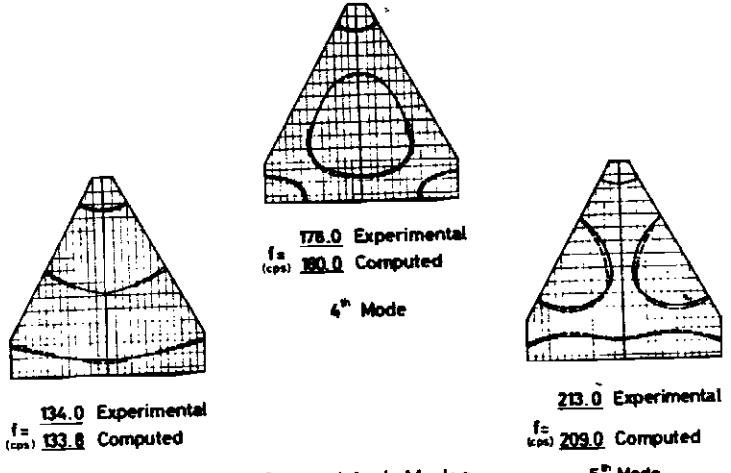

f = (cps) 134.0 Experimental
133.6 Computed

3th Mode

f = (cps) 178.0 Experimental
180.0 Computed

4th Mode

f = (cps) 213.0 Experimental
209.0 Computed

5th Mode

Symmetrical Modes
Frequencies and Nodal Lines

Fig.I.44

II. Plates and Shells

II. 1 Introduction

The present Chapter reviews some of the work on plates and shells carried out at the Institut für Statik und Dynamik der Luft-und Raumfahrtkonstruktionen since 1962. In view of the very extended nature of the theoretical investigations it is only possible to give here a resumé of the main trends together with some characteristic examples. We discuss first the application of oblique co-ordinates to plane stress and plate bending problems using a matrix formulation whereby particular attention is paid to a proper dual presentation of force (stress) and displacement (strain) formulae. This has not been the case in past work and leads, if not treated with due finesse to unnecessarily complex and fortuous expressions. Following these introductory developments, we give an apercu of the theory of bending of parallelogram plates with arbitrary anisotropic behaviour. The method used is based on the natural mode technique, both as far as stiffness and lumped mass are concerned. The derived kinematically consistant lumped mass includes the effect of rotary inertia which allows a neat extension of the theory to take account of in-plane loads and predict the onset of buckling. It is shown that the relevant geometrical stiffnesses[3] are effectively derived from corresponding component matrices for the lumped masses. Subsequently the plane stress problem of a parallelogram element[3] with four nodal points is reviewed on the basis of natural modes and the inclusion of anisotropic behaviour. The theory of bending and stretching of parallelogram elements satisfies all kinematic compatibility conditions; it is here restricted to plates of uniform thickness, but the analysis for varying thickness is available[30]. Having set up the bending and membrane stiffnesses of a single parallelogram element, it is simple to obtain the corresponding stiffness matrix for a shell consisting of an assembly of parallelogram elements.

The second element considered in this Section is the anisotropic triangle under membrane and bending action for which we derive once more a concise expression by the use of natural modes, which show again their superiority. The idealized model in question, which has three nodal points does not satisfy everywhere the kinematic compatibility conditions and hence does not lead automatically to an exact solution as the number of elements is increased. Nevertheless the accuracy of the proposed expressions has been proven to be good for practical purposes. The effect of initial strains as may arise from thermal or plasticity effects is also included. A triangular shell element with six nodal points is discussed in Ref. 30, but cannot be included here for lack of space. It improves markedly the accuracy of our computations.

There follow a number of specific examples to the above theories on the statics and dynamics of parallelogram plates. Good agreement of our finite element method with experimental and analytical results, where available, is demonstrated. Also given are a number of applications of triangular elements which appear to yield, contrary to other opinions, reliable results. This is demonstrated, inter alia, for circular plates and spherical shells. Furthermore we present an application of the theory to a sandwich

type non-circular cylindrical fuselage and compare the results with experimental data. Given the complex nature of the problem and the ignoring of some important influences, like the out of plane bending stiffness of the frames and their torsional stiffness, it is considered that the method leads to an acceptable prediction of stresses and deflexions.

II.2 Transformation Rules for Parallelogram Elements

In what follows we present a succinct account of the transformation rules as applied to co-ordinates, forces and displacements, as well as moments and rotations. We immediately start with the three-dimensional case but assume thereby that the obliquity is restricted to the Ox, Oy axes whereas the Oz axis remains perpendicular to the Oxy plane.

II.2a Basic Transformation Notions

Let us consider two distinct co-ordinate systems $OXYZ$ and $O'xyz$ respectively; Fig. II.1a,b. It is thereby useful to assume that $OXYZ$ is a fixed system determining the geometry of the complete structure and that $O'xyz$ appertains to a particular element. The angles included by OX, OY and $O'x$, $O'y$ are designated by β and α respectively. A point A is located by the vector OA and the co-ordinates V_x, V_Y, V_Z, the components V_x, V_Y of which are derived by the standard construction for the parallelogram of forces. At the same time we can refer the point A to the system $O'xyz$ and define it by the vector $O'A$ with the co-ordinates U_x, U_y, U_z and the vector OO'. We introduce the (3 x 1) vectors

$$V = \{ V_x \quad V_Y \quad V_Z \} \tag{II,1}$$

$$U = \{ U_x \quad U_y \quad U_z \} \tag{II,2}$$

and the transformation matrix

$$\mathcal{L} = \begin{bmatrix} C_{xX} & C_{xY} & C_{xZ} \\ C_{yX} & C_{yY} & C_{yZ} \\ C_{zX} & C_{zY} & C_{zZ} \end{bmatrix} \tag{II,3}$$

where C_{ij} stands for

$$C_{ij} = \cos(i, J) \tag{II,3a}$$

We also require

$$\mathcal{L}_\alpha = \frac{1}{S_\alpha^2} \begin{bmatrix} 1 & -C_\alpha & 0 \\ -C_\alpha & 1 & 0 \\ 0 & 0 & S_\alpha^2 \end{bmatrix}, \quad \mathcal{L}_\beta = \frac{1}{S_\beta^2} \begin{bmatrix} 1 & -C_\beta & 0 \\ -C_\beta & 1 & 0 \\ 0 & 0 & S_\beta^2 \end{bmatrix} \tag{II,4}$$

Here

$$S_\alpha = \sin\alpha \ , \quad C_\alpha = \cos\alpha \ , \quad S_\beta = \sin\beta \ , \quad C_\beta = \cos\beta \tag{II,5}$$

If U_o , $V_{o'}$ are the vectors or column matrices defining the position of the origins O and O' with respect to the systems $O'xyz$ and $OXYZ$ respectively, we find

$$U = U_o + \mathcal{L}_\alpha \mathcal{L} V \tag{II,6}$$

$$V = V_{o'} + \mathcal{L}_\beta \mathcal{L}^t U \tag{II,7}$$

It is furthermore useful to select in addition two cartesian systems $O'\bar{x}\bar{y}\bar{z}$, $O\bar{X}\bar{Y}\bar{Z}$, the $O'\bar{z}$ and $O\bar{Z}$ of which coincide with $O'z$ and OZ respectively; see Figs. II.2a.b. Hence the $O'\bar{x}\bar{y}$ and $O\bar{X}\bar{Y}$ systems are co-planar with $O'xy$ and OXY.

We start with the familiar transformations

$$\bar{U} = \bar{U}_o + \bar{\mathcal{L}}\, \bar{V} \tag{II,8}$$

$$\bar{V} = \bar{V}_{o'} + \bar{\mathcal{L}}^t U \tag{II,9}$$

where the definitions of the (3 x 1) vectors $\bar{U}, \bar{V}$ etc. are evident and

$$\bar{\mathcal{L}} = \begin{bmatrix} C_{\bar{x}X} & C_{\bar{x}Y} & C_{\bar{x}Z} \\ C_{\bar{y}X} & C_{\bar{y}Y} & C_{\bar{y}Z} \\ C_{\bar{z}X} & C_{\bar{z}Y} & C_{\bar{z}Z} \end{bmatrix} \tag{II,10}$$

Note that in the present case $\bar{\mathcal{L}}$ is a unitary matrix

$$\bar{\mathcal{L}}\bar{\mathcal{L}}^t = I_3 \tag{II,10a}$$

Relations (8), (9) follow also from Eqs. (6), (7) for $\alpha = \beta = \frac{\pi}{2}$

We next consider the transformation connecting the oblique and cartesian co-ordinates

$$\bar{U} = \bar{\mathcal{L}}_o U \quad , \quad \bar{V} = \bar{\mathcal{L}}_o V \tag{II,11}$$

Here

$$\bar{\mathcal{L}}_o = \begin{bmatrix} C_{\bar{x}x} & C_{\bar{x}y} & 0 \\ C_{\bar{y}x} & C_{\bar{y}y} & 0 \\ 0 & 0 & 1 \end{bmatrix} \ , \quad \bar{\mathcal{L}}_o = \begin{bmatrix} C_{\bar{x}X} & C_{\bar{x}Y} & 0 \\ C_{\bar{y}X} & C_{\bar{y}Y} & 0 \\ 0 & 0 & 1 \end{bmatrix} \tag{II,12}$$

Using the notation of Figs.II.2 we may also write Eqs.(12) in the form

$$\bar{\mathcal{L}}_o = \begin{bmatrix} \cos\alpha_x & \cos\alpha_y & 0 \\ \sin\alpha_x & \sin\alpha_y & 0 \\ 0 & 0 & 1 \end{bmatrix} , \quad \bar{\mathcal{L}}_o = \begin{bmatrix} \cos\beta_X & \cos\beta_Y & 0 \\ \sin\beta_X & \sin\beta_Y & 0 \\ 0 & 0 & 1 \end{bmatrix} \qquad (II,12a)$$

The inverse relations are

$$U = \mathcal{L}_o \bar{U} \quad , \quad V = \mathcal{L}_o \bar{V} \qquad (II,13)$$

in which

$$\mathcal{L}_o = \bar{\mathcal{L}}_o^{-1} = \frac{1}{S_\alpha} \begin{bmatrix} C_{yy} & -C_{xy} & 0 \\ -C_{yx} & C_{xx} & 0 \\ 0 & 0 & S_\alpha \end{bmatrix} = \frac{1}{S_\alpha} \begin{bmatrix} \sin\alpha_y & -\cos\alpha_y & 0 \\ -\sin\alpha_x & \cos\alpha_x & 0 \\ 0 & 0 & S_\alpha \end{bmatrix} \qquad (II,14)$$

and $\mathcal{L}_o$ is obtained by evident changes of suffixes and angles.

Substitution of Eqs. (11) into Eq.(8) and premultiplying with $\bar{\mathcal{L}}_o^{-1} = \mathcal{L}_o$ we obtain

$$U = U_o + \mathcal{L}_o \bar{\mathcal{L}} \bar{\mathcal{L}}_o V \qquad (II,15)$$

We immediately observe that

$$\bar{\mathcal{L}} \bar{\mathcal{L}}_o = \begin{bmatrix} C_{xX} & C_{xY} & C_{xZ} \\ C_{yX} & C_{yY} & C_{yZ} \\ C_{zX} & C_{zY} & C_{zZ} \end{bmatrix} = \begin{bmatrix} C_{xX} & C_{xY} & C_{xZ} \\ C_{yX} & C_{yY} & C_{yZ} \\ C_{zX} & C_{zY} & C_{zZ} \end{bmatrix} \qquad (II,16)$$

the last relation of which follows from the identity of the $O\bar{z}$ and Oz axis. Next we re-write Eq.(15) in the form,

$$U = U_o + \mathcal{L}_o \bar{\mathcal{L}}_o^{t,-1} \bar{\mathcal{L}}_o^t \bar{\mathcal{L}} \bar{\mathcal{L}}_o V \qquad (II,15a)$$

We easily confirm that

$$\bar{\mathcal{L}}_o^t \bar{\mathcal{L}} \bar{\mathcal{L}}_o = \mathcal{L} \qquad (II,16a)$$

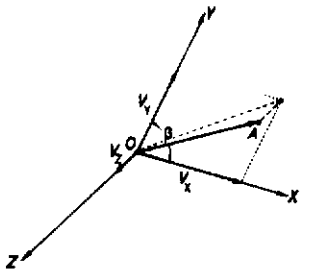

Oblique Basic System
Co-ordinates and Force Components
Fig.II.1a

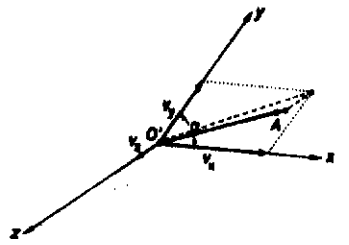

Oblique Local System of Axes
Co-ordinates and Force Components
Fig.II.1b

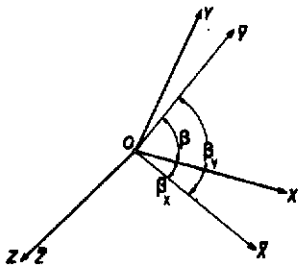

Oblique and Cartesian Basic System of Axes
Fig.II.2a

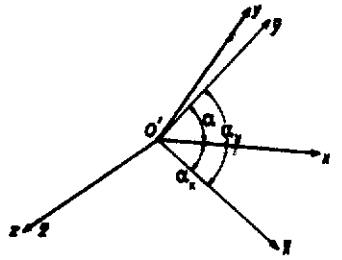

Oblique and Cartesian Local System of Axes
Fig.II.2b

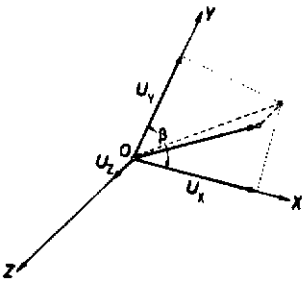

Oblique Basic System of Axes
Displacement Components
Fig.II.3a

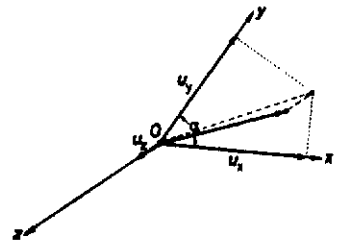

Oblique Local System of Axes
Displacement Components
Fig.II.3b

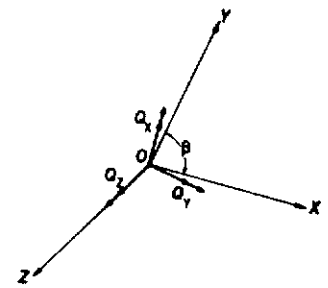

Oblique Basic System of Axes
Moment Components
Fig.II.4a

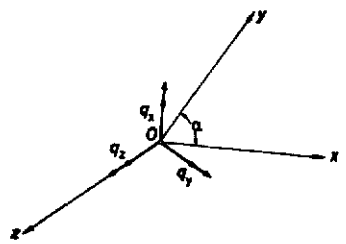

Oblique Local System of Axes
Moment Components
Fig.II.4b

Also

$$\mathcal{L}_o \bar{\mathcal{L}}_o^{t,-1} = \bar{\mathcal{L}}_o^{-1} \bar{\mathcal{L}}_o^{t,-1} = \mathcal{L}_\alpha \qquad (II,16b)$$

Substitution of Eqs.(16a), (16b) in Eq.(15a) yields once more relation (8).

Another important set of transformations applies to vectors or (3 x 1) column matrices whose elements are not defined by the parallelogram rule of resolution but by the projections of the vector onto the oblique axes; Figs.II,3a,b. Since it is subsequently proved that this rule applies to displacement vectors the relative position of the origins O and O' is unimportant and may be ignored. Naturally, for cartesian co-ordinates the two definitions of the components of a vector coincide. To differentiate our new approach from the previous one we use here the symbol u, U etc. to define the column matrices. Thus, we introduce with respect to the oblique axes $OXYZ$ and $Ox_1y_1z_1$

$$U = \{ U_X \quad U_Y \quad U_Z \} \qquad (II,17)$$

$$u = \{ u_{x_1} \quad u_{y_1} \quad u_{z_1} \} \qquad (II,18)$$

At the same time we refer the vectors to the cartesian axes $O\bar{X}\bar{Y}\bar{Z}$, $O\bar{x}_1\bar{y}_1\bar{z}_1$ and have

$$\bar{U} = \{ \bar{U}_{\bar{X}} \quad \bar{U}_{\bar{Y}} \quad \bar{U}_{\bar{Z}} \} \qquad (II,19)$$

$$\bar{u} = \{ \bar{u}_{\bar{x}_1} \quad \bar{u}_{\bar{y}_1} \quad \bar{u}_{\bar{z}_1} \} \qquad (II,20)$$

The transformation rules (8) and (9) take now the form

$$\bar{u} = \bar{\mathcal{L}} \bar{U} \quad , \quad \bar{U} = \bar{\mathcal{L}}^t \bar{u} \qquad (II,21)$$

where $\bar{\mathcal{L}}$ is once more given by Eq.(10). We next confirm without difficulty that

$$u = \bar{\mathcal{L}}_o^t \bar{u} \quad , \quad U = \bar{\mathcal{L}}_o^t \bar{U} \qquad (II,22)$$

which are seen to be dual to Eqs.(11), $\bar{\mathcal{L}}_o$, $\bar{\mathcal{L}}_o$ being specified in Eqs.(12),(12a).

Premultiplying the first of Eqs.(21) by $\bar{\mathcal{L}}_o^t$ and using the inverse of the second of Eqs.(22) we find

$$u = \bar{\mathcal{L}}_o^t \bar{\mathcal{L}} \bar{\mathcal{L}}_o^{t,-1} U = \bar{\mathcal{L}}_o^t \bar{\mathcal{L}} \bar{\mathcal{L}}_o \bar{\mathcal{L}}_o^{-1} \bar{\mathcal{L}}_o^{t,-1} U$$

Noting Eq.(16a) and the relation in the $OXYZ$ system corresponding to Eq.(16b) we find

$$u = \mathcal{L}\,\mathcal{L}_\beta\, U \tag{II,23}$$

Similarly we obtain

$$U = \mathcal{L}^t \mathcal{L}_\alpha\, u \tag{II,24}$$

Note the interesting differences between Eqs.(6),(7) and (23),(24). As we shall see in the following Section the two sets represent dual relations.

II.2b Transformations for Forces and Displacements

All the necessary developments for writing the transformation rules for forces and displacements have already been completed in the preceding Section. This may be immediately confirmed by considering the invariant expression for the work W. To this purpose let $\bar{v}, v, \bar{V}, V$ and $\bar{u}, u, \bar{U}, U$ designate force and displacement vectors in accordance with the specification laid down above.

We easily confirm that

$$\begin{aligned} W &= \tfrac{1}{2}\bar{v}^t\bar{u} = \tfrac{1}{2}\bar{V}^t\mathcal{L}^t\mathcal{L}\bar{U} = \tfrac{1}{2}\bar{V}^t\bar{U} \\ &= \tfrac{1}{2}V\mathcal{L}_o^t\bar{\mathcal{L}}^{t,-1}U = \tfrac{1}{2}V^tU = \tfrac{1}{2}v^tu \end{aligned} \tag{II,25}$$

We collect for subsequent convenience all relevant transformation rules. Thus, in cartesian systems

$$\bar{v} = \bar{\mathcal{L}}\bar{V} \quad , \quad \bar{V} = \bar{\mathcal{L}}^t\bar{v} \tag{II,26}$$

$$\bar{u} = \bar{\mathcal{L}}\bar{U} \quad , \quad \bar{U} = \bar{\mathcal{L}}^t\bar{u} \tag{II,27}$$

Also for the transformation from a cartesian into an oblique system and vice versa we have

$$\bar{V} = \bar{\mathcal{L}}_o V \quad , \quad \bar{v} = \bar{\mathcal{L}}_o^t v \tag{II,28}$$

$$\bar{U} = \mathcal{L}_o^t U \quad , \quad \bar{u} = \mathcal{L}_o^t u \tag{II,29}$$

and

$$V = \mathcal{L}_o\bar{V} \quad , \quad v = \mathcal{L}_o\bar{v} \tag{II,30}$$

$$U = \bar{\mathcal{L}}_o^t\bar{U} \quad , \quad u = \bar{\mathcal{L}}_o^t\bar{u} \tag{II,31}$$

It is sometimes useful to split the transformations (28) to (31) into a two stage operation using in addition to the cartesian system $O\bar{x}\bar{y}\bar{z}$ (or $O\bar{X}\bar{Y}\bar{Z}$) also an intermediate cartesian system $Ox'y'z$ (or $OX'Y'Z$) where Ox' (OX') coincides with the Ox (OX) of the oblique system. The relevant formulae are easily set up; see Section II.2d.
Finally, the relations between two oblique systems of axes are

$$v = \varepsilon_\alpha L V \quad , \quad V = \varepsilon_\beta L^t v \qquad (II,32)$$

$$u = L \varepsilon_\beta U \quad , \quad U = L^t \varepsilon_\alpha u \qquad (II,33)$$

II,2c Transformations for Moments and Rotations

Whilst the transformations for the forces and displacements follow immediately from the relevent expressions of Section II.2a some extension of our theory is necessary to develop the transformations for moments and rotations. In an oblique system $OXYZ$ an applied moment Q is represented by three components Q_X, Q_Y, Q_Z which are defined in such a manner, that the moment vectors Q_X, Q_Y are contained in the OXY plane and are perpendicular to the OY and OX axes respectively, and that Q_Z is directed along the OZ axis. This allows us to express Q_X, Q_Y, Q_Z in terms of forces and co-ordinates by the same formulae as if it were a cartesian system. Thus, for a force $V = \{V_X\ V_Y\ V_Z\}$ acting at the point $\{XYZ\}$ the oblique components Q_X, Q_Y, Q_Z become

$$Q_X = YV_Z - ZV_Y \quad , \quad Q_Y = ZV_X - XV_Z \quad , \quad Q_Z = XV_Y - YV_X \qquad (II,34)$$

Note that whilst $Z = \bar{Z}$ and $V_Z = V_{\bar{Z}}$, Q_Z is different from $Q_{\bar{Z}}$. The definition of a rotation P in an oblique co-ordinate system $OXYZ$ which is dual to that of Q, fixes the components P_X, P_Y, P_Z as angles of rotation measured in the OYZ, OZX, OXY planes respectively. Our exposé on oblique moments and rotations is, of course, equally applicable to the alternative oblique co-ordinate system $Ox\bar{y}z$; see Figs. II 4a, b, 5a, b.

We start with the evident cartesian transformations

$$\bar{q} = \bar{L}\bar{Q} \quad , \quad \bar{Q} = \bar{L}^t \bar{q} \qquad (II,35)$$

and

$$\bar{p} = \bar{L}\bar{P} \quad , \quad \bar{P} = \bar{L}^t \bar{p} \qquad (II,36)$$

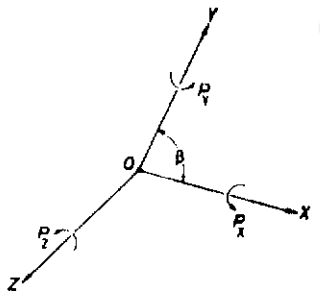

Oblique Basic System of Axes
Rotation Components
Fig.II.5a

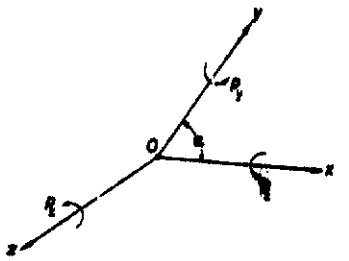

Oblique Local System of Axes
Rotation Components
Fig.II.5b

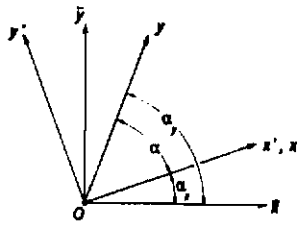

Oblique and Cartesian System of Axes
Fig.II.6

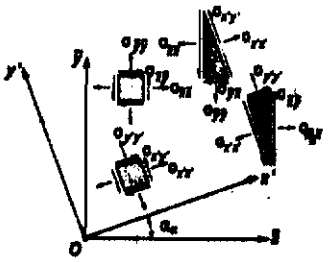

Cartesian Transformation of Stresses
Fig.II.7

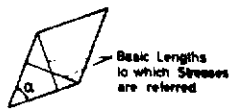

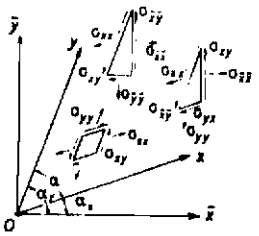

Oblique Transformation of Stresses
Fig.II.8

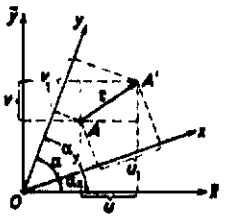

Cartesian and Oblique Components of Displacements
Fig.II.9

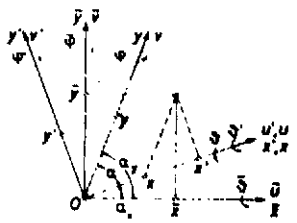

Oblique and Cartesian Rotation
Fig.II.10

which are identical to the corresponding relations (26), (27) for forces and displacements. We now introduce the oblique systems $Oxyz$, $OXYZ$ and obtain for the moments in accordance with our above aperçu the relations

$$Q = \frac{1}{s_\beta} \bar{\mathcal{L}}_o^t \bar{Q} \quad , \quad q = \frac{1}{s_\alpha} \bar{\mathcal{L}}_o^t \bar{q} \tag{II,37}$$

and

$$\bar{Q} = s_\beta \mathcal{L}_o^t Q \quad , \quad \bar{q} = s_\alpha \mathcal{L}_o^t q \tag{II,38}$$

The corresponding expressions for the rotations are

$$P = s_\beta \mathcal{L}_o \bar{P} \quad , \quad p = s_\alpha \mathcal{L}_o \bar{p} \tag{II,39}$$

and

$$\bar{P} = \frac{1}{s_\beta} \bar{\mathcal{L}}_o P \quad , \quad \bar{p} = \frac{1}{s_\alpha} \bar{\mathcal{L}}_o p \tag{II,40}$$

We confirm from the relevant work expression

$$\frac{1}{2} \bar{Q}^t \bar{P} = \frac{1}{2} \bar{q}^t \bar{p} = \frac{1}{2} Q^t P = \frac{1}{2} q^t p \tag{II,41}$$

that the vectors Q , P (and q, p) are the correct dual expressions for the moments and rotations in an oblique system. The remark made subsequent to Eqs.(28) to (30) applies here again.

We finally seek to transform the moments and rotations from one oblique system $O\,xyz$ into another $OXYZ$ and vice versa. We start with the relations for the moments. Premultiplying the first of Eqs.(35) with $\frac{1}{s_\alpha} \bar{\mathcal{L}}_o^t$ and using the inverse of the first of Eqs.(37) we find

$$q = \frac{s_\beta}{s_\alpha} \bar{\mathcal{L}}_o^t \bar{\mathcal{L}} \bar{\mathcal{L}}_o^{t,-1} Q = \frac{s_\beta}{s_\alpha} \mathcal{L} \mathcal{L}_\beta Q \tag{II,42}$$

Similarly

$$Q = \frac{s_\alpha}{s_\beta} \mathcal{L}^t \mathcal{L}_\alpha q \tag{II,43}$$

For the rotations we proceed similarly and find

$$p = \frac{s_\alpha}{s_\beta} \mathcal{L}_\alpha \mathcal{L} P \tag{II,44}$$

and

$$P = \frac{s_\beta}{s_\alpha} \mathcal{L}_\beta \mathcal{L}^t p \tag{II,45}$$

It may be preferable for the unification of the theory to specify a slightly different vectorial representation for the moments and rotations in the oblique system. Thus, if the moments and rotations are given by

$$q' = s_\alpha q \quad , \quad Q' = s_\beta Q \tag{II,46}$$

and

$$p' = \frac{1}{s_\alpha} p \quad , \quad P' = \frac{1}{s_\beta} P \tag{II,47}$$

where dashes designate the new definition of the vectors, Eqs.(44) to (45) take the form

$$q' = \mathcal{L} \mathcal{L}_\beta Q' \quad , \quad Q' = \mathcal{L}^t \mathcal{L}_\alpha q' \tag{II,48}$$

and

$$p' = \mathcal{L}_\alpha \mathcal{L} P' \quad , \quad P' = \mathcal{L}_\beta \mathcal{L}^t p' \tag{II,49}$$

We now observe the interesting result that the moments (rotations) transform in an oblique system as the displacements (forces); c.f. Eqs. (32),(33). We do not pursue the issue in this paper.

II.2d Transformations for Stresses and Strains, Elastic Properties of the Material

We start with the cartesian definition of stresses and strains and revert subsequently to the more useful oblique specification. Let us consider initially two cartesian systems $O\bar{x}\bar{y}$ and $Ox'y'$ as shown in Fig.II.6, and assume that the stresses and strains are known with respect to $O\bar{x}\bar{y}$. Following Section I and Refs.12, 13 we introduce as stress and strain vectors the expressions

$$\bar{\sigma} = \{ \sigma_{\bar{x}\bar{x}} \quad \sigma_{\bar{y}\bar{y}} \quad \sqrt{2}\, \sigma_{\bar{x}\bar{y}} \} \tag{II,50}$$

$$\bar{\varepsilon} = \{ \varepsilon_{\bar{x}\bar{x}} \quad \varepsilon_{\bar{y}\bar{y}} \quad \frac{1}{\sqrt{2}} \varepsilon_{\bar{x}\bar{y}} \} \tag{II,51}$$

and

$$\sigma' = \{ \sigma_{x'x'} \quad \sigma_{y'y'} \quad \sqrt{2}\, \sigma_{x'y'} \} \tag{II,52}$$

$$\varepsilon' = \{ \varepsilon_{x'x'} \quad \varepsilon_{y'y'} \quad \frac{1}{\sqrt{2}} \varepsilon_{x'y'} \} \tag{II,53}$$

Following Eq.(56) of Ref.13, the two-dimensional transformation rules connecting σ' with $\bar{\sigma}$ and $\bar{\epsilon}$ with ϵ' are given (see Fig.II,7) by

$$\sigma' = B\,\bar{\sigma} \qquad \text{and} \qquad \bar{\epsilon} = B^t \epsilon' \tag{II,54}$$

Since B is a unitary matrix $(B^t B = I_3)$ we also have the dual relations

$$\bar{\sigma} = B^t \sigma' \qquad \text{and} \qquad \epsilon' = B\,\bar{\epsilon} \tag{II,54a}$$

In accordance with Ref.13, B is given (see also Fig.II.4) by

$$B = \begin{bmatrix} c_{\alpha x}^2 & s_{\alpha x}^2 & \sqrt{2}\, s_{\alpha x} c_{\alpha x} \\ s_{\alpha x}^2 & c_{\alpha x}^2 & -\sqrt{2}\, s_{\alpha x} c_{\alpha x} \\ -\sqrt{2}\, s_{\alpha x} c_{\alpha x} & \sqrt{2}\, s_{\alpha x} c_{\alpha x} & (c_{\alpha x}^2 - s_{\alpha x}^2) \end{bmatrix} \tag{II,55}$$

where

$$s_{\alpha x} = \sin \alpha_x \quad , \quad c_{\alpha x} = \cos \alpha_x \tag{II,55a}$$

We next demonstrate the application of the transformation rules (54),(54a) to the determination of the elasticity modulus E' associated with the vectors σ', ϵ' viz.

$$\sigma' = E' \epsilon' \tag{II,56}$$

Assume that we know the, in general, anisotropic modulus $\bar{E}$ for the stresses and strains $\bar{\sigma}$ and $\bar{\epsilon}$,

$$\bar{\sigma} = \bar{E}\,\bar{\epsilon} \tag{II,56a}$$

Premultiplication of Eq.(56a) with B and substitution of the second of Eqs.(54) yields in conjunction with the first of Eqs.(54),

$$E' = B \bar{E} B^t \qquad \text{or} \qquad E'^{-1} = B^t E^{-1} B. \tag{II,57}$$

The correctness of our above transformations may also be confirmed by the invariant strain energy expression per unit area and thickness of plate

$$U_i = \tfrac{1}{2}\, \bar{\sigma}^t \bar{\epsilon} = \tfrac{1}{2}\, \sigma'^t \epsilon' \tag{II,58}$$

We now take up the more interesting problem of oblique stresses and strains. Contrary to the usual designations of stresses we adopt here as their definition the corresponding resultant forces per unit cross-sectional area, measured perpendicular to the direction of the so-called direct stresses or forces. (Fig.II.8). The stress vector σ in the oblique system is then given by

$$\sigma = \{ \sigma_{xx} \quad \sigma_{yy} \quad \sqrt{2}\ \sigma_{xy} \} \qquad (II,59)$$

The oblique strains are usually expressed as derivatives of the components u_1, v_1 of the displacements as laid down in Section V.2b. We have

$$\varepsilon = \{ \varepsilon_{xx} \quad \varepsilon_{yy} \quad \frac{1}{\sqrt{2}} \varepsilon_{xy} \} \qquad (II,60)$$

where

$$\varepsilon_{xx} = \frac{\partial u_1}{\partial x} \ , \ \varepsilon_{yy} = \frac{\partial v_1}{\partial y} \ , \ \varepsilon_{xy} = \left\{ \frac{\partial u_1}{\partial y} + \frac{\partial v_1}{\partial x} \right\} \qquad (II,61)$$

and u_1, v_1 are given (see Eqs.(31) and Fig.II.9)

$$\begin{bmatrix} u_1 \\ v_1 \end{bmatrix} = \begin{bmatrix} c_{\alpha x} & s_{\alpha x} \\ c_{\alpha y} & s_{\alpha y} \end{bmatrix} \begin{bmatrix} \bar{u} \\ \bar{v} \end{bmatrix} = \begin{bmatrix} 1 & 0 \\ c_\alpha & s_\alpha \end{bmatrix} \begin{bmatrix} c_{\alpha x} & s_{\alpha x} \\ -s_{\alpha x} & c_{\alpha x} \end{bmatrix} \begin{bmatrix} \bar{u} \\ \bar{v} \end{bmatrix} \qquad (II,62)$$

The two-stage transformation refers to an initial rotation of the cartesian system $O\bar{x}\bar{y}$ (displacements $\bar{u}, \bar{v}$) into the position $Ox'y'$ (displacements u', v') and subsequent change into the oblique system Oxy (displacements u_1, v_1).
Application of simple statics leads to the transformations

$$\sigma = \mathfrak{A}^t \bar{\sigma} \qquad \text{or} \qquad \bar{\sigma} = \mathfrak{A}^{t,-1} \sigma = \mathfrak{B} \sigma \qquad (II,63)$$

where

$$\mathfrak{A}^t = \frac{1}{s_\alpha^2} \begin{bmatrix} s_{\alpha y}^2 & c_{\alpha y}^2 & -\sqrt{2}\, s_{\alpha y} c_{\alpha y} \\ s_{\alpha x}^2 & c_{\alpha x}^2 & -\sqrt{2}\, s_{\alpha x} c_{\alpha x} \\ -\sqrt{2}\, s_{\alpha x} s_{\alpha y} & -\sqrt{2}\, c_{\alpha x} c_{\alpha y} & (s_{\alpha x} c_{\alpha y} + s_{\alpha y} c_{\alpha x}) \end{bmatrix} \qquad (II,64)$$

and

$$\mathfrak{B} = \begin{bmatrix} c_{\alpha x}^2 & c_{\alpha y}^2 & \sqrt{2}\, c_{\alpha x} c_{\alpha y} \\ s_{\alpha x}^2 & s_{\alpha y}^2 & \sqrt{2}\, s_{\alpha x} s_{\alpha y} \\ \sqrt{2}\, s_{\alpha x} c_{\alpha x} & \sqrt{2}\, s_{\alpha y} c_{\alpha y} & (s_{\alpha x} c_{\alpha y} + s_{\alpha y} c_{\alpha x}) \end{bmatrix} \qquad (II,65)$$

also

$$s_{\alpha x} = \sin\alpha_x \ , \ s_{\alpha y} = \sin\alpha_y \ , \ c_{\alpha x} = \cos\alpha_x \ , \ c_{\alpha y} = \cos\alpha_y \ . \qquad (11,55b)$$

Before proceeding to the corresponding strain transformations we observe that the expression (63) could, of course, also be built up in two steps, in which one first transforms from the basic cartesian system $O\bar{x}\bar{y}$ to the rotated one $Ox'y'$ and thus completes the transformation for the oblique system Oxy ; see also our statement on force transformation in Section II.2C. We easily confirm that the matrices α^t may be written as the respective products

$$\alpha^t = AB \ , \ \beta = \alpha^{t,-1} = B^t A^{-1} = B^t C^t \qquad (11,66)$$

where

$$A = \frac{1}{s_\alpha^2}\begin{bmatrix} s_\alpha^4 & c_\alpha^2 & -\sqrt{2}\, s_\alpha c_\alpha \\ 0 & 1 & 0 \\ 0 & -\sqrt{2}\, c_\alpha & s_\alpha \end{bmatrix} \qquad (11,67)$$

and

$$C^t = \begin{bmatrix} 1 & c_\alpha^2 & \sqrt{2}\, c_\alpha \\ 0 & s_\alpha^2 & 0 \\ 0 & \sqrt{2}\, s_\alpha c_\alpha & s_\alpha \end{bmatrix} \qquad (11,68)$$

The transformation matrix B is given in Eq.(55).

To obtain the strain transformation rules we first write,

$$\varepsilon_{xx} = \frac{\partial u_1}{\partial x} = \frac{\partial u_1}{\partial \bar{x}}\frac{\partial \bar{x}}{\partial x} + \frac{\partial u_1}{\partial \bar{y}}\frac{\partial \bar{y}}{\partial x}$$

$$\varepsilon_{yy} = \frac{\partial v_1}{\partial y} = \frac{\partial v_1}{\partial \bar{x}}\frac{\partial \bar{x}}{\partial y} + \frac{\partial v_1}{\partial \bar{y}}\frac{\partial \bar{y}}{\partial y} \qquad (11,69)$$

$$\varepsilon_{xy} = \frac{\partial u_1}{\partial y} + \frac{\partial v_1}{\partial x} = \frac{\partial u_1}{\partial \bar{x}}\frac{\partial \bar{x}}{\partial y} + \frac{\partial u_1}{\partial \bar{y}}\frac{\partial \bar{y}}{\partial y} + \frac{\partial v_1}{\partial \bar{x}}\frac{\partial \bar{x}}{\partial x} + \frac{\partial v_1}{\partial \bar{y}}\frac{\partial \bar{y}}{\partial x}$$

The detailed operations in Eq.(69) gain in clarity, if we remember that the co-ordinate derivations contained therein essentially define the transformation of rotation. Thus, if ϑ, φ and $\bar{\vartheta}, \bar{\varphi}$ denote rotations about the cartesian axes $O\bar{x}\bar{y}$ and the oblique Oxy we have, using Eqs.(14), (39),

$$\begin{bmatrix} \vartheta \\ \varphi \end{bmatrix} = \begin{bmatrix} S_{\alpha y} & -C_{\alpha y} \\ -S_{\alpha x} & C_{\alpha x} \end{bmatrix} \begin{bmatrix} \bar{\vartheta} \\ \bar{\varphi} \end{bmatrix} = \begin{bmatrix} S_{\alpha} & -C_{\alpha} \\ 0 & 1 \end{bmatrix} \begin{bmatrix} C_{\alpha x} & S_{\alpha x} \\ -S_{\alpha x} & C_{\alpha x} \end{bmatrix} \begin{bmatrix} \bar{\vartheta} \\ \bar{\varphi} \end{bmatrix} \qquad (II,70)$$

where the second or product transformation refers again to a two-stage operation, first from the cartesian system $O\bar{x}\bar{y}$ (rotations $\bar{\vartheta}, \bar{\varphi}$) into the cartesian system $Ox'y'$ (rotations ϑ', φ'), and then the oblique system Oxy (rotations ϑ, φ), see also Fig.II.10. At the same time we may write

$$\begin{bmatrix} \vartheta \\ \varphi \end{bmatrix} = \begin{bmatrix} \frac{\partial \bar{y}}{\partial y} & -\frac{\partial \bar{x}}{\partial y} \\ -\frac{\partial \bar{y}}{\partial x} & \frac{\partial \bar{x}}{\partial x} \end{bmatrix} \begin{bmatrix} \bar{\vartheta} \\ \bar{\varphi} \end{bmatrix} \qquad (II,71)$$

which, applying the first of Eqs.(11), is easily seen to coincide with Eq.(70).

Substitution of the relevant expressions from Eqs.(69),(70),(71) into Eq.(69) leads to the required strain transformation rules

$$\bar{\varepsilon} = \alpha \varepsilon \qquad \text{and} \qquad \varepsilon = \alpha^{-1} \bar{\varepsilon} = \mathcal{B}^t \bar{\varepsilon} \qquad (II,72)$$

which are seen to be dual to Eqs.(63). We also confirm that

$$\alpha = B^t A^t \qquad \text{and} \qquad \mathcal{B}^t = CB \qquad (II,66a)$$

Let us now express the elasticity relation in the oblique system in the usual form

$$\sigma = E\varepsilon \qquad (II,73)$$

Using an argument similar to that leading to Eq.(57) we find

$$E = \alpha^t \bar{E} \alpha \qquad \text{or} \qquad E^{-1} = \mathcal{B}^t \bar{E}^{-1} \mathcal{B}. \qquad (II,74)$$

Following Eqs.(1,98,99) we write E in the form

$$E = E'\nu = E' \begin{bmatrix} \nu_{11} & \nu_{12} & \sqrt{2}\,\nu_{13} \\ \nu_{21} & \nu_{22} & \sqrt{2}\,\nu_{23} \\ \sqrt{2}\,\nu_{31} & \sqrt{2}\,\nu_{32} & 2\,\nu_{33} \end{bmatrix} \qquad (II,75)$$

where the coefficients ν_{ij} are non-dimensional and E' a suitable measure of the modulus.

Consider, for example, the specific case of an isotropic material. Applying Eqs.(66a) and remembering that as a result of the isotropy it suffices to apply A^t and C in place of α and β^t we obtain

$$E = \frac{E}{(1-\nu^2)} \frac{1}{S_\alpha^4} \begin{bmatrix} 1 & c_\alpha^2 + \nu s_\alpha^2 & -\sqrt{2}\, c_\alpha \\ c_\alpha^2 + \nu s_\alpha^2 & 1 & -\sqrt{2}\, c_\alpha \\ -\sqrt{2}\, c_\alpha & -\sqrt{2}\, c_\alpha & (1 + c_\alpha^2 - \nu s_\alpha^2) \end{bmatrix} \qquad (11,76)$$

and

$$E^{-1} = \frac{1}{E} \begin{bmatrix} 1 & c_\alpha^2 - \nu s_\alpha^2 & \sqrt{2}\, c_\alpha \\ c_\alpha^2 - \nu s_\alpha^2 & 1 & \sqrt{2}\, c_\alpha \\ \sqrt{2}\, c_\alpha & \sqrt{2}\, c_\alpha & (1 + c_\alpha^2 + \nu s_\alpha^2) \end{bmatrix} \qquad (11,77)$$

where ν is Poisson's Ratio.

We conclude this Section by establishing the strain energy expression U_{ie} per unit area in oblique stress and strain expressions. Using the cartesian formulae and Eqs.(62) and (62a) we confirm

$$U_{ie} = \frac{1}{2} \bar{\sigma}^t \bar{\varepsilon} = \frac{1}{2} \sigma^t \beta^t \alpha \varepsilon = \frac{1}{2} \sigma^t \varepsilon \qquad (11,78)$$

which proves that the selected stress and strain expressions σ and ε are correctly paired; this is in contrast to the usual definition in the relevant technical literature[20]. The total strain energy per unit thickness of an oblique panel is found to be

$$U_i = \int U_{ie}\, dA = S_\alpha \iint \sigma^t \varepsilon\, dx\, dy \qquad (11,78a)$$

Finally, for a plate under bending and stretching, the unit displacement theorem, governing the Matrix Displacement method, leads to the following formula for a typical stiffness coefficient

$$1 \cdot k_{ij} = S_\alpha \int \varepsilon_i^t \sigma_j\, dV = S_\alpha \int \varepsilon_j^t \sigma_i\, dV \qquad (11,79)$$

where $\varepsilon_j\ (\varepsilon_i)$ are the strain distributions due to unit (generalized) displacements $i\ (j)$ and $\sigma_j\ (\sigma_i)$ the associated stresses. In the following Sections we apply a matrix generalization of Eq.(79).

II.3 Introductory Notions on the Bending of Oblique Plates

In this Section we introduce the kinematic modes of a parallelogram element in bending. These ensure, as long as the obliquity is not changed, the satisfaction of the kinematic compatibility conditions throughout the plate. The chosen mathematical expressions equally apply to parallelogram and rectangular elements as long as they are used in the corresponding natural co-ordinate system, i.e. oblique and cartesian respectively. The adopted model has four nodal points at the corners of each element.

To start with we consider a few points on the adopted notation. The reader's attention is, in particular, drawn to the non-dimensional specification of the co-ordinates, (see Fig.I.8 and Tables I.2 and II.1).

$$\xi = 2x/a \quad , \quad \eta = 2y/b \tag{II,80}$$

We also use a non-dimensional measure of the deflexion

$$\omega = w/\ell \tag{II,81}$$

where ℓ is a suitable length. Since in accordance with our Introduction in II.1 we ignore transverse shear deformations the bending behaviour of the plate is described in addition to ω by the slopes or rotations

$$\theta = \frac{\partial w}{\partial y} = 2\mu \frac{\partial \omega}{\partial \eta} \quad , \quad \phi = -\frac{\partial w}{\partial x} = -2\lambda \frac{\partial \omega}{\partial \xi} \tag{II,82}$$

where

$$\lambda = \ell/a \quad , \quad \mu = \ell/b \tag{II,83}$$

Naturally, for a skew plate, expressions (82) are to be understood in the oblique sense laid down in II.2c. The reader should note that the signs of the rotations (82) are those associated with a right-handed co-ordinate system; hence the 'minus' for ϕ .

We now define the state of deformation of the plate at any point x, y or ξ, η by the (3 x 1) vector

$$\mathbf{w} = \{ \omega \quad \theta \quad \phi \} \qquad (3 \times 1) \tag{II,84}$$

As discussed in Chapter I the standard Matrix Displacement method uniquely describes the deformed shape of an element in terms of its nodal displacements. Hence in the present case the corresponding determining vector is the (12 x 1) matrix

$$\mathbf{\rho} = \{ \rho_1 \quad \rho_2 \quad \rho_3 \quad \rho_4 \} \tag{II,85}$$

in which

$$\rho_i = \{ \omega_i \quad \theta_i \quad \phi_i \} \qquad (3 \times 1) \tag{II,85a}$$

reproduces the deflexion and rotations at a typical nodal point L . Eq.(85) shows that the kinematic behaviour of a plate under bending with four nodal points can be described by a function containing $4 \times 3 = 12$ constants. Alternatively we may say that 12 component modes can be found for any given vector ρ .

Following our introduction of natural modes in Ref.3 and the relevant exposé in Section I, we solve here the problem using this more rational and elegant approach. Correspondingly we consider the kinematic state as a combination of three rigid body modes ρ_o and nine pure straining modes ρ_N . The alternative formulation of the state of deformation is hence, as in Eq.(I,2)

$$\rho' = \{\rho_N \quad \rho_o\} \tag{II,86}$$

The choice of the straining modes is to a certain extent arbitrary as long as they are linearly independent and ensure kinematic compatibility. We select as unit ρ_N the non-dimensional polynomials reproduced in Fig.II.11. It is now possible to write the vector w as

$$w = [\omega_N \quad \omega_o]\{\rho_N \quad \rho_o\} = \omega_e \rho' \tag{II,87}$$

where the (12 x 12) matrix ω_e is reproduced in ful in Table II.1 and is derived from the adopted modes in Fig.II.11. The first(12 x 1)row of ω_e , which reproduces the deflexions ω_N and ω_o of the nine straining and three rigid body modes, is denoted by ω_e . Once ρ' is known the deformation is fixed by Eq.(87).

It is next necessary to establish the matrix transformations relating the vectors ρ' and ρ . To this purpose we use the theory as set out in Section I. Thus, applying Eqs.(I,6,7) we have

$$\rho = A_e \rho' = [A_N \quad A_o]\rho' \tag{I,88}$$

and the inverse relation

$$\rho' = A_e^{-1}\rho = a_e \rho = \begin{bmatrix} a_N \\ a_o \end{bmatrix}\rho \tag{II,89}$$

In the present case the dimensions of a_N and a_o are (9 x 12) and (3 x 12), whilst those of A_N and A_o are (12 x 9) and (12 x 3), It is relatively simple to set up the required a_e directly, but it may be preferable to proceed here by inversion from A_e , which may be written down by inspection; see Table II.2. The matrix a_e is reproduced in Tables II.3,3a.Eq.(89) may be split into the two matrix expressions for ρ_N and ρ_o , as in Eqs. (I,5,6a).

Note that all above derivations assume that w, ρ', ρ are referred to the oblique co-ordinate system $O x y z$. If the solution of a particular problem is to be based on a cartesian reference system $O x' y' z$, we may derive the relevant a_e either by an additional transformation (which is preferable from the programming point of view) or through an ab initio formation of a_e for the relevant co-ordinate system. For example, Table II.4 reproduces the a_e for the cartesian system $O x' y' z$ The alternative method of a subsequent transformation is easily established from Eq.40, in Section II.2c.

If we denote for the time being the a_e for the oblique and cartesian systems with a_{es} and a_{ec} respectively, we find

$$a_{ec} = a_{es} \mathcal{F} \tag{II,90}$$

where

$$\mathcal{F} = \begin{bmatrix} I_4 & O_4 & O_4 \\ O_4 & sI_4 & -cI_4 \\ O_4 & O_4 & I_4 \end{bmatrix} \tag{II,91}$$

which follows also by direct inspection of a_{ec}.

Having obtained the relation (88) we can immediately express W in terms of ρ via

$$W = \varpi_e a_e \rho - \Pi_e \rho \tag{II,92}$$

where

$$\Pi_e = \varpi_e a_e \tag{II,93}$$

We complete this Section by referring briefly to the corresponding developments for the associated generalized forces R, P' and P.

Following Eqs.(I,9,10) of Chapter I the force vectors P' and P associated with ρ' and ρ are put in the form

$$P' = \left\{ P_N \quad P_o \right\} \tag{II,94}$$

and

$$P = \left\{ P_1 \quad P_2 \quad P_3 \quad P_4 \right\} \tag{II,95}$$

Here P_N is a (9 x 1) vector of self-equilibrating forces and P_o a (3 x 1) vector of external resultants acting over the body or surface of the element. P_o itself is written

$$P_o = \left\{ P_{oz}\, \ell \quad M_{ox} \quad M_{oy} \right\} \tag{II,96}$$

where P_{oz} is the total external load in the z -direction and M_{ox}, M_{oy} the (oblique) external moments about the O_x, O_y axes respectively. The component vectors P_i of (95) are clearly of the form

$$P_i = \left\{ P_z\, \ell \quad M_x \quad M_y \right\}_i \tag{II,97}$$

$a_e = \frac{a_n}{a_0}$ $\quad l$ = Reference Length; $\lambda = l/a$, $\mu = l/b$; $\xi = 2x/a$, $\eta = 2y/b$, $\omega = w/l$

$\omega = w/l$ $\quad \delta = 2\lambda \frac{\partial \omega}{\partial \xi}$ $\quad \varphi = -2\lambda \frac{\partial \omega}{\partial \xi}$

$$a^1_n = \begin{bmatrix}
\frac{1}{16\lambda}(1-\xi^2) & 0 & \frac{1}{4}\xi & 1\\
\frac{1}{16\mu}(1-\eta^2) & -\frac{1}{4}\eta & 0 & 2\\
-\frac{1}{16\lambda}\xi(1-\xi^2) & 0 & \frac{1}{8}(1-3\xi^2) & 3\\
-\frac{1}{16\mu}\eta(1-\eta^2) & -\frac{1}{8}(1-3\eta^2) & 0 & 4\\
-\frac{1}{32\lambda}\eta(1-\xi^2)(3-\eta^2) & -\frac{3\mu}{16\lambda}(1-\xi^2)(1-\eta^2) & -\frac{1}{8}\xi\eta(3-\eta^2) & 5 > p_n\\
-\frac{1}{32\mu}\xi(3-\xi^2)(1-\eta^2) & \frac{1}{8}\xi\eta(3-\xi^2) & \frac{3\lambda}{16\mu}(1-\xi^2)(1-\eta^2) & 6\\
\frac{1}{32\lambda}\xi\eta(1-\xi^2)(3-\eta^2) & \frac{3\mu}{16\lambda}\xi(1-\xi^2)(1-\eta^2) & -\frac{1}{16}\eta(1-3\xi^2)(3-\eta^2) & 7\\
-\frac{1}{32\mu}\xi\eta(3-\xi^2)(1-\eta^2) & \frac{1}{16}\xi(3-\xi^2)(1-3\eta^2) & -\frac{3\lambda}{16\mu}\eta(1-\xi^2)(1-\eta^2) & 8\\
\frac{1}{4}\xi\eta & \frac{\mu}{2}\xi & -\frac{\lambda}{2}\eta & 9
\end{bmatrix}$$

$$a^1_0 = \begin{bmatrix}
\frac{1}{8} & 0 & 0 & 1'\\
-\frac{1}{8\lambda}\xi & 0 & \frac{1}{4} & 2 > p_0\\
\frac{1}{8\mu}\eta & \frac{1}{4} & 0 & 3
\end{bmatrix}$$

Matrix a_e for Natural Straining and Rigid Body Modes of Parallelogram Plate Element — Table II.1

l = Reference Length; $\lambda = l/a$, $\mu = l/b$; $\omega = w/l$

$A_e = [\, A_n \,|\, A_0 \,] =$

	p_n 1	2	3	4	5	6	7	8	9	p_0 10	11	12	
1	·	·	·	·	·	·	·	·	$+\frac{1}{4}$	$+\frac{1}{4}$	$+\frac{1}{8}\lambda$	$-\frac{1}{8}\mu$	
2	·	·	·	·	·	·	·	·	$-\frac{1}{4}$	$+\frac{1}{4}$	$-\frac{1}{8}\lambda$	$-\frac{1}{8}\mu$	
3	·	·	·	·	·	·	·	·	$+\frac{1}{4}$	$-\frac{1}{4}$	$-\frac{1}{8}\lambda$	$+\frac{1}{8}\mu$	ω
4	·	·	·	·	·	·	·	·	$-\frac{1}{4}$	$+\frac{1}{4}$	$+\frac{1}{8}\lambda$	$+\frac{1}{8}\mu$	
5	·	$+\frac{1}{4}$	·	$+\frac{1}{4}$	·	$+\frac{1}{4}$	·	$+\frac{1}{4}$	·	·	·	$+\frac{1}{4}$	
6	·	$+\frac{1}{4}$	·	$+\frac{1}{4}$	·	$-\frac{1}{4}$	·	$-\frac{1}{4}$	·	·	·	$+\frac{1}{4}$	
7	·	$-\frac{1}{4}$	·	$-\frac{1}{4}$	·	$+\frac{1}{4}$	·	$-\frac{1}{4}$	·	·	·	$+\frac{1}{4}$	δ
8	·	$-\frac{1}{4}$	·	$+\frac{1}{4}$	·	$-\frac{1}{4}$	·	$+\frac{1}{4}$	·	·	·	$+\frac{1}{4}$	
9	$-\frac{1}{4}$	·	$-\frac{1}{4}$	·	$-\frac{1}{4}$	·	$-\frac{1}{4}$	·	·	·	$+\frac{1}{4}$	·	
10	$+\frac{1}{4}$	·	$-\frac{1}{4}$	·	$+\frac{1}{4}$	·	$-\frac{1}{4}$	·	·	·	$+\frac{1}{4}$	·	φ
11	$+\frac{1}{4}$	·	$-\frac{1}{4}$	·	$-\frac{1}{4}$	·	$+\frac{1}{4}$	·	·	·	$+\frac{1}{4}$	·	
12	$-\frac{1}{4}$	·	$-\frac{1}{4}$	·	$+\frac{1}{4}$	·	$+\frac{1}{4}$	·	·	·	$+\frac{1}{4}$	·	

Transformation Matrix A_e for Oblique System *Oxy* — Table II.2

$a_e = \frac{a_n}{a_0}$ $\quad l$ = Reference Length; $\lambda = l/a$, $\mu = l/b$; $\omega = w/l$

$a^1_n =$

	p_n 1	2	3	4	5	6	7	8	9	
1	·	·	$+2\lambda$	$+2\mu$	·	·	$+2\lambda$	$+2\mu$	$+1$	1
2	·	·	-2λ	$+2\mu$	·	·	-2λ	$+2\mu$	-1	
3	·	·	-2λ	-2μ	·	·	$+2\lambda$	$+2\mu$	$+1$	
4	·	·	$+2\lambda$	-2μ	·	·	-2λ	-2μ	-1	
5	·	$+1$	·	$+1$	·	$+1$	·	$+1$	·	
6	·	$+1$	·	$+1$	·	-1	·	-1	·	
7	·	-1	·	$+1$	·	$+1$	·	-1	·	
8	·	-1	·	$+1$	·	-1	·	$+1$	·	
9	-1	·	-1	·	$+1$	·	$+1$	·	·	
10	$+1$	·	-1	·	-1	·	$+1$	·	·	
11	$+1$	·	-1	·	$+1$	·	-1	·	·	
12	-1	·	$+1$	·	$+1$	·	$+1$	·	·	

$a^1_0 =$

	p_0 1	2	3	
1	$+1$	-2λ	-2μ	1
2	$+1$	2λ	-2μ	2
3	-1	-2λ	$+2\mu$	3
4	$+1$	$+2\lambda$	$+2\mu$	4
5	·	·	·	1
6	·	·	·	2
7	·	·	·	3
8	·	·	·	4
9	·	·	·	5
10	·	·	·	6
11	·	·	·	7
12	·	·	·	8

Transformation Matrix a_e for Oblique System Oxy — Table II.3

$b_e = \frac{b_n}{b_0}$ $\quad l$ = Reference Length; $\lambda = l/a$, $\mu = l/b$; $\omega = w/l$

$a_e = d_e b_e d_n$

$b^1_n =$

	p_n 1	2	3	4	5	6	7	8	9	
1	·	·	$+1$	$+1$	·	·	$+1$	$+1$	$+1$	1
2	·	·	-1	$+1$	·	·	-1	-1	-1	
3	·	·	-1	-1	·	·	$+1$	$+1$	$+1$	
4	·	·	$+1$	-1	·	·	-1	-1	-1	
5	·	$+1$	·	$+1$	·	$+1$	·	$+1$	·	
6	·	$+1$	·	$+1$	·	-1	·	-1	·	
7	·	-1	·	$+1$	·	$+1$	·	-1	·	
8	·	-1	·	$+1$	·	-1	·	$+1$	·	
9	-1	·	-1	·	$+1$	·	$+1$	·	·	
10	$+1$	·	-1	·	-1	·	$+1$	·	·	
11	$+1$	·	-1	·	$+1$	·	-1	·	·	
12	-1	·	$+1$	·	$+1$	·	$+1$	·	·	

$b^1_0 =$

	p_0 1	2	3	
1	$+1$	$+1$	-1	1
2	$+1$	-1	-1	2
3	$+1$	-1	$+1$	3
4	$+1$	$+1$	$+1$	4
5	·	·	·	1
6	·	·	·	2
7	·	·	·	3
8	·	·	·	4
9	·	·	·	5
10	·	·	·	6
11	·	·	·	7
12	·	·	·	8

$d_e = 2\lambda\ 2\mu\ 2\lambda\ 2\mu\ 2\lambda\ 2\mu\ 2\lambda\ 2\mu\ 1\ \ 1\ \ 2\lambda\ 2\mu$

$d_n = 1,\ \frac{1}{2\mu}\lambda,\ \frac{1}{2\lambda}\mu$

Transformation Matrix a_e for Oblique System Oxy — Table II 3a

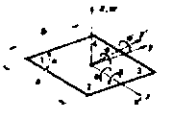

$a_0 = \begin{bmatrix} a_0 \\ a_0 \end{bmatrix}$

l = Reference Length
$\lambda = l/a$ $\mu = l/b$
$w = w'/l$
s = sine c = cosine

$a_0^1 x$

	P_0 1	2	3	4	5	6	7	8	9	
	0	0	$+2\lambda$	$+2\mu$	0	0	$+2\lambda$	$+2\mu$	+1	
	0	0	-2λ	$+2\mu$	0	0	-2λ	-2μ	−1	
	0	0	-2λ	-2μ	0	0	$+2\lambda$	$+2\mu$	+1	
	0	0	$+2\lambda$	-2μ	0	0	-2λ	-2μ	−1	
	0	$+s$	0	$+s$	0	$+s$	0	$+s$	0	
	0	$+s$	0	$+s$	0	$-s$	0	$-s$	0	
	0	$-s$	0	$+s$	0	$+s$	0	$-s$	0	
	0	$-s$	0	$+s$	0	$-s$	0	$+s$	0	
	−1	$-c$	−1	$-c$	−1	$-c$	−1	$-c$	0	
	+1	$-c$	−1	$-c$	+1	$+c$	−1	$+c$	0	
	+1	$+c$	−1	$-c$	−1	$-c$	+1	$+c$	0	
	−1	$+c$	−1	$-c$	+1	$+c$	+1	$-c$	0	

$a_0^1 =$

	P_0 1	2	3	
	+1	$+2\lambda$	-2μ	1
	+1	-2λ	-2μ	2
	+1	-2λ	$+2\mu$	3
	+1	$+2\lambda$	$+2\mu$	4
	0	0	0	1
	0	0	0	2
	0	0	0	3
	0	0	0	4
	0	0	0	1
	0	0	0	2
	0	0	0	3
	0	0	0	4

w | θ' | ψ'

Transformation Matrix a_0 for Cartesian System Oxy' Table II.4

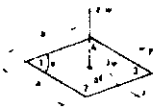

l = Reference Length
$\lambda = l/a$ $\mu = l/b$

Natural Stiffness Matrix (9 x 9) for g'th Element of Plate

$$k_{mq} = \frac{E' t^3}{12}\left[d_1 q_1 d_1 + d_2 q_2 d_2 + d_3 q_3 d_3\right]$$

Complete Stiffness Matrix (12 x 12) for g'th Element

$$k_g = a_{0g}^t\, k_{mq}\, a_{0g}$$

Unassembled Stiffness Matrix for s Elements of Plate

$$k = \left[k_1 \quad k_2 \quad k_s\right]$$

Total Stiffness Matrix for Plate

$$K = a^t k a$$

Elastic Modulus Matrix Defined by

$$\begin{bmatrix} \sigma_{xx} \\ \sigma_{yy} \\ \sqrt{2}\sigma_{xy} \end{bmatrix} = E' \begin{bmatrix} 1 & \nu_{12} & \sqrt{2}\nu_{13} \\ \nu_{21} & 1 & \sqrt{2}\nu_{23} \\ \sqrt{2}\nu_{31} & \sqrt{2}\nu_{32} & 2\nu_{33} \end{bmatrix} \begin{bmatrix} \varepsilon_{xx} \\ \varepsilon_{yy} \\ \frac{1}{\sqrt{2}}\varepsilon_{xy} \end{bmatrix}$$

$$d_1 = \sqrt{\frac{\lambda}{\mu}}\left[1 \quad 1 \quad 1 \quad 1 \quad \frac{\mu}{\lambda} \quad \frac{\lambda}{\mu} \quad 1 \quad \frac{\lambda}{\mu} \quad 1\right]$$

$$d_2 = \sqrt{\frac{\mu}{\lambda}}\left[1 \quad 1 \quad 1 \quad 1 \quad \frac{\mu}{\lambda} \quad \frac{\lambda}{\mu} \quad \frac{\mu}{\lambda} \quad 1 \quad 1\right]$$

$$d_3 = \sqrt{\lambda\mu}\left[\frac{1}{\mu} \quad \frac{1}{\lambda} \quad \frac{1}{\mu} \quad \frac{1}{\lambda} \quad \frac{1}{\mu} \quad \frac{1}{\lambda} \quad \frac{1}{\lambda} \quad \frac{1}{\mu} \quad 1\right]$$

For Isotropic Rectangular Element $\nu_{11} = \nu_{22} = 1$, $\nu_{12} = \nu$, $\nu_{13} = \nu_{23} = 0$, $\nu_{33} = \frac{1-\nu}{2}$, $\nu_{12} + 2\nu_{33} = 1$
$E' = E/(1-\nu^2)$

$q_1 = \frac{1}{4}$

ν_{11}								
	$3\nu_{11}$		$2\nu_{13}$		ν_{12}			
		$2\nu_{13}$		$\frac{4}{9}(\nu_{12}+2\nu_{13})$		$\frac{8}{9}\nu_{12}$		
		ν_{12}		$\frac{8}{9}\nu_{13}$		$\frac{2}{9}\nu_{12}$		
							$\frac{51}{36}\nu_{11}$	$\frac{9}{36}\nu_{13}$
							$\frac{9}{36}\nu_{13}$	$\frac{2}{36}\nu_{11}$

$q_2 = \frac{1}{4}$

			$3\nu_{23}$		ν_{22}		$2\nu_{23}$	
			ν_{22}		$\frac{16}{9}\nu_{23}$		$\frac{8}{9}\nu_{23}$	
			$2\nu_{23}$		$\frac{8}{9}\nu_{23}$		$\frac{4}{9}(\nu_{12}+2\nu_{13})$	
								$\frac{2}{36}\nu_{12}$
								$\frac{8}{36}\nu_{23}$

$q_3 = \frac{1}{4}$

	ν_{12}							$-4\nu_{12}$
								$-4\nu_{23}$
					$\frac{6}{5}\nu_{12}$			
				$\frac{6}{5}\nu_{12}$				
				$\frac{6}{5}\nu_{12}$	$\frac{17}{36}\nu_{11}$			
				$\frac{6}{5}\nu_{12}$		$\frac{17}{36}\nu_{22}$		
							$\frac{12}{25}(\nu_{12}+2\nu_{33})$	$\frac{1}{25}(37\nu_{12}+4\nu_{33})$
							$\frac{1}{25}(37\nu_{12}+4\nu_{33})$	$\frac{12}{25}(\nu_{12}+2\nu_{33})$
	$-4\nu_{12}-4\nu_{33}$							$16\nu_{33}$

Stiffness Matrix for Anisotropic Parallelogram Plate Element Table II.5

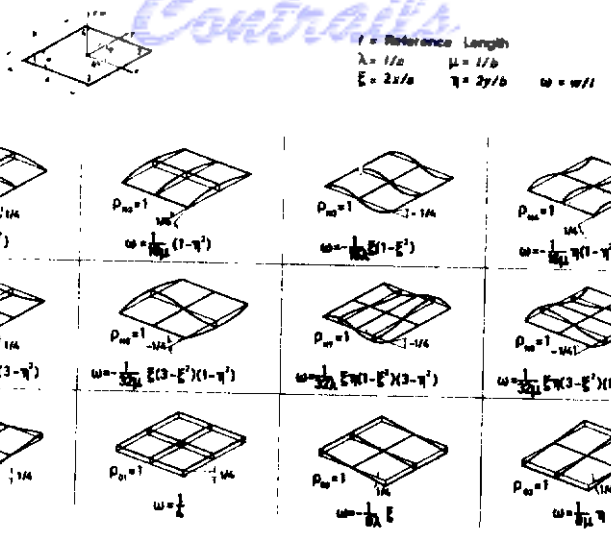

Straining and Rigid Modes for Parallelogram Plate Element Fig. II.11

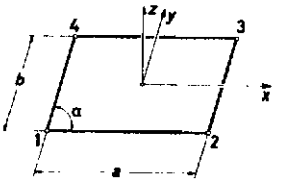

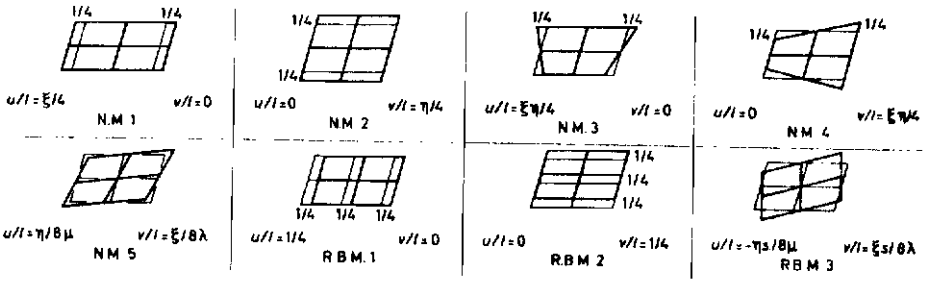

Parallelogram Membrane Element with Four Nodal Points

Fig. II.12

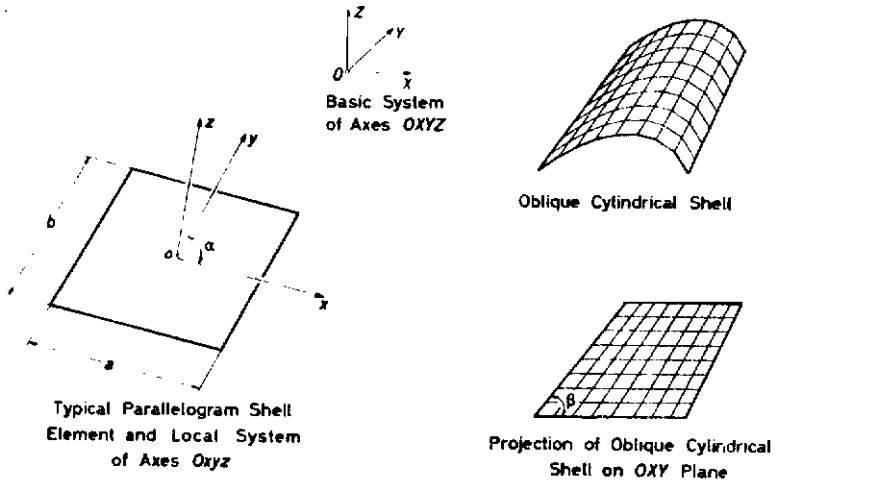

Oblique Cylindrical Shell with Parallelogram Elements

Fig. II.13

The dual relation to Eq.(89) is

$$P = a_e^t P' = a_N^t P_N + a_o^t P_o \qquad (II,98)$$

If the resultant body and surface forces acting on the plate element are zero, i.e., $P_o = O$, Eq.(98) reduces as in Section I to

$$P = a_N^t P_N \qquad (II,99)$$

and P are hence in the present case a self-equilibrating set of forces and moments. Eqs.(I,5, II,99) are applied in the subsequent Section to the derivation of the stiffness k of a parallelogram element in bending.

Assume next that at the point (x,y) of the plate characterized by the deformation vector w there act a generalized force

$$R = \{ P_z \ell \quad M_x \quad M_y \} \qquad (II,100)$$

Application of the principle of the invariance of work shows that the nodal force vector P_e corresponding to R is given by

$$P_e = \Pi_e^t R \qquad (II,101)$$

Note that in the present case the force P_e is not self-equilibrating. A generalization of Eq.(101) is considered in Section II.5.

II.4 The Stiffness Matrix of a Parallelogram Element in Bending

The derivation of the (12 x 12) stiffness matrix k_g of a typical element g is conveniently based on its (9 x 9) natural stiffness k_N. In the subsequent derivation we omit the suffix g until the final formation of the matrix k of the stiffnesses of the unassembled elements.

To find k_N we essentially have to generalize Eq.(79) for an individual stiffness coefficient k_{ij}. We start by establishing the explicit expression for the strain vector ε at a distance z from the neutral axis. To achieve this we have first to establish the displacements u_1, v_1, as defined in Section II.2b. A simple geometrical consideration leads to

$$u_1 = -z\theta = -z\frac{\partial w}{\partial x}, \quad v_1 = z\phi = -z\frac{\partial w}{\partial y} \qquad (II,102)$$

where the derivatives are, of course, referred to the oblique co-ordinate system. Using Eqs.(102) in formulae (60) and (61) we obtain

$$\varepsilon = z \left\{ -\frac{\partial^2 w}{\partial x^2} \quad -\frac{\partial^2 w}{\partial y^2} \quad -\sqrt{2}\,\frac{\partial^2 w}{\partial x \partial y} \right\} \qquad (II,103)$$

Let us next set up the (3 x 9) matrix $\mathfrak{E}_N = \frac{z}{\ell}\,\mathfrak{A}_N$, the nine columns of which are the vectors $\mathfrak{E}_i$ corresponding to the nine natural modes $\rho_N = 1$. By definition

$$\mathfrak{E} = \mathfrak{E}_N \rho_N = \frac{z}{\ell}\,\mathfrak{A}_N \rho_N \tag{II,104}$$

The corresponding stress vector $\mathfrak{S}$ is obtained from Eq.(73).

Introducing the non-dimensional co-ordinates ξ, η the parameters λ, μ and a deflexion ω_i of a typical natural straining mode i, the corresponding strain vector $\mathfrak{E}_{Ni}$ becomes

$$\mathfrak{E}_{Ni} = \frac{2z}{\ell}\left\{-2\lambda^2\omega_{\xi\xi} \qquad -2\mu^2\omega_{\eta\eta} \qquad -2\sqrt{2}\,\lambda\mu\,\omega_{\xi\eta}\right\}_i \tag{II,105}$$

We may now assemble the (3 x 9) matrix $\mathfrak{A}_N$ by straightforward differentiation of the first row ω_N of the (3 x 9) matrix $\mathfrak{W}_N$. In fact, if we define the (3 x 1) operator ϑ^2 as

$$\vartheta^2 = \left\{-2\lambda^2\frac{\partial^2}{\partial\xi^2} \qquad -2\mu^2\frac{\partial^2}{\partial\eta^2} \qquad -2\sqrt{2}\,\lambda\mu\frac{\partial^2}{\partial\xi\partial\eta}\right\} \tag{II,106}$$

we have

$$\mathfrak{A}_N = \vartheta^2\omega_N \tag{II,107}$$

After this preparatory work we proceed to the derivation of $\mathfrak{k}_N$. We first apply the generalization of Eq.(79), given by Eq.(I,22), in the form

$$\mathfrak{k}_N = \int_V \mathfrak{E}_N^t\,\mathfrak{E}\,\mathfrak{E}_N\,dV = \int_V \frac{z^2}{\ell^2}\,\mathfrak{A}_N^t\,\mathfrak{E}\,\mathfrak{A}_N\,dV \tag{II,108}$$

Introducing Eqs.(75,107) and integrating over z we obtain in conjunction with the non-dimensional co-ordinates ξ, η

$$\mathfrak{k}_N = \frac{E'}{12\lambda\mu}\,s_4\int_{-1}^{+1}\int_{-1}^{+1}\mathfrak{A}_N^t\,\mathfrak{V}\,\mathfrak{A}_N\,d\xi\,d\eta \tag{II,109}$$

For a homogeneous element of constant thickness t, but arbitrary anisotropy $\mathfrak{V}$, the stiffness $\mathfrak{k}_N$ is reproduced in full in Table II, 5. It may be considerably simplified in the case of isotropy, especially if the element is rectangular. However, our ASKA operates as a general purpose programme, so that there is no point in developing programmes for special cases. Nevertheless, some readers may be interested in the result for a rectangular element, so that we reproduce further the corresponding expression for its stiffness matrix in a suitable form.

Having obtained the natural stiffness k_N we proceed to the derivation of the fully expanded (12 x 12) stiffness matrix k referred to the basic system $O\,x\,y$, which is in accordance with Eq.(I,23)

$$k = a_N^t k_N a_N \tag{II,110}$$

The stiffness k may be referred either to oblique or cartesian co-ordinate systems. The corresponding a_N may be read from Tables II.3, 4; see also Eq.(91). For computational purposes it proves most convenient (especially in conjunction with ASKA) to carry out the congruent transformation as part of the general purpose programme in the computer itself, and not to establish the explicit expressions for the elements of k. However, as a matter of interest for the more specialized reader we reproduce in Table II.6 the matrix k for an isotropic rectangular element; its programming is particularly straightforward in conjunction with Boolean orders. The stiffness k for an arbitrary anisotropic quadrilateral may be found in full in Ref.30. This last publication also contains a considerable number of extensions to our theory of practical interest. Thus it derives inter alia the stiffness k for an anisotropic parallelogram with a thickness t varying in accordance with the expression

$$t = t_o + t_I \xi + t_{II} \eta + t_{III} \xi\eta \tag{II,111}$$

The constants t_o to t_{III} may easily be determined in terms of the thicknesses t_1 to t_4 at the nodal points 1 to 4. A further significant advance to our theory covers arbitrary, anisotropic quadrilateral plates. The reproduction of all these data would exceed by far the limits of this article.

II.5 Stiffness of the Unassembled and Assembled Plate; Local Displacement Relations for the Plate

Following our usual analysis, the stiffness k of the unassembled plate elements is the diagonal supermatrix

$$k = \lceil k_1\ k_2 \cdots k_q \cdots k_s \rfloor \tag{II,112}$$

each element of which is of order (12 x 12) and based on the same co-ordinate system, oblique or cartesian. We then require the relation between the (generalized) nodal displacements φ_q of each element q (sub-vector of order (12 x 1)) and the vector r of these displacements as referred to the n nodal points of the plate as a whole. This is given by the standard Boolean matrix transfomation

$$\varphi = a\, r \tag{II,113}$$

where φ, a supervector of order (12s x 1), is

$$\varphi = \{ \varphi_1\ \varphi_2 \cdots \varphi_q \cdots \varphi_s \} \tag{II,114}$$

We also have the dual expression connecting the loads P and R associated with φ and r respectively

$$R = a^t P \qquad (II,115)$$

where all forces and displacements are measured on the system of axes chosen for k. In the presence of thermal differential strain η_Δ between the upper and lower surfaces their effect may be included in the analysis by our initial load concept J. In the present case, J is the (12s x 1) supervector

$$J = \{ J_1 \; J_2 \cdots J_g \cdots J_s \} \qquad (II,116)$$

and Ref.13 indicates how the sub-vector J_g may be set up for any given η_Δ distribution. This derivation is, of course, equally applicable to η_Δ arising from plasticity and time-dependent viscous effects, as discussed in Chapter III.

The load-displacement relationship for the plate as a whole is now given by Eq.(I,25) which we reproduce here for convenience,

$$R = K r + a^t J \qquad (II,117)$$

Here K, the stiffness of the assembled structure, is in our usual notation

$$K = a^t k a \qquad (II,118)$$

Having obtained r the stresses are easily established as shown in detail in Ref.30.

II.6 The Generalized Load Vector P_e due to an Arbitrary Transverse Load Distribution

We now take up in more detail the formation of the load vector R and apply some of the basic ideas of Section II.3, in particular Eqs. (91, 102). Assume that the element g is subjected to an arbitrary system of distributed and/or concentrated forces $p(x,y)$ or P in the z -direction. We may also allow for the effect of distributed or concentrated moments. In the latter case we write the (3 x 1) load vector of the plate in the form

$$p = \{ p_{zz} \; p_{zx} \; p_{zy} \} \qquad (II,119)$$

where the components may be discontinuous functions of (x,y). In accordance with our specification of a non-dimensional deflexion ω, the p_{zz} arising from a distributed loading p must be written as pl and has the dimensions lbf/in, as p_{zx} and p_{zy}. Our Matrix Displacement method essentially requires that all loads be applied at the nodal points. To obtain the kinematically equivalent lumped load vector P_e acting at the nodal points it is most convenient to apply the Unit Displacement method of Ref.1, which we write here in the form

$$\varphi^t P_e = \int \pi^t p \, dA \qquad (II,120)$$

where π is the generalized displacement vector of Eq. (84) and dA an element of plate area. Using Eq.(92) we obtain for oblique co-ordinates,

$$\rho^t P_e = s\,\rho^t \iint \Pi_e^t\, p\, dx\, dy = s\,\rho^t a_e^t \iint \omega_e^t p\, dx\, dy \qquad (II,120a)$$

Hence P_e , a (12 x 1) vector is given by

$$P_e = s \iint \Pi_e^t\, p\, dx\, dy = s\, a_e^t \iint \omega_e^t p\, dx\, dy \qquad (II,121)$$

Eq.(123) may also be derived fromEq.(101) by the substitution

$$m = s\, p\, dx\, dy \qquad (II,122)$$

and subsequent integration. Consider the simple case, when

$$p_{zz} = p_o l = \text{const.} \qquad (II,123)$$

and external moments are acting on the plate. Application of ω_e from Table II.3 leads to the simple result

$$P_e = \sin\alpha \frac{p_o l^3}{16\lambda\mu} a_e^t \left\{ \frac{2}{3\mu} \quad \frac{2}{3\lambda} \quad 0 \quad 0 \quad 0 \quad 0 \quad 0 \quad 0 \quad 4 \quad 0 \quad 0 \right\} \qquad (II,124)$$

It is immediately observed that the tenth element, arising from the rigid body translation, yields the standard equal distribution of the transverse load at the four nodal points. The first and second elements are on the other hand due to the first two natural straining modes and generate moments at the nodal points. The structure of P_e is seen more clearly by carrying out a premultiplication with a_e^t . We find

$$P_e = \sin\alpha \frac{p_o l^3}{4\lambda\mu} \left\{ 1 \quad 1 \quad 1 \quad 1 \quad +\frac{1}{6\mu} \quad +\frac{1}{6\mu} \quad -\frac{1}{6\mu} \quad -\frac{1}{6\mu} \quad -\frac{1}{6\lambda} \quad +\frac{1}{6\lambda} \quad +\frac{1}{6\lambda} \quad -\frac{1}{6\lambda} \right\} \qquad (II,124a)$$

We next consider an extension of the above technique, which proves particularly useful when p varies in a complex and irregular manner over the surface. At the same time the procedure serves as a useful introduction to the generalized lumped mass concept, expounded in the following Section. The proposed technique is based on the idea that in many instances it may suffice to represent p by an approximate distribution in terms of the assumed kinematic modes ω_e ; in mathematical terms we establish a finite series expansion of p based on the ω_e functions. For the present purpose we limit the presentation to the particular case of a transverse load p_{zz} and zero applied moments. We first define the given p in terms of the ordinates and gradients of the function $p(x,y)$ at the nodal points 1,2,3,4. Writing

$$P_i = p_o l\, \eta_v \qquad (II,125)$$

where p_o is a reference pressure and η_v the non-dimensional (12 x 1) vector

$$\mathfrak{p}_v = \left\{ \frac{p_1}{p_0} \quad \frac{p_2}{p_0} \quad \frac{p_3}{p_0} \quad \frac{p_4}{p_0} \quad \left(\frac{\partial(p/p_0)}{\partial(y/\ell)}\right)_1 \quad \left(\frac{\partial(p/p_0)}{\partial(y/\ell)}\right)_2 \quad \left(\frac{\partial(p/p_0)}{\partial(y/\ell)}\right)_3 \quad \left(\frac{\partial(p/p_0)}{\partial(y/\ell)}\right)_4 \right.$$
$$\left. -\left(\frac{\partial(p/p_0)}{\partial(x/\ell)}\right)_1 \quad -\left(\frac{\partial(p/p_0)}{\partial(x/\ell)}\right)_2 \quad -\left(\frac{\partial(p/p_0)}{\partial(x/\ell)}\right)_3 \quad -\left(\frac{\partial(p/p_0)}{\partial(x/\ell)}\right)_4 \right\}$$

(II, 126)

where the minus sign associated with the gradients in the xz-plane arise from the adopted sign convention for φ. We now represent the loading p at any station (ξ, η) by the approximate expansion

$$p = \omega_e a_e \mathfrak{p}_v \qquad \text{(II, 127)}$$

where ω_e is the (1 x 12) deflexion matrix defined following Eq.(87). Substituting Eq.(127) into Eq.(123), we find

$$P_e = \frac{s p_0 \ell^3}{16 \lambda \mu} a_e^t \left[\int_{-1}^{+1} \int_{-1}^{+1} \omega_e^t \omega_e \, d\xi \, d\eta \right] a_e \mathfrak{p}_v \qquad \text{(II, 128)}$$

Carrying out a straightforward integration, we obtain

$$P_e = \frac{s p_0 \ell^3}{16 \lambda \mu} a_e^t \vartheta \mathfrak{A} \vartheta a_e \mathfrak{p}_v \qquad \text{(II, 129)}$$

where the (12 x 1) diagonal matrix ϑ and the square matrix $\mathfrak{A}$ are given in Table II.7. Having established the load vector P_e for all elements we put

$$P = \{ P_{e1} \; P_{e2} \cdots P_{eq} \cdots P_{es} \} \qquad \text{(II, 130)}$$

and find the resultant load vector R at the nodal points from the Boolean transformation Eq.(166) in Section III.5.

II.7 The Kinematically Consistent Lumped Mass Matrix

We now apply our ideas to a kinematically consistent lumped mass matrix briefly expanded in Section I.3 to parallelogram plates under bending. The developments of the preceding Section are thereby of immediate applicability. In what follows we not only take account of translational inertia but also include the contribution from rotational inertia of the plate. Strictly, this is only justified, when transverse shear strains - ignored here but not in the basic Ref.30 - are admitted. However, the present complete inertia theory has the advantage of leading naturally into the overall expression of the geometrical stiffness (see Section V), which determines the buckling phenomenon of the plate under arbitrary in-plane loading.

We start by writing the distributed mass per unit area as a (3 x 3) matrix

l = Reference Length

$\lambda = \frac{l}{a} \qquad \mu = \frac{l}{b}$

$k = k_\sigma + k_b$

$k_\sigma = \frac{E' t^3}{12} b_1 \left[\left(\frac{\lambda}{\mu}\right)^2 𝔄 + \left(\frac{\mu}{\lambda}\right)^2 𝔅 + ℭ \right] b_1 \qquad E' = E/(1-\nu^2)$

$k_b = \frac{E' t^3}{12} b_2 𝔇 b_2$

$b_1 = \left[(\lambda\mu)^{\frac{1}{2}} I_3 \quad \left(\frac{\lambda}{\mu}\right)^{\frac{1}{2}} I_3 \quad \left(\frac{\mu}{\lambda}\right)^{\frac{1}{2}} I_3 \right]$

$b_2 = \left[(\lambda\mu)^{\frac{1}{2}} I_3 \quad I_3 \quad I_3 \right]$

$$𝔄 = \frac{1}{70} \begin{bmatrix}
+352 & +68 & -68 & -352 & +165 & +45 & +45 & +165 & +46 & -24 & +24 & -46 \\
+68 & +352 & -352 & -68 & +45 & +165 & +165 & +45 & +24 & -46 & +46 & -24 \\
-68 & -352 & +352 & +68 & -45 & -165 & -165 & -45 & -24 & +46 & -46 & +24 \\
-352 & -68 & +68 & +352 & -165 & -45 & -45 & -165 & -46 & +24 & -24 & +46 \\
 & & & & +104 & +36 & +18 & +52 & +22 & +13 & +13 & +22 \\
 & & & & +36 & +104 & +52 & +18 & -13 & -22 & -22 & -13 \\
 & & & & +18 & +52 & +104 & +36 & +13 & +22 & +22 & +13 \\
 & & & & +52 & +18 & +36 & +104 & -22 & -13 & -13 & -22 \\
 & & \text{symmetric} & & & & & & +8 & -6 & +6 & -8 \\
 & & & & & & & & -6 & +8 & -8 & +6 \\
 & & & & & & & & +6 & -8 & +8 & -6 \\
 & & & & & & & & -8 & +6 & -6 & +8
\end{bmatrix}$$

$$𝔅 = \begin{bmatrix} b_1 & 0 & 0 \\ 0 & 0 & b_1 \\ 0 & b_1 & 0 \end{bmatrix} 𝔄 \begin{bmatrix} b_1 & 0 & 0 \\ 0 & 0 & b_1 \\ 0 & b_1 & 0 \end{bmatrix}$$

$$\text{where} \quad b_1 = \begin{bmatrix} 1 & \cdot & \cdot & \cdot \\ \cdot & \cdot & \cdot & 1 \\ \cdot & \cdot & 1 & \cdot \\ \cdot & 1 & \cdot & \cdot \end{bmatrix}$$

$$ℭ = \frac{1}{50} \begin{bmatrix}
+196 & -196 & +196 & -196 & +79 & -79 & -19 & +19 & +79 & +19 & -19 & -79 \\
-196 & +196 & -196 & +196 & -79 & +79 & +19 & -19 & -19 & -79 & +79 & +19 \\
+196 & -196 & +196 & -196 & +19 & -19 & -79 & +79 & +19 & +79 & -79 & -19 \\
-196 & +196 & -196 & +196 & -19 & +19 & +79 & -79 & -79 & -19 & +19 & +79 \\
 & & & & +16 & -16 & +4 & -4 & +61 & -6 & -1 & +6 \\
 & & & & -16 & +16 & -4 & +4 & +6 & -61 & -6 & +1 \\
 & & & & +4 & -4 & +16 & -16 & -1 & +6 & +61 & -6 \\
 & & & & -4 & +4 & -16 & +16 & -6 & +1 & +6 & -61 \\
 & & \text{symmetric} & & & & & & +16 & -4 & +4 & -16 \\
 & & & & & & & & -4 & +16 & -16 & +4 \\
 & & & & & & & & +4 & -16 & +16 & -4 \\
 & & & & & & & & -16 & +4 & -4 & +16
\end{bmatrix}$$

$$𝔇 = \frac{1}{10} \begin{bmatrix}
-16 & +16 & -16 & +16 & -13 & +13 & +1 & -1 & -13 & -1 & +1 & +13 \\
+16 & -16 & +16 & -16 & +13 & -13 & -1 & +1 & +1 & +13 & -13 & -1 \\
-16 & +16 & -16 & +16 & -1 & +1 & +13 & -13 & -1 & -13 & +13 & +1 \\
+16 & -16 & +16 & -16 & +1 & -1 & -13 & +13 & +13 & +1 & -1 & -13 \\
 & & & & \cdot & \cdot & \cdot & \cdot & -24 & +2 & 0 & -2 \\
 & & & & \cdot & \cdot & \cdot & \cdot & -2 & +24 & +2 & 0 \\
 & & & & \cdot & \cdot & \cdot & \cdot & 0 & -2 & -24 & +2 \\
 & & & & \cdot & \cdot & \cdot & \cdot & +2 & 0 & -2 & +24 \\
 & & \text{symmetric} & & & & & & \cdot & \cdot & \cdot & \cdot \\
 & & & & & & & & \cdot & \cdot & \cdot & \cdot \\
 & & & & & & & & \cdot & \cdot & \cdot & \cdot \\
 & & & & & & & & \cdot & \cdot & \cdot & \cdot
\end{bmatrix}$$

Elastic Stiffness Matrix for a Rectangular Element

Table II.6

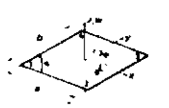

l = Reference Length

$\lambda = l/a \qquad \mu = l/b \qquad s = \sin\alpha \qquad c = \cos\alpha$

m = Plate Mass / Unit Area

r = Radius of Gyration ($t/2\sqrt{3}$ for solid plate)

Lumped Mass Matrix for g'th Element of Plate

$$m = \frac{\rho l^4}{\lambda\mu}\, s \left[a_N' \;\; a_D' \right] \left[\ldots \; [illegible] \; \left[\lambda^2 𝔅_1 + \mu^2 𝔅_2 + \lambda\mu c 𝔅_3\right] b_1 \right] \left[a_N \;\; a_D \right]$$

Unassembled Mass Matrix for s-Elements of Plate

$m = \left[m_1 \quad m_g \quad m_s \right]$

Total Mass Matrix for Plate

$M = a' m a$

$$𝔄 = \begin{bmatrix}
[illegible] & 1 & \cdot & \cdot & \cdot & \cdot & \cdot & \cdot & \cdot & 1 & \cdot & \cdot \\
1 & \frac{6}{5} & \cdot & \cdot & \cdot & \cdot & \cdot & \cdot & \cdot & 1 & \cdot & \cdot \\
\cdot & \cdot & \frac{10}{21} & \cdot & \cdot & \frac{5}{42} & \cdot & \cdot & \cdot & \cdot & 1 & \cdot \\
\cdot & \cdot & \cdot & \frac{10}{21} & \frac{5}{42} & \cdot & \cdot & \cdot & \cdot & \cdot & \cdot & -1 \\
\cdot & \cdot & \cdot & \frac{5}{42} & \frac{17}{42} & \cdot & \cdot & \cdot & \cdot & \cdot & \cdot & -1 \\
\cdot & \cdot & \frac{5}{42} & \cdot & \cdot & \frac{17}{42} & \cdot & \cdot & \cdot & \cdot & 1 & \cdot \\
\cdot & \cdot & \cdot & \cdot & \cdot & \cdot & \frac{34}{3} & 9 & 1 & \cdot & \cdot & \cdot \\
\cdot & \cdot & \cdot & \cdot & \cdot & \cdot & 9 & \frac{34}{3} & 1 & \cdot & \cdot & \cdot \\
\cdot & \cdot & \cdot & \cdot & \cdot & \cdot & 1 & 1 & [illegible] & \cdot & \cdot & \cdot \\
1 & 1 & \cdot & \cdot & \cdot & \cdot & \cdot & \cdot & \cdot & 1 & \cdot & \cdot \\
\cdot & \cdot & 1 & \cdot & \cdot & 1 & \cdot & \cdot & \cdot & \cdot & 3 & \cdot \\
\cdot & \cdot & \cdot & -1 & -1 & \cdot & \cdot & \cdot & \cdot & \cdot & \cdot & 3
\end{bmatrix}$$

$$𝔅_1 = \begin{bmatrix}
3 & \cdot & \cdot & \cdot & \cdot & \cdot & \cdot & \cdot & \cdot & \cdot & \cdot & \cdot \\
\cdot & \cdot & \cdot & \cdot & \cdot & \cdot & \cdot & \cdot & \cdot & \cdot & \cdot & \cdot \\
\cdot & \cdot & \frac{8}{5} & \cdot & \cdot & 1 & \cdot & \cdot & \cdot & \cdot & \cdot & \cdot \\
\cdot & \cdot & \cdot & \cdot & \cdot & \cdot & \cdot & \cdot & \cdot & \cdot & \cdot & \cdot \\
\cdot & \cdot & \cdot & \cdot & \frac{88}{21} & \cdot & \cdot & \cdot & \cdot & \cdot & \cdot & \cdot \\
\cdot & \cdot & 1 & \cdot & \cdot & 4 & \cdot & \cdot & \cdot & \cdot & 5 & \cdot \\
\cdot & \cdot & \cdot & \cdot & \cdot & \cdot & \frac{17}{7} & \frac{3}{7} & \cdot & \cdot & \cdot & \cdot \\
\cdot & \cdot & \cdot & \cdot & \cdot & \cdot & [illegible] & [illegible] & 2 & \cdot & \cdot & \cdot \\
\cdot & \cdot & \cdot & \cdot & \cdot & \cdot & \cdot & 2 & 12 & \cdot & \cdot & \cdot \\
\cdot & \cdot & \cdot & \cdot & \cdot & \cdot & \cdot & \cdot & \cdot & \cdot & \cdot & \cdot \\
\cdot & \cdot & \cdot & \cdot & \cdot & 5 & \cdot & \cdot & \cdot & \cdot & [illegible] & \cdot \\
\cdot & \cdot & \cdot & \cdot & \cdot & \cdot & \cdot & \cdot & \cdot & \cdot & \cdot & \cdot
\end{bmatrix}
\quad
𝔅_2 = \begin{bmatrix}
\cdot & \cdot & \cdot & \cdot & \cdot & \cdot & \cdot & \cdot & \cdot & \cdot & \cdot & \cdot \\
\cdot & 3 & \cdot & \cdot & \cdot & \cdot & \cdot & \cdot & \cdot & \cdot & \cdot & \cdot \\
\cdot & \cdot & \cdot & \cdot & \cdot & \cdot & \cdot & \cdot & \cdot & \cdot & \cdot & \cdot \\
\cdot & \cdot & \cdot & \frac{8}{5} & 1 & \cdot & \cdot & \cdot & \cdot & \cdot & \cdot & \cdot \\
\cdot & \cdot & \cdot & 1 & 4 & \cdot & \cdot & \cdot & \cdot & \cdot & \cdot & -5 \\
\cdot & \cdot & \cdot & \cdot & \cdot & \frac{88}{21} & \cdot & \cdot & \cdot & \cdot & \cdot & \cdot \\
\cdot & \cdot & \cdot & \cdot & \cdot & \cdot & \frac{4}{7} & \frac{3}{7} & 2 & \cdot & \cdot & \cdot \\
\cdot & \cdot & \cdot & \cdot & \cdot & \cdot & \frac{3}{7} & \frac{17}{7} & \cdot & \cdot & \cdot & \cdot \\
\cdot & \cdot & \cdot & \cdot & \cdot & \cdot & 2 & \cdot & 12 & \cdot & \cdot & \cdot \\
\cdot & \cdot & \cdot & \cdot & \cdot & \cdot & \cdot & \cdot & \cdot & \cdot & \cdot & \cdot \\
\cdot & \cdot & \cdot & \cdot & \cdot & \cdot & \cdot & \cdot & \cdot & \cdot & \cdot & \cdot \\
\cdot & \cdot & \cdot & \cdot & -5 & \cdot & \cdot & \cdot & \cdot & \cdot & \cdot & 9
\end{bmatrix}$$

$$𝔅_3 = \begin{bmatrix}
\cdot & \cdot & \cdot & \cdot & \cdot & \cdot & 1 & \cdot & 6 & \cdot & \cdot & \cdot \\
\cdot & \cdot & \cdot & \cdot & \cdot & \cdot & \cdot & 1 & 6 & \cdot & \cdot & \cdot \\
\cdot & \cdot & \cdot & \cdot & -1 & \cdot & \cdot & \cdot & \cdot & \cdot & \cdot & \cdot \\
\cdot & \cdot & \cdot & \cdot & \cdot & -1 & \cdot & \cdot & \cdot & \cdot & \cdot & \cdot \\
\cdot & \cdot & -1 & \cdot & \cdot & -6 & \cdot & \cdot & \cdot & \cdot & -5 & \cdot \\
\cdot & \cdot & \cdot & -1 & -6 & \cdot & \cdot & \cdot & \cdot & \cdot & \cdot & 5 \\
1 & \cdot & \cdot & \cdot & \cdot & \cdot & \cdot & \cdot & \cdot & \cdot & \cdot & \cdot \\
\cdot & 1 & \cdot & \cdot & \cdot & \cdot & \cdot & \cdot & \cdot & \cdot & \cdot & \cdot \\
6 & 6 & \cdot & \cdot & \cdot & \cdot & \cdot & \cdot & \cdot & \cdot & \cdot & \cdot \\
\cdot & \cdot & \cdot & \cdot & \cdot & \cdot & \cdot & \cdot & \cdot & \cdot & \cdot & \cdot \\
\cdot & \cdot & \cdot & \cdot & -5 & \cdot & \cdot & \cdot & \cdot & \cdot & \cdot & 9 \\
\cdot & \cdot & \cdot & \cdot & \cdot & 5 & \cdot & \cdot & \cdot & \cdot & 9 & \cdot
\end{bmatrix}$$

$a_1' = \left[6\lambda \;\; 6\mu \;\; 10\lambda \;\; 10\mu \;\; 5\lambda \;\; 5\mu \;\; 70\lambda \;\; 70\mu \;\; [illegible] \;\; 1 \;\; 6\lambda \;\; 6\mu \right]$

$a_2' = \left[3\lambda \;\; 3\mu \;\; 3\lambda \;\; 3\mu \;\; 5\lambda \;\; 5\mu \;\; 5\lambda \;\; 5\mu \;\; 3 \;\; 1 \;\; 3\lambda \;\; 3\mu \right]$

Lumped Mass Matrix for Parallelogram Plate Element

Table II.7

$$\mathcal{M} = m \begin{bmatrix} l^2 & 0 & 0 \\ 0 & i_{xx}^2 & i_{xy}^2 \\ 0 & i_{yx}^2 & i_{yy}^2 \end{bmatrix} \qquad \text{(II,131)}$$

where m is the actual mass per unit area and i_{xx}, i_{yy}, i_{xy} are the radii of gyration associated with rotational inertia, the coupling term i_{xy} arising when using oblique co-ordinates. The factor l^2 is introduced for dimensional consistency. We now show how the coupling term i_{xy} may be established. Consider the alternative (2 x 1) vectors P' and P of the rotations with respect to the cartesian and oblique systems $Ox'y'$ and Oxy of axes; thus

$$P' = \{\vartheta' \quad \varphi'\} \qquad \text{and} \qquad P = \{\vartheta \quad \varphi\} \qquad \text{(II,132)}$$

Following Eq.(39) they are related by

$$P' = \frac{1}{s_\alpha} \begin{bmatrix} 1 & c_\alpha \\ 0 & s_\alpha \end{bmatrix} P \qquad \text{(II,133)}$$

The amplitude of the kinetic energy per unit area of the plate due to rotational inertia alone may be put in the alternative forms

$$\frac{m}{2} P'^t \begin{bmatrix} i^2 & 0 \\ 0 & i^2 \end{bmatrix} P' = \frac{m}{2} P^t \begin{bmatrix} i_{xx}^2 & i_{xy}^2 \\ i_{yx}^2 & i_{yy}^2 \end{bmatrix} P$$

Substitution of Eq.(133) into the last expression yields

$$\begin{bmatrix} i_{xx}^2 & i_{xy}^2 \\ i_{yx}^2 & i_{yy}^2 \end{bmatrix} = \frac{i^2}{s_\alpha^2} \begin{bmatrix} 1 & c_\alpha \\ c_\alpha & 1 \end{bmatrix} \qquad \text{(II,134)}$$

Hence for a homogeneous parallelogram element Eq.(131) becomes

$$\mathcal{M} = m \begin{bmatrix} l^2 & 0 & 0 \\ 0 & \frac{i^2}{s_\alpha^2} & \frac{i^2}{s_\alpha^2} c_\alpha \\ 0 & \frac{i^2}{s_\alpha^2} c_\alpha & \frac{i^2}{s_\alpha^2} \end{bmatrix} \qquad \text{(II,131a)}$$

We may now proceed to the derivation of the lumped mass matrix and assume that the element is oscillating with a circular frequency ω *. The inertia force corresponding to the mass matrix of Eq.(131) or (131a) per unit area of plate is

* The temporary use of ω to denote circular frequency should not lead to confusion with the symbol ω for the non-dimensional displacement in the z -direction

$$\mathcal{R}_i = -\mathfrak{m}\ddot{x} = -\mathfrak{m}\Pi_e\ddot{\rho} \qquad (II,135)$$

Since the motion is harmonic we find

$$\hat{\mathcal{R}}_i = \omega^2 \mathfrak{m}\Pi_e\hat{\rho} \qquad (II,135a)$$

The equivalent inertia force vector $\hat{P}_i$ corresponding to the amplitude vector $\hat{\rho}$ may be obtained from

$$\hat{P}_i = \omega^2 \mathfrak{m}\hat{\rho} \qquad (II,136)$$

where $\mathfrak{m}$ is the (12 x 12) lumped mass matrix we seek. To obtain $\mathfrak{m}$ we may either apply Eq.I,26a immediately or use the Unit Displacement method in a form analogous to Eq.(120) to find

$$\hat{\rho}^t\hat{P}_i = \iint \hat{x}^t\hat{\mathcal{R}}_i\, dA \qquad (II,137)$$

and introducing the non-dimensional oblique co-ordinates

$$\hat{\rho}^t\hat{P}_i = \frac{\ell_s^2}{4\lambda\mu}\int_{-1}^{+1}\int_{-1}^{+1}\hat{x}^t\hat{\mathcal{R}}_i\, d\xi\, d\eta \qquad (II,137a)$$

Using Eqs.(135a),(136) we obtain

$$\hat{\rho}^t\mathfrak{m}\hat{\rho} = \frac{\ell_s^2}{4\lambda\mu}\hat{\rho}^t\left[\int_{-1}^{+1}\int_{-1}^{+1}\Pi_e^t\,\mathfrak{m}\,\Pi_e\, d\xi\, d\eta\right]\hat{\rho} \qquad (II,137b)$$

or finally

$$\mathfrak{m} = \frac{\ell_s^2}{4\lambda\mu}\int_{-1}^{+1}\int_{-1}^{+1}\Pi_e^t\mathfrak{m}\,\Pi_e\, d\xi\, d\eta = \frac{\ell_s^2}{4\lambda\mu}\, a_e^t\left[\iint \omega_e^t\mathfrak{m}\,\omega_e\, d\xi\, d\eta\right]a_e \qquad (II,138)$$

Note the important, and at first surprising result that translational (or rotational) inertia gives, in general, rise not only to lumped translational (or rotational) inertias, but also to lumped rotational (translational) inertias at the four nodal points. If $\mathfrak{m}$ is only given at the four corners of an element it is reasonable to describe a variation for $\mathfrak{m}$ in accordance with Eq. 11 this more general theory is rehearsed in Ref.30. Here we restrict ourselves to a homogeneous element of constant thickness t and reproduce in Table II.7 the matrix expression for $\mathfrak{m}$ in a form most suitable for computer operations using ASKA. We may, of course, carry out explicitly the matrix operations in Eq. (138), the corresponding result may be found in Ref.30. The reader will observe that the pure translational component of $\mathfrak{m}$ is as to be expected formally similar to Eq.(129) for the generalized static force in the z -direction.

Having established $\mathfrak{m}$ for a parallelogram element in the basic co-ordinate system the total mass matrix M of the plate corresponding to the stiffness K is found from the congruent Boolean transformation (120) which reads here,

$$M = a^t m a \qquad (II,139)$$

The above derivation of m may be applied either to an oblique or a cartesian system Oxy or $Ox'y'$ respectively as long as the appropriate a_e is selected. Alternatively, having obtained m explicitly in one co-ordinate system, we may use the transformations (39,40) to find m for the other.

II.8 Combined Effect of Transverse and In-Plane Loads; Buckling

The developments of the last Section may be used to establish the equivalent nodal loads arising from a set of known membrane stresses

$$\sigma_{xx}, \sigma_{yy}, \sigma_{xy}$$

which for a parallelogram element are, in general, understood to be specified in the oblique directions. The equivalent nodal loads associated with the displacement vector ρ are, in accordance with the classical plate theory, dependent on the rotations $\vartheta = \frac{\partial w}{\partial y}$, $\varphi = -\frac{\partial w}{\partial x}$ (see e.g. Morley[20]) Hence they may be derived by considering a pseudo-rotational inertia

$$t\sigma_i = \begin{bmatrix} \sigma_{xx} t & \sigma_{yx} t \\ \sigma_{xy} t & \sigma_{yy} t \end{bmatrix} \qquad (II,140)$$

in place of

$$\frac{i^2}{3^2} \begin{bmatrix} 1 & c \\ c & 1 \end{bmatrix}$$

and remembering the difference of definition in the oblique stresses between Morley[20] and the present publication.

Assuming for the sake of generality the joint presence of transverse loads, whose effect is approximated as in Eq.(129), we obtain for an element with constant thickness t the generalized load matrix

$$P = \frac{p_0 l^3}{16\lambda\mu} S\, a_e^t \vartheta^t \alpha \vartheta a_e \rho_v$$

$$\frac{\sigma_0 t l^2}{16\lambda\mu} S\, a_e^t \vartheta_i^t \left[\omega_{xx} \lambda^2 \mathcal{B}_1 + \omega_{yy} \mu^2 \mathcal{B}_2 - \omega_{xy} \lambda\mu \mathcal{B}_3 \right] \vartheta_i a_e \rho \qquad (II,141)$$

where

$$\sigma_{xx} = \sigma_0 \omega_{xx}, \quad \sigma_{yy} = \sigma_0 \omega_{yy}, \quad \sigma_{xy} = \sigma_0 \omega_{xy} \qquad (II,141a)$$

The change of sign of the term in ω_{xy} in Eq.(141) against that of the corresponding term in Table II.7 is due to the definition of φ as $-\frac{\partial w}{\partial x}$. Eq.(141) yields in conjunction with the stiffness matrix K all the necessary data to set up the equation governing the buckling of parallelogram plates. To this purpose we first denote the elastic stiffness of the plate no longer as K but as K_E,

given as before by Eq.(118). We next introduce the concept of geometrical stiffness k_G of the element first defined in Ref.3, which proves extremely useful in analysing large displacements and buckling phenomena (see also Chapter V). In the present case we find it helpful to specify the geometrical stiffnesses $k_{Gxx}, k_{Gyy}, k_{Gxy}$, associated with the stresses $\sigma_{xx}, \sigma_{yy}, \sigma_{xy}$ by

$$k_{Gxx} = \frac{\ell^2}{16}\frac{\lambda}{\mu}\, a_e^t \vartheta_i^t \mathcal{L}_1 \vartheta_i a_e$$

$$k_{Gyy} = \frac{\ell^2}{16}\frac{\mu}{\lambda}\, a_e^t \vartheta_i^t \mathcal{L}_2 \vartheta_i a_e \qquad \text{(II,142)}$$

$$k_{Gxy} = -\frac{\ell^2}{16}\, a_e^t \vartheta_i^t \mathcal{L}_3 \vartheta_i a_e$$

If the in-plane loading contains all component stresses $\sigma_{xx}, \sigma_{yy}, \sigma_{xy}$ in fixed ratios ω_{xx}, ω_{yy} ω_{xy}, the geometrical stiffness of the combined loading is

$$k_G = \frac{\ell^2 s}{16\lambda\mu}\, a_e^t \vartheta_i^t \left[\omega_{xx}\lambda^2 \mathcal{L}_1 + \omega_{yy}\mu^2 \mathcal{L}_2 - \omega_{xy}\lambda\mu \mathcal{L}_3\right] \vartheta_i a_e \qquad \text{(II,143)}$$

It is convenient for buckling investigations to apply a change of sign and to write

$$\sigma_b = -\sigma_0 \qquad \text{(II,144)}$$

Establishing next the total geometrical stiffness of the plate K_G by the Boolean transformation

$$K_G = a^t k_G a \qquad \text{(II,145)}$$

we find that the equilibrium condition for the plate takes the concise form

$$\left[K_E - \sigma_b t K_G\right] r = 0 \qquad \text{(II,146)}$$

or

$$\left[\frac{1}{\sigma_b t} I - K_E^{-1} K_G\right] r = 0 \qquad \text{(II,146a)}$$

which reduces the determination of the buckling stress to an eigenvalue problem.

II.9 The Plane Stress Problem of a Parallelogram Element; Basic Notions

For our theory on shells idealized into an assembly of parallelogram elements we also require the stiffness and generalized mass associated with a membrane state of stress. The first part of our problem has been solved in Ref.3 (Appendix IV), but it is convenient to reformulate our theory on the basis of natural displacements and stiffnesses.

Consider again a typical parallelogram element, see Fig.II.12. In general it is preferable to refer its stiffness, etc., to the oblique system $O x y$ and to define correspondingly the nodal displacements u_i, v_i . Since the membrane state has three rigid body freedoms, the complete specification of all eight nodal displacements requires the introduction of five natural modes. These are reproduced together with the rigid body modes in Fig.II.12 , whereby the definition of displacements u_2, v_1 and the rotation ψ is in accordance with Eqs.(3) and (39); see also Eq.(102) for the in-plane displacements under bending. Analoguous to Section II.3 we now introduce the two alternative (8 x 1) vectors describing the membrane state of deformation of an element. First the standard vector of the eight nodal displacements

$$\rho = \frac{1}{\ell}\{u_1 \quad v_1\} \tag{II,147}$$

where

$$u_1 = \{u_1 \quad u_2 \quad u_3 \quad u_4\}_1$$
$$v_1 = \{v_1 \quad v_2 \quad v_3 \quad v_4\}_1 \tag{II,147a}$$

and we find it convenient to apply a different sequence from that used in Section I. Also

$$\rho' = \{\rho_N \quad \rho_0\} \tag{II,148}$$

Here ρ_N is the (5 x 1) natural displacement vector and ρ_0 the (3 x 1) rigid body motion vector. For reasons of consistency we apply the same non-dimensional representation of the displacements as in the case of the bending of plates. Following the set of modes chosen in Fig.II.12 the (2 x 1) vector

$$\pi = \frac{1}{\ell}\{u_1 \quad v_1\} \tag{II,149}$$

specifying the oblique displacements u_1, v_1 at any point (ξ, η) of the plate may be expressed as

$$\pi = [\mathfrak{B}_N \quad \mathfrak{B}_0]\{\rho_N \quad \rho_0\} = \mathfrak{B}_e \rho' \tag{II,150}$$

where the (2 x 8) matrix $\mathfrak{B}_e$ composed of the (2 x 5) and (2 x 3) submatrices $\mathfrak{B}_N$ und $\mathfrak{B}_0$ is given by

$$\mathfrak{B}_e = \left[\begin{array}{ccccc:ccc} \xi/4 & \xi\eta/4 & 0 & 0 & \ell/8\mu & 1/4 & 0 & -\ell\xi/8\mu \\ 0 & 0 & \ell/4 & \xi\eta/4 & \xi/8\lambda & 0 & 1/4 & \xi\xi/8\lambda \end{array}\right] \tag{II,151}$$

In accordance with our procedure we now have to establish the relationship between ρ' and ρ and vice versa. We start with the slightly more evident form

$$\rho = A_e \rho' = \left[A_N \;\; A_o \right] \rho' \tag{II,152}$$

where

$$\left[A_N \,\middle|\, A_o \right] = \left[\begin{array}{cccccccc}
-1/4 & +1/4 & 0 & 0 & -1/8\mu & +1/4 & 0 & +s_4/8\mu \\
+1/4 & -1/4 & 0 & 0 & -1/8\mu & +1/4 & 0 & +s_4/8\mu \\
-1/4 & +1/4 & 0 & 0 & +1/8\mu & +1/4 & 0 & -s_4/8\mu \\
-1/4 & -1/4 & 0 & 0 & +1/8\mu & +1/4 & 0 & -s_4/8\mu \\
0 & 0 & -1/4 & +1/4 & -1/8\lambda & 0 & 1/4 & -s_4/8\lambda \\
0 & 0 & -1/4 & -1/4 & +1/8\lambda & 0 & 1/4 & +s_4/8\lambda \\
0 & 0 & +1/4 & +1/4 & +1/8\lambda & 0 & 1/4 & +s_4/8\lambda \\
0 & 0 & +1/4 & -1/4 & -1/8\lambda & 0 & 1/4 & -s_4/8\lambda
\end{array}\right] \tag{II,153}$$

Straightforward inversion of Eq. (153) by mere addition or subtraction of rows leads to

$$a_e = \begin{bmatrix} a_N \\ a_o \end{bmatrix} = d_{p1} b_e d_{p2} \tag{II,154}$$

where

$$b_e = \begin{bmatrix} b_N \\ b_o \end{bmatrix} = \left[\begin{array}{cccccccc}
-1 & +1 & +1 & -1 & 0 & 0 & 0 & 0 \\
+1 & -1 & +1 & -1 & 0 & 0 & 0 & 0 \\
0 & 0 & 0 & 0 & -1 & -1 & +1 & +1 \\
0 & 0 & 0 & 0 & +1 & -1 & +1 & -1 \\
\hline
-1 & -1 & +1 & +1 & -1 & +1 & +1 & -1 \\
+1 & +1 & +1 & +1 & 0 & 0 & 0 & 0 \\
0 & 0 & 0 & 0 & +1 & +1 & +1 & +1 \\
+1 & +1 & -1 & -1 & -1 & +1 & +1 & -1
\end{array}\right] \tag{II,155}$$

and

$$d_{p1} = \left[\tfrac{1}{\mu} I_2 \;\; \tfrac{1}{\lambda} I_2 \;\; 1 \;\; \tfrac{1}{\mu} \;\; \tfrac{1}{\lambda} \;\; \tfrac{1}{s_4} \right]$$

$$d_{p2} = \left[\mu I_4 \;\; \lambda I_4 \right] \tag{II,156}$$

Eq. (154) is for computational convenience split into a factorial matrix expression, in which b_e is an extended Boolean matrix and d_{p1}, d_{p2} are diagonal matrices dependent on the geometry of the parallelogram.

Having established a_e, the relation (150) may be expressed in terms of ρ as

$$\gamma = \omega_e a_e \rho' = \Pi_e \rho' \qquad (II,157)$$

where once more Π_e stands for

$$\Pi_e = \omega_e a_e \qquad (II,157a)$$

If it proves preferable to operate with a cartesian system $Ox'y'$, the corresponding a_e may be set up most conveniently by an additional transformation (see also Eqs. (93,94)). Thus, keeping in mind that ρ, ρ' express displacements, we find in conjunction with Eqs.(30,31)

$$a_{ec} = a_{es} \mathcal{F}_m \qquad (II,158)$$

where

$$\mathcal{F}_m = \begin{bmatrix} I_4 & 0 \\ c_\alpha I_4 & s_\alpha I_4 \end{bmatrix} \qquad (8 \times 8) \qquad (II,159)$$

and the suffices C and S are temporarily attached to a_e to denote cartesian and oblique systems of reference respectively.

The generalized forces (or rather moments) corresponding to the non-dimensional displacements ρ' and ρ are

$$P' = \{ P_N \quad P_o \} \qquad (8 \times 1) \qquad (II,160)$$

and

$$P = \{ P_1 \quad P_2 \quad P_3 \quad P_4 \} \qquad (8 \times 1) \qquad (II,161)$$

where

$$P_i = l \{ U_i \quad V_i \} \qquad (2 \times 1) \qquad (II,161a)$$

If the resultant surface and body forces on the element are zero, relationship (99) holds again, and

$$P = a_N^t P_N \qquad (II,162)$$

Assume next that at any point (x,y) of the plate there act a generalized force

$$\mathcal{R} = l \{ P_{ox} \quad P_{oy} \} \qquad (II,163)$$

We find that the kinematically equivalent nodal forces are given by

$$P_e = \Pi_e^t \mathcal{R} \qquad (II,164)$$

The reader is also referred to Sections II.3,6,the basic argumentation of which is applicable to the present case.

II.10 Stiffness and Lumped Mass of a Membrane. Parallelogram Element

We now apply the (2 x 5) natural mode matrix ϖ_N of Eqs.(150, 151) to the determination of the natural stiffness k_N . The strain vector ε in oblique co-ordinates is expressed (see also Eq.(104), as

$$\varepsilon = \alpha_N \rho_N \tag{II,165}$$

where

$$\alpha_N = \vartheta \varpi_N \tag{II,166}$$

and ϑ is the differential operator

$$\vartheta^t = \begin{bmatrix} 2\lambda\frac{\partial}{\partial\xi} & 0 & 2\frac{\mu}{\sqrt{2}}\frac{\partial}{\partial\eta} \\ 0 & 2\mu\frac{\partial}{\partial\eta} & 2\frac{\lambda}{\sqrt{2}}\frac{\partial}{\partial\xi} \end{bmatrix} \tag{II,167}$$

Using Eqs. (150, 151) we find

$$\alpha_N = \frac{1}{2}\begin{bmatrix} \lambda & \lambda\eta & 0 & 0 & 0 \\ 0 & 0 & \mu & \mu\xi & 0 \\ 0 & \frac{\mu\xi}{\sqrt{2}} & 0 & \frac{\lambda\eta}{\sqrt{2}} & \frac{1}{\sqrt{2}} \end{bmatrix} \tag{II,168}$$

The natural stiffness k_N may now be established via Eq.(108) and becomes here

$$k_N = \frac{E'\ell^2}{4\lambda\mu} S_\alpha \int_{-1}^{+1}\int_{-1}^{+1} t\, \alpha_N^t \vartheta\, \alpha_N \, d\xi\, d\eta \tag{II,169}$$

For an element of constant thickness t we obtain

$$k_N = \frac{E't\ell^2}{4} S_\alpha \begin{bmatrix} \nu_{11}\left(\frac{\lambda}{\mu}\right) & 0 & \nu_{12} & 0 & \frac{\nu_{13}}{\mu} \\ 0 & \frac{1}{3}\left[\nu_{11}\left(\frac{\lambda}{\mu}\right)+\nu_{33}\left(\frac{\mu}{\lambda}\right)\right] & 0 & \frac{1}{3}\left[\nu_{13}\left(\frac{\lambda}{\mu}\right)+\nu_{23}\left(\frac{\mu}{\lambda}\right)\right] & 0 \\ \nu_{12} & 0 & \nu_{22}\left(\frac{\mu}{\lambda}\right) & 0 & \frac{\nu_{23}}{\lambda} \\ 0 & \frac{1}{3}\left[\nu_{13}\left(\frac{\lambda}{\mu}\right)+\nu_{13}\left(\frac{\mu}{\lambda}\right)\right] & 0 & \frac{1}{3}\left[\nu_{22}\left(\frac{\mu}{\lambda}\right)+\nu_{33}\left(\frac{\lambda}{\mu}\right)\right] & 0 \\ \frac{\nu_{13}}{\mu} & 0 & \frac{\nu_{23}}{\lambda} & 0 & \frac{\nu_{33}}{\lambda\mu} \end{bmatrix} \tag{II,170}$$

which may be split into two component matrices depending only on the elastic constants and pre- and postmultiplied with diagonal matrices containing the non-dimensional parameters λ and μ. We may now establish the full (8 x 8) membrane stiffness matrix $\mathbf{k}_M$ based on the displacement vector ρ by the standard transformation

$$\mathbf{k}_M = \mathbf{a}_N^t \mathbf{k}_N \mathbf{a}_N \qquad (II,171)$$

which may be based either on an oblique or cartesian system of axes. In this analysis of a pure membrane state of stress it is preferable to adopt the sequential order

$$\bar{\rho} = \frac{1}{\ell}\left\{ u_1 \quad v_1 \quad u_2 \quad v_2 \quad u_3 \quad v_3 \quad u_4 \quad v_4 \right\} \qquad (II,172)$$

for the displacements. The associated stiffness matrix $\mathbf{k}_M$ is easily established using Boolean location matrices $\mathbf{T}$ as in Ref.3.

The total stiffness $\mathbf{K}$ of the membrane is set up by the congruent Boolean transformation Eqs.(I,24) and (118) . For any given external load vector $\mathbf{R}$ and initial load vector $\mathbf{J}$ on the elements, the displacements are found by the standard Eqs.(I,25) and (117) ; strains and stresses are then easily determined.

We conclude this Section by deriving the kinematically consistent lumped mass matrix $\mathbf{m}_M$ associated with the displacement function $\boldsymbol{\varpi}_e$. To this purpose we first relate the (2 x 2) matrices $\mathbf{m}_s$ and $\mathbf{m}_c$ corresponding to a mass m per unit area, and associated with the oblique and cartesian systems Oxy and $Ox'y'$ respectively. We write

$$\mathbf{m}_s = \ell^2 \begin{bmatrix} m_{xx} & m_{xy} \\ m_{yx} & m_{yy} \end{bmatrix} \quad , \quad \mathbf{m}_c = m\ell^2 \mathbf{I}_2 \qquad (II,173)$$

Considering the amplitude of kinetic energy and applying the transformation of Eqs. (29, 31) we obtain

$$\mathbf{m}_s = \frac{m\ell^2}{S_\alpha^2} \begin{bmatrix} 1 & -c_\alpha \\ -c_\alpha & 1 \end{bmatrix} \qquad (II,173a)$$

The required (8 x 8) lumped mass matrix $\mathbf{m}$ becomes then

$$\mathbf{m} = \frac{m\ell^4}{4\lambda\mu S_\alpha} \mathbf{a}_e^t \left[\int_{-1}^{+1} \int_{-1}^{+1} \boldsymbol{\varpi}_e^t \begin{bmatrix} 1 & -c_\alpha \\ -c_\alpha & 1 \end{bmatrix} \boldsymbol{\varpi}_e \, d\xi \, d\eta \right] \mathbf{a}_e \qquad (II,174)$$

the detailed derivation of which is straightforward.

However, it proves simpler to derive first the cartesian mass matrix $\mathbf{m}_c$ proceeding directly from an alternative definition of $\boldsymbol{\Pi}_e$ corresponding to non-dimensional unit nodal displacements in the cartesian directions. We easily confirm that $\boldsymbol{\Pi}_e$ is then the diagonal supermatrix

$$\boldsymbol{\Pi}_e = \begin{bmatrix} \boldsymbol{\Pi}_{e_1} & & \boldsymbol{\Pi}_{e_1} \end{bmatrix} \qquad (2 \times 8) \qquad \text{(II, 175)}$$

where $\boldsymbol{\Pi}_{e_1}$ is the (1×4) submatrix.

$$\boldsymbol{\Pi}_{e_1} = \frac{1}{4}\begin{bmatrix} (1-\xi)(1-\eta) & (1+\xi)(1-\eta) & (1+\xi)(1+\eta) & (1-\xi)(1+\eta) \end{bmatrix} \qquad \text{(II, 175a)}$$

Here ξ and η are referred to the oblique axes. The mass matrix $\mathbf{m}_c$ is now

$$\mathbf{m}_c = \frac{m\ell^4}{4\lambda\mu} s_\alpha \int_{-1}^{+1}\int_{-1}^{+1} \boldsymbol{\Pi}_e^t \boldsymbol{\Pi}_e \, d\xi \, d\eta \qquad \text{(II, 176)}$$

The integration in the oblique sense is straightforward and we find

$$\mathbf{m}_c = \frac{m\ell^4}{36\lambda\mu} s_\alpha \begin{bmatrix} \mathbf{G}_m & \mathbf{0}_4 \\ \mathbf{0}_4 & \mathbf{G}_m \end{bmatrix} \qquad \text{(II, 176a)}$$

where

$$\mathbf{G}_m = \begin{bmatrix} 4 & 2 & 1 & 2 \\ 2 & 4 & 2 & 1 \\ 1 & 2 & 4 & 2 \\ 2 & 1 & 2 & 4 \end{bmatrix} \qquad \text{(II, 176b)}$$

We may next obtain $\mathbf{m}_s$ by the transformation

$$\mathbf{m}_s = \frac{1}{s_\alpha^2}\begin{bmatrix} s_\alpha \mathbf{I}_4 & -c_\alpha \mathbf{I}_4 \\ \mathbf{0}_4 & \mathbf{I}_4 \end{bmatrix} \mathbf{m}_c \begin{bmatrix} s_\alpha \mathbf{I}_4 & \mathbf{0}_4 \\ -c_\alpha \mathbf{I}_4 & \mathbf{I}_4 \end{bmatrix} \qquad \text{(II, 177)}$$

which derives from Eqs. (29, 31). The final result is

$$m_s = \frac{m\ell^4}{36\lambda\mu s_\alpha}\begin{bmatrix} G_m & -c_\alpha G_m \\ -c_\alpha G_m & G_m \end{bmatrix} \qquad (II,178)$$

Having m_s or m_c for a single element, the total lumped mass matrix associated with the membrane state of stress is determined from the Boolean transformation of the type (138).

This completes the basic analysis of the membrane state of stress of a parallelogram element with four nodal points.

II.11 Stiffness and Lumped Mass of a Parallelogram Element Referred to the Basic Co-ordinate System $OXYZ$ of a Shell

We are now in a position to analyse the statics and dynamics of a shell consisting of an assembly of parallelogram elements; see Fig.II.13. To this purpose we first introduce a number of extensions to the definition of the relevant complete displacement vectors. The following two sequential orders of these vectors are thereby of importance

$$\rho = \{ \rho_x \ \rho_y \ \rho_z \ \vartheta \ \varphi \ \psi \} \qquad (24 \times 1) \quad (II,179)$$

and

$$\bar{\rho} = \{ \rho_{1d} \ \rho_{2d} \ \rho_{3d} \ \rho_{4d} \ \rho_{1r} \ \rho_{2r} \ \rho_{3r} \ \rho_{4r} \} \qquad (24 \times 1) \quad (II,180)$$

where, for example,

$$\rho_x = \{ u_1 \ u_2 \ u_3 \ u_4 \} \ , \quad \vartheta = \{ \vartheta_1 \ \vartheta_2 \ \vartheta_3 \ \vartheta_4 \} \ (4 \times 1) \quad (II,181a)$$

$$\rho_{1d} = \{ u_1 \ v_1 \ w_1 \} \ , \quad \rho_{1r} = \{ \vartheta_1 \ \varphi_1 \ \psi_1 \} \qquad (3 \times 1) \quad (II,181b)$$

The elemental stiffness and mass matrix associated with the vector ρ are now

$$k_e = \lceil k_M \ k_B \ 0 \rfloor \ , \quad m_e = \lceil m_M \ m_B \ 0 \rfloor \qquad (24 \times 24) \ (II,182)$$

In Eq.(182) the in-plane torsional stiffness and corresponding lumped mass are ignored; see, however, Ref.30. To obtain the stiffness $\bar{k}_e$ and mass $\bar{m}_e$ related to $\bar{\rho}$ we apply the congruent Boolean law location transformation

$$\bar{k}_e = T_e^t k_e T_e \qquad \bar{m}_e = T_e^t m_e T_e \qquad (II,183)$$

where

$$T_e = \lceil T \quad T \rfloor \qquad (24 \times 24) \ (II,184)$$

and

$$T = \begin{bmatrix} E_{11} & E_{21} & E_{31} & E_{41} \\ E_{12} & E_{22} & E_{32} & E_{42} \\ E_{13} & E_{23} & E_{33} & E_{43} \end{bmatrix} \qquad (12 \times 12) \qquad (II, 184a)$$

Here E_{ij} are Boolean or location matrices of order (4x3) containing a single unit element in the position (i,j).

We next proceed to refer the matrices $\bar{k}_e$ and $\bar{m}_e$ to the common or basic co-ordinate system $OXYZ$ of the structure, which may be either oblique or cartesian, the position of the origin O being in this context of no relevance. To find the required transformation matrix, we have merely to use the relations (33) for the displacements and (44) for the rotations. Then let us define the (24 x 24) diagonal super matrix

$$\mathcal{F} = \begin{bmatrix} \mathcal{F}_d & \mathcal{F}_r \end{bmatrix} \qquad (II, 185)$$

where

$$\mathcal{F}_d = \begin{bmatrix} \mathcal{L} \mathcal{L}_\beta & \mathcal{L} \mathcal{L}_\beta & \mathcal{L} \mathcal{L}_\beta & \mathcal{L} \mathcal{L}_\beta \end{bmatrix} \qquad (12 \times 12) \qquad (II, 186)$$

and

$$\mathcal{F}_r = \begin{bmatrix} \frac{S_\alpha}{S_\beta} \mathcal{L}_\alpha \mathcal{L} & \frac{S_\alpha}{S_\beta} \mathcal{L}_\alpha \mathcal{L} & \frac{S_\alpha}{S_\beta} \mathcal{L}_\alpha \mathcal{L} & \frac{S_\alpha}{S_\beta} \mathcal{L}_\alpha \mathcal{L} \end{bmatrix} (12 \times 12) \quad (II, 186a)$$

Here the matrices $\mathcal{L}$, $\mathcal{L}_\alpha$, $\mathcal{L}_\beta$ are given by Eqs.(3) and (4). Eq.(185) is the most general transformation matrix and presumes that both the local $Oxyz$ and basic $OXYZ$ systems may be oblique. The simplification arising when either of these co-ordinate systems is cartesian is evident.

The elemental stiffness and mass matrix are now

$$k = \mathcal{F}^t \bar{k}_e \mathcal{F} \quad , \quad m = \mathcal{F}^t \bar{m}_e \mathcal{F} \qquad (II, 187)$$

and are of order (24 x 24).

The stiffness and mass matrices of the assembled structure are clearly

$$K = a^t k a \quad , \quad M = a^t m a \qquad (II, 188)$$

which may be used to solve any static or dynamic problem of a shell with the prescribed geometry via the standard relation

$$R = K r + a^t J \qquad (II,118)$$

The transformation of the complete nodal load (or rather moment) vector P is dual to that of Eq.(185) as may be immediately confirmed from Eqs.(32),(42),(43).

A number of examples computed at ISD show excellent agreement with exact (where available) and experimental results. One important aspect in the solution of these problems arises when four parallelogram elements attached to a nodal point are co-planar. In this case the kinematic freedom ψ at this nodal point is ignorable in the sense of Ref.3.

II.12 Anisotropic Triangular Element under Membrane and Bending Action, Basic Notions

A further element used by the writer over the last four years or so, in the analysis of shells is that of a triangular element under bending and membrane action. Similar investigations have been carried out by other authors, especially by the active group at Berkeley under R.W.Clough[22,23]. All investigators stress the positive aspects of the triangular element which arise from its adaptability but note at the same time some serious shortcomings due to a partial satisfaction of the kinematic compatibility conditions at the boundary. Thus we have within the Matrix Displacement method the rather unusual example of a type of element whose deficiency with respect to kinematic compatibility does not automatically ensure convergence to the exact result as the number of elements is increased. At the same time, the author, as he pointed out in his Main Lecture[31] to the Royal Aeronautical Society, had relatively good experience as shown in a number of examples with his own procedure initiated in 1962 based on the natural flexibility or stiffness concept[3].

In the following Section, this unpublished theory to which he first referred publicly in his Trondheim Lectures[34], at the beginning of 1963 is rehearsed. As in the original analysis of triangular elements under plane stress three nodal points are assigned at the vertices to each triangular element. A more elaborate theory, corresponding to that in Ref.15 is to appear in a forthcoming publication[30]. After completion of this work the author's attention was drawn to Ref.23, where Clough discussesd succinctly some of the shortcomings of the past approaches to the triangular element.

We start with some basic geometrical and numerical matrices required in the main theory. First, we introduce the (3 x 3) diagonal matrices of the lengths and cosines of the included angles,

$$l = \begin{bmatrix} l_\alpha & & \\ & l_\beta & \\ & & l_\gamma \end{bmatrix} \qquad (II,189)$$

$$c = \begin{bmatrix} c_\alpha & & \\ & c_\beta & \\ & & c_\gamma \end{bmatrix} \qquad (II,190)$$

and the eccentricity matrix μ of the vertices (Fig.II.15) with respect to the opposite side

$$\mu = \begin{bmatrix} \mu_\alpha & & \\ & \mu_\beta & \\ & & \mu_\gamma \end{bmatrix} = l^{-1} \begin{bmatrix} l_+^2 - l_-^2 \end{bmatrix} l^{-1} \qquad (3 \times 3)\ (II,191)$$

where the meaning of the suffices + and - corresponds to that in Ref.3. Another basic matrix required in the analysis is

$$A = \begin{bmatrix} 1 & c_\gamma^2 & c_\beta^2 \\ & 1 & c_\alpha^2 \\ \text{symmetric} & & 1 \end{bmatrix} \qquad (3 \times 3) \qquad (II,192)$$

We next form three (9 x 9) diagonal supermatrices whose diagonal elements of order (1 x 3) contain, in turn, the direction cosines of the sides, in-plane normals and out-plane normals, denoted by subscripts T, N, V respectively. The three sets of axes T, N, V form in each case, as shown in Fig.II.15 a right-hand coordinate system. We write

$$\mathcal{L}_T = \begin{bmatrix} \mathcal{L}_{T\alpha} & \mathcal{L}_{T\beta} & \mathcal{L}_{T\gamma} \end{bmatrix} \qquad (9 \times 9) \qquad (II,193)$$

$$\mathcal{L}_N = \begin{bmatrix} \mathcal{L}_{N\alpha} & \mathcal{L}_{N\beta} & \mathcal{L}_{N\gamma} \end{bmatrix} \qquad (9 \times 9) \qquad (II,194)$$

$$\mathcal{L}_V = \begin{bmatrix} \mathcal{L}_v & \mathcal{L}_v & \mathcal{L}_v \end{bmatrix} \qquad (9 \times 9) \qquad (II,195)$$

No suffix is required for $\mathcal{L}_V$ since the three axes vertical to the plane of the triangle are necessarily parallel. Refs.3, 15 indicate how $\mathcal{L}_{T_i}$ is set up in the computer. For $\mathcal{L}_N$ and $\mathcal{L}_V$ we may construct a number of matrix formulae, but we only reproduce here a pair of expressions which, although not the simplest, are symmetrical. Thus, for $\mathcal{L}_N$

$$\mathcal{L}_N = \frac{l_+ l_-}{2\Omega} \mathcal{L}_T \left[\mathcal{L}_{T-}^t \mathcal{L}_{T+} - \mathcal{L}_{T+}^t \mathcal{L}_{T-} \right] \qquad (II,194a)$$

The advance and regress orders + and - refer in the present case to the diagonal submatrices, but in the following formula for $\mathcal{L}_V$,

$$\mathcal{L}_V = \mathcal{L}_{N+} \mathcal{L}_{T-}^d - \mathcal{L}_{N-} \mathcal{L}_{T+}^d \qquad (II,195a)$$

$\mathcal{L}_{T-}^d$, $\mathcal{L}_{T+}^d$ are read in one order as diagonal (9 x 9) matrices. In contrast to Eq.(194a) the suffixes + and - indicate that the elements within each submatrix are advanced or regressed respectively. We also require the following difference and addition matrices

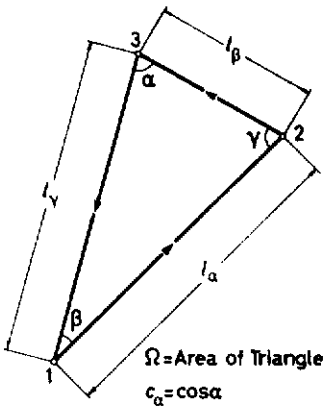

Basic Geometry of Triangle

Fig.II.14

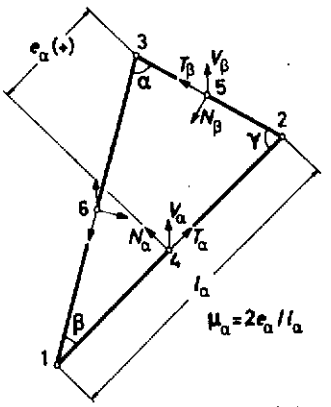

Right-Handed System of Axes *T,N,V* Based on Each Side of Triangle

Fig. II.15

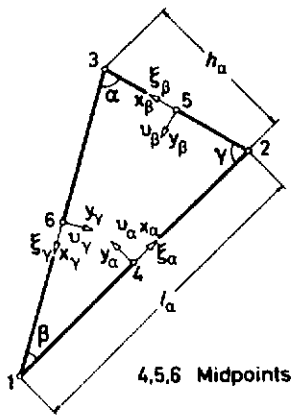

Coordinate Systems ξ,υ Based on Each Side of Triangle

Fig.II.16

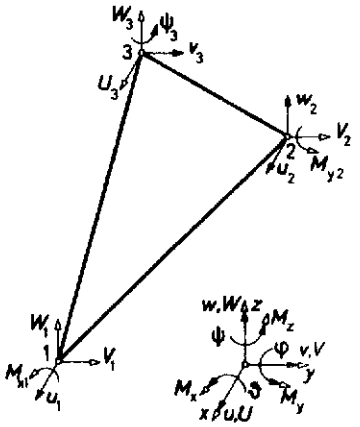

Cartesian Definition of Forces (Moments) and Displacements (Rotations)

Fig.II.17

$$D = \begin{bmatrix} -I_3 & I_3 & O_3 \\ O_3 & -I_3 & I_3 \\ I_3 & O_3 & -I_3 \end{bmatrix} \quad (9 \times 9) \qquad (II,196)$$

$$A = \begin{bmatrix} I_3 & I_3 & O_3 \\ O_3 & I_3 & I_3 \\ I_3 & O_3 & I_3 \end{bmatrix} \quad (9 \times 9) \qquad (II,197)$$

$$D_3 = \begin{bmatrix} -1 & 1 & 0 \\ 0 & -1 & 1 \\ 1 & 0 & -1 \end{bmatrix} \quad (3 \times 3) \qquad (II,198)$$

Finally, following Fig.I.16 we use two kinds of non-dimensional co-ordinates. Firstly we have, as in Ref.15

$$\xi_\alpha = 2x_\alpha/l_\alpha \quad , \quad \xi_\beta = 2x_\beta/l_\beta \quad , \quad \xi_\gamma = 2x_\gamma/l_\gamma \qquad (II,199)$$

which is formed as a diagonal matrix

$$\xi = \begin{bmatrix} \xi_\alpha & \xi_\beta & \xi_\gamma \end{bmatrix} \quad (3 \times 3) \qquad (II,200)$$

and secondly

$$\upsilon_\alpha = y_\alpha/h_\alpha \quad , \quad \upsilon_\beta = y_\beta/h_\beta \quad , \quad \upsilon_\gamma = y_\gamma/h_\gamma \qquad (II,201)$$

In contrast to Section I.3 we use here the symbol υ in place of ξ for the natural triangular co-ordinates.

II.13 Natural and Cartesian Definition of Displacements and Forces, Elastic Properties

As in our main account of the Matrix Displacement method in Chapter I two sets of displacements are required for the analysis, denoted as natural and cartesian ones. The procedure includes in each case the effect of membrane action.

We start with the complete cartesian force and displacement vectors which are arranged in the sequence

$$P = \{P_d \quad P_r\} \qquad \varrho = \{\varrho_d \quad \varrho_r\} \ (18\times 1) \quad (II,202)$$

The suffices d and r stand for displacements (forces) and rotations or slopes (moments). We start by defining the submatrices P_d and P_r as

$$P_d = \{P_1 \quad P_2 \quad P_3\} \ , \ P_r = \{\Omega_1 \quad \Omega_2 \quad \Omega_3\} \ (9\times 1) \quad (II,203)$$

in which (see Fig. II.17)

$$P_i = \{U_i \quad V_i \quad W_i\} \ , \ \Omega_i = \{M_{xi} \quad M_{yi} \quad M_{xyi}\} \ (3\times 1) \quad (II,204)$$

Similarly, for the displacement vectors

$$\varrho_d = \{\varrho_1 \quad \varrho_2 \quad \varrho_3\} \ , \ \varrho_r = \{\omega_1 \quad \omega_2 \quad \omega_3\} \ (9\times 1) \quad (II,205)$$

in which

$$\varrho_i = \{u_i \quad v_i \quad w_i\} \ , \ \omega_i = \{\vartheta_i \quad \varphi_i \quad \psi_i\} \ (3\times 1) \quad (II,206)$$

We next define the natural forces and displacements, and assume that the membrane part is identical to that used in Refs. 3, 13 and corresponds to a constant strain or stress field. To understand the proposed procedure for the bending contribution, let us first consider in some detail the moment distribution in an element. In analogy to the method adopted in Ref. 3, but in contrast to the classical cartesian measure m_{xx}, m_{yy}, m_{xy}, we use the component moments $m_\alpha, m_\beta, m_\gamma$ acting parallel to the three sides $l_\alpha, l_\beta, l_\gamma$ respectively. Hence, the bending action at any point of the triangular element is represented by the (3 x 1) vector

$$m_N = \{m_\alpha \quad m_\beta \quad m_\gamma\} \qquad (II,207)$$

We observe that the true state of stress is obtained by the <u>superposition</u> of $m_\alpha, m_\beta, m_\gamma$; (see also the relevant discussion in Ref. 3). However, at variance with the membrane analysis of the triangular element, it is not possible to assume that the bending stresses or moments are constant over the triangle. This may be seen <u>inter alia</u> by the necessity of transferring shear forces, which requires varying bending moments. Let us also examine the number of kinematic degrees of freedom which enter into the bending of the plate. These are seen to be 3 x 3 = 9 representing one translation or deflexion and two slopes at each nodal point. The natural modes are hence 9 - 3 = 6. As such, we select here

three symmetric and three antisymmetric moment distributions m_S, m_A and corresponding deformations parallel to each side. In extension of Eq.(207), the vector m_N can now be written as

$$m_N = m_S + \frac{1}{3} m_A = \left[I_3 \quad \cdot \frac{1}{3} \right] \{ m_S \quad m_A \} \qquad (II,208)$$

where

$$m_S = \{ m_{S\alpha} \quad m_{S\beta} \quad m_{S\gamma} \}, \quad m_A = \{ m_{A\alpha} \quad m_{A\beta} \quad m_{A\gamma} \} \qquad (II,208a)$$

A simple argument on the equilibrium applied on either of the sides $(1,3)$, $(1,3_1)$, $(1,3_2)$ of the plate containing the triangle shown in Figs. II, 18, 19 leads to the expression

$$\{ T_{S\alpha} \quad T_{A\alpha} \} = \Omega \ell_\alpha^{-1} \{ m_{S\alpha} \quad m_{A\alpha} \} \qquad (II,209)$$

where $T_{S\alpha}, T_{A\alpha}$ are the measures of the resultant moments at the nodal points 1,2 acting in the plane of the side ℓ_α. No resultant occurs at 3. Corresponding expressions may be set up for the other two pairs of symmetric and antisymmetric component moments. The six generalized moments T_S and T_A and six corresponding slopes ϑ_S and ϑ_A shown in Figs. II.18.19 together with the appropriate units are the natural forces and displacements adopted here.* We should point out that the convention of symmetry and antisymmetry is in each case to be understood with respect to the midpoint of the corresponding side. Note that no transverse forces and nodal deflexions enter directly in this natural definition. With this background we write

$$P_N = \{ P_{NM} \quad P_{NB} \}, \quad \vartheta_N = \{ \vartheta_{NM} \quad \vartheta_{NB} \}_{(9\times1)} \qquad (II,210)$$

Here the submatrices of the force vector are

$$P_{NM} = \{ P_\alpha \quad P_\beta \quad P_\gamma \}_{(3\times1)}, \quad P_{NB} = \{ T_S \quad T_A \}_{(6\times1)} \qquad (II,211)$$

in which P_α, P_β, P_γ denote pairs of forces acting at the vertices in line with the corresponding sides (see Fig. II.20) and T_S, T_A are given by

$$T_S = \{ T_{S\alpha} \quad T_{S\beta} \quad T_{S\gamma} \}, \quad T_A = \{ T_{A\alpha} \quad T_{A\beta} \quad T_{A\gamma} \}_{(3\times1)} \qquad (II,212)$$

where T_{Si} and T_{Ai} are the aforementioned symmetric and antisymmetric nodal moments acting at the two vertices of the side ℓ_i, their vectorial direction being specified by $\mathcal{L}_{Ni}$.

---

* The reader is also referred to Ref.3, which analyses in a similar manner the much simpler problem of a beam.

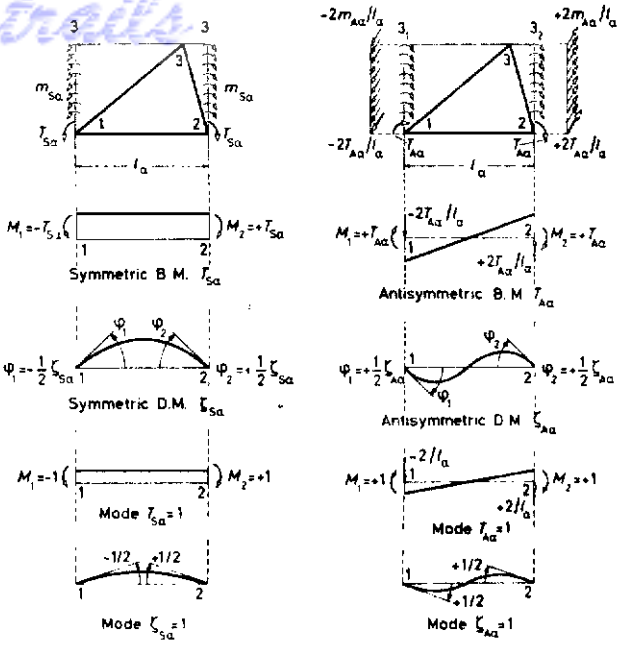

Symmetric Bending Mode of Plate Parallel to Side l_α Modes $T_{S\alpha}$ and $\zeta_{S\alpha}$

Fig II.18

Antisymmetric Bending Mode of Plate Parallel to Side l_α, Modes $T_{A\alpha}$ and $\zeta_{A\alpha}$

Fig. II.19

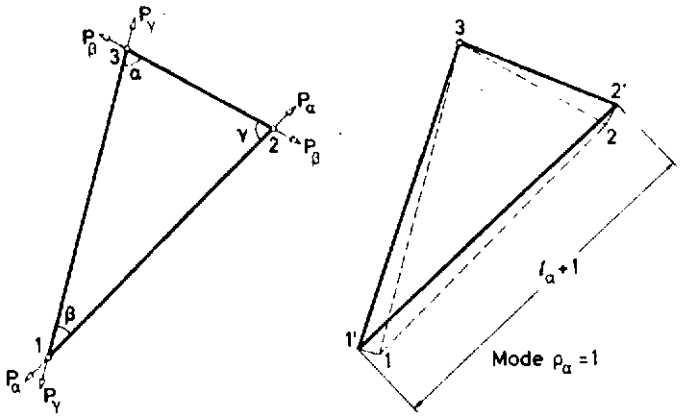

Natural Membrane Loads and Elongations

Fig. II.20

Correspondingly, the natural displacement vectors ϱ_{NH}, ϱ_{NB} are described by

$$\varrho_{NH} = \{\varrho_\alpha \quad \varrho_\beta \quad \varrho_\gamma\}^{(3\times1)},\ \varrho_{NB} = \{\jmath_S \quad \jmath_A\}^{(6\times1)} \qquad (II,213)$$

where ϱ_i is the total elongation of the side ℓ_i (Fig.II.20) and

$$\jmath_S = \{\jmath_{S\alpha} \quad \jmath_{S\beta} \quad \jmath_{S\gamma}\},\ \jmath_A = \{\jmath_{A\alpha} \quad \jmath_{A\beta} \quad \jmath_{A\gamma}\}^{(3\times1)} \qquad (II,214)$$

in which the $\jmath_S$ and $\jmath_A$ vectors describe symmetric and antisymmetric deformation modes.

It is a matter of some interest that the natural vectors should strictly have 18 - 6 = 12 rows and not 9 as used above. The reason for the reduced dimension is due to our ignoring of the in-plane rotational stiffness at the nodal points. As a result, when investigating a flat portion of a shell, we have to ignore a rotational degree of freedom, preferably associated with the axis nearest to the perpendicular of the plane in question. The procedure is akin to ignoring the membrane degrees of freedom described in Ref.3.

Following a similar but more complex argument to that applied in the case of the beam in Ref.3 we confirm the dual relations

$$\varrho_N = a_N \varrho \quad , \quad P = a_N^t P_N \qquad (II,215)$$

where

$$a = \left[\begin{array}{c} a_{NM} \\ \hline a_{NB} \end{array}\right] = \left[\begin{array}{cc} \mathcal{L}_T D & 0 \\ \hline 0 & \mathcal{L}_N D \\ 2\ell^{-1} D_3 \mathcal{L}_V & \mathcal{L}_N A \end{array}\right]^{(9\times18)} \qquad (II,216)$$

In Eq.(216) a_{NM} and a_{NB} are of dimensions (3 x 18) and (6 x 18) and refer to the membrane and bending actions respectively. All matrices used in Eq.(216) are given in Eqs.(189) to (200).

We also require, in what follows, the relation between total natural strains ε_N and natural component stresses σ_N as defined in Refs.3 and 13 in the form (see also Section I.5)

$$\varepsilon_N = \mathcal{E}_N^{-1} \sigma_N \qquad (II,217)$$

where $\mathcal{E}_N$ is the so-called (3 x 3) natural modulus of elasticity and may include arbitrary anisotropy (6 constants)[15]. The connection between $\mathcal{E}_N$ and the cartesian measure E is discussed in Ref.13.

II.14 Natural and Cartesian Stiffness of a Triangular Element

The derivation of the bending stiffness of a triangular element follows closely that developed in Refs.3 and 13 for the corresponding membrane stiffness. In particular the natural stiffness is established

here too by inversion of the flexibility matrix f_{NB} . The motivation for this preference cannot be adequately explained in the present limited space. To obtain f_{NB} , which relates P_{NB} and ϱ_{NB} by the matrix expression

$$\varrho_{NB} = f_{NB} P_{NB} \tag{II,218}$$

we first note that the vector m_N of Eq.(208) may be derived from P_{NB} via the formula (see Eqs.(208), (209), (211))

$$m_N = \frac{1}{\Omega} l \begin{bmatrix} I_3 & \xi \end{bmatrix} P_{NB} = b P_{NB} \tag{II,219}$$

To derive the (6 x 6) flexibility matrix we use the Unit Load method, which in the present case, after integration over the thickness t , leads to

$$f_{NB} = \int_V \sigma^t \varepsilon \, dV = 12 \int \frac{1}{t^3} b^t \varepsilon_N^{-1} b \, d\omega \tag{II,220}$$

For constant thickness the integration over the area is straightforward and yields

$$f_{NB} = \begin{bmatrix} f_{SS} & f_{SA} \\ f_{AS} & f_{AA} \end{bmatrix} = \frac{12}{\Omega t^3} \begin{bmatrix} l \varepsilon_N^{-1} l & \frac{1}{6} l \varepsilon_N^{-1} l \mu \\ \frac{1}{6} \mu l \varepsilon_N^{-1} l & \varepsilon_N^{-1} \cdot i_T^2 \end{bmatrix} \tag{II,221}$$

Here the meaning of the suffices in the submatrices f_{SS} , f_{SA} etc., is self-evident and the dot in $\varepsilon_N^{-1} \cdot i_T^2$ indicates an element by element multiplication of the two (3 x 3) matrices. i_T^2 may be considered as a (3 x 3) matrix of the squares of the radii of gyration with respect to the coordinate system ξ_α , ξ_β , ξ_γ . We have,

$$i_T^2 = \frac{1}{3} \left[l \left[2 I_3 - A \right] l - 2 l_- \varepsilon_- \varepsilon_+ l_+ \right] \tag{II,222}$$

and having established f_{NB} , we derive k_{NB} by direct inversion

$$k_{NB} = f_{NB}^{-1} \tag{II,223}$$

As a matter of fact, we may obtain an explicit matrix expression for k_{NB} , but omit this here. We next introduce the membrane stiffness from Refs.3, 13 in the form

$$k_{NM} = \frac{1}{\Omega t} l^{-1} \varepsilon_N l^{-1} \tag{II,224}$$

The complete natural stiffness k_N is then the (9 x 9) diagonal matrix

$$k_N = \begin{bmatrix} k_{NH} & \\ & k_{NB} \end{bmatrix} \tag{II,225}$$

Finally, the (18 x 18) cartesian stiffness based on the (18 x 1) vectors P, ρ is

$$k = a_N^t k_N a_N \tag{II,226}$$

The complete stiffness matrix K of the shell is obtained from our usual Boolean assembly with the matrix a (3,15). Hence the displacements and rotations at the nodal points derive from*

$$\tau = K^{-1} R \tag{II,227}$$

To find the stresses, we may use for the membrane components the method developed in Ref.3,13. Determination of the bending stresses may immediately proceed to cartesian components using the corresponding subvector of ρ. However, it is preferable first to establish $\rho_{NB} = a_{NB} \rho$, from which the natural strains and stresses may be deduced. A still better procedure uses the loading vector P_{NB} obtained from

$$P_{NB} = k_{NB} \rho_{NB} = k_{NB} a_{NB} \rho \tag{II,228}$$

Hence, the component moments and stresses are found from Eq.(219), where the determining matrix takes particularly simple forms at the vertices and the C.G. For example, the natural component at the vertex 3 is given by

$$b_3 = \frac{1}{\Omega} \begin{bmatrix} I_3 & \begin{bmatrix} \mu_\alpha & +1 & -1 \end{bmatrix} \end{bmatrix} \tag{II,229}$$

also at the C.G.

$$b_{CG} = \frac{2}{\Omega} \begin{bmatrix} I_3 & \frac{1}{3}\mu \end{bmatrix} \tag{II,229a}$$

where μ_3 is the eccentricity vector of the C.G.

Following our successful technique in the membrane case it is advisable to average at each nodal point or middle of the sides the cartesian vectors m of all adjoining triangles and hence derive the principal bending stresses.

* We cannot discuss here the derivation of the generalized force vector R arising from distributed static and inertia loads (see Ref.30).

II.15 Effect of Initial Strains

The final Section deals with the effect of initial strains due to plasticity, thermal actions, etc. The problem is effectively solved once the (9 x 1) natural initial displacement vector

$$\rho_{N\eta} = \{\rho_{M\eta} \quad \rho_{B\eta}\} \tag{II,230}$$

is established, whose notation and sequential order follows that of the second of Eqs.(210) for ρ_N, the suffix N being omitted in (230) for typographical economy. Let us assume that the initial strains imposed on the triangle are prescribed as six (3 x 1) natural vectors at the vertices 1,2,3 in the form (see in this connection Ref.16)

$$\begin{matrix} \eta_{M1} \;,\; \eta_{M2} \;,\; \eta_{M3} & \text{membrane components} \\ \eta_{B1} \;,\; \eta_{B2} \;,\; \eta_{B3} & \text{bending components} \end{matrix} \tag{II,231}$$

As far as the membrane vector $\rho_{M\eta}$ is concerned, a straighforward argument (e.g. application of the Unit Load method), using the assumed constant membrane state of elastic strain in the triangle, shows that the problem is equivalent to laying down an average value for $\overline{\eta}_M$ within the triangle. Hence, in accordance with Refs.3 and 13, the natural initial membrane load vector becomes

$$\rho_{M\eta} = l\,\overline{\eta}_M = \frac{1}{3} l \{\eta_{M1} + \eta_{M2} + \eta_{M3}\} \tag{II,232}$$

The initial load vector J_{NM} is hence

$$J_{NM} = -k_{NM}\rho_{M\eta} \tag{II,233}$$

Let us next consider the more complex determination of $\rho_{B\eta}$. The variation of the bending strain vector η_B within the triangle is taken to be linear* and this is most neatly expressed in terms of the given η_B at the vertices using the non-dimensional coordinates v of Eq.(201) in the form (note that $v_\alpha + v_\beta + v_\gamma = 1$)

$$\eta_B = v_\alpha \eta_{B3} + v_\beta \eta_{B1} + v_\gamma \eta_{B2} \tag{II,234}$$

To derive ρ_{NB}, we apply the Unit Load method and note that the generalized strain corresponding to the moment m_N is the initial curvature vector η_B/t assuming that the initial strain varies linearly across the thickness. We obtain for constant t

* The question is to be discussed in greater detail in another communication[30].

$$\rho_{N8} = \int \tfrac{1}{t} B^{t} \eta_{8}\, d\omega = \tfrac{1}{t}\left[\left\{I_3 \quad \tfrac{1}{2}\mu\right\} l \bar{\eta}_{8} - \tfrac{1}{6}\left\{0 \quad l\left[\lambda_{\alpha}\eta_{\beta 3} + \lambda_{\beta}\eta_{\beta 2} + \lambda_{\gamma}\eta_{\beta 1}\right]\right\}\right] \quad (11,235)$$

where

$$\bar{\eta}_{8} = \tfrac{1}{3}\left[\eta_{\beta 1} + \eta_{\beta 2} + \eta_{\beta 3}\right] \quad (11,236)$$

and $$\lambda_{\alpha} = c_{\alpha}\begin{bmatrix} 0 & -\frac{l_{\gamma}}{l_{\beta}} & \frac{l_{\beta}}{l_{\gamma}} \end{bmatrix}, \quad \lambda_{\beta} = c_{\beta}\begin{bmatrix} \frac{l_{\gamma}}{l_{\alpha}} & 0 & -\frac{l_{\alpha}}{l_{\gamma}} \end{bmatrix}$$

$$\lambda_{\gamma} = c_{\gamma}\begin{bmatrix} -\frac{l_{\beta}}{l_{\alpha}} & \frac{l_{\alpha}}{l_{\beta}} & 0 \end{bmatrix} \quad (11,237)$$

If $\eta_{3} = \bar{\eta}_{8}$ is constant over the triangle, Eq.(235) reduces to the physically evident formula

$$\rho_{8\eta} = \tfrac{1}{t}\left\{I_3 \quad \tfrac{1}{3}\mu\right\} l \eta_{8} \quad (11,238)$$

The corresponding initial natural load vector J_{N8} is hence

$$J_{N8} = -k_{N8}\rho_{8\eta} \quad (11,239)$$

and we finally obtain the (18 x 1) cartesian load vector J from the expression

$$J = a_{N}^{t}\left\{J_{NM} \quad J_{N8}\right\} \quad (11,240)$$

Eq.(240) reduces to a very simple form in the cases of isotropic elastic and thermal behaviour and constant differential thermal strain over the triangle thickness (see for example Ref.16). We omit this here for reasons of space and remember that a general purpose programme is necessarily based on the most general formulae (233), (239), (240).

11.16 Applications of the Matrix Displacement Method to Plates and Shells.

Our first applications of the matrix analysis to plates were naturally enough, to laterally loaded rectangular plates of uniform thickness with edge conditions for which exact solutions were known, i.e., edges simply supported. The agreement using a typical grid of 6 x 6 elements was good, but, at first surprisingly, the most troublesome boundary condition was that of simple support. However, the finite element approach being based upon the classical theory of thin plates, inevitably incorporates difficulties of the latter associated with such edge conditions. When laterally loaded parallelogram plates are analysed, whenever edges are simply supported, the convergence to a known result as a function of

the number of elements employed was still less satisfactory than for rectangular elements, the difficulties increasing with the angle of sweep. The classical thin plate theory predicts a singularity at the obtuse-angled corners, whereby the principal bending moments become infinite. This happens at these corners for all boundary conditions except where both edges are clamped or both are free. However, as mentioned above, difficulties even occur with rectangular, simply supported plates due to the form of boundary condition employed. For a simply supported edge of a rectangular plate, the true conditions are $\omega = 0$ and $m_x = 0$ at the edge (x = const). We seek a kinematic form for use in the Displacement method and set $\omega = \phi = 0$ along the edge (x = const.), whereas one would set $\omega = \theta = \phi = 0$ for a clamped edge (x = const). When one comes to the corner element, the condition $\phi = 0$ along (x = const.)imposes a clamping along the adjacent side (y = const) at the corner point. For a parallelogram plate the same applied, since the rotations are referred to the oblique coordinate system.

Two cures have been tried with success: first, a finer grid near the edges of the plate,giving elongated elements parallel to the plate edge, rather than using a finer net everywhere; this method yielded excellent results for rectangular plates. The second is to relax the boundary condition of zero rotation at the corner point itself. The latter works remarkably well with parallelogram plates, and this artifice appears to be justified, since there is no change in accuracy (even to the fifth significant figure) in the central deflection of a rectangular plate (where the singularity does not arise) due to this relaxed boundary condition.

Fig.II.21 shows the highly satisfactory degree of accuracy obtainable with a moderate number of elements for a simply supported square plate with uniform lateral loading, for which the exact solution is well known. When the plate is swept through 45 degrees (II.23), the source of comparative data is the result of an electric analogue investigation by Rushton (Ref.35). As always with the Displacement method, the stiffness is overestimated and so the calculated deflection is very slightly smaller than it should be. The maximum principal bending moments are, however, fractionally greater than given by Rushton. A case of interest to civil engineers is the 'swept bridge', i.e., a plate with two opposite edges simply supported and the other pair free. Our deflections, using 6 x 6 and 12 x 12 grids, lie respectively three and seven percent above a value obtained experimentally for 45-degree sweep, whereas a finite difference solution was 18 percent higher (Fig.II.22). When the plate is further swept, so that the angle at an acute corner is reduced to 30 degrees, the comparison is with Morley's[20] analytical version of the oblique coordinates theory (Fig.II.24). The matrix deflection is again slightly too small, but now the moments also. Typical data regarding our application, including times of computation, are given in Fig.II.25, and also illustration of the effect of grid modifications on the accuracy achieved and the numerical accuracy as a function of the size of calculation, i.e., grid fineness. There is clearly a point beyond which loss of numerical accuracy outweighs the better representation of the structure. The principal bending moments and deflection contours are also represented for simply supported elongated parallelogram plates in Figs. II.26.27 and for a rhomboid plate with central point load in Fig.II.28. Fig.II.29 gives a table of results for uniformly loaded, fully built-in plates of various sweep angles and aspect ratios. These are a few cases where a comparison by Morley

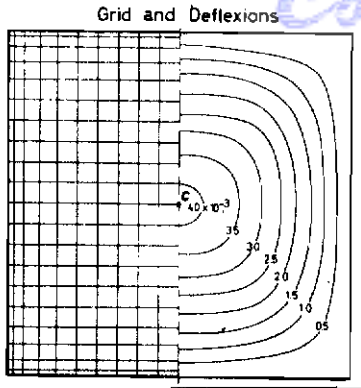

	Exact	D.M.
$w / \frac{pA^4}{D}$	4.06×10^{-3}	4.052×10^{-3}

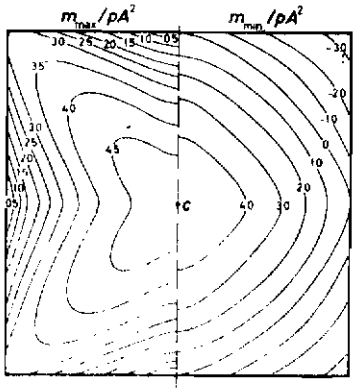

Principal Moments

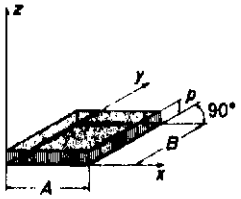

	Exact	D.M.
$m_{max,c}/pA^2$	4.79×10^{-2}	4.754×10^{-2}

Simply Supported Square Plate under Uniform Loading
Fig.II. 21

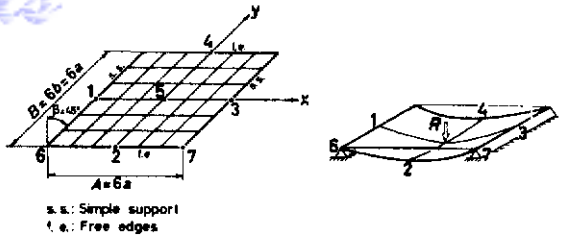

s. s.: Simple support
f. e.: Free edges

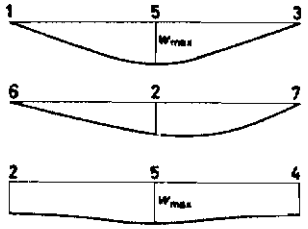

Deflexions

Point			
2 and 4	5		5
$\frac{m_{max}}{R}$	$\frac{m_{max}}{R}$	$\frac{m_{min}}{R}$	$\frac{w_{max}}{RA^2/D}$
0·09131 [0·0903]	0·393 [0·443] (0·370) ⟨0·384⟩	0·192 [0·237] (0·257) ⟨0·200⟩	0·0103 [0·0106] (0·0117) ⟨0·0099⟩

[ ] 12 x 12 Grid with Size of Elements Decreasing
( ) JENSEN, Finite Difference
⟨ ⟩ Test

Deflexions and Moments of a Skew Bridge under Concentrated Load R at Centre Fig.II.22

	Rushton	D M
$w_c / \frac{pA^4}{D}$	1.34×10^{-3}	1.29917×10^{-3}

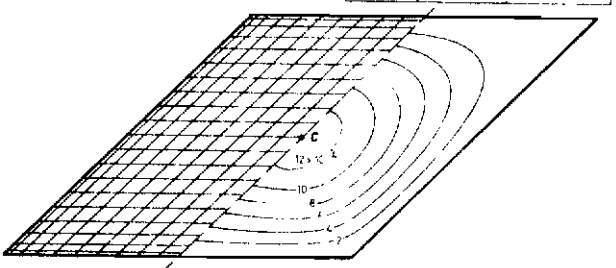

Grid and Deflexions

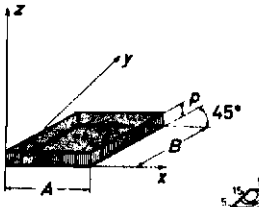

	Rushton	D M.
$m_{max,c}/pA^2$	0.0317	0.0324572
$m_{min,c}/pA^2$	0.0216	0.021424

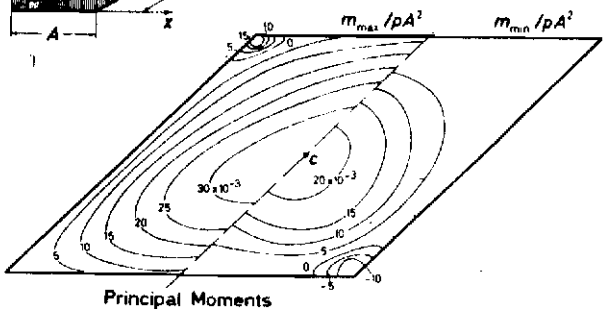

Principal Moments

Simply Supported Swept Plate under Uniform Loading
($\alpha = 45°$, $B = A$) Fig II. 23

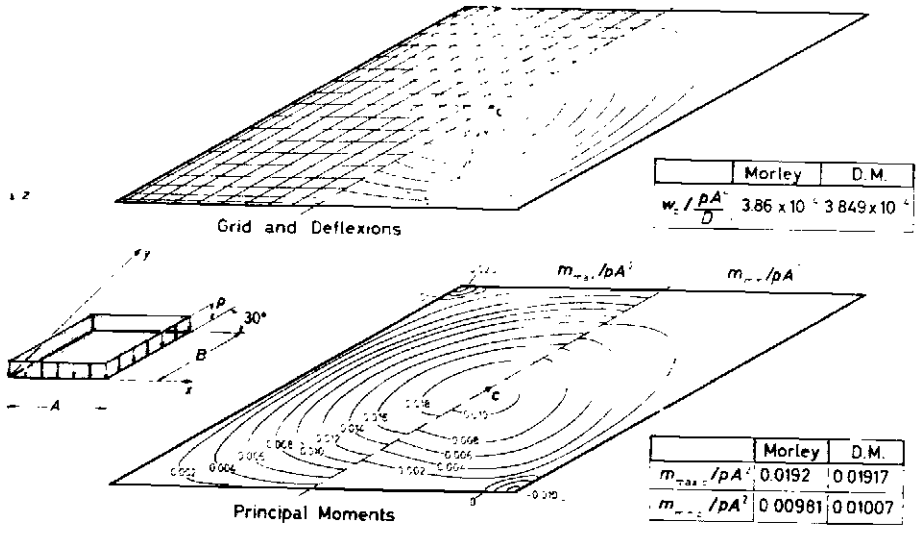

	Morley	D.M.
$w_c / \frac{pA^4}{D}$	3.86×10^{-3}	3.849×10^{-3}

	Morley	D.M.
$m_{max\,c}/pA^2$	0.0192	0.01917
$m_{min\,c}/pA^2$	0.00981	0.01007

Simply Supported Swept Plate under Uniform Loading ($\alpha = 30°$, $B = A$) Fig.II.24

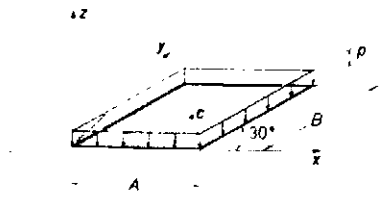

Number of Elements	Number of Unknowns	Computing Time without Parallel Processing	Numerical Accuracy of Solution
6 x 6	103	43s	> 5
12 x 12	415	4m 47s	> 4
20 x 20	1167	17m 52s	> 3 Dec Digits

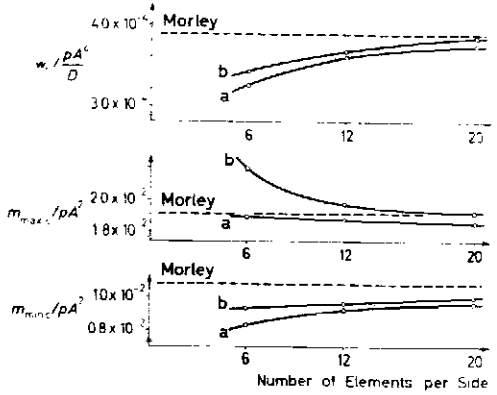

Deflexions and Principal Moments at Centre for Various Divisions of Plate

a: Plate Divided into Identical Elements
b: Size of Elements Decreasing towards the Edges

Simply Supported Swept Plate under Uniform Loading ($\alpha = 30°$, $B = A$)
Solution by Matrix Displacement Method Using Parallelogram Plate Elements Fig.II.25

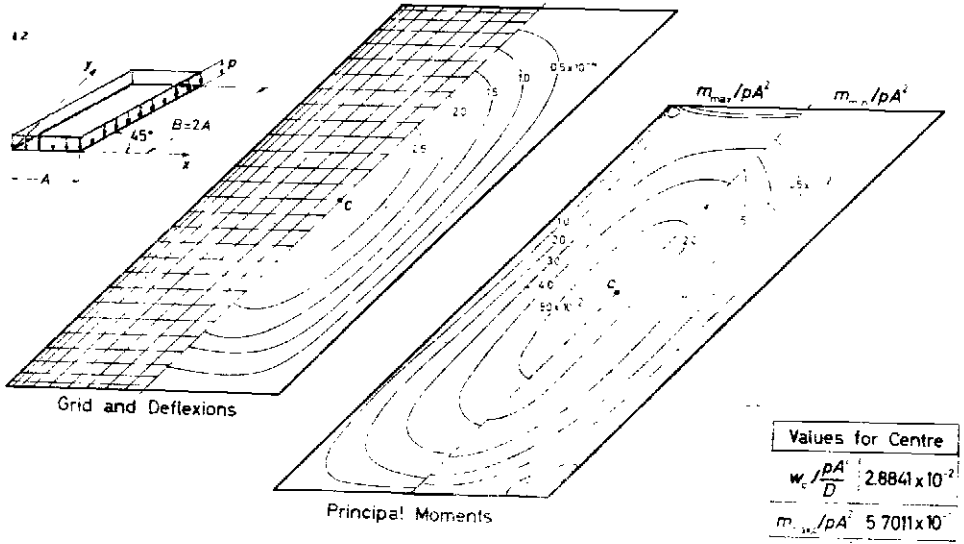

Values for Centre	
$w_c / \frac{pA^4}{D}$	2.8841×10^{-2}
$m_{max\,c}/pA^2$	5.7011×10^{-2}
$m_{min\,c}/pA^2$	2.1363×10^{-2}

Simply Supported Swept Plate under Uniform Loading ($\alpha = 45°$, $B = 2A$) Fig. II 26

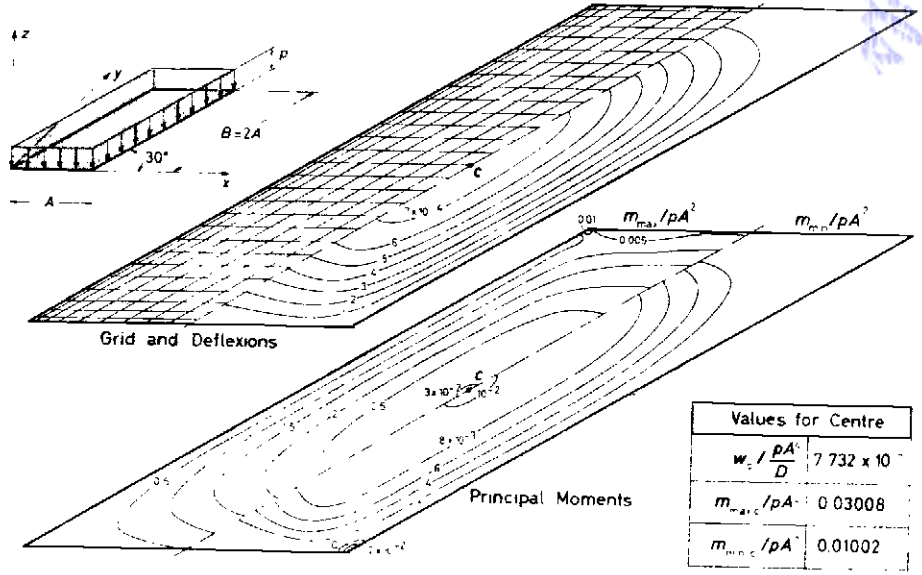

Values for Centre	
$w_c / \frac{pA^4}{D}$	7.732×10^{-3}
$m_{max\,c}/pA^2$	0.03008
$m_{min\,c}/pA^2$	0.01002

Simply Supported Swept Plate under Uniform Loading ($\alpha = 30°$, $B = 2A$) Fig II.27

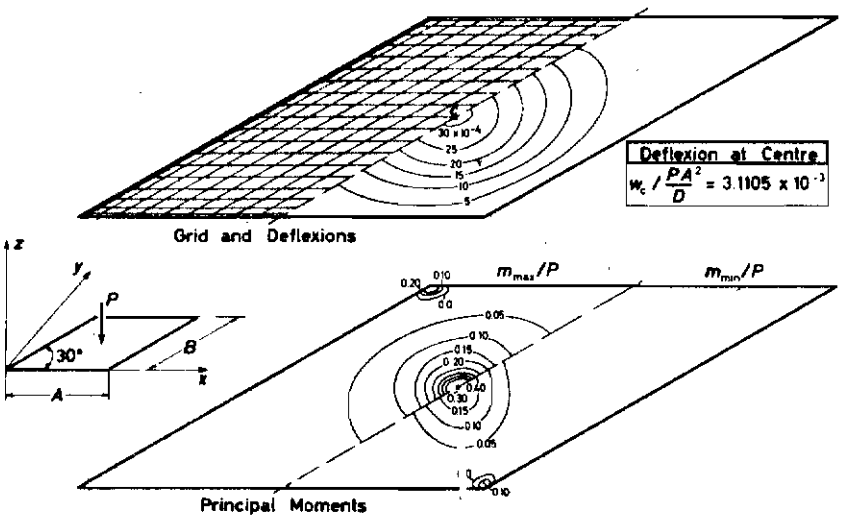

Simply Supported Swept Plate under a Concentrated Load
($\alpha = 30°$, $B = A$) Fig.II.28

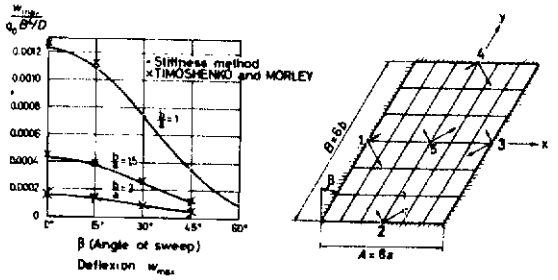

		Point					
		1 and 3		2 and 4		5	
Mode	β	m_1/q_0B^2	m_2/q_0B^2	m_1/q_0B^2	m_2/q_0B^2	m_1/q_0B^2	m_2/q_0B^2
1	0	-0·0135	-0·0489 (-0·0513)	-0·0489 (-0·0513)	-0·0135	0·0226 (0·0231)	0·0226 (0·0231)
	15°	-0·0119	-0·0399	-0·0399	-0·0199	0·0186	0·0232
	30°	-0·0081	-0·0275	-0·0275	-0·0081	0·0139	0·0202
	45°	-0·0040	-0·0139	-0·0139	-0·0040	0·0086	0·0158
	60°	-0·0013	-0·0046	-0·0013	-0·0048	0·0039	0·0084
1·5	0	-0·0092	-0·0327 (-0·0336)	-0·0237 (-0·0253)	-0·0062	0·0085 (0·0090)	0·0158 (0·0163)
	15°	-0·0084	-0·0279	-0·0183	-0·0055	0·0078	0·0149
	30°	-0·0062	-0·0208	-0·0124	-0·0036	0·0061	0·0126
	45°	-0·0036	-0·0121	-0·0063	-0·0018	0·0039	0·0090
	60°	-0·0015	-0·0051	-0·0006	-0·0022	0·0018	0·0049
2	0	-0·0058	-0·0198 (-0·0207)	-0·0137 (-0·0143)	-0·0032	0·0038 (0·0039)	0·0102 (0·0103)
	15°	-0·0054	-0·0179	-0·0096	-0·0029	0·0035	0·0096
	30°	-0·0042	-0·0139	-0·0066	-0·0020	0·0027	0·0078
	45°	-0·0026	-0·0087	-0·0037	-0·0011	0·0018	0·0063
	60°	-0·0012	-0·0041	-0·0004	-0·0015	0·0009	0·0027

( ) Results by Timoshenko, Morley

Deflexions and Bending Moments for a Fully Built-in Swept Plate under Uniform Loading Fig.II.29

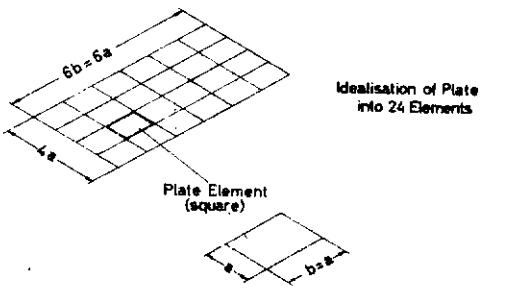

Idealisation of Plate into 24 Elements

f = Frequency cps

Mode	1	2	3	4	5
f/f_{exact}	1·000	1·002	1·007	1·008	1·010

Frequencies for Uniform Rectangular Simply Supported Plate

Matrix Displacement Solution by Finite Elements and Lumped Masses

Fig.II.30

or from Timoshenko[8] exists but, for the most part, we have filled it in with matrix results. Since the completion of this work, still more reliable data (not reproduced here) have been obtained with finer and graduated grids.

Using an eigenvalue subroutine and the kinematically consistent lumped mass matrix, extraordinarily good agreement was also obtained for the natural frequencies and mode shapes of uniform rectangular plates with simply supoorted edges (Fig.II.30). Of course, the analytical solutions being exact, afforded comparison to any desired level of accuracy. For the family of swept uniform cantilever plates shown in Fig.II.31, very good agreement with experiment was also achieved for their vibration frequencies. The calculated frequencies for the first eight modes are shown as a function of sweep angle up to 60 degrees. Agreement was still very good in the fifth mode, the highest for which the experimental data were available. Again, the consistent mass matrix was employed, of course, but rotational inertia was not taken into account. Using 25 elements as indicated, a typical time required on the computer for any one case (90 unknowns) was about four minutes. Another analogy, expounded in Section II.8, emerges when the rotational as well as the translational inertia of vibrating plates is taken into account; viz., the additional inertia matrix has the same form as the matrix for a loading directly proportional to the displacement curvature, i.e., as in buckling problems. Some buckling results for built-in rectangular and swept plates, shown in Fig.II.32, display remarkable agreement once again with analytical solutions. ($D = Et^3/12(1-\nu^2)$ is the usual plate stiffness). The maximum deviation quoted of three percent, using a 7 x 7 uniform grid, is reduced to one percent when a 12 x 12 grid is employed in swept plates. The cartesian shear loading case is something of a quirk amenable to solution by analytical means, whereas oblique shear, as is more commonly considered, is not. In Table II.8 we reproduce some data on the buckling of swept plates for different boundary conditions and aspect ratio. The accuracy of the results could have been improved by a graduation of the grid.

As to triangular plate elements to fit an arbitrary boundary, the first case tried was on a clamped rhomboid plate with 60-degree included angle under uniform lateral loading (Fig.II.36). The agreement with available theory and comparison with a corresponding parallelogram partitioning was quite good, using 72 elements in a 6 x 6 oblique grid, the central deflection being within about four percent of the theoretical; similar conclusions apply to the bending moments at the centre. As already mentioned, triangular plate elements do not necessarily satisfy kinematic compatibility between nodal points, so some loss of accuracy compared with parallelograms is to be expected. The results of an analysis of a circular plate under uniformly distributed load are shown in Figs. II.33.34 for two edge conditions, together with statistics regarding the computation in Fig.II.35.

II.17 Shells

One of our first exercises was on a spherical cap, loaded radially for simply-supported (Fig.II.37) and built-in edge (Fig.II.38) conditions. The same grid was used as for the circular plate mentioned above (Fig.II.35). The cases and loading chosen are ones for which analytical results were available

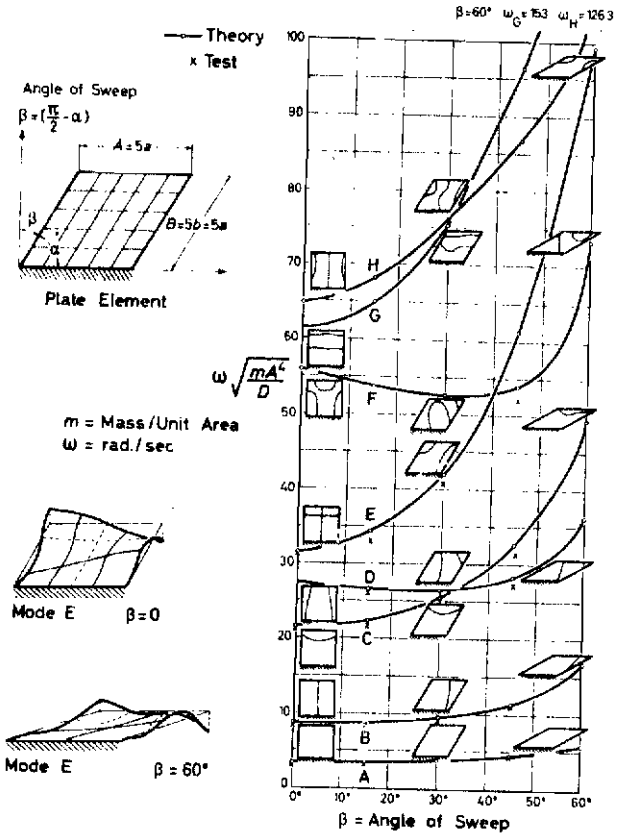

Frequencies and Modes for Swept Cantilever Plate

Fig.II.31

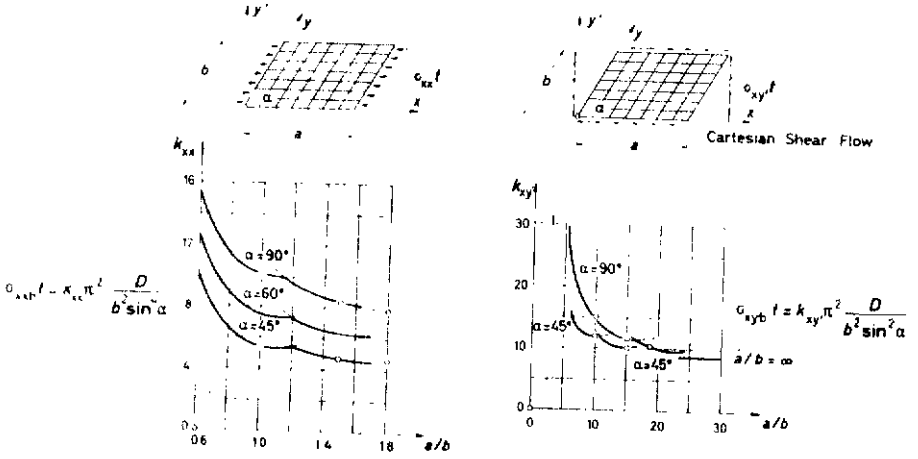

*Computed by Matrix Displacement Method

Maximum Difference from Results of Timoshenko and Wittrick for a 7 x 7 (12 x 12) Grid 3% (1%)

Buckling of Fully Built-in Oblique Plates

Fig.II.32

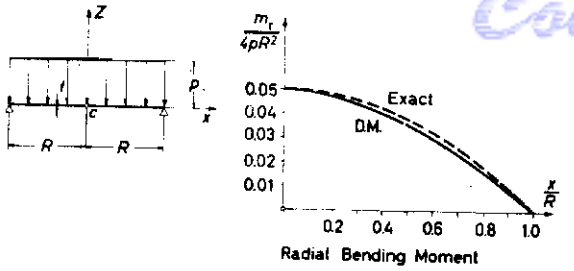

Values for Centre	Exact	D.M.
$\frac{w_c}{16pR^4/D}$	4.232×10^{-3}	4.175×10^{-3}
$\frac{m_c}{4pR^2}$	0.05	0.04997

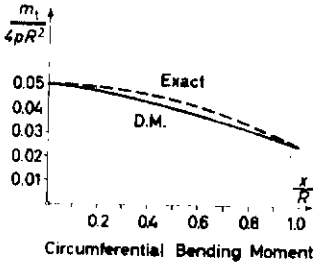

Simply Supported Circular Plate
under Uniform Loading (ν=0.2)

Fig.II.33

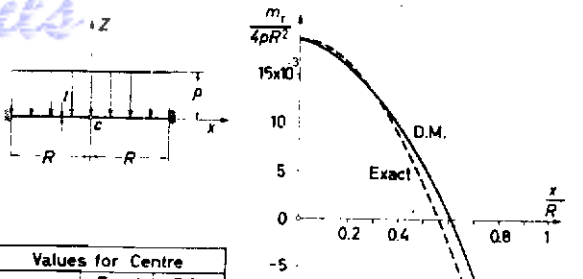

Values for Centre	Exact	D.M.
$\frac{w_c}{16pR^4/D}$	9.766×10^{-4}	9.650×10^{-4}
$\frac{m_c}{4pR^2}$	1.875×10^{-2}	1.886×10^{-2}

Values for Boundary	Exact	D.M.
$\frac{m_r}{4pR^2}$	-3.125×10^{-1}	-2.863×10^{-2}
$\frac{m_t}{4pR^2}$	-0.625×10^{-2}	-0.655×10^{-2}

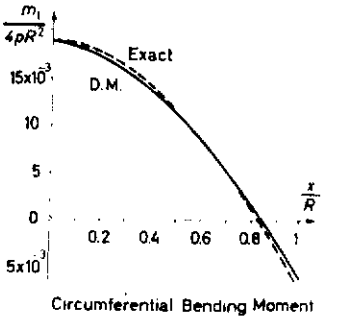

Built-in Circular Plate
under Uniform Loading (ν=0.2)

Fig.II.34

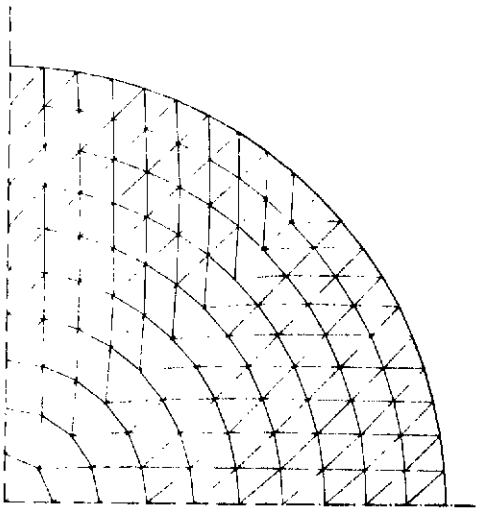

Grid for Quadrant of Plate
(also used for Spherical Shell)

	Simply Supported	Built-in
Number of Elements	200	200
Number of Unknowns	322	280
Computer time (without parallel processing)	11m 30s	8m 53s

Circular Plates under Uniform Pressure
Analysis by Matrix Displacement Method

Fig. II. 35

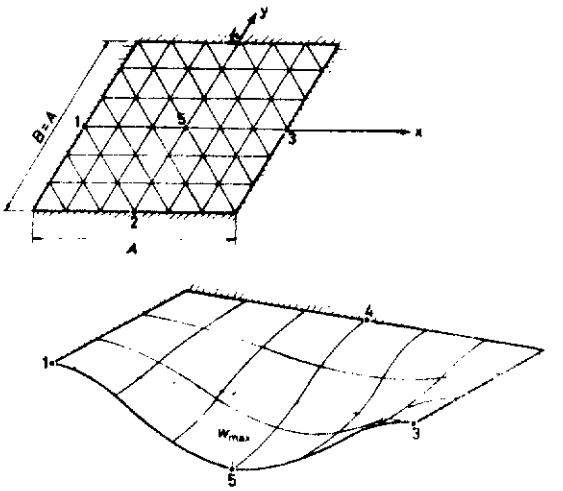

	Maximum Deflexion $\frac{w_{max}}{q_0A^4/D}$	Bending Moments $\frac{m}{q_0A^2}$			
		Point 1, 2, 3, 4		Point 5	
		m_I	m_{II}	m_I	m_{II}
Triangular Elements	0·897	-0·0083	-0·0265	0·0151	0·0219
Parallelogram Elements	0·949	-0·0081	-0·0275	0·0139	0·0202

Built-in Parallelogram Plate under Uniform Loading using Triangular Elements Fig.II.36

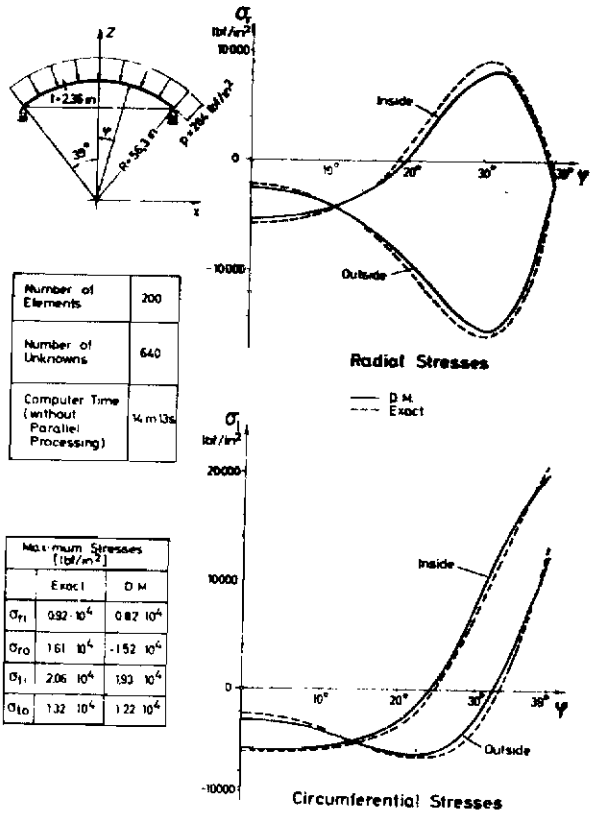

Number of Elements	200
Number of Unknowns	640
Computer Time (without Parallel Processing)	14 m 13s

Maximum Stresses [lbf/in²]	Exact	D.M
σ_{ri}	0.92 · 10^4	0.82 10^4
σ_{ro}	1.61 10^4	-1.52 10^4
σ_{ti}	2.06 10^4	1.93 10^4
σ_{to}	1.32 10^4	1.22 10^4

Simply Supported Spherical Shell
under Uniform Pressure (ν = 0.2) Fig. II. 37

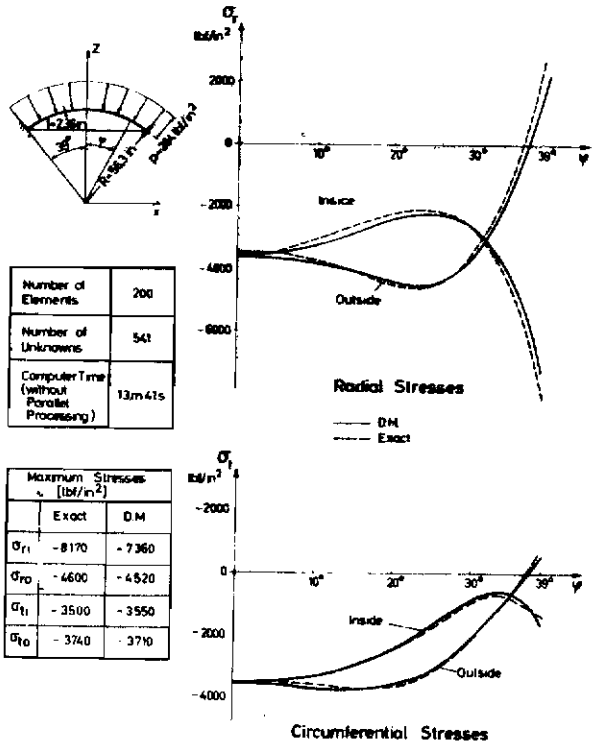

Number of Elements	200
Number of Unknowns	541
Computer Time (without Parallel Processing)	13m 41s

Maximum Stresses [lbf/in²]	Exact	D.M
σ_{ri}	-8170	-7360
σ_{ro}	-4600	-4520
σ_{ti}	-3500	-3550
σ_{to}	-3740	-3710

Built-in Spherical Shell
under Uniform Pressure (ν=0.2)

Fig. II. 38

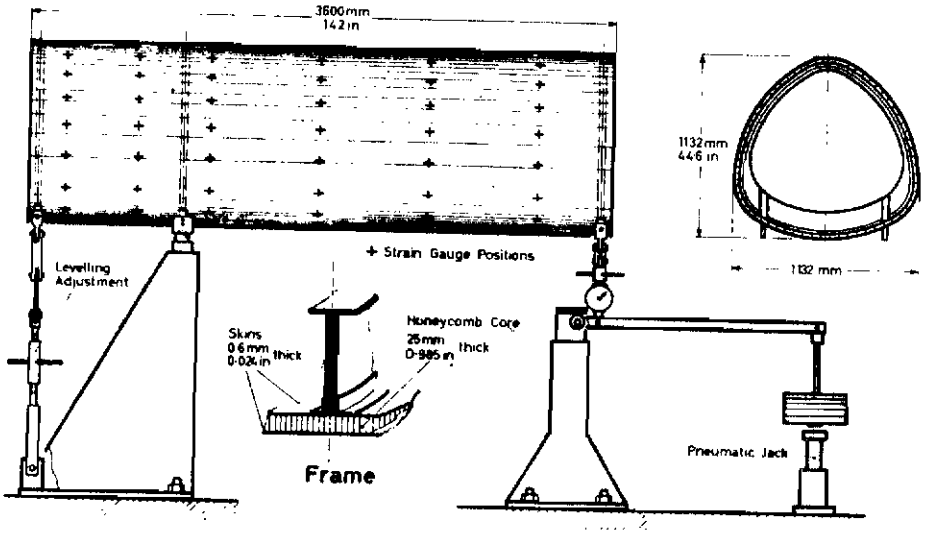

Construction and Geometry of Sandwich Type Fuselage Fig. II. 39

(see Timoshenko/Woinowsky-Krieger); these were computed for $\nu = 0.2$ by the original author. Good agreement is seen to have been achieved by the Matrix Displacement method, analysing one-quarter of the shell.

A more complicated application was on a cylindrical, non-circular sandwich fuselage which was built and tested, described in the following section. It was clear from the outset that, despite the use of a metal honeycomb core, its shear strains could not be neglected, and that an accurate analysis would have to await the development of shell elements to allow for shear deformations. However, good agreement was achieved, using the analysis grid shown in Fig. II.40 for the symmetrical loading case (see Fig. II.39). Equivalent shell properties were derived from the sandwich facings and shear deformations other than in the plane of the element ignored. The three frames were represented by beam elements with stiffnesses referred to displacements and rotations offset from their neutral axis, i.e., measured on the inside surface of the shell. There was, by this means, no need to assume an effective width of shell working with the frame in bending.

As shown in Fig. II.41, there is quite good agreement in the axial stresses between calculation and experiment. Surprisingly perhaps, the tip deflection (duly corrected) is rather greater than by calculation (8.2 v. 7.9 mm) for 1000 Kp total tip load. This may be attributed to the directionality of membrane triangles and the exaggerated stiffness they produce. Clearly, the greater part of the deflection ensues from membrane deformations of the shell. A similar axial stress distribution around the shell cross-section, both in membrane and shell-bending components, is obtained from calculation and test. The calculation appears in places to overestimate somewhat the shell-bending contribution, which probably is reduced by the finite deformability of the sandwich core. For this symmetrical loading case, only one half of the shell was analysed, inserting appropriate symmetrical boundary conditions at the centre plane. It is planned to solve one half for the antisymmetric case additionally and to obtain the final results for an asymmetrical loading by superposition. Although an inversion of the whole stiffness matrix is not undertaken unless the complete flexibility be explicitly required, there is a worthwhile time saving on the machine, when two systems of equations of half the size are solved. The additional programming time is minimized by the facilities in ASKA.

II.18 The Sandwich Fuselage Test

In the design and testing of the sandwich fuselage, as much use as possible was made of the experience gained from the 'membrane' fuselage built and tested at Imperial College as experimental verification of the fuselage analysis (Ref.2) by the Matrix Force method, reported in Ref.3, additional data on which are given in an Appendix to this paper. Firstly, the same jig was used for bonding the three segments, so that the external contour was the same. The sandwich dimensions chosen yielded the same order of distributed circumferential bending stiffness as that afforded by the light frames in the membrane fuselage. Obviously, the sandwich shell had a much higher bending stiffness in the longitudinal direction than the membrane shell. However, the fuselage bending stiffness was much the same, as the thicker sandwich skins (2 x 0.024 in. compared with 2 x 0.012 in.) balanced out the additional booms provided in the membrane fuselage. The three heavy frames where the loading

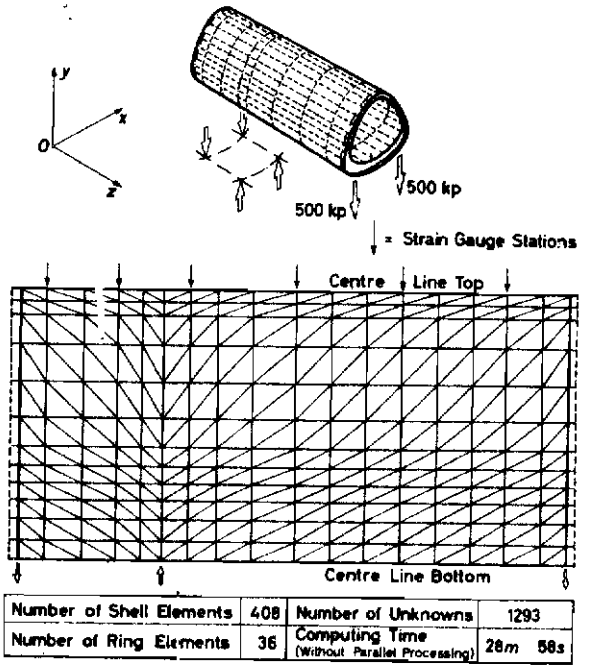

Number of Shell Elements	408	Number of Unknowns	1293
Number of Ring Elements	36	Computing Time (Without Parallel Processing)	28m 58s

Fuselage Analysis - Grid and Computing Details
Fig. II.40

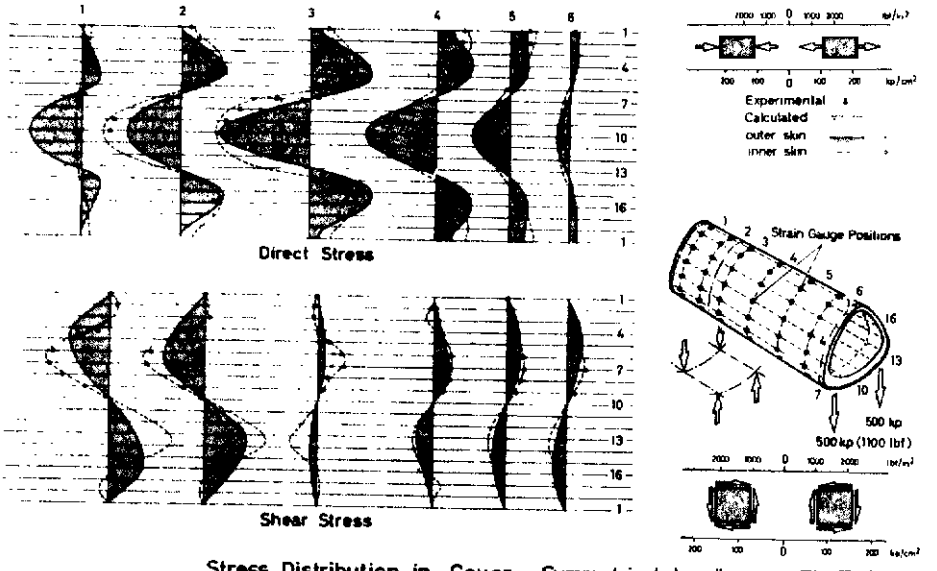

Stress Distribution in Cover - Symmetrical Loading Fig. II. 41

was applied were made with similar dimensions to those of the first fuselage, where their strength had proved quite adequate.

Two bonding processes were available to us: (a) Redux-bonding in an autoclave under heat (150°C) and pressure, curing taking altogether two to three hours, or (b) using Araldite epoxy resin adhesive curing in 24 hours at room temperature under contact pressure, the mixed components having a pot life of about 1/2 hour. The former process yields rather more reliable and stronger bonds and was used wherever possible. The sandwich segments were bonded with Redux and simultaneously the inserts for the longitudinal butt-joints and attachment angles for the heavy frames. Pressings for the heavy frames and the aforesaid angles were formed from 2024 Alclad sheet. The frames had thin sandwich webs which were Redux-bonded in halves to ensure flatness and then cold-glued back to back. Loads were applied vertically at two points, symmetrically disposed on each frame. For this purpose, steel bars were glued into place in the frame between the flanges of the pressings.

Since the longitudinal booms had been deleted, so was the loading case in which a moment was applied at the free end. The three remaining cases to be investigated, one symmetrical and two asymmetrical, involved merely vertical loads applied at the tip. In the asymmetrical cases, the reaction at the other end was to be on alternate sides. The loading and rear support frames were so designed that vertical loads could be applied at either side or in the centre. A yoke was used to distribute a central load equally between each pair of loading points on the end frames in the symmetrical loading case. The support reactions in all loading cases were thereby statically determinate, and colinear loading was achieved through shackle links at the end frames and ball seats at the centre frame, one of which had the freedom to move sideways.

The loading was applied via a lever system with 10:1 mechanical advantage, using 20 Kp weights. At both ends, a levelling adjustment was provided to ensure vertical loading of the horizontal fuselage, at least initially. The weights rested on a pneumatic jack which was lowered slowly in order to apply a loading to the fuselage for a few seconds at a time; i.e., sufficiently short for a group of measurements to be taken, without the measuring bridge's balance having time to vary due to drift or temperature changes. The fuselage was also lagged with plastic foam sheeting to minimize the effect of draughts.

Strain measurements in the shell were made using ninety-eight 45 degree rosettes on the inner and outer skins of one side of the fuselage. A check rosette was affixed on the other side (inside and out) at each of six measuring stations, making a grand total of 110 rosettes. Bending strains in the rings were measured at some ten radial stations, plus a check station on the other side. Strains were measured on both inner flanges of the symmetrical frame sections and also on the inner angles where they were bonded to the inside skin of the shell. It has been intended to employ an automatic strain recording system, but it proved possible to conduct the measurements manually and rapidly using a 10-channel switching bridge connected to a digital voltmeter. The strain gauges (462 in all) were connected in groups of 10 via special connectors, which included also common leads to rosettes, groups of gauges and leads to a dummy gauge for temperature compensation. One dummy gauge in the neighbourhood was used for each set of 10 gauges. It was bonded to a piece of sheet aluminium which was then taped to the shell. Had the automatic recording system been ready in time, the gauges were to

be read in groups of 100 (connected in groups of 10 as above) and the results punched on paper tape in the form of unbalance voltages before loading, under load and after loading. These were then to be processed directly in the computer.

In the symmetrical loading case, symmetry of strains was assumed and confirmed by the check gauges on the other side of the fuselage. For the asymmetrical cases, the tip load was to be applied first on one side, and then on the other, and the check strains should correspond alternately to the full set from the case where the loading be applied on the other side.

The stiffness of the construction materials was checked on coupons taken from the sheets used. For sheet Alclad, the thickness was also measured, as this varies considerably from the nominal for thinner gauges. For the shell material, tests were conducted on a bonded sandwich specimen to include the stiffening effect of the aluminium honeycomb core (1/4 in.cell, 0.002 in.foil) and the cured adhesive film with its glasscloth carrier. These items accounted for an additional stiffness of some six percent in tension and a little less in bending. Sandwich specimens were also employed to measure the shear stiffness of the honeycomb core in its two principal directions.

Deflections under load were measured, using a theodolite, along the centre line of the fuselage bottom, and at the steel bar inserts where loads were applied and reacted. Measurement to 10^{-3} mm was possible by this method and detected significant deflections of the massive support frame. Thus, from the measurements, rigid-body rotation of the fuselage, due to support deflections, could be eliminated.

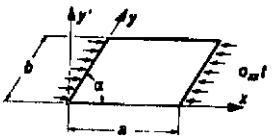

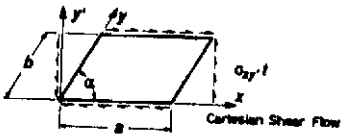

		s_{xxyy}			s_x f_x s_{yy}			b_x f_x s_{yy}			b_x f_x b_{yy}			b_{xxyy}		
	a/b \ α	90°	60°	45°	90°	60°	45°	90°	60°	45°	90°	60°	45°	90°	60°	45°
k_{xx}	1.0	4.025 (4.00)	3.283	2.411	1.406 (1.44)	1.155	0.738	1.857 (1.70)	1.239	0.776	4.85	3.44	2.20	10.15 (10.07)	7.740	5.298
	1.5	4.270 (4.347)	3.363	2.627	0.860 (0.890)	0.612	0.38	1.296 (1.340)	0.857	0.559	2.54	1.804	1.147	8.389 (8.33)	6.830	4.498
	1.8	4.083 (4.04)	3.171	2.288	0.728 (0.756)	0.498	0.188	1.294 (1.34)	0.834	0.504	2.102	1.513	0.989	8.157 (8.11)	6.335	4.425
$k_{xy'}$	1.0	9.365 (9.34)	5.301	4.521	4.80	1.479	0.987	5.005	1.731	1.099	8.62	5.40	4.21	14.885 (15.0)	12.516	12.204
	1.5	7.129 (7.1)	6.017	5.364	2.41	0.894	0.553	2.896	1.224	0.868	4.12	3.081	2.557	11.670	10.590	10.321
	1.8	6.606 (6.6)	5.64	4.915	1.877	0.754	0.371	2.486	1.263	0.771	3.207	2.547	2.248	11.128	10.267	9.980

s = Simply Supported , f = Free , b = Built-in , Edges parallel to x (y) axis are defined by suffices x (y)
( ) = Analytical Data

$$\sigma_{xxb} t = k_{xx} \pi^2 \frac{D}{b^2 \sin^2 \alpha}$$

$$\sigma_{xyb} t = k_{xy'} \pi^2 \frac{D}{b^2 \sin^2 \alpha}$$

Buckling Coeficients k for Oblique Plates under Compression and Cartesian Shear for Various Boundary Conditions
Analytical and M.D. (12x12 Grid) Results

Table II.8

III. Elasto-Plastic Analysis of Three-Dimensional Media

III.1 Introduction

Though the basic principles and equations of the matrix theory of structures are essentially concerned with linear systems, non-linear systems may easily be brought within their scope by representing the non-linear relations as a series of linear steps. Many problems have already been treated successfully this way. The particular type of non-linear relation with which we concern ourselves in this chapter is that for the stress-strain properties of the material. In the most general case, this relation may not be simply non-linear, but also dependent on time and the stress-strain history. At present, the state of knowledge in this field is neither as certain nor as comprehensive as could be desired. It is open to argument whether completely general constitutive equations can be formed to cover all cases, or even whether this is desirable. But in practice, analyses which are made are usually concerned with fairly distinct phenomenological descriptions of the material properties such as plasticity, creep and viscoelasticity. In their introduction into the Matrix Displacement theory; however, all these share the common property that they can be described in terms of incremental strain/stress laws with time, temperature and direction of strain in relation to previous history as further parameters. Given these data, either in functional or tabular form, the principles of solution by the Matrix Displacement method are the same for all types of behaviour. We restrict ourselves in what follows to strain hardening, elasto-plastic materials and to fix ideas, assume the Prandtl-Reuss equations and the von Mises yield criterion for calculation of the stress/strain relations in the plastic regime. The presentation is equally applicable to large displacements and strains, provided the experimental data are available.

For the step-by-step calculations, two distinct incremental techniques are possible. Thus, we may calculate an effective tangent modulus, which describes directly the incremental stress/strain relation, allowing for plasticity and distinquishing between increase of plastic strain and unloading. From this, the tangent stiffnesses are computed and hence the incremental displacements for the linear step. The alternative method is to operate always with the elastic stiffness and to represent the plasticity effects as initial loads. This latter method appears, at present, to have some computational advantages when local unloading may occur and is the one discussed in the following sections.

For a three-dimensional continuum, tetrahedral elements are the most generally useful, since they can be fitted to arbitrary boundaries and changed in size throughout the body, so as to give a more detailed representation in regions of particular importance. These may be of the constant stress type[12, 13] or be permitted linear variation of stress and strain (Section I). Tetrahedral elements have the further advantage that large displacements may also be allowed for simply by incorporating the geomentrical stiffness[12, 13]. In two dimensions, the corresponding element is the triangle.

III.2 General Incremental Stress/Strain Law

Whatever the nature of the deformational characteristics of a three-dimensional continuum, we may define an incremental stress/strain law in the form

$$\gamma_\Delta = \eta_\Delta + \varepsilon_\Delta = \eta_{\Theta\Delta} + \eta_{P\Delta} + \eta_{C\Delta} + \varepsilon_\Delta = \eta_{\Theta\Delta} + \eta_{P\Delta} + \eta_{C\Delta} + E^{-1}\sigma_\Delta \qquad \text{(III.1)}$$

where all lower case symbols are (6 x 1) vectors or column matrices. Their components or elements may be measured in any coordinate system, e.g., as the natural strains introduced in Refs. 3, 12, 13. The specific meaning of the vector symbols in Eq. (1) is

γ_Δ	= incremental total strain	$\eta_{P\Delta}$	= incremental plastic strain
ε_Δ	= incremental elastic strain	$\eta_{C\Delta}$	= incremental creep strain
$\eta_{\Theta\Delta}$	= incremental thermal strain	σ_Δ	= incremental stress

E is the generalised (6 x 6) elasticity modulus as given in Refs. (12,13), and need not be constant, i.e., non-linear elasticity is allowed for, but requires careful definition especially in the unloading stage, since it is, in general, a function of the preceding loading history. E may, moreover, vary with temperature. Fig. III.1 illustrates typical stress/strain diagrams in the presence of temperature and its effect on the elastic limit and proof stress. Anisotrophy of the material is easily included in our theory, as is inhomogeneity, as long as each element is taken to be homogeneous. However, we assume in our present discussion that the material is isotropic.

Assuming for simplicity a cartesian system of axes, we write the incremental strain and stress vectors in the form

$$\gamma_\Delta = \left\{ \gamma_{xx} \quad \gamma_{yy} \quad \gamma_{zz} \quad \tfrac{1}{\sqrt{2}}\gamma_{xy} \quad \tfrac{1}{\sqrt{2}}\gamma_{yz} \quad \tfrac{1}{\sqrt{2}}\gamma_{zx} \right\}_\Delta \qquad \text{(III.2)}$$

$$\sigma_\Delta = \left\{ \sigma_{xx} \quad \sigma_{yy} \quad \sigma_{zz} \quad \sqrt{2}\sigma_{xy} \quad \sqrt{2}\sigma_{yz} \quad \sqrt{2}\sigma_{zz} \right\}_\Delta \qquad \text{(III.3)}$$

Expressions analogous to γ_Δ may be given for η_Δ, $\eta_{\Theta\Delta}$, $\eta_{P\Delta}$. The generalised Young's Modulus E for a three-dimensional isotropic body is then most conveniently put in the form

$$E^{-1} = \frac{1}{2G}\mu_e = \frac{1}{2G}\left[I_6 - \frac{\nu}{1+\nu}\begin{bmatrix} E_3 & O_3 \\ O_3 & O_3 \end{bmatrix}\right] \qquad \text{(III.4)}$$

or

$$E = 2G\mu_e^{-1} = 2G\left[I_6 + \frac{\nu}{1-2\nu}\begin{bmatrix} E_3 & O_3 \\ O_3 & O_3 \end{bmatrix}\right] \qquad \text{(III.4a)}$$

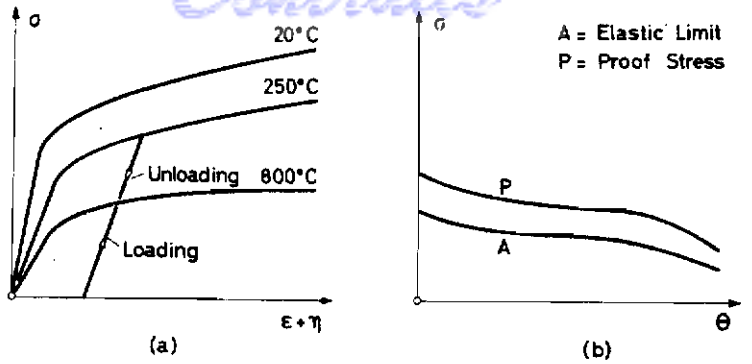

Characteristic Stress-Strain-Temperature Diagrams

Fig.III.1

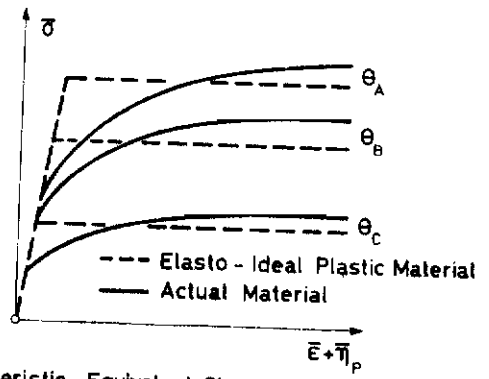

Characteristic Equivalent Stress-Equivalent Strain Diagram for Different Temperatures

Fig. III.2

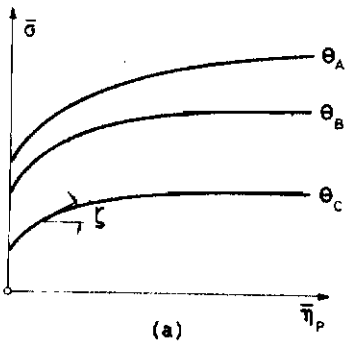

Characteristic Equivalent Stress-Equivalent Plastic Strain Diagrams for Different Temperatures

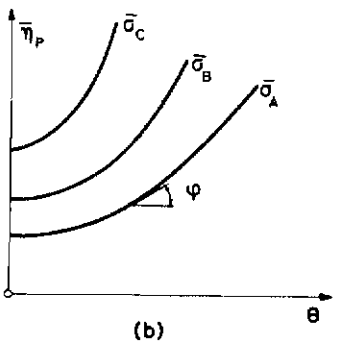

Characteristic Equivalent Plastic Strain-Temperature Diagrams for Different Equivalent Stresses

Fig. III.3

Here G is the shear modulus, ν Poisson's ratio, and E_3 a (3 x 3) matrix fully populated with 'ones'. Before proceeding to the plastic strains we must consider first the yield criterion.

III.3 Yield Criterion

When operating with the digital computer, it is, in principle, possible to allow for any yield condition in association with strain hardening. The law need not be given as an analytical expression, but can be fed into the machine in tabular form. We base our consideration here on the von Mises criterion. This is founded on the so-called equivalent stresses $\bar{\sigma}$ and strains $\bar{\gamma}$ ($\bar{\eta} \propto \bar{\varepsilon}$) which, for present purposes, are best written as *

$$\bar{\sigma} = \left[\sigma_d^t \sigma_d - \sigma_{d-}^t \sigma_d + \tfrac{3}{2} \sigma_s^t \sigma_s\right]^{1/2} \qquad \text{(III.5)}$$

$$\bar{\gamma} = \tfrac{2}{3}\left[\gamma_d^t \gamma_d - \gamma_{d-}^t \gamma_d + \tfrac{3}{2} \gamma_s^t \gamma_s\right]^{1/2} \qquad \text{(III.6)}$$

where σ_d and σ_s (γ_d and γ_s) are the two (3 x 1) submatrices of the total stress (strain) vector corresponding to the direct and shear components respectively. For example,

$$\sigma = \{\sigma_d \quad \sigma_s\} = \{\sigma_{xx} \quad \sigma_{yy} \quad \sigma_{zz} \quad \sqrt{2}\sigma_{xy} \quad \sqrt{2}\sigma_{yz} \quad \sqrt{2}\sigma_{zx}\} \qquad \text{(III.7)}$$

Hence

$$\sigma_d = \{\sigma_{xx} \quad \sigma_{yy} \quad \sigma_{zz}\}, \quad \sigma_s = \{\sqrt{2}\sigma_{xy} \quad \sqrt{2}\sigma_{yz} \quad \sqrt{2}\sigma_{zx}\} \qquad \text{(III.7a)}$$

Similarly

$$\gamma_d = \{\gamma_{xx} \quad \gamma_{yy} \quad \gamma_{zz}\}, \quad \gamma_s = \{\tfrac{1}{\sqrt{2}}\gamma_{xy} \quad \tfrac{1}{\sqrt{2}}\gamma_{yz} \quad \tfrac{1}{\sqrt{2}}\gamma_{zx}\} \qquad \text{(III.8)}$$

The subscript "-" indicates a single regression of the elements of a vector. Thus,

$$\sigma_{d-} = \{\sigma_{yy} \quad \sigma_{zz} \quad \sigma_{xx}\}, \quad \gamma_{d-} = \{\gamma_{yy} \quad \gamma_{zz} \quad \gamma_{xx}\} \qquad \text{(III.9)}$$

The formulation (5) and (6) for the yield criteria is very suitable for operations on a digital computer in conjunction with a matrix interpretation scheme.

If $\bar{\sigma}$ at the current loading step is found to exceed the critical value, which may include the effect of work hardening due to previous plastic straining, additional plastic deformation will take place. We may also include the effect of a temperature increment Θ_Δ in the yield criterion by re-writing Eq. (5) in the form

$$\left[\sigma_d^t \sigma_d - \sigma_{d-}^t \sigma_d + \tfrac{3}{2}\sigma_s^t \sigma_s\right]^{1/2} = \bar{\sigma}_o + \frac{\partial \bar{\sigma}}{\partial \Theta} \cdot \frac{\Theta_\Delta}{2} \qquad \text{(III.5a)}$$

* These formulae may also be expressed concisely in terms of natural stresses or strains.

Given the necessary experimental data, the application of Eq. (5a) proves straightforward. Fig. III.2 shows some typical $\bar{\sigma}$ versus $\bar{\varepsilon}_\Delta + \bar{\eta}_{p\Delta}$ curves, and the corresponding diagrams for ideal plastic behaviour.

III.4 Plastic and Thermal Strains

Following the basic philosophy of Hill's classical work [9] on a mathematically consistent theory of work hardening, we may reformulate the Prandtl-Reuss stress/strain equations in conjunction with the von Mises criterion in a suitable matrix dress. (As stated previously, we could operate equally well with any other more general constitutive equation.) For an isotropic and plastically incompressible body we find for the incremental non-elastic straining vector η_Δ, whose elements are ordered as in Eq. (2), the simple matrix expression

$$\eta_\Delta = \beta_\Delta \mu_p \sigma + \eta_{\theta\Delta} e \tag{III.10}$$

where σ is the total stress vector of Eq. (7), $\eta_{\theta\Delta}$ the thermal strain increment and

$$\mu_p = \left[\begin{bmatrix} I_3 & O_3 \\ O_3 & \frac{1}{2} I_3 \end{bmatrix} - \frac{1}{3} \begin{bmatrix} E_3 & O_3 \\ O_3 & O_3 \end{bmatrix} \right] \tag{III.11}$$

$$e = \{ 1 \quad 1 \quad 1 \quad 0 \quad 0 \quad 0 \} \tag{III.12}$$

β_Δ is a non-constant scalar, which depends on the plastic and thermal straining history and hence may vary from point to point. Substitution of Eq. (11) into the yield criterion specified by $\bar{\eta}_\Delta$ leads to Hill's result,

$$\beta_\Delta = \frac{3}{2} \cdot \frac{\bar{\eta}_{p\Delta}}{\bar{\sigma}} \tag{III.13}$$

$\bar{\eta}_{p\Delta}$ is the equivalent plastic strain derived from an expression of the type (6) with $\eta_{p\Delta}$ in place of γ.

Let us now assume that we have the diagrams or tabular data of the $\bar{\sigma}$ versus $\bar{\eta}_p$ relations for various temperatures suitably stored in the computer; whence corresponding information may be construed for the $\bar{\eta}_p$ versus Θ relations for various stresses $\bar{\sigma}$ (see, for example, Figs. III.3a,3b). To the first approximation, we obtain

$$\bar{\eta}_{p\Delta} = \frac{\partial \bar{\eta}_{p\Delta}}{\partial \bar{\sigma}} \delta\bar{\sigma} + \frac{\partial \bar{\eta}_{p\Delta}}{\partial \Theta} \delta\Theta = \frac{1}{J} \bar{\sigma}_\Delta + \varphi \Theta_\Delta \tag{III.14}$$

where

$$J = \frac{\partial \bar{\sigma}}{\partial \bar{\eta}_{p\Delta}} \quad , \quad \varphi = \frac{\partial \bar{\eta}_{p\Delta}}{\partial \Theta} \tag{III.15}$$

are the slopes of the diagrams in Fig. III.3 and $\bar{\sigma}_\Delta$, Θ_Δ are the incremental changes in $\bar{\sigma}$ and Θ ; note that $\bar{\jmath}_\Delta$ is evaluated from an expression of the type (5) with σ_Δ in place of σ . Substitution of Eq. (14) in (13) yields

$$\beta_\Delta = \frac{3}{2}\left(\frac{1}{J}\bar{\sigma}_\Delta + \varphi\Theta_\Delta\right)\frac{1}{\bar{\sigma}} \qquad \text{(III.16)}$$

It is evident that for a plastically isotropic material the $\bar{\sigma}$ versus $\bar{\eta}_p$ information required to obtain J and φ , may be deduced from uniaxial tests $\sigma_i - \gamma_i$ for a sequence of temperatures Θ ; see Fig. III.3. In fact, for such a loading we immediately confirm that

$$\bar{\sigma} = \sigma \quad , \quad \bar{\eta}_p = \eta_p = \gamma - \varepsilon = \gamma - \frac{\sigma}{E} \qquad \text{(III.17)}$$

To illustrate the application of this procedure to the calculation of J , let us assume that the uniaxial strain η_p is given by a modified Ramberg–Osgood expression of the type

$$\eta_p = \frac{1.1\sigma_l}{mE}\left[\left(\frac{\sigma}{1.1\sigma_l}\right)^m - \left(\frac{1}{1.1}\right)^m\right] \qquad \text{(III.18)}$$

where σ_l is the elastic limit and m a constant. Using Eqs. (16), (17) in the first of Eq. (15) we find

$$\frac{1}{J} = \frac{1}{E}\left(\frac{\bar{\sigma}}{1.1\sigma_l}\right)^{m-1} \qquad \text{(III.15a)}$$

III.5 Method of Solution of the Elasto-Plastic Problem

To understand the basic philosophy of our technique, we first assume that the initial strain vectors η of all constituent elements are known, irrespective of their origin. Then the problem may be solved directly by applying the idea of inital loads. From Ref. 1 or Eq. (1.25) we have

$$R = K_E r + a^t J \qquad \text{(III.19)}$$

where R and r are the external load and displacement vectors at the nodal points. K_E is the elastic stiffness and J the elastic loads arising at the nodal points, if all initial strains are suppressed; a is a Boolean or location matrix. If the effect of large displacements is being included, we must substitute the total stiffness $K_E + K_G$ for K_E in Eq. (19). Refs. 11, 12, 13 show in detail how the K_E , K_G and J may be set up for anisotropic, constant stress triangular and tetrahedron elements where the initial vector η is allowed to be arbitrary. K_E and J for tetrahedral and triangular membrane elements with linear varying strain are established in Chapter I and Ref 15 respectively, for triangular plate bending elements in Ref. 17. For example, for a

typical tetrahedron element subject to a uniform thermal strain $\eta = \alpha\,\Theta$, the (12 x 1) vector J of the x, y, z components of the initial loads is simply

$$J = -\eta\, k\, \psi \tag{III.20}$$

where k is the (12 x 12) cartesian stiffness of the element and ψ the (12 x 1) vector

$$\psi = \{\psi_1 \quad \psi_2 \quad \psi_3 \quad \psi_4\} \tag{III.21}$$

in which

$$\psi_i = \{x_i \quad y_i \quad z_i\}$$

In practice, plastic and creep strains are not known in advance. Solution of the problem is then necessarily incremental (either direct or preferable iterative). We start by establishing in our load cycle (see Fig. III.4) the load R_A and temperature Θ_A for which the elastic limit A is just reached at some point within the structure. The subsequent loading is then represented by a sequence of steps R_Δ and Θ_Δ as indicated in Fig. III.4. For each increment we apply the linearised equation

$$R_\Delta = K_\varepsilon r_\Delta + a^t J_\Delta \tag{III.22}$$

There remains the vital problem of establishing the J_Δ associated with the initially unknown strain η_Δ. We have applied with success on the computer the following two procedures:

a. The direct incremental approach

Assuming that the analysis of a typical preceding step $j-1, j$ has been completed, we obtain from its results $\vec{\sigma}$, $\vec{\sigma}_\Delta$, $1/f$, β_Δ and hence $\eta_{p\Delta}$ from Eq. (10). This $\eta_{p\Delta}$ is then fed into the subsequent step $j, j+1$ and added to the current $\eta_{\Theta\Delta}$. Hence, we determine J and solve Eq. (22) for r_Δ from which we derive the solution of the step $j, j+1$ and so on; Figs. III.5a,b. Thus, starting with point A, we find in turn the points B, C, D of the time-displacement history. If unloading occurs, this is not taken into account until the next step, which then operates under purely elastic conditions. This method is seen to include at each incremental step (a) the directly associated thermal strain vector $\eta_{\Theta\Delta}$ and (b) the preceding plastic strain vector $\eta_{p\Delta}$. The question of further loading after unloading is discussed after the iterative method.

b. The iterative incremental approach

The first loop of each loading step in analyzed elastically. The calculation of the subsequent loops is based on an average value of $1/f$ from which the relevant η_Δ are obtained and hence r_Δ from Eq. (22). This mean value of $1/f$ is in each case set up using the final $1/f$ of the antecedent step $j-1, j$ and the $1/f$ derived at the end of the preceding loop of the current step $j, j+1$. We may repeat these operations until convergence to a point B_1 is achieved. Note that in each loading step the $\eta_{p\Delta}$ of the preceding step is ignored, since it has been processed in the relevant computation. Fig. 5b shows a sequence of equilibrium positions B_1, C_1, D_1 etc.,

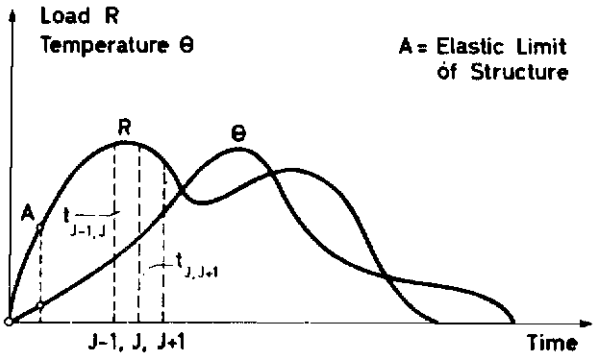

Load Temperature Cycle

Fig.III.4

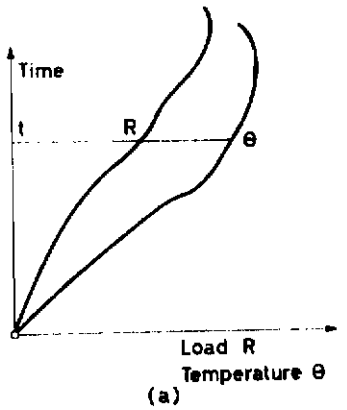

Load Temperature History

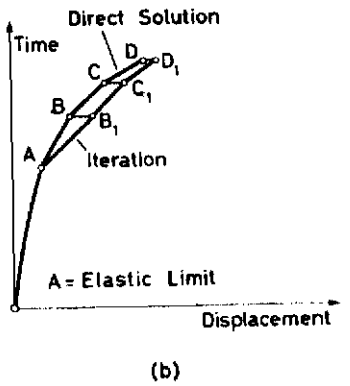

Direct and Iterative Incremental Solution of Elasto-Plastic Problem

Fig. III.5

attained by this procedure.* This second method is evidently more accurate, but more time consuming. It is necessary to check out at each iteration if loading or unloading occurs. At the same time, high accuracy is, in general, achieved after three iterations. In our experience the direct approach proves sufficiently accurate for engineering purposes as long as small enough intervals are chosen. However, it may be best in practice to apply an intermediate procedure with fewer loading steps but allowing for a finite number of iterations, say two or three, for each increment.

In either of the two procedures, the programming must also provide for the case when loading follows an unloading sequence. To take account of strain hardening β_Δ is held zero until the current $\bar{\sigma}$ is found to exceed the highest equivalent stress $\bar{\sigma}_{max}$ (not σ_l) achieved (and stored) in the previous loading history. In fact, this is best realised by introducing initially a column matrix with an entry σ_l corresponding to each element. As plasticity occurs and spreads in the loading history, the corresponding σ_l entries are changed into the appropriate $\bar{\sigma}_{max} > \sigma_l$.

It follows that the incremental $\bar{\sigma}_\Delta$ of Eq. (16) for a current step $j, j+1$ may always be written (when positive) in the form

$$\bar{\sigma}_\Delta = \bar{\sigma}_{j+1} - \bar{\sigma}_{max} \qquad \text{(III.23)}$$

where $\bar{\sigma}_{max}$ is the highest equivalent stress achieved in the previous loading history of the element. The above argument applies for a constant temperature case $\theta_\Delta = 0$. The factor β_Δ, when positive, is then evaluated from Eq. (16) in conjunction with Eq. (15). In the presence of a temperature history we may allow for a negative $\bar{\sigma}_\Delta$ as long as θ_Δ is sufficiently large to yield a positive β_Δ; in this case, $\bar{\sigma}_{max}$ must correspond to the current temperature.

III.6 Examples of Elasto-Plastic Analysis

Two problems which have been analysed by the direct increment method are illustrated in Figs. III.6 to 15. Both consist of flat, square plates of constant thickness, loaded by a uniform shear flow at the edges and both have a central hole, giving rise to stress concentrations. In each case, the analysis was carried out for a quarter of the plate, by taking advantage of the symmetry about the diagonals. For the square hole with rounded corners $(r/a = 0.2)$, constant strain triangular elements (TRIM3) were used and the finer grid adjacent to the hole is shown in Figs. III.6, 7. The number of nodal points, triangles and unknowns is 309, 556 and 603, respectively. Results are given first for the elastic analysis in the form of non-dimensional principal stress contours and show a stress concentration factor of 8.25 as compared with 8.04 obtained analytically[19] for an infinite plate with the same shape of hole; Fig. III.8, 8a. From the end of the elastic range, load was applied in a series of 48 steps for which the direct incremental method was used. A final 49th step had

* The differences between the results of the two methods are exaggerated in Fig. 5b for illustrative purposes.

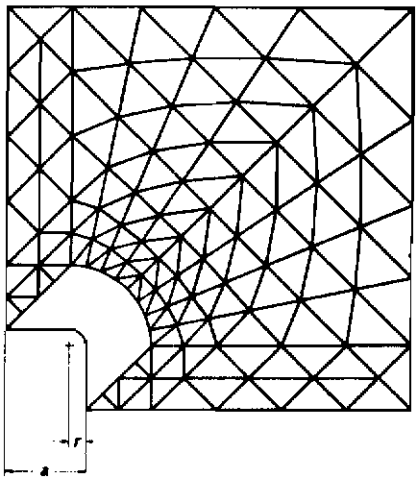

Plate with Central Hole; $r/a = 0.2$
Outer Grid for TRIM 3 Elements
Fig.III.6

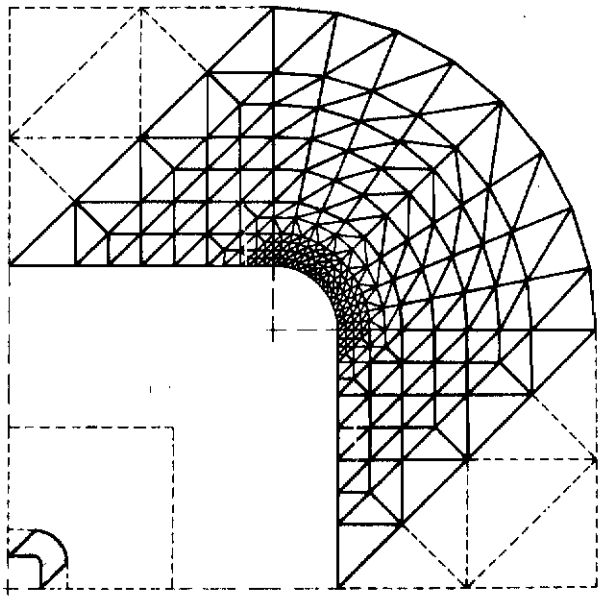

Plate with Central Hole; $r/a = 0.2$
Inner Grid for TRIM 3 Elements Fig.III.7

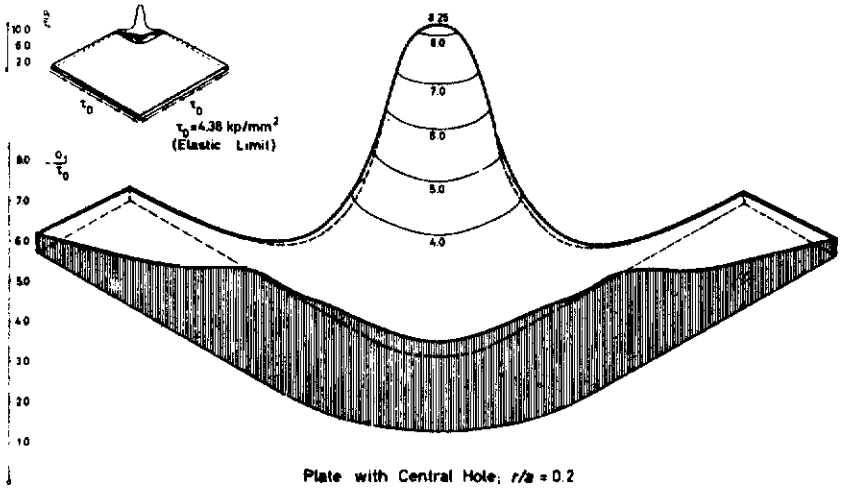

Plate with Central Hole; $r/a = 0.2$
Applied Uniform Stress T_a (TRIM 3 Elements)
Principal Stress σ_1 (Elastic State) Fig. III. 8

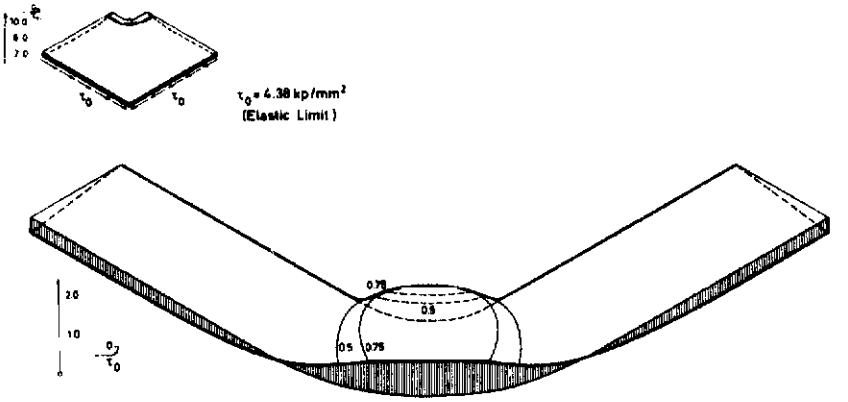

Plate with Central Hole; $r/a = 0.2$
Applied Uniform Stress T_a (TRIM 3 Elements)
Principal Stress σ_2 (Elastic State) Fig. III. 8a

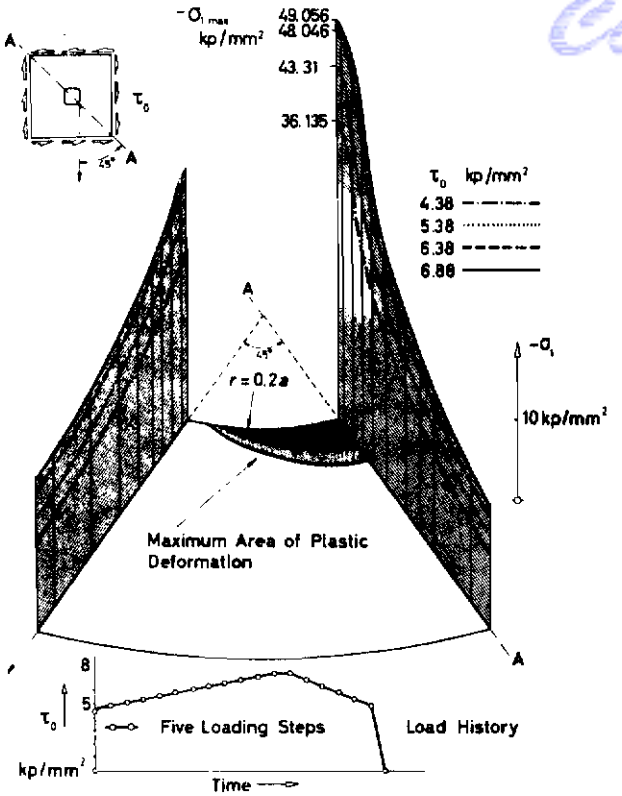

τ_0 in kp/mm²	4.38	4.63	4.88	5.13	5.38	5.63	5.88	6.13	6.38	6.63	6.88	6.88
$-\sigma_{1\,max}$ / τ_0	8.25	8.23	8.20	8.13	8.05	7.96	7.82	7.70	7.53	7.33	7.13	7.11

Plate with Central Hole $r/a = 0.2$
Stress Distribution in Elasto - Plastic Regime (Load Increasing)
Fig.III.9

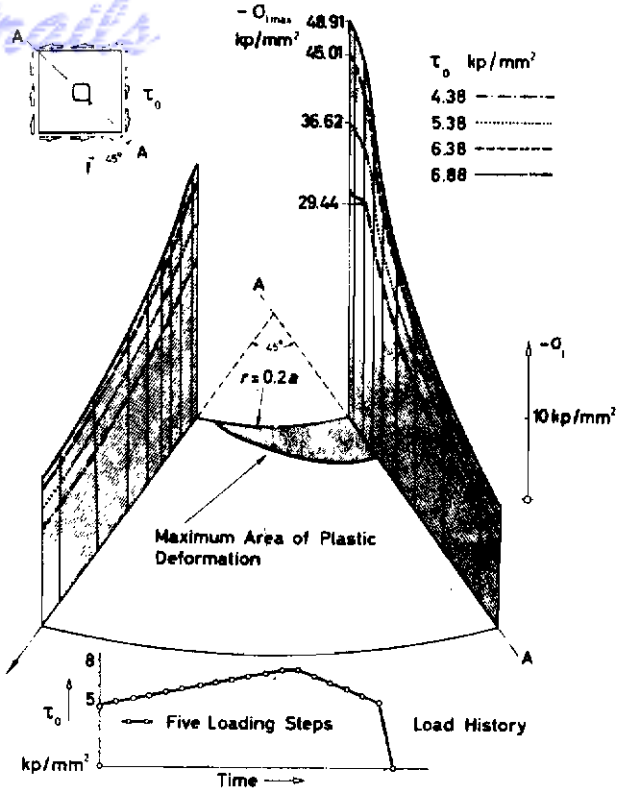

τ_0 in kp/mm²	6.88	6.38	5.88	5.38	4.88	4.38
$-\sigma_{1\,max}$ / τ_0	7.11	7.055	6.91	6.80	6.65	6.72

Plate with Central Hole $r/a = 0.2$
Stress Distribution in Elasto - Plastic Regime (Load Decreasing)
Fig.III.10

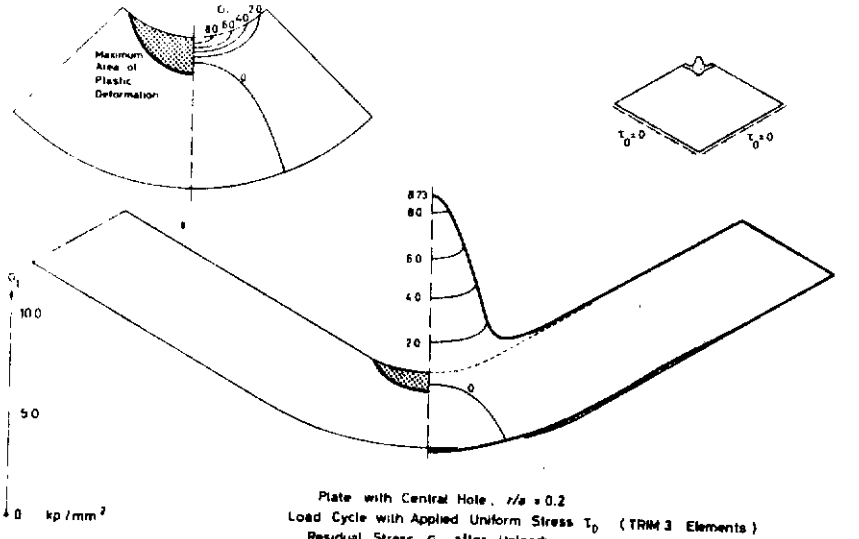

Plate with Central Hole, $r/a = 0.2$
Load Cycle with Applied Uniform Stress τ_0 (TRIM 3 Elements)
Residual Stress σ_1 after Unloading
Fig.III.11

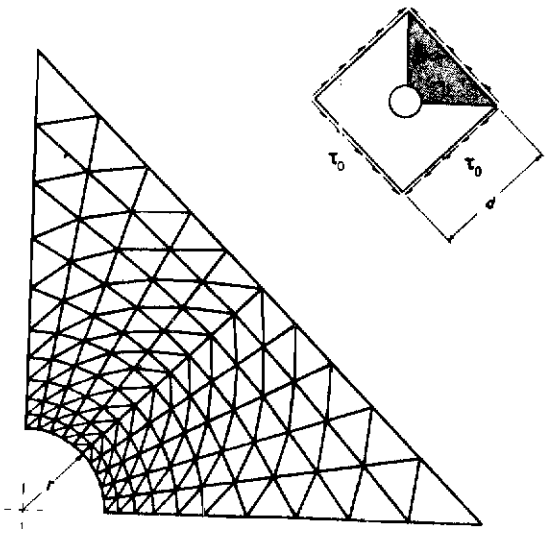

Plate with Circular Hole; $r/d = 0.125$
TRIM 6 Elements

Fig. III. 12

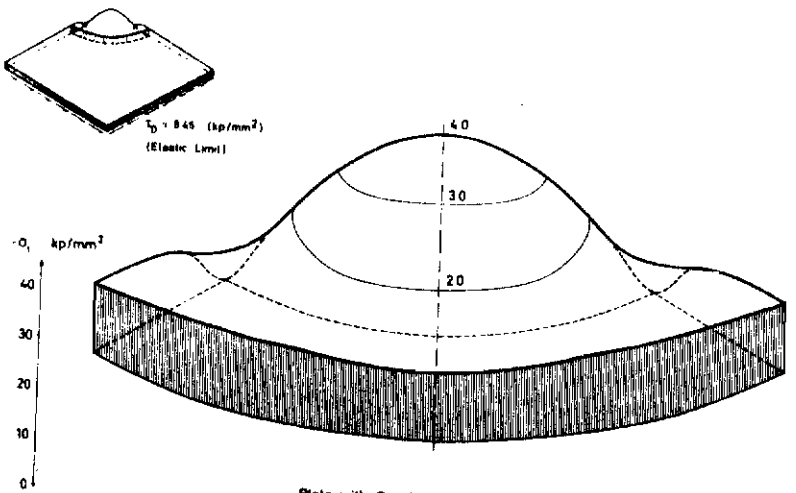

Plate with Circular Hole under Shear τ_0
Elastic Solution for TRIM 6 Elements
Principal Stress σ_1

Fig. III 13

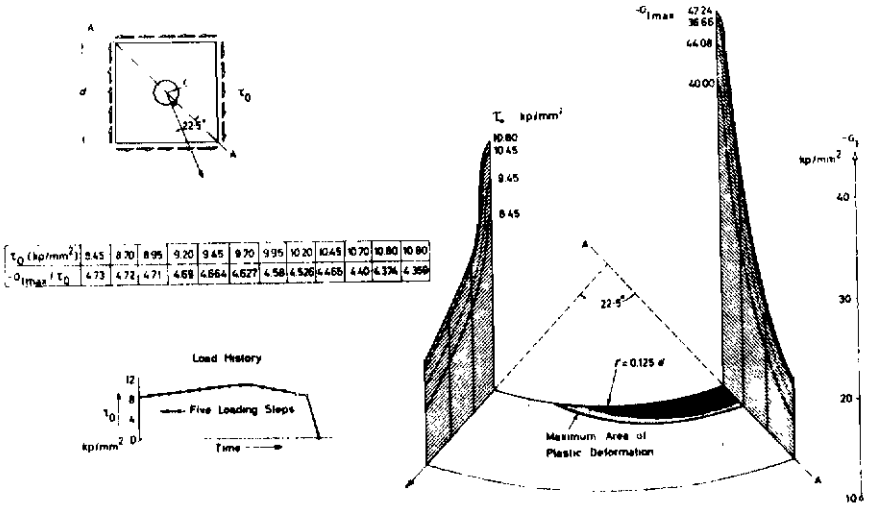

Plate with Circular Hole r/d = 0.125 under Shear Loading (TRIM 6 Elements)
Stress Distribution in Elasto-Plastic Regime (Load Increasing) Fig III 14

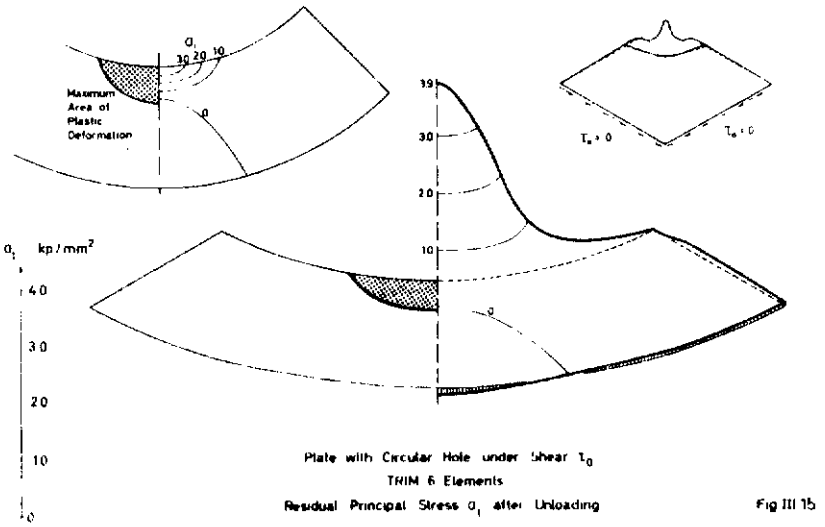

Plate with Circular Hole under Shear τ_0
TRIM 6 Elements
Residual Principal Stress σ_1 after Unloading Fig III 15

zero load increment in order to give the final elasto-plastic state from which the unloading calculation proceeded. The stress distribution σ_1 at four loading steps are reproduced in Fig. III.9 and Fig. III.10 reproduces the corresponding information for four unloading steps. It is confirmed that the stresses in the latter stage are in agreement with those deduced by subtraction of the elastic stresses, associated with the current load decrement, from the stresses of maximum load level. Fig. III.11 illustrates the residual stress σ_1 after removal of the external load. The computing line for each loop was 6' 50".

Similar results appear in the remaining figures for the plate with circular hole. However, in this case, the triangular elements used were allowed linearly varying stresses (TRIM6) and the grid of Fig.III.12 is correspondingly coarser. The number of nodal points, triangles and unknowns is now 441, 200 and 840. The analytical solution[8] for an elastic infinite plate yields a stress concentration factor of 4.0; this compares with 4.7 given by the present analysis of the finite plate; see Fig.III.13.

Since the development of plastic-strains would obviously be limited to the elements in the vicinity of the hole, the elements were divided into two groups and the plastic strain calculations were carried out only for the inner group. This afforded some shortening of the computation time, but would not, of course, be possible in a more general problem. The programming for the calculations was entirely with ASKA, except for the calculation of the incremental initial loads J_Δ, which had not then been incorporated into ASKA. The computing time per loop was 7' 48". The stress σ_1 at four loading steps is shown graphically in Fig. III.14, whilst Fig. III.15 reproduces the final residual stresses σ_1.

The last example is also being analysed by the iterative incremental method and the corresponding result is to be presented at the Symposium itself.

IV. Plastic Collapse Load

IV.1 Introduction

The detailed analysis of structures with plastic strains demands inevitably a step-by-step calculation, as discussed in the previous chapter, owing to the non-conservative nature of the plastic deformation. If the effect of strain hardening is neglected, i.e. the material is assumed to be elastic-perfectly plastic, the calculation of stress and strain history in a loading cycle becomes computationally difficult, if not impossible. On the other hand, the structure now exhibits a definite collapse load, at which unrestrained plastic deformation sets in, and whose calculation does not require a detailed study of the stress-strain history. Calculations of collapse load have been used for some time for the limit design of structures and in recent years the technique of linear programming has been employed in such calculations. Applications have, however, been limited to skeletal structures, such as pin- and stiff-jointed frameworks, for which plastic hinges can be assumed. This method does not seem to have been applied to large scale aircraft structures, possibly owing to the difficulty of idealising these into manageable standard components, to which a simple yield criterion can be assumed. In what follows, a stressed skin structure is represented by flange members taking only direct stress and panels which carry only shear stress. The material behaviour is taken to be elastic-perfectly plastic, so that a yield stress or load can be specified for each component, although the tensile yield limit and the compressive yield limit may differ in magnitude. In compression and also in shear, the yield limits may be imposed by buckling considerations, rather than by plastic deformation. However, the effect, as far as the calculations are concerned, is the same. Up to the yield limit, the component is assumed to deform elastically (though this is not an essential part of the theory); strains beyond the yield limit produce no increase in stress.

The structural model is thus an extension, to incorporate yield properties, of the classical Wagner model of a stressed-skin structure, on which the Force method of analysis has been widely and successfully used for the elastic analysis.

The applied loads on the structure are assumed to increase proportionally, so that the loading matrix can be written as $\lambda \mathbf{R}$. The column vector $\mathbf{R}$ defines the loading for some standard magnitude, represented by $\lambda = 1$, and we seek to establish the value of λ when the structure collapses. Prior to collapse, the plastic strain is 'contained' by the elastic strain and must be of the same order. The deformations can therefore be assumed to be small, and calculations of equilibrium and kinematic relations based on the undeformed geometry of the structure.

Under these assumptions, two approaches to the problem are possible, which have the same dual relationship as the Force and Displacement methods of analysis and also the dual relationship of the maximisation and minimisation problems in linear programming. The first method investigates the collapse of the structure from the point of view of statical equilibrium and considers possible load

paths which do not violate the yield limits. The second method tackles the problem kinematically by examining possible collapse mechanisms, produced by plastic deformation in a sufficient number of structural elements. Since the plastically deforming members must be carrying loads equal to their respective yield limits, the collapse load corresponding to a given mechanism is obtained by considering virtual displacements in the collapse mode.

Based on these ideas, the following dual theorems on the plastic collapse of structures have been known for some time.[6,7]

(a) 1st Theorem

The collapse load of a structure is the maximum load for which a stress distribution, satisfying all equilibrium conditions and nowhere exceeding the yield limits, can be found.

(b) 2nd Theorem

The collapse load of a structure is the minimum load which is in equilibrium with the yield stresses of the plastically deforming members in a collapse mechanism.

The applications of these two theorems to the calculation of collapse loads by linear programming methods are now considered separately.

IV.2 The Force Method

With the applied load matrix written as λR, the stress (internal force) matrix S of the m idealised structural elements is given by

$$\begin{aligned} S &= \lambda\, b_0 R + b_1 X \\ &= \lambda\, S_0 + b_1 X \end{aligned} \qquad \text{(IV.1)}$$

where $S_0 = b_0 R$ gives a statically-consistent system of forces in the elements in equilibrium with R and b_1, the self-equilibrating forces corresponding to the n redundancies X. Eq.(1) thus expresses the equilibrium conditions of the structure. Any statically possible stress system is obtained by assigning suitable values to the redundancies. The condition that these stresses must not exceed the yield limits can be stipulated as

$$Y_L \leq S \leq Y_u \qquad \text{(IV.2)}$$

where Y_u and Y_L are the column matrices of the upper and lower yield limits.

According to the Theorem I theretore, we have to find the maximum value of λ for which the matrix S, given in Eq.(1), satisfies the restrictions in (2). In the usual linear programming formulation, the unknown variables are λ and X ($n+1$ in all), and the problem can be stated as follows:

To maximise a linear function

$$\lambda = [1 \quad 0] \begin{bmatrix} \lambda \\ X \end{bmatrix}, \qquad \text{(IV.3)}$$

where the variables $\begin{bmatrix} \lambda \\ X \end{bmatrix}$ are subject to the restrictions

$$Y_L \leq [S_o \; b_1]\begin{bmatrix}\lambda \\ X\end{bmatrix} \leq Y_u \qquad (IV.4)$$

The method of solution follows closely the standard linear programming practice, with a slight modification to allow for the different upper and lower bounds without having to double the size of the problem, the details of which will not be elaborated here. Suffice it to say that the first step of the linear programming routine determines a load factor λ, which is limited by the yielding of a member, and each subsequent step finds a new load path (column X) for which a higher load is carried through the structure. The maximum λ is reached when the path is blocked by the yielding of the members, and no alternative can be found to enable a higher load to be carried. It is interesting that though the magnitude of the collapse load is not affected by the choice of b_1 and b_0, unless b_1 is very badly chosen and leads to computational difficulties, the pattern of the plastic deformation may vary considerably. Moreover the stress distribution over the remainder of the structure is not fixed since in general fewer than $n+1$ elements become plastic and the equilibrium conditions are insufficient to determine the complete stress system.

The computer programming for this method is quite straightforward, and solutions are shown for a singly-symmetrical two cell wing (Fig.IV.1) (18 redundancies, 69 members), and a tapered delta wing (Figs. IV.2 and 3) (66 redundancies, 198 members). No special computational difficulty was encountered.

Structures with cut-outs, either initially in the design or due to subsequent modification present no difficulties. It is only necessary to consider them to be filled in, so that the structure is regularised and the b_0 and b_1, matrices remain unchanged, and put the yield limits of these cut-out members in the Y_L and Y_u matrices to zero. The calculation proceeds in exactly the same manner as for structures with no cut-outs.

IV.3 The Displacement Method

Let τ be a column matrix of p independent displacements (linear or angular) at the nodal points of the idealised structure, and υ the column matrix of strains in the m structural members. The matrix relation

$$\upsilon = a\tau \qquad (IV.5)$$

then transforms the displacements τ into the true strains of the elements υ by the geometrical matrix a. Note that in this Chapter the matrix a is not merely the Boolean location matrix used in the remainder of the paper, but incorporates also the transformation into the natural strains, represented elsewhere by the matrix a_N for the individual elements. Also, to emphasize the duality with the Force method, the element strain matrix is denoted by υ instead of the usual ε_N. Generally, for a redundant structure, m is greater than p. In fact, $m-p$ gives the number of redundancies n.

A collapse mechanism can be represented by a system of displacements τ and the kinematically

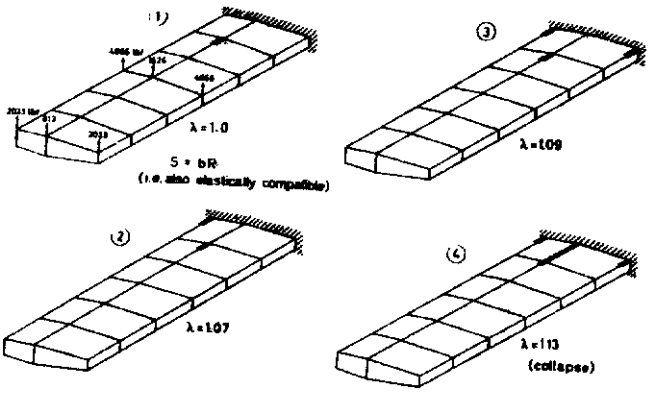

Example of Plastic Collapse by Force Method
$S = \lambda bR + b_0 X$

Fig. IV.1

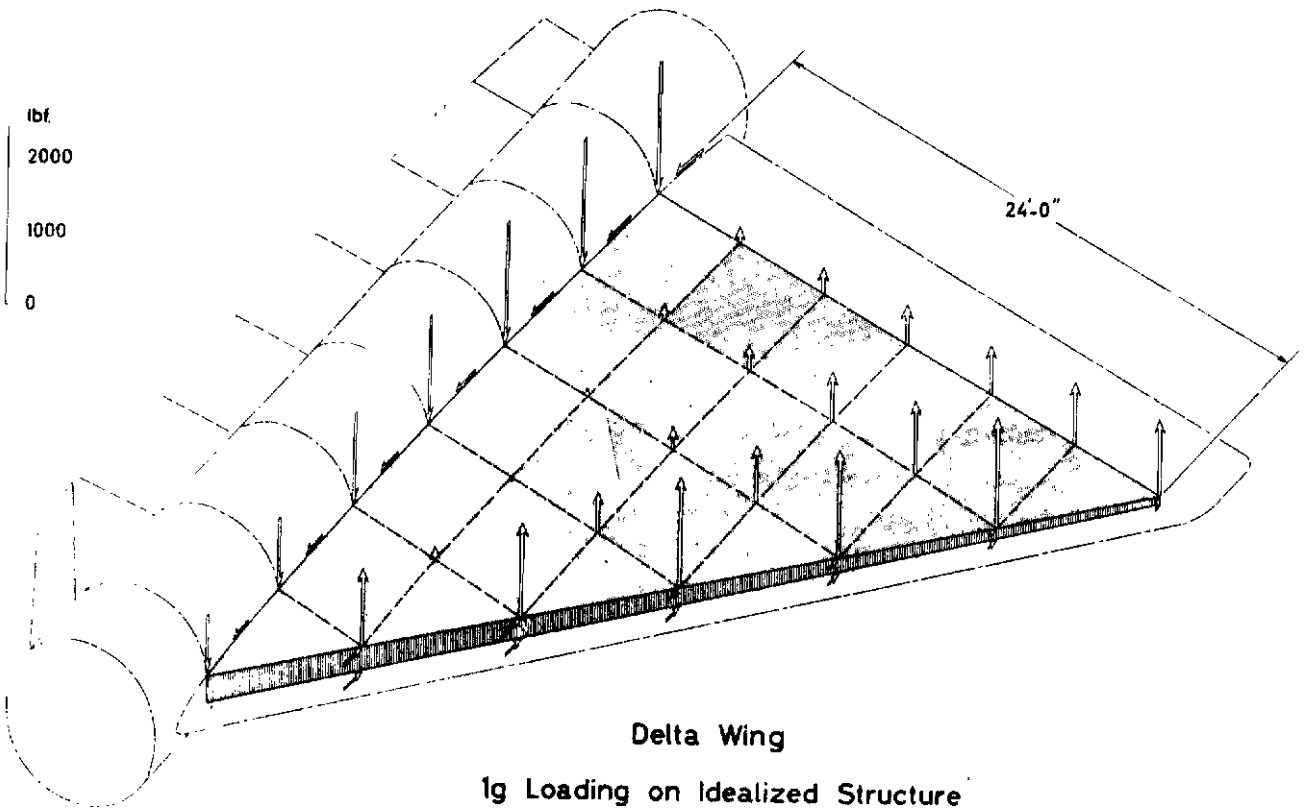

Delta Wing

1g Loading on Idealized Structure

Fig. IV.2

consistent strains υ . Each column of the a matrix, say the j^{th} column, can be construed as a basic mechanism corresponding to a displacement $r_j = 1$. Then the matrix Eq.(5) specifies all possible collapse mechanisms as a combination of the p basic mechanisms $r_1, r_2, \cdots, r_p$.

The strains υ in a collapse mechanism can be considered as being caused by the yielding of those members under the applied load λR . In other words, λR is equilibrated by a system of forces, of which those in the members involved in the collapse mechanism are equal to the yield forces, with the sign consistent with the deformation.

By the Principle of Virtual Work, which is simply a restatement of the equilibrium condition, we have

$$\lambda R^t r = Y^t \upsilon \tag{IV.6}$$

where $Y_i = (Y_u)_i$ (the upper yield limit) if $\upsilon_i > 0$

$= (Y_L)_i$ (the lower yield limit) if $\upsilon_i < 0$.

It is therefore possible to find the value of λ corresponding to every collapse mechanism. Notice that it is not necessary to know the entire system of stresses which equilibrates the external load. The only stresses concerned are those in the members involved in the collapse mechanism, which are equal to the appropriate yield limits. The second theorem of plastic collapse then states that the actual collapse load is the minimum of all possible values of λ thus found. This is once again a linear programming problem.

We may assign an arbitrary value to one of the possible displacements r_j to represent the collapse mechanism. But it is more convenient to normalise the displacements with respect to the loads R .

$$R^t r = 1 \tag{IV.7}$$

Then Eq.(6) becomes

$$\lambda = Y^t \upsilon \tag{IV.6a}$$

Regarding both r and υ as unknown variables, the problem can now be represented in the following form:

To minimise the linear function

$$\lambda = \begin{bmatrix} 0 & Y^t \end{bmatrix} \begin{bmatrix} r \\ \upsilon \end{bmatrix} \tag{IV.6b}$$

where

$$\begin{matrix} & p & m \\ 1 & \\ m & \end{matrix} \begin{bmatrix} R^t & 0 \\ -a & I \end{bmatrix} \begin{bmatrix} r \\ \upsilon \end{bmatrix} = \begin{bmatrix} 1 \\ 0 \end{bmatrix} \tag{IV.8}$$

Apart from the Y matrix, which has to be selected from Y_u or Y_L according to whether v is positive or negative, this is once again a standard linear programming problem, but the routine has to be modified in order to allow for the uncertain nature of the Y matrix.

It can be shown, by the inversion of a part of the a matrix, that this problem is precisely the dual problem (in the linear programming sense) of the Force method formulated in Eqs.(3) and (4), the solution of one is equal to the solution of the other. That is, if the idealisation of the two approaches are identical, which may not always be the case.

There are p displacements r and m strains v in Eq.(8). Each variable is associated with a column of the $(m+1)\times(p+m)$ matrix. Thus, the variable r_j is associated with the column $\begin{bmatrix} R_j \\ -a_j \end{bmatrix}$ and the variable v_i with the column $\begin{bmatrix} 0 \\ e_i \end{bmatrix}$ where e_i is the i^{th} unit vector (i.e. a column of zeros with a 1 in the i^{th} place).

For the initial solution, we may take one r variable, say r_1, corresponding to which it can be arranged for $R_1 \neq 0$, together with all the v variables as the basic variables. That is to say, the minor

$$M_1 = \begin{bmatrix} R_1 & 0 \\ -a_1 & I \end{bmatrix} \qquad \text{(IV.9)}$$

taken from the large matrix in Eq.(8) will be non-singular and have an inverse

$$M_1^{-1} = \begin{bmatrix} 1/R_1 & 0 \\ a_1/R_1 & I \end{bmatrix} \qquad \text{(IV.10)}$$

which gives values to the basic variables

$$\begin{bmatrix} r_1 \\ v \end{bmatrix} = \begin{bmatrix} 1/R_1 & 0 \\ a_1/R_1 & I \end{bmatrix}\begin{bmatrix} 1 \\ 0 \end{bmatrix} = \begin{bmatrix} 1/R_1 \\ a_1/R_1 \end{bmatrix} \qquad \text{(IV.11)}$$

while the rest of the variables are assumed to be zero

$$r_2 = r_3 = \ldots\ldots = r_p = 0 . \qquad \text{(IV.12)}$$

Eqs. (11) and (12) together satisfy Eq.(8) and constitute a possible solution to the problem. In fact, it represents simply the mechanism with displacements $r_1 = 1/R_1$, $r_j = 0, j \neq 1$, and corresponding strains $v = a_1/R_1$. The value of λ associated with the mechanism can be evaluated immediately from Eq.(6a) after the appropriate Y is chosen.

Next, the variable r_2 is brought into the basic set, replacing one of the v's, say v_ℓ. This is achieved by replacing the column $\begin{bmatrix} 0 \\ e_\ell \end{bmatrix}$ associated with the variable v_ℓ, by the column $\begin{bmatrix} R_2 \\ -a_2 \end{bmatrix}$ in the matrix M_1. The new matrix M_2 will be different from M_1 in only one column, and the new inversion M_2^{-1} can be obtained rapidly from M_1^{-1} by a simple algorithm without resorting

to the usual matrix inversion routine. The choice of the variable v_ℓ to be replaced depends on the criterion that the resulting value of λ must not be higher than the initial one. This step, in fact, finds a combination of the mechanisms r_1 and r_2. The new combination results in a mechanism with a lower λ, if possible, otherwise r_2 will have zero value in the solution and the original mechanism will not be changed.

Each subsequent step brings a new r variable into the basic set, replacing one of the v variables, at the same time lowering the value of λ if possible. Since the columns of the a matrix represent distinct mechanisms and must therefore be linearly independent, the matrix M_i is at no stage singular and the inverse M_i^{-1} always exists.

Thus, after p steps, all the r displacement variables will be included in the basic set, together with $m+1-p = n+1$ of the v variables. They will have values given in the first column of the inverse matrix M_0^{-1}, the remaining $p-1$ non-basic v variables will have zero values. At this stage, the mechanism is formed by a combination of all the basic mechanisms $r_1, \ldots, r_p$.

It may still be possible to change the mechanism by exchanging a basic v with a non-basic v variable. The criterion must always be that the resulting mechanism gives a decrease in the value of λ. Otherwise there will be no point in the exercise. In effect this step can be interpreted physically as a study of the possible load ranges, for equilibrium, in the elements not so far included. Those in which this load range falls outside the yield limit will clearly lead to a reduction in λ when included in the mechanism.

The iteration routine used in the computer program follows the usual linear programming procedure, but with modifications for the special nature of the problem. One complication arises because the correct Y for a member can only be decided after the sign of the strain v is known. Though one procedure would be to express the function

$$\lambda = Y^t v$$

in the form

$$\lambda = \frac{1}{2} \sum_m \left[Y_u (|v| + v) - Y_\ell (|v| - v) \right] \qquad \text{(IV.13)}$$

this would require the introduction of a further m variables $|v|$ and considerably increase the size of the problem. To obviate this, a restriction is imposed on the interchange of v variables in the second phase of the calculations, so that changes of the variables already included in the mechanism do not involve a change in sign. A change of mechanism which necessitates a reversal of sign for an element must therefore be brought about in two stages, with zero as an intermediate value.

Mainly due to this, the computer programming for the Displacement method is more complicated than that for the Force method. Problems successfully tackled so far have been chiefly fairly simple skeletal structures, on which various aspects of the method were tested. A typical example is the simple cantilever with 16 idealised flanges and 8 webs and 16 independent displacements which is shown in Fig.IV.4. The figure illustrates how the collapse mechanism is progressively established in

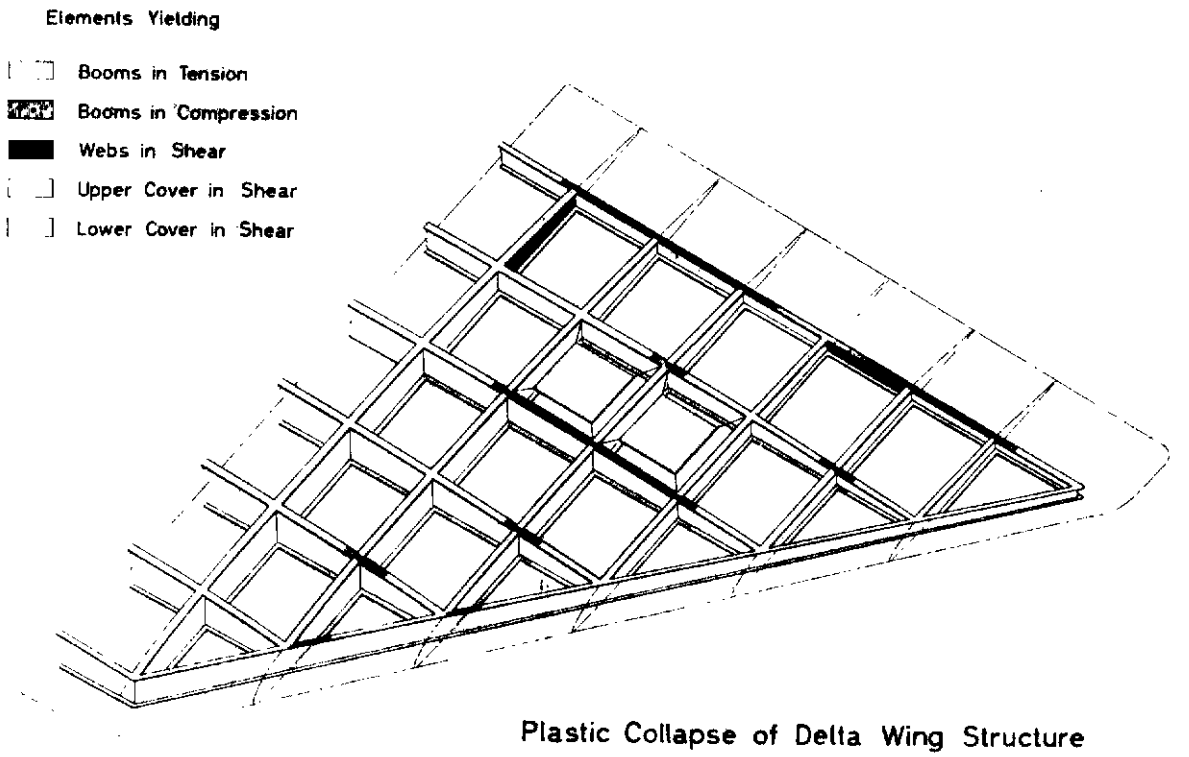

Plastic Collapse of Delta Wing Structure under 3.88g Loading Fig. IV.3

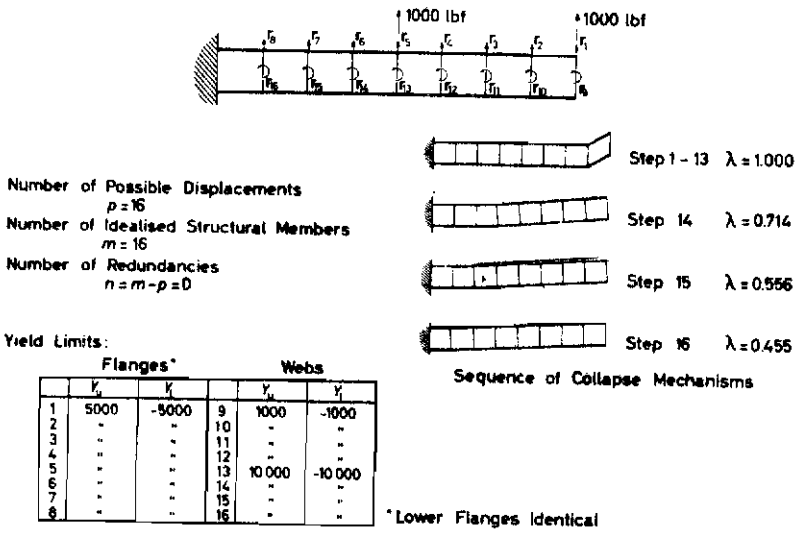

Plastic Collapse of Idealized Beam by Displacement Method Fig. IV.4

the course of the calculation. The structure is statically determinate and the collapse load obvious, but it gives a fairly severe test from the linear programming point of view. In fact, the nearer the number of possible displacements p is to the number of members m, the more unsuitable the problem is for the Displacement method. Attempts to solve the delta-wing problem of Fig.IV.2, successfully tackled by the Force method, have so far not yielded the correct collapse mechanism and load. This is believed to be due to the difficulty of forming consistently the $\mathbf{a}$ matrix for the idealised structure with twisted shear panels in the cover.

It appears also that, for a large problem, the solution is very sensitive to rounding errors. During the calculation for the tapered delta wing, for example, there were 175 idealised members and 119 displacements. It required, therefore, 119 iterations to bring all the τ variables in. It was found that rounding errors soon crept into the inverse matrix $\mathbf{M}^{-1}$, and unless anything numerically less than a small number μ is replaced by zero, the iteration procedure does not give a consistent answer at all. The number μ has to be set according to the magnitude of the numbers involved in each problem, and the accuracy of the computer used for the calculation. If set too small, it will have no effect. If set too large, it will discard relevant information and produce a wrong answer. For the problem in question, the numbers in the $\mathbf{M}^{-1}$ matrix are of the order 10^{-5}, and the machine used has an accuracy of about 9-10 decimal places. The correct setting of the number μ would be around 10^{-14}. In fact, a consistent result was produced when μ is set between 10^{-12} to 10^{-16}. The program stopped before 119 iterations, (because an τ variable could not be brought in without increasing λ 1), when μ was set at 10^{-11}; and the value of λ went on decreasing indefinitely when μ was set at 10^{-19}!

IV.4 Comparison of Methods

Of the two approaches, the Force method is undoubtedly the easier to program and is the more suitable for problems where the degree of redundancy is much smaller than the number of structural members. However, it does require the determination of the $\mathbf{b}_0$ and $\mathbf{b}_1$ matrices, which necessitates a prior statical analysis and, in particular, the specification of suitable redundancies. On the other hand, the assembly of the $\mathbf{a}$ matrix, being purely geometrical, is very straight-forward, so that, once the general computer program has been written for the Displacement method, problems can be solved by comparatively unskilled operators. Given that the idealisations are the same for the two methods, the statistical analysis for the Force method can be regarded as a particl solution of the equilibrium equations

$$\mathbf{a}^t \mathbf{S} = \mathbf{R} \qquad \text{(IV.14)}$$

However, if the problem is not to be sensitive to round-off error, the redundancies must be chosen with care. As in the familiar elastic analysis it is preferable to use standard sets of self-equilibrating force systems to form the columns of the $\mathbf{b}_1$ matrix, rather than simply to choose certain of the element loads as redundancies and solve Eq.(IV.14). Thus for novel structures, some skill and experience are necessary though for standard types of structure, automatic methods can be devised for computing $\mathbf{b}_1$.(Ref.2). In general the Displacement method is more suitable for structures where

the number of redundancies is high in relation to the number of elements, or to the number of displacements. This is again similar to the situation for the elastic analysis. There remains only the question of round-off error in connection with large problems. This is a topic requiring further investigation before problems with several hundred displacements can be confidently tackled.

V. Rehearsal of Finite Displacement Theory and Applications

V.1 Introduction

Structural analysis of engineering systems may usually be based on the geometry of the undeformed structure. This ignoring of non-rigid body displacements presumes, in general, that strains and displacements are small. If in addition the stress-strain relation is taken to be linear, the theory is reduced to a standard linear matrix formulation. At the same time we should remember that this analysis allows, as shown in Section III, the inclusion of initial strains or stresses and thus, via an incremental or iterative procedure the solution of non-linear problems involving plasticity and time-dependent viscous effects. The applications given there were, however, restricted to small displacements and strains.

We all know that there are classes of engineering problems where it is impossible to ignore the effect of deformations. The first one that comes to ones mind is the classical type of initial buckling or elastic instability of a strut or flat plate. Essentially these instability effects involve a bifurcation of equilibrium (see Fig. V.1), the point of bifurcation occuring at the critical load. An important point to keep in mind is that this phenomenen arises through displacements yielding a stable equilibrium position basically different from that prior to instability. For example, in the case of the ideal straight strut which is initially subjected to pure compression, buckling leads to bending introducing moments. The calculation of the critical load(s) is essentially an eigenvalue problem.

Looking beyond the above standard instability classes, there are a number of cases where the deformations reach such a magnitude, that the relations between displacements and strains, forces and stresses can no longer be based on the initial geometry. As a result our problem becomes non-linear. We may classify these problems broadly in two categories : The first displaying a stiffening and the second a slackening (softening) effect with increasing loads and displacements. Two elementrary examples are shown in Figs. V 2, 3. Patticularly interesting is the limiting case of a vanishing tangential stiffness which leads to a snap-through type of instability arising in arches, shells, etc.. The example of Fig. V, 4 displays in fact all facets of the class of problems presently under discussion. Thus, within certain ranges of geometric parameters, we find that the following phenomena occur for this model :

1) For negative values of R , a rise of the stiffness as $|R|$ increases.
2) For positive values of R
   a) A decrease of stiffness followed smoothly by an increase of the stiffness as the arch reverses its position.
   b) Alternatively, the decrease of stiffness may occur up to a critical value of R_b followed by a symmetrical snap-through of the arch into a reversed position and a sub-

sequent stiffening.

c) Finally we may have the case where the decrease of the stiffness is followed by a type of snap-through in conjunction with antisymmetrical buckling, leading ultimately again to a stiffening as under 2 a) or b).

These cases are illustrated on a number of examples in Section V.5.

As a matter of fact, there are many additional interesting aspects to the problem. Thus, if we do not impose a loading but a displacement we clearly can circumvent the primary snap-through until we reach a reversed position of the arch. If antisymmetrical buckling modes are not a determining factor the transition to the stiffening proceeds smoothly as under 2 b). On the other hand, if antisymmetrical modes are critical, the decrease of load, following the state of zero tangential stiffness, is suddenly halted, and leads to a secondary snap-through into the ascending stiffening R versus r path; see Ref. (29).

In the above problems, the source of the non-linear behaviour is basically the effect of change of geometry on the equilibrium relations. At the same time, we may still retain in many instances the notion that the behaviour of each element is linear with respect to its natural strains and stresses. In fact, the phenomena in question have in common that they may give rise to large displacements whilst the strains remain small.

The aforementioned category of problems may be broadened further by allowing also for large strains as is the case, for example, for rubber and similar materials, which may experience strains of the order of 100% and more and still remain elastic. In general, the elastic law connecting incremental natural stresses and strains is non-linear, anisotropic and dependent on the magnitudes of the strains. These large strains are very easily incorporated in the theory as demonstrated in Refs. 3, 11, 12, 13 as long as the elements do not change their basic shape. This occurs, e.g., for pin-jointed members in a framework and two-and three-dimensional media idealized by triangular and tetrahedron elements of constant strain. In fact, in these applications the general analysis proposed in Ref. 3 is immediately applicable, irrespective of the magnitude of the strains. The problem presents itself differently if the element changes the nature of its geometry continuously as is the case for a beam element in a stiff-jointed structure which may be initially straight or curved in accordance with a specific analytic expression. Here the strain history modifies continuously the configuration and the inclusion of large strains in the elements necessitates a corresponding extension of the theory. In slight alteration of our argument, we may say that the aforementioned first group of elements is characterized by the fact that the instantaneous elastic stiffness is at any stage of the deformation always derived by the same formula originally proposed for infinitely small strains .In the second group this is not any longer true. In fact, this may not even apply in the presence of small strains.

Consider, for example, once more a straight beam element whose stiffness essentially derives from the E.T.B. and its adjuncts. Now, when the structure deforms, the element will in general be bent and its elastic stiffness may be materially affected in the presence of an end load, an extreme case occurring when the end load is compressive and equal to the buckling load of the element yielding a vanishing elastic stiffness. This effect may be simulated by an inherent or natural geometric

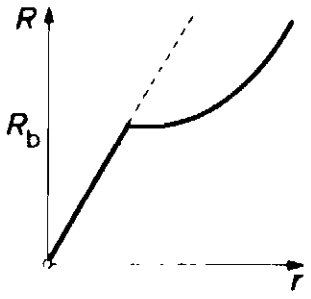

Bifurcation of Equlibrium
Instability

Fig.V.1

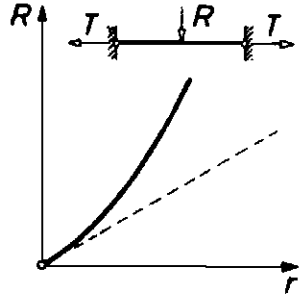

Non-linear Behaviour of System
Stiffening Effect with Large Displacements
(Due to Induced Tension T in Beam)

Fig.V.2

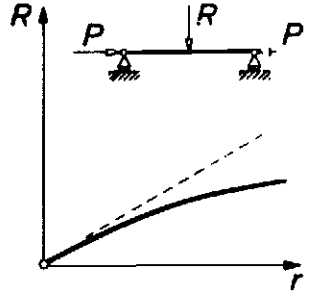

Non-linear Behaviour of System
Softening Effect with Large Displacements
(Due to Applied Compression Load P on Beam)

Fig.V.3

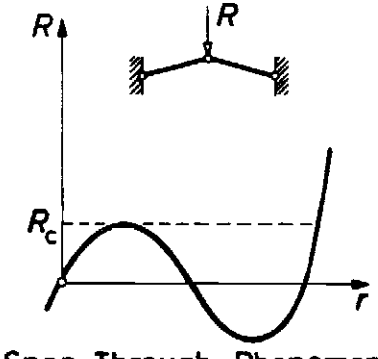

Snap-Through Phenomenon
Secondary Instability

Fig.V.4

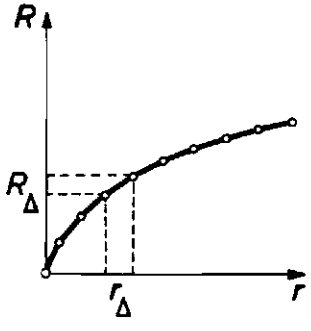

Large Displacement Analysis
Incremental Linearization

Fig.V.5

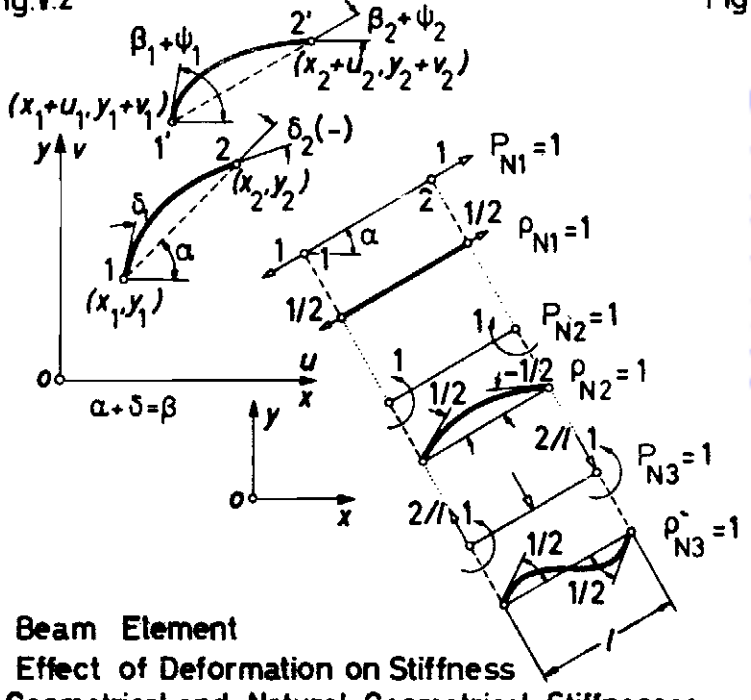

Beam Element
Effect of Deformation on Stiffness
Geometrical and Natural Geometrical Stiffnesses

Fig.V.6

stiffness of the beam element, which should not be confused with the geometrical stiffness of Ref. 3, arising from the change of direction of the natural loads applied on the elements as the structure is deformed. It is, of course, possible to account in problems involving beams and shells also for truly large strains. But in developing all relevant theory one has to keep in mind the limitations of such concepts as E.T.B., etc. In view of this the specific application of the analysis to a beam and arch given in Section V.5 is strictly limited to small strains in the elements although the basic theory reviewed below is, in principle, also applicable to large strains.

V.2 Modification of Matrix Displacement Analysis for Large Displacements

The extension of the standard Matrix Displacement analysis into the non-linear region of large deformations and strains may be accomplished by an iterative or incremental technique in each case suitably linearized. As a matter of fact, the latter method may be considered to include also the possibility of an iterative approach. We restrict ourselves here to the more useful incremental linearization approach and refer the reader to Fig. V.5, showing a typical load displacement histogram as computed in linearized steps. Briefly the technique amounts to analysing each incremental load and/or thermal step R_Δ, θ_Δ on the basis of the geometry obtained by the deformations of the preceding step. Within each loading step we apply the linearized equation of the standard matrix displacement method with one but salient difference. To pinpoint this last essential point of our theory, let us ignore for the moment the elastic effects arising in a typical load increment and assume that the element, in equilibrium under the natural nodal loads P_N, is displaced in space by q_Δ. Clearly the new position of the element gives rise to incremental changes in the cartesian components of the natural loads P_N which have to be accounted for when setting up the equilibrium condition corresponding to the end of the current loading step. The practical execution and understanding of the method is greatly helped through the introduction of a geometrical stiffness k_G which expresses in the succinct form $P_{G\Delta} = k_G q_\Delta$ the aforementioned changes in the nodal loads on the element. Naturally, the element is also undergoing an elastic deformation in the current loading step, which expresses itself by an increment $P_{N\Delta}$ of the natural load vector. Its influence on the equilibrium conditions is included as in the small displacement theory. The total stiffness of the element which enters in each incremental loading is seen to be $k = k_E + k_G$. At the conclusion of each loading step we have to establish the new geometry and relevant data of the structure and form the vector $P_N + P_{N\Delta}$ of the natural load which enters in the geometrical stiffness of the subsequent step.

It is of great importance to realize that the basic simplicity of the above method first presented in Ref. 3 and elucidated further in Refs. 11, 12, 13 is exclusively due to the conception of the natural loads and displacement vectors P_N and q_N of an element and the associated natural elastic stiffness k_{NE}. Without these fundamental ideas the analysis becomes extremely involved and unpratical. As a by-product of these lines of thought we also introduced the natural strain and stress vectors which take a particularly neat and useful form for triangular and tetrahedron elements and contribute to the conciseness of the theory. This confirms our statements in Section I, 1, 2 that the

concepts of natural loads and displacements have remoulded the Matrix Displacement theory and greatly accelerated its development even in the small displacement-strain range. The exposition of the relevant theory in Ref. 3 was to a certain extent, and not unnaturally, guided by intuitive arguments, notwithstanding the correctness of the analysis and results. In what follows we reformulate the basic theory on a purely kinematic basis, which is more in line with the presentation of the small displacement theory in Section I.

V.3 Theory of Incremental Linearization

Let the initial geometry of an element be described by a vector γ_0 which includes all allowable freedoms at the nodal points. At the end of the first incremental loading step the geomtry of the element is defined by the vector

$$\gamma_1 = \gamma_0 + g_{\Delta 1} \tag{V,1}$$

The same process continues in each loading step and we may write for a typical ith increment, defined by its beginning (i,+) and end (i+1,-)

$$\gamma_i = \gamma_{i-1} + g_{\Delta i} \tag{V,2}$$

Note the differential and corresponding incremental relations

$$\delta\gamma = \delta g \quad \text{and} \quad \gamma_\Delta = g_\Delta \tag{V,3}$$

The principle of superposition is clearly applicable to the natural nodal loads P_N and we may write that the accumulated P_N at the stage (i+1,-) is given by

$$P_{N,i} = P_{N,i-1} + P_{N,\Delta i} \tag{V,4}$$

Remembering the transformation rules Eq. (I,5, 11 a) we first observe that the matrix a_N is here a function of the current geometry. We are nevertheless entitled to use Eq. (I,11 a) in the form

$$P_i = a_{Ni}^t \, P_{N,i} \tag{V,5}$$

as long as we remember the dependence of a_N on the geometry. It is at the same time obvious that the dual relation Eq. (I,5) between g_N and g is only meaningful in the incremental sense. Our developments may be clearer if we precede where necessary the incremental presentation by the exact differential formulation. Hence we write

$$\delta g_N = a_N \, \delta g \quad \text{and} \quad g_{N\Delta} = a_N \, g_\Delta \tag{V,6}$$

where the suffix i of the loading step is dropped. The differential form may also be expressed as

$$a_N = \frac{\partial g_N}{\partial g} = \frac{\partial g_N}{\partial \gamma} \qquad (\nu \times q) \tag{V,7}$$

which, in accordance with the rule of differentiation for matrices becomes

$$a_N = \{ a_{N1} \quad a_{N2} \cdots\cdots a_{N\delta} \cdots\cdots a_{N\nu} \} \tag{V,8}$$

where a typical δ^{th} row is given by

$$a_{N\delta} = \frac{\partial g_{N\delta}}{\partial g} = \left[\frac{\partial g_{N\delta}}{\partial g_1} \quad \frac{\partial g_{N\delta}}{\partial g_2} \cdots\cdots\cdots \frac{\partial g_{N\delta}}{\partial g_q} \right] \tag{V,9}$$

Note that ν is the number of natural modes and q the total number of nodal displacements of the element. The definition of Eqs. (8),(9) is not intended to serve as a guide for the setting up of the a_N matrix, but as an illustration of its functional significance.

If we now proceed to the $(i+1)$th loading step, starting at $(i,+)$ and ending at $(i+1,-)$ the equilibrium condition on the element becomes

$$P + \delta P = (a_N^t + \delta a_N^t)(P_N + \delta P_N) \tag{V,10}$$

which upon application of Eq.(5) and exclusion of higher order differentials reduces to

$$\delta P = a_N^t \delta P_N + \delta a_N^t P_N = \delta (a_N^t P_N) \tag{V,11}$$

the last expression of which follows immediately from Eq.(5). The finite difference form of Eq.(11) is,

$$P_\Delta = a_N^t P_{N\Delta} + a_{N\Delta}^t P_N \tag{V,12}$$

A perusal of Eq.(12) indicates that the first term is merely the standard contribution of the linear theory due to elastic and initial strain effects in the current step. In fact, we may write

$$P_{N\Delta} = k_N g_{N\Delta} + J_{N\Delta} = k_N a_N g_\Delta + J_{N\Delta} \tag{V,13}$$

where k_N is the natural elastic stiffness computed at $(i,+)$. Let us now look at the second term which clearly represents the effect of change of geometry on the equilibrium conditions of the element. Expanding the expression by the ν rows $a_{N\delta\Delta}$ of $a_{N\Delta}$ we find (see also Eq.(4.7) of Ref. 3)

$$a_{N\Delta}^t P_N = \sum_{\delta=1}^{\nu} P_{N\delta} a_{N\delta\Delta}^t \tag{V,14}$$

It is next necessary to determine the incremental rows $a_{N\delta\delta}$ of $a_{N\delta}$. Proceeding initially in a formal manner, we find in accordance with the matrix differentiation rules and subsequent finite difference reduction

$$\delta a_{N\delta}^t = \frac{\partial a_{N\delta}^t}{\partial g} \delta g = \left[\frac{\partial a_{N\delta}^t}{\partial g_1} \quad \frac{\partial a_{N\delta}^t}{\partial g_2} \cdots\cdots \frac{\partial a_{N\delta}^t}{\partial g_j} \cdots\cdots \frac{\partial a_{N\delta}^t}{\partial g_q} \right] \delta g \tag{V,15}$$
$$= \Lambda_\delta \delta g$$

and

$$a^{t}_{N\delta\Delta} = \Lambda_\delta g_\Delta \tag{V,16}$$

where Λ_δ is, clearly, a symmetrical matrix. In fact, using Eq.(9) we may write

$$\Lambda_\delta = \frac{\partial a^{t}_{N\delta}}{\partial g} = \left[\frac{\partial^2 g_{N\delta}}{\partial g_j \partial g_p}\right] \tag{V,17}$$

We may now reformulate the second term in Eq.(12) to read

$$a^{t}_{N\Delta} P_N = \left[\sum_{\delta=1}^{\nu} P_\delta \Lambda_\delta\right] g_\Delta = k_G g_\Delta \tag{V,18}$$

where

$$k_G = \sum_{\delta=1}^{\nu} P_\delta \Lambda_\delta \tag{V,19}$$

is the geometrical stiffness of Ref. 3.Eq.(17) is merely of formel interest and a more useful expression is obtained, using the identity (3), which yields

$$\Lambda_\delta = \frac{\partial a^{t}_{N\delta}}{\partial \gamma} = \left[\frac{\partial a^{t}_{N\delta}}{\partial \gamma_1} \quad \frac{\partial a^{t}_{N\delta}}{\partial \gamma_2} \quad \cdots\cdots \quad \frac{\partial a^{t}_{N\delta}}{\partial \gamma_j} \quad \cdots\cdots \quad \frac{\partial a^{t}_{N\delta}}{\partial \gamma_q}\right] \tag{V,20}$$

which may be used to confirm the results for the geometrical stiffnesses of a pin-jointed member obtained in Ref. 3 by a pure geometrical argument.

We next rewrite Eq.(11) using Eqs.(13) and (19) in the form

$$\begin{aligned} P_\Delta &= a^{t}_{N} k_N a_N g_\Delta + a^{t}_{N} J_{N\Delta} + k_G g_\Delta \\ &= \left[k_E + k_G\right] g_\Delta + J_\Delta = k g_\Delta + J_\Delta \end{aligned} \tag{V,21}$$

where

$$k_E = a^{t}_{N} k_N a_N \quad , \quad k = k_E + k_G \tag{V,22}$$

are the instantaneous elastic and total stiffness matrices of the element respectively and

$$J_\Delta = a^{t}_{N} J_{N\Delta} \tag{V,23}$$

is the incremental initial load vector. All these matrices are defined at the beginning of the current load increment and are referred to the basic coordinate system. Having established the basic information for a single element, we proceed to the analysis of the complete structure over the current step. Thus we have the incremental form of expression (I,25)

$$R_\Delta = K r_\Delta + a^{t} J_\Delta \tag{V,24}$$

where

$$K = K_E + K_G = a^t k_E a + a^t k_G a = a^t k a \qquad (V,25)$$

Hence,

$$r_\Delta = K^{-1}\left[R - a^t J_\Delta\right] \quad \text{and} \quad g_\Delta = a\, r_\Delta \qquad (V,26)$$

It is now possible to calculate for any element, say j, the incremental natural strains and loads

$$g_{\Delta j} = a_j\, r_\Delta \quad , \quad g_{N\Delta j} = a_N g_{\Delta j} \quad , \quad P_{N\Delta j} = k_{Nj} g_{N\Delta j} + J_{N\Delta j} \qquad (V,27)$$

The total natural load vector for the jth element which is operative for the next step (i+1)+, (i+2)- is now

$$P_{Nj} = \sum^{i+1} P_{N\Delta j} = \sum^{i+1} k_{Nj}\, g_{N\Delta j} + \sum^{i+1} J_{N\Delta j} \qquad (V,28)$$

Ref. 13 indicates how to compute the initial load vector for any distribution of initial strains in an anisotropic material.

For small strains it is often possible to assume k_N constant as long as there are no temperature effects on elastic moduli. However, since all our finite displacement work is based on general purpose programmes such simplifications are ignored and k_N computed anew at each step. For further comments on the instantaneous elastic stiffness see following paragraph.

The complete procedure after fixing the incremental load temperature history may be summarized as follows, where g (effectively a, r) is the vector denoting the geometry of the assembled structure:

1) Start by computing for each element a_N, k_N, $\vec{r}_{N\Delta}$ based on the undeformed geometry g_0. Assemble the total (purely elastic) stiffness K_E and initial load resultants at the nodal points $a^t J_\Delta$ and proceed to compute r_Δ, $g_{N\Delta}$, $P_{N\Delta}$.

2) For each subsequent step, say ith, between (i,+) and (i+1,-) compute a_N, k_N, k_G, $J_{N\Delta}$ based on the geometry $g_i = g_{i-1} + r_{\Delta,i}$ at the end of the antecedent step. Hence assemble total stiffness K and find r_Δ, $g_{N\Delta}$, $P_{N\Delta}$ and $P_N = \sum P_{N\Delta}$

As a limiting case of the above general considerations let us consider the problem of classical instability. Although this is, as mentioned before, essentially a small displacement problem, we use the large displacement formulation in order to show its integration into the general theory. Prior to instability of an ideal straight or flat structure, say a strut or plate, we have the standard equilibrium equation for small displacements

$$K_E r = R \qquad (I,25)$$

which in the unbent position effectively only expresses a uniform compressive action on the structure. The natural loads P_N of an element are proportional to the load resultant, say R. Since the critical value R_b at buckling is unknown we introduce an arbitrary measure $\bar{R}$ and set

$$R = \lambda \bar{R} \qquad P_N = \lambda \bar{P}_N \qquad (V,29)$$

where $\bar{R}$ and $\bar{P}_N$ are known vectors determined by $\bar{R}$ and λ an undetermined numerical factor. The bifurcation of equilibrium at R_b or the corresponding λ involves a displacement vector r_Δ whose influence on the initial load vector $P_N = \lambda \bar{P}_N$ can be ignored to the first approximation in agreement with our previous theory. Hence any buckling or equilibrium in a bent position under a constant load R is expressed by

$$K_G = a^t k a \tag{V,30}$$

where

$$\left[K_E + \lambda \bar{K}_G\right] r_{\Delta e} = 0 \tag{V,31}$$

The geometrical stiffness k_G of each element is here determined from

$$k_G = \sum_{\delta=1}^{\nu} \bar{P}_{N\delta} \Lambda_\delta \tag{V,32}$$

on the basis of the undeformed geometry and is hence known. Eq.(V,30) represents a typical eigenvalue problem with $r_{\Delta e}$ the eigenvector and λ the eigenvalue and need not concern us here. As stated in Ref. 3 the method is immediately applicable to instability problems due to thermal and other initial strain problems.

A more interesting aspect of the theory arises when we seek to compute the post-buckling behaviour following a classical instability problem. Here we face the difficulty that we have first to establish a starting point for our operation by finding a stable bent shape of the initially straight structure subject to a load slightly in excess of the buckling load. Our aim may be achieved by a number of procedures.

We reproduce here one we found successful. To start with, we select a load vector R which represents a slight increase of the applied critical load R_b, and assign to it a bowed position of the structure defined by a displacement vector $r_{\Delta 1}$, incorporating the eigenvector $r_{\Delta e}$ with a finite amplitude. The latter may be chosen either from an intelligent guess or approximate theory, if available. To fix ideas, but without any loss of generality, let us consider the specific case of a strut in the Ox direction; buckling taking place in the Oxy plane. Since the eigenvector $r_{\Delta e}$ is based on the theory of infinitely small displacements, it does not include any u_Δ displacements, which are necessarily present in any finite displacement analysis. We could take account of their influence by introducing the corresponding end load in the P_{N1} vector. However, it is more consistent and in line with the subsequent steps if we compute the u_Δ from the compression strains in the strut (assumed to be straight) due to the applied end load. In addition we may incorporate the shortening due to bowing , which is strictly a higher order effect. This finalizes the construction of the complete $r_{\Delta 1}$ vector.

Assigning the suffix o to data associated with the straight position, the new geometry is given by

$$g_1 = g_o + r_{\Delta 1} \tag{V, 2a}$$

The natural vector P_{N1} of a typical element appropriate to the position 1 is obtained from Eq.(13) which takes here the form

$$P_{N1} = P_{N\Delta 1} = k_{N0}\, \varrho_{N\Delta 1} = k_{N0}\, a_{N0}\, \varrho_{\Delta 1} \qquad (V,13a)$$

If the vector $r_{\Delta 1}$, were correctly known, the following equilibrium position would evidently hold*

$$a^t \left\{ a_{N1}^t\, P_{N1} \right\} = R_1 \qquad (V,33)$$

However, it is unlikely that this will be the case and it is hence necessary to apply an iteration procedure. To this purpose we find for the geometry (1), K_{E1}, K_{G1}, $K_1 = K_{E1} + K_{G1}$ and obtain a correction $r_{\Delta 2}$ to the displacement from

$$K_1 r_{\Delta 2} + a^t \left\{ a_{N1}^t\, P_{N1} \right\} = R_1 \qquad (V,34)$$

Solving for $r_{\Delta 2}$ we determine

$$P_{N2} = P_{N1} + P_{N\Delta 2} = P_{N1} + k_{N1}\, a_{N1}\, \varrho_{\Delta 2} \qquad (V,13b)$$

and the new geometry

$$\varrho_2 = \varrho_1 + r_{\Delta 2} \qquad (V,2b)$$

We deduce hence a_{N2}, K_{E2}, K_{G2} and may find the third correction $r_{\Delta 3}$ so on until full convergence is achieved, which is, in general, very quickly. Once the initial post-buckling position is known, the subsequent computation with increasing load proceeds as in the standard finite deflexion technique.

V.4 Modification of Elastic Stiffness Due to Deformations at Small Strains; Beam Element.

We mentioned previously that in the presence of small strains the elastic stiffness of an element may be decisively effected through its deformation. We illustrate this point on the example of the beam, briefly but incompletely referred to in Ref. 3. Considering Fig. V 6, we introduce the following vectors defining the geometry and displacement of an element

$$\gamma = \left\{ x_1 \quad y_1 \quad \delta_1 \quad x_2 \quad y_2 \quad \delta_2 \right\}$$
$$\varrho = \left\{ u_1 \quad v_1 \quad \psi_1 \quad u_2 \quad v_2 \quad \psi_2 \right\} \qquad (V,35)$$

where $\delta = \beta - \alpha$ and $\delta_1 = \delta_2 = 0$ for an initially straight beam. For the natural modes defined in Fig. V.6 the natural stiffness of a uniform straight beam of cross-section B and moment of inertia I is, in accordance with Ref. 3,

$$k_{NE} = \frac{E}{l} \begin{bmatrix} B & & \\ & I & \\ & & 3I \end{bmatrix} \qquad (V,36)$$

which corresponds to the natural load and displacement vectors

* the bracketed expression indicates the corresponding vector of all constituent elements.

$$P_N = \{ P_{N1} \; P_{N2} \; P_{N3} \}$$
$$\delta_N = \{ \delta_{N1} \; \delta_{N2} \; \delta_{N3} \} \qquad (V,37)$$

for subsequent convenience we use in Eq.(36) the symbol k_{NE} in place of the previous k_N. The cartesian elastic stiffness referred to the system $Oxyz$ is

$$k_E = a_N^t k_{NE} a_N \qquad (V,38)$$

where (see Eqs. (4),(84), & (4),(89) [3])

$$a_N = \begin{bmatrix} -c_1 & -s & 0 & c_1 & s & 0 \\ 0 & 0 & 1 & 0 & 0 & -1 \\ -\frac{2}{\ell}s_1 & \frac{2}{\ell}c_1 & 1 & \frac{2}{\ell}s_1 & -\frac{2}{\ell}c_1 & 1 \end{bmatrix} \qquad (V,39)$$

and

$$s_1 = \sin\alpha, \qquad c_1 = \cos\alpha \qquad (V,40)$$

Now once the beam is deformed it is seen that the end load component P_{N1}, will have a stiffening or softening effect on the stiffnesses associated with δ_{N2}, δ_{N3}, depending on its being a tension or compressive force. Assuming that the modes δ_{N2}, δ_{N3} of Fig. V.7 are still applicable in the presence of P_{N1} (which is, of course, an approximation even for small strains), we find, applying the unit displacement method, the natural geometrical stiffness of the bent element in the form

$$k_{GN} = P_1 \frac{\ell}{4} \begin{bmatrix} 0 & \frac{1}{3} & \frac{1}{5} \end{bmatrix} \qquad (V,41)$$

Hence the total natural stiffness of a beam element is

$$k_N = k_{EN} + k_{GN} \qquad (V,42)$$

We observe that k_N becomes singular when the stiffnesses corresponding to P_{N2} or P_{N3} vanish. The associated critical values of P_{N1}

$$P_{N1b} = -12\,EI/\ell^2, \quad P_{N3b} = -60\,EI/\ell^2 \qquad (V,43)$$

which should be compared with the exact values .

$$P_{N1b} = -\pi^2 EI/\ell^2, \quad P_{N3b} = -4\pi^2 EI/\ell^2 \qquad (V,43a)$$

The influence of these substantial errors in the instability values of an individual element are not, in general, significant since in a composite stiff-jointed structure it is unlikely that such critical compressive loads will act on individual elements, especially if the partitioning is chosen in a sensible manner. It is, of course, equally possible to determine more accurate values k_N. We may, for example, choose the well-known exact expressions with hyperbolic or trigonometric functions as long as we remember that they are restricted to small strains of the element. The effective elastic stiffness k_N should be used where necessary in all relevant formulae in place of k_{NE}; this may be particularly

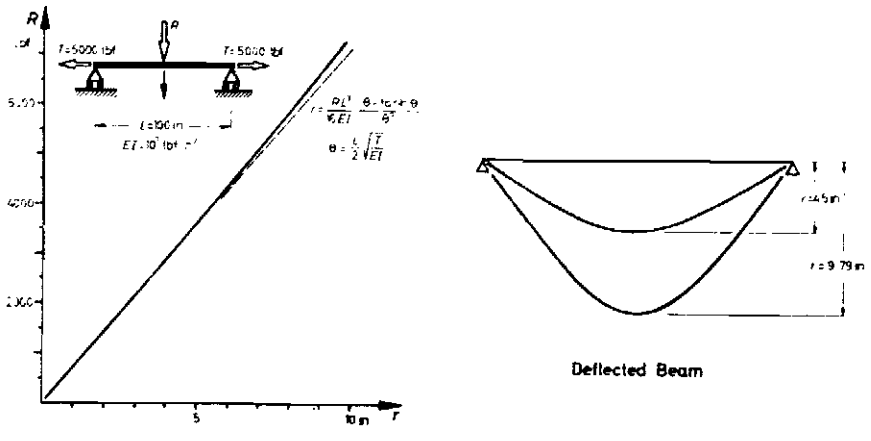

Large Displacement Behaviour of Beam under Transverse Load and Constant Tension

Fig.V.7

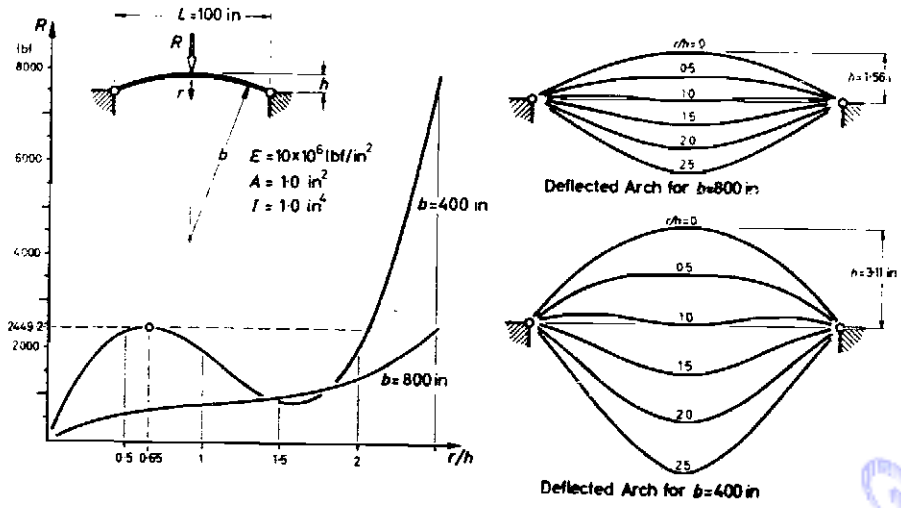

Large Displacement Behaviour of Arch under Central Load and Snap-through

Fig.V.8

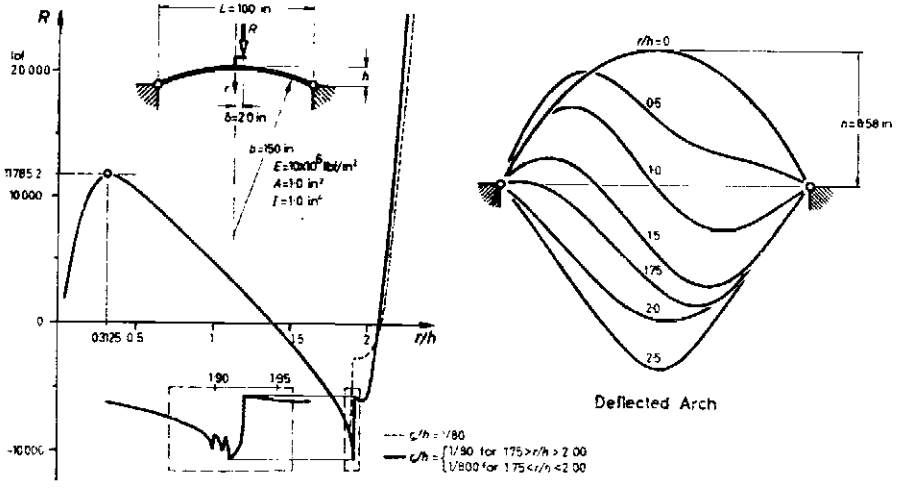

Large Displacement Behaviour and Snap-through of Eccentrically Loaded Arch δ=2·0 in

Fig.V.9

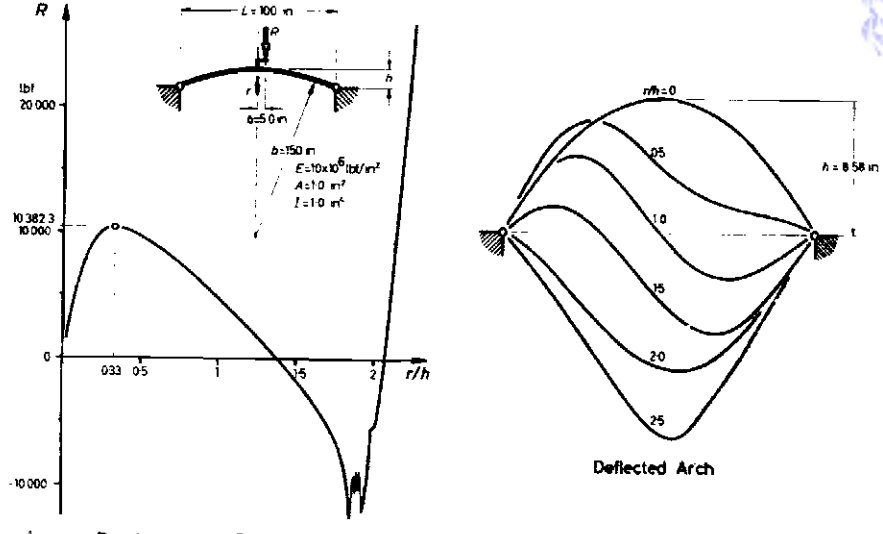

Large Displacement Behaviour and Snap-through of Eccentrically Loaded Arch δ=5·0 in

Fig. V.10

important in the expression for P_N , see Eqs. (13, 13a). The total cartesian elastic stiffness is now

$$k_E = a_N^t k_N a_N \qquad (V,44)$$

We next require the geometrical stiffness of the beam element associated with the natural load vector P_N , which we write

$$k_g = \sum^{3} P_\delta \Lambda_\delta \qquad (V,45)$$

and have partially discussed in Ref. 3. However, the derivation given there is incomplete as far as the influence of the shear force $2P_{N3}/\ell$ due to the mode P_{N3} is concerned. Starting with the end load P_M , we find applying Eq. (4, 100) of Ref. 3 or directly Eq.(20)

$$\Lambda_1 = \frac{\partial a_{N1}}{\partial \gamma} = \frac{1}{\ell} \Delta^t \left[E_1 - T_1 \right] \Delta \qquad (V,46)$$

where E_1 , and T_1 , are the (3 x 3) matrices

$$E_1 = \begin{bmatrix} I_2 & 0 \\ 0 & 0 \end{bmatrix} \qquad T_1 = \begin{bmatrix} c_2 & s_2 & 0 \\ s_2 & -c_2 & 0 \\ 0 & 0 & 0 \end{bmatrix} \qquad (V,46a)$$

and

$$s_2 = \sin 2\alpha , \quad c_2 = \cos 2\alpha \qquad (V,46b)$$

Δ is the (3 x 6) difference matrix

$$\Delta = \left[-I_3 \quad I_3 \right] \qquad (V,46c)$$

We note that the symmetrical bending moment distribution P_{N2} evidently does not give rise to a geometrical stiffness and

$$\Lambda_2 = 0 \qquad (V,47)$$

There only remains to establish Λ_3 . This is most easily achieved by writing the third row a_{N3} of a_N in the form

$$\ell a_{N3}^t = \left\{ -2s \quad 2c \quad \ell \quad 2s \quad -2c \quad \ell \right\}$$
$$= 2 T a_{N1}^t + \left\{ 0 \quad 0 \quad \ell \quad 0 \quad 0 \quad \ell \right\} \qquad (V,48)$$

where T is the Boolean operator

$$T = \left[T_1 \quad T_1 \right] \qquad (V,49)$$

and

$$T_1 = \begin{bmatrix} 0 & 1 & 0 \\ -1 & 0 & 0 \\ 0 & 0 & 1 \end{bmatrix} \qquad (V,49a)$$

Differentiating Eq.(48) with respect to γ and noting that, since $d\ell = d\varsigma_1$

$$\frac{\partial \ell}{\partial \gamma} = a_{N1} \qquad (V,50)$$

we obtain

$$\ell \Lambda_3 + a_{n3}^t a_{n1} = 2T\Lambda_1 + \{0\ 0\ a_{n1}\ 0\ 0\ a_{n1}\}$$

This expression is easily seen to reduce to

$$\Lambda_3 = \frac{2}{\ell^2} \Delta^t \mathcal{T}_2 \Delta \qquad (V,51)$$

where

$$\mathcal{T}_2 = \begin{bmatrix} -s_2 & c_2 \\ c_2 & s_2 \end{bmatrix} \qquad (V,51a)$$

V.5 Examples of Large Displacement Analysis to Beams and Arches

Following the general remarks above on large displacements and the snap-through (Durchschlag) type of instability, two illustrative examples are given of the application of the theory. The first deals with the large displacement behaviour of a beam, under a constant tension, when loaded transversely at the centre. For the geometry and loading given in Fig. V.7 the tension load is equal in magnitude to about half the first Euler buckling load in compression and thus exerts an appreciable stiffening influence on the beam. The figure shows the load-displacement relation determined from the usual small displacement theory; alongside the result of a step-by-step calculation using 30 load increments $R_\Delta = 2.50$ lbf. The initial slope is seen to agree very closely with the analytical result and the curve displays the slight stiffening effect to be expected as the displacements build up. It should be noted that the ends of the beam were allowed to move inward as it bent.

A more complicated load displacement relation is obtained for an initially curved beam if the ends are restrained from outward movement and the loading is such as to decrease the curvature. Depending on the geometry and elastic properties, a multi-valued relation may obtain, so that snapping through from an unstable equilibrium position to another stable one, becomes possible. In Figs. V,8 to 10 three examples of such a structure are illustrated.

The incremental analysis of this system is much the same as for the straight beam, in fact a large part of the computer programme was common to the two sets of computations. An important difference was that, for the arch, the central deflexion was incremented, instead of the applied loading, in order to keep the calculation stable and to obtain the complete load displacement curves. For the two systems of Fig. V.8, displacement increments $r_\Delta = h/20$ were applied successively, up to a maximum displacement $r = 2.5\,h$. For the flatter arch (b = 800 in.), the passage of the system through the region $r = h$ produced only a weak inflexion in the load deflexion curve. However, a decrease in radius of curvature to b = 400 in. gave a system in which the inflexion was so large as to produce a local negative slope, and hence the possibility of a symmetrical snapping with a force-controlled loading.

In the third arch (Fig. V.9,10) the radius was decreased to 150 in. and in this case, the end load developed between the supports exceeded the second Euler buckling load (of the straightened beam). Thus the beam could be expected to be unstable in the near straight configuration and to pass through with a near antisymmetrical buckled form. In order to avoid any computing instability in this mode, the load was applied with two alternative slight eccentricities of d = 2.0 and 5.0 in., as shown in the figures. First, calculations were made with displacement increments $\gamma_A = h/80$. The system passed smoothly through until, when nearly in the inverted position, a sudden jump occurred. This is associated with a secondary snapping, which is also revealed in the analytic study of the problem [29]. In a second calculation, the displacement steps in this region were decreased to $\gamma_A = h/800$ and the resulting load-displacement curve is shown in more detail in diagrams to Figs. V, 9 and 10. This more refined calculation reacts to the instability first by an oscillation, prior to the jump, which is reduced in magnitude. After the jump, both curves settle down immediately to a stable behaviour, running close together and virtually parallel.

For all the problems of this section, the structure was represented by 20 compressible beam elements. A natural geometric stiffness k_{NG} as well as the elastic one k_{NE} was allowed for each element and in addition to the main geometrical stiffness k_B. Because of the differences in the support conditions, the stiffness matrices for the complete, supported structures were of order 60 x 60 for the beam and 59 x 59 for the arches.

V.6 Two-Dimensional Application for Large Displacements and Strains; Rubber Plate Calculation and Experiment

A rubber plate 400 mm square, 10.2 mm thick, with a 100 mm diameter central hole was the subject of finite displacement analysis by the method of Ref. 3 and an experimental verification. A tensile loading was applied uniformly distributed over the width at all loading stages. A pre requisite of the calculation was a determination of the elastic anisotropic properties of the rubber as a function of (large) strains. These data, after reduction, were supplied to the computer in the form of a table of instantaneous values of elastic (tangent) modulus and Poisson's ratio as functions of the current total principal strains. (These total strains are the sums of preceding incremental strains which, in the limit, for infinitesimal steps, would be the logarithmic strains.)

The calculation was carried out for one-quarter of the plate, using the large displacement version of ASKA employing 800 TRIM3 elements. The grid, in principle the same as that in Figs. III. 6,7, contained 441 nodal points with 840 degrees of freedom (unknowns). The first cycle (small displacement) analysis was carried out for a load of 10 kp and the resulting principal strains computed for each element. By linear interpolation, the elastic constants for each element in the next cycle were extracted from the tables and the cycle calculated for the basis of the large displacement theory of Ref. 3, with an additional 10 kp load applied to the instantaneous geometry. The shape of the plate is shown in Fig.V.11 after five and ten loading steps (P = 50, 100 kp), whereby the highest

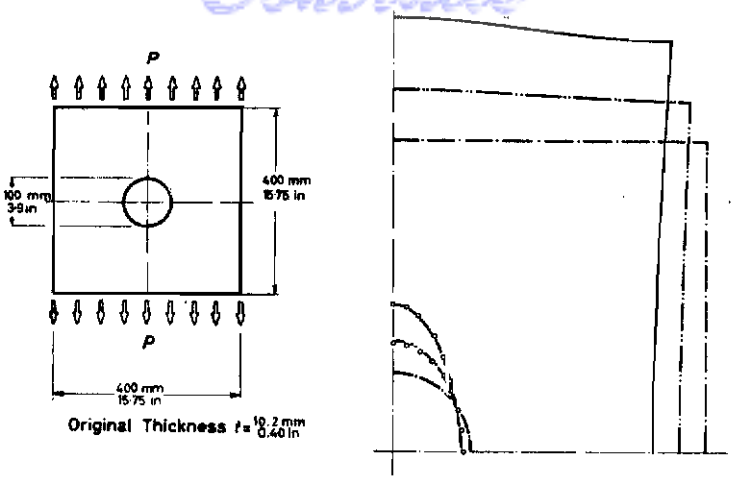

Rubber Plate Analysis
Deformations

Fig. V.11

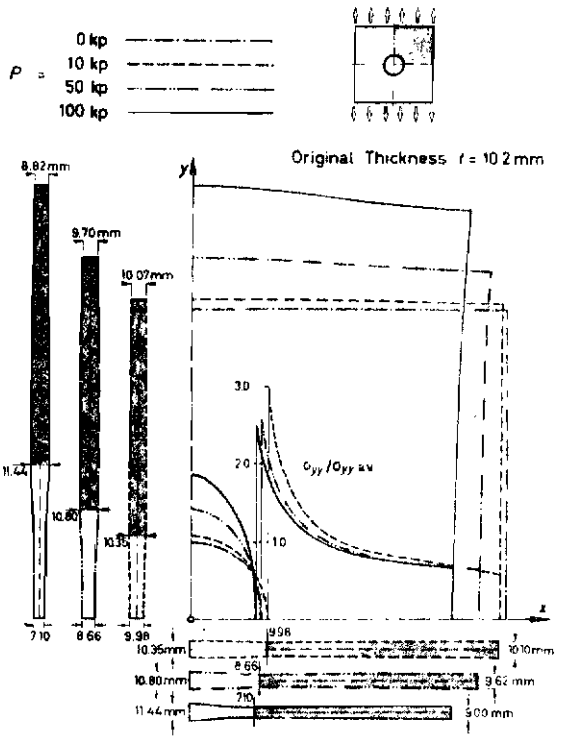

Rubber Plate Analysis
Variation of $\sigma_{yy}/\sigma_{yy\,av}$ and Thickness

Fig. V.12

total strains at the edge of the hole were 0.38 and 0.67, respectively. The agreement between calculated and measured displacements at the edge of the hole is seen to be remarkably good. Each loop of the calculation took 43 min., of which 7 min. were required to form $k = k_E + k_G$ 8 min. for K, and 8 min. for its inversion; k_G is the geometrical stiffener given in Ref. 3. A further 7 min. was consumed in calculating the new geometry, principal stresses and strains, and searching the tables. All the stored data were 'saved' in each loop, i.e., transferred from store to magnetic tape, so that the calculation could be interrupted and resumed as necessary. This SAVe routine required 11 min. each time.

To perform the experiment, a special self-contained loading rig was mounted on the massive frame of a digital plotting table. An approximation to a uniform loading was obtained by gluing a number of short metal segments to each end of the plate on both surfaces, whereby these ends were permitted some freedom to assume differential axial displacements and to contract laterally. A microscope was fitted to the plotting head so that fine markings made on the unstrained plate could be located in the cross-wires and the coordinates read from the x- and y-Vernier scales.

In Fig. V.12, plots are presented of the transverse distribution of direct stress σ_{yy} at the narrowest section for P = 10 kp (small strains), 50 and 100 kp; from which it is seen that the stress concentration factor based on the current nett area decreases slightly with increasing load, but not as much as would be predicted by small displacement theory based on the current geometry with the ellipsoidal hole. Also indicated on the diagram are the changes in the sheet thickness along both axes of symmetry.

V.7 Three-Dimensional Application with Large Displacements and Strains, 'Rubber' Cube

For this calculation, the three-dimensional body chosen was the cube with an ellipsoidal cavity considered in Section I.7. Here, constant elastic properties of the same order as those of soft rubber were assumed, viz., E = 0.1 kp/mm^2, ν = 0.43. Of course, in principle, non-linear and anisotropic elastic behaviour could have been taken into account, but the experimental data mentioned in the preceding section were restricted to the two-dimensional case. As in Section I.7, one-eighth of the body was analysed (with suitably symmetrical boundary conditions), using the same grid with 442 nodal points for the 1797 TETRA4 elements and 1145 unknowns in the calculation. The loop time of about 128m included 3m 20s to form the a, 23m to assemble k, a further 41m to assemble K and 40m for its inversion; the element stiffnesses contain the additional geometrical stiffness component k_G (Refs. 11-13) which increased somewhat the assembly time of k. These times, particularly the last, were somewhat prolonged by the need to use the less immediately accessible mass storage FASTRAND drum, because the capacity of the quick-access drums was insufficient.

The leading case calculated was a uniform tension on effectively a small displacement solution, opposite end faces applied in eight steps. From the first step, a stress concentration factor of 3.43 was obtained with overall elongation of 5 percent; see Fig. V.13. After four loops, the SCF

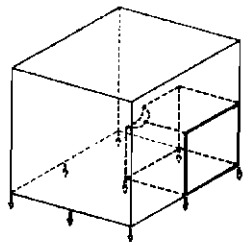

Cube with Ellipsoidal Cavity under Uniform Stress
$\sigma_{yy} = 5 \times 10^{-3}$ kp/mm^2

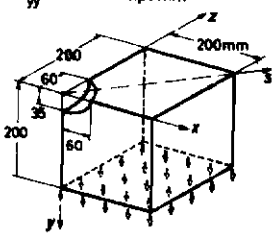

One Eighth of Space of Cube (Computed Model)

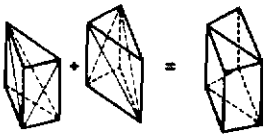

Tetrahedron Components of Typical Quadrilateral Prisma A

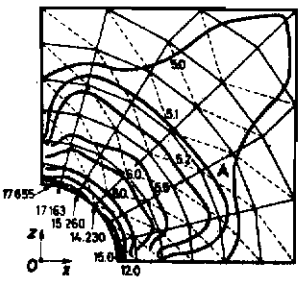

σ_{yy} Contours in Oxz Plane

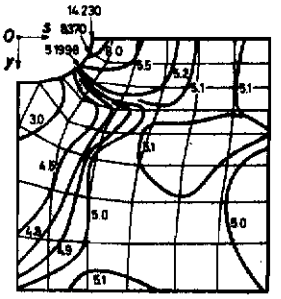

σ_{yy} Contours in Oys Plane

$E = 0.1$ kp/mm^2
$V = 0.43$

Stress Concentration in a Rubber Cube with Ellipsoidal Cavity
(Small Displacement Theory) Fig.V.13

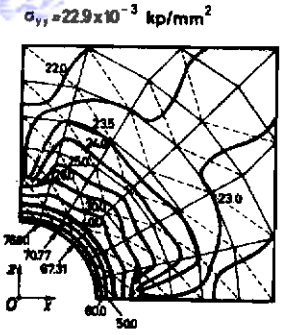

$\sigma_{yy} = 22.9 \times 10^{-3}$ kp/mm^2

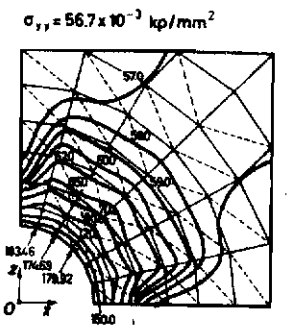

$\sigma_{yy} = 56.7 \times 10^{-3}$ kp/mm^2

σ_{yy} Contours in Oxz Plane

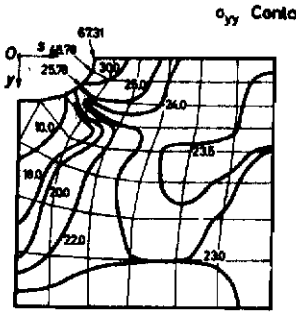

Fourth Loading Step

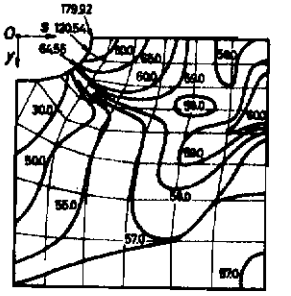

Eighth Loading Step

σ_{yy} Contours in Oys Plane
$E = 0.1$ kp/mm^2
$V = 0.43$

Stress Concentration in a Rubber Cube with Ellipsoidal Cavity
(Large Displacement Theory) Fig.V.14

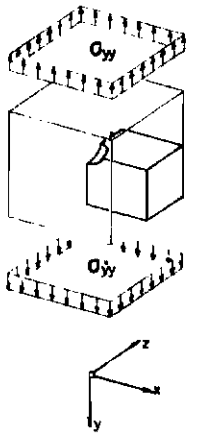

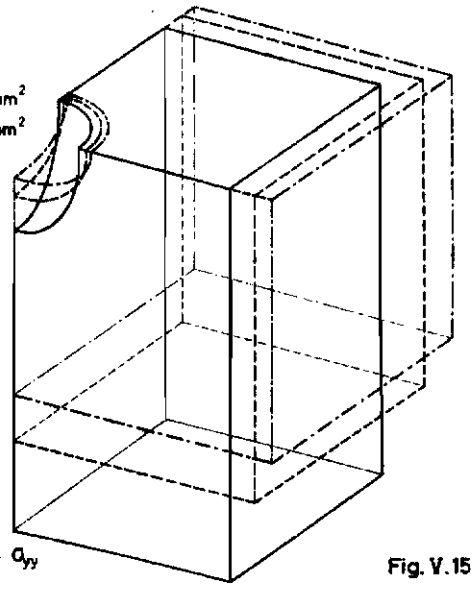

Deformation of Cube with Central Ellipsoidal Cavity under Uniaxial Stress σ_{yy}

Fig. V.15

had further decreased to 3.24 and the extension reached 59.8 percent; see Fig. V.14, which shows also the stress contours of σ_{yy} at the central plane perpendicular to the direction of loading and at a diagonal section. The changes in the geometry are depicted in Fig. V.15 after four and eight loading steps, respectively.

VI. On the Optimisation of Aircraft Structures

VI.1 Introduction

The aim in our studies has been to define as general a structural arrangement as possible within a given geometrical envelope and loading, and to obtain a minimum structure weight by iteration, i.e. by adjustment of sheet thicknesses and boom areas to obtain the desired, as far as possible, uniform stress level, and repeating the calculation for the stress distribution until convergence is achieved.

One might attempt to seek a closed solution to this design problem, but this founders for several reasons. Firstly, any closed solution would need to specify the uniform allowable stress, and therefore the desired uniform strain. However, this uniform strain may be positive or negative, and in any but a trivially simple structure the sign will not be known in advance for all members. The wrong choice leads to absurd results! Secondly, the range of variation of material thicknesses is restricted. Ideally, one might arrive at some sort of framework to sustain the idealized load distribution for an airframe. However, an outside covering with a stiffness causing it to carry a significant part of the overall (as opposed to local) loads is necessary to maintain the outside aerodynamic shape, and this, together with the advantages accruing from having the material in a structure disposed as far as possible from the centre brings us back to our familiar stressed-skin construction. The outside skin thickness may be determined purely by the surface pressure loading or practical considerations of manufacture and handling, or may be defined by stability requirements of the composite structure into which it is integrated in order to carry the overall loads. The former type of requirement sets a lower bound to the admissible range of sheet thicknesses. The latter consideration concerning stability and the supporting structure merely adds to the complication of the problem.

The closed solution approach also falls down because even in some very simple structures and loading cases, a field of uniform strain satisfying equilibrium is kinematically impossible, except perhaps for a particular geometrical arrangement. However, an aircraft is not designed by just one loading case, so the optimisation refers to the stress envelope. As we have seen, there must be supporting structure, which adds to the degree of static indeterminancy, so that any attempt at the optimisation of an airframe requires a high-speed digital computer.

A further general remark on structural design concerning in particular long-range supersonic aircraft is that the aerodynamic parameters are well known. For all high-performance aircraft, weight-saving is vital. A question can be put as follows: "Here is the broad picture of what is required from the aerodynamic and operational standpoint. Within this fairly wide set of conditions, what would be the best layout from the structural point of view?" This question cannot be answered with much confidence at present.

VI.2 Theoretical Considerations

It can be readily proved that if a member in an elastic structure be modified, by factoring its cross-sectional area in the ratio of actual to ideal stresses to raise (lower) the stress to the desired level, the resulting stress in the member will in fact be higher (lower) than that sought. Clearly, successive iterations lead to an oscillating value of the thickness of the member, and it is found that in certain circumstances the convergence by this simple procedure to the asymptotic value can be very slow indeed. Any practical structure is made either from sheet material of standard thicknesses or is fabricated to certain tolerances. Therefore, the thickness of a member is strictly not a continuous variable. A stepwise nature of the admissible variation does, in fact, exercise a "damping" on the oscillation, leading to a much more rapid convergence than would otherwise result.

One also finds that the predetermined minimum allowable thickness also has an important effect. If only one loading case be considered, and free variation of member thicknesses be allowed, the structure tends to reduce to a simple statically determinate one, somewhat removed from the sort actually required. Consideration of more than one loading case and a lower limit on thickness prevent this happening.

A further type of theoretical investigation we have pursued is that in which a multiply-redundant system is optimised as described above, and then small geometric variations allowed in order to seek a lower weight. The simple plane problem considered, employing about 240 unknowns by the Displacement method incurred very long computing times, and no conclusive results have as yet been obtained. Upper and lower limits for flange areas and sheet thicknesses are prescribed, together with their admissible increments. An important consideration which did emerge quickly was that the structural idealization may lead to spurious results. The two-dimensional field was subdivided into constant-strain flange and triangular sheet elements, the latter having the inherent disadvantage of their crude representation of the stress variation. Without the imposition of upper and lower limits on the sheet th ck-nesses, a grotesque arrangement derived, clearly due to the inadequacy of the representation of the sheet by simple triangular elements.

VI.3 Applications to a Supersonic Transport Aircraft

The effort has been devoted to a pair of layouts for a hypothetical supersonic transport aircraft in the Concorde category. Sets of coordinates for wind-tunnel models were supplied together with simplified aerodynamic data. The first layout was a fully-integrated wing-fuselage arrangement[31], whereas the second had a fuselage nose blending into an ogee delta wing. (The Concorde itself has discrete wings and fuselage, albeit of similar shape and might be a fourth or fifth member of a systematic series of variations). The first wing was examined with a plane middle surface and the second with camber. Due to the camber, a fairly orthodox supersonic lift distribution was to be expected in cruising flight, but at subsonic approach incidence, and in limiting manoeuvres at all flight speeds a separated flow would result, giving strong vortices above the wing causing high suctions on the upper surface (and thereby a large proportion of the total lift) at about 3/4 of the local semi-span measured

from the aircraft centre-line (Fig.VI.1).

The aircraft were to be of the same order of size as the Concorde, so a quoted weight breakdown for the latter was taken and further broken down to obtain plausible mass distributions with correct C.G. positions. (Fig.VI.2). From these distributions came the inertia loadings for the structure.

Supplied with the coordinates were broad indications as to the positions of the cabin and engines assumed in deriving the aerodynamic shape and from these a structural layout was deduced. As the aerodynamic date were in the form of lift distributions rather than surface pressures, sandwich construction 1.6 in. (4 cm) thick was assumed for the outer skinning with a separate inner cabin wall. The centroid of the sandwich was taken to be 0.8 in. inside the outer contour, except where the total wing thickness was less than 6 in. It was then assumed that a full-depth sandwich was employed, making the effective structural depth equal to that of the wing itself. The above sandwich configurations extended right to the edges of the wing. Provision for control surfaces would only cause local changes in the load distribution. A frame pitch of 20 in. was assumed in the region of the cabin (the usual value in modern transport aircraft) and a multiple of this used to fix a grid for the analysis. The aircraft were to be 168 ft. long (2016 ins.), and the length was divided into 20 stations for the analysis grid, so each idealized frame was to represent five actual frames. The same pitch was taken in the 'wing' region and assumed to represent a number of spars, at probably between 20 and 40 in. pitch, the latter being taken here. Hence, each idealized spar represented 2 1/2 actual ones. Rib locations were chosen at conveniently spaced stations for which coordinates were given, so as to yield triangular skin elements of reasonable proportions. (See Fig.VI.3, only the nodal points at the corners of elements are indicated). The cabin for the exercise was assumed to be circular in cross-section, with a single wall thickness fixed at 18 swg (0.048 in.), although a flattened cabin section composed of circular arcs with a floor would utilize the internal volue more efficiently. The representation of the cabin was done as follows:

Lumped frames were considered at 100 in. intervals, with a web thickness corresponding to 20 swg (0.036 in.) at 20 in. frame pitch. The flanges of the lumped frames then comprised an effective width of the cabin wall and outer skin sandwich, arbitrarily taken to be 60 in. (12 in. per frame). Between the frames and their neutral surfaces, triangular sheet elements were employed in the calculation which represented the composite fuselage's contribution to longitudinal bending of the aircraft, and to torsion, had antisymmetric loading cases been considered.

The above idealization appears reasonable for frame segments at the top and bottom of the fuselage, but questionable for others where the fuselage blends into the wing. However, we think that the chosen arrangement of elements overcomes these objections, since we assumed beam elements (frame segments) all round the cabin, but these are connected to triangular sheet elements at nodal points, which are then joined to spar elements in the wing region of this integrated structure (Fig, VI.4). Since sheet material loaded in its plane, as represented by these triangles, is much stiffer than a bending member (a basic assumption in all aircraft structures!), the assumed values of bending stiffness of the frame segments at the cabin sides will be relatively unimportant.

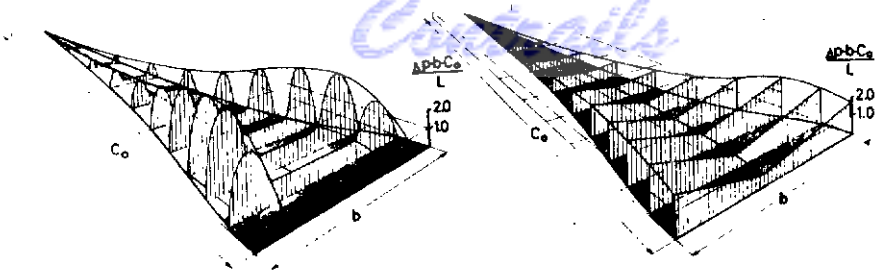

Subsonic (Approach)

Supersonic (Cruise)

Lift Distributions

Fig.VI.1

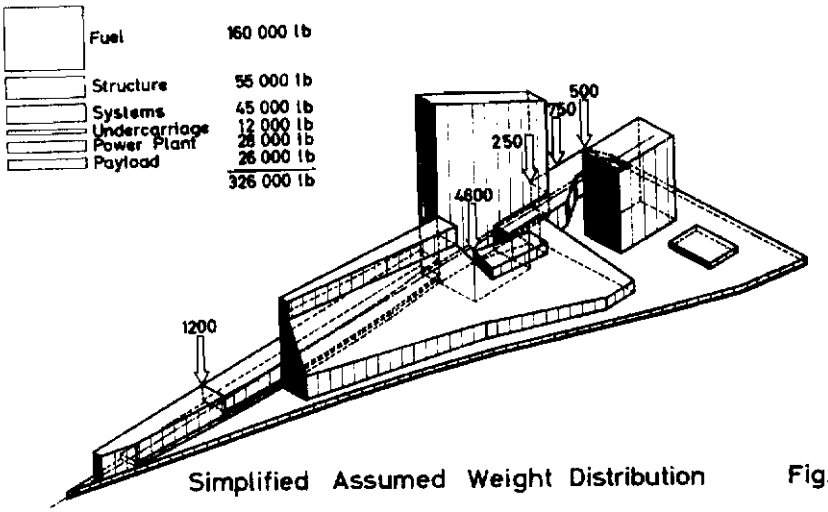

Simplified Assumed Weight Distribution

Fig.VI.2

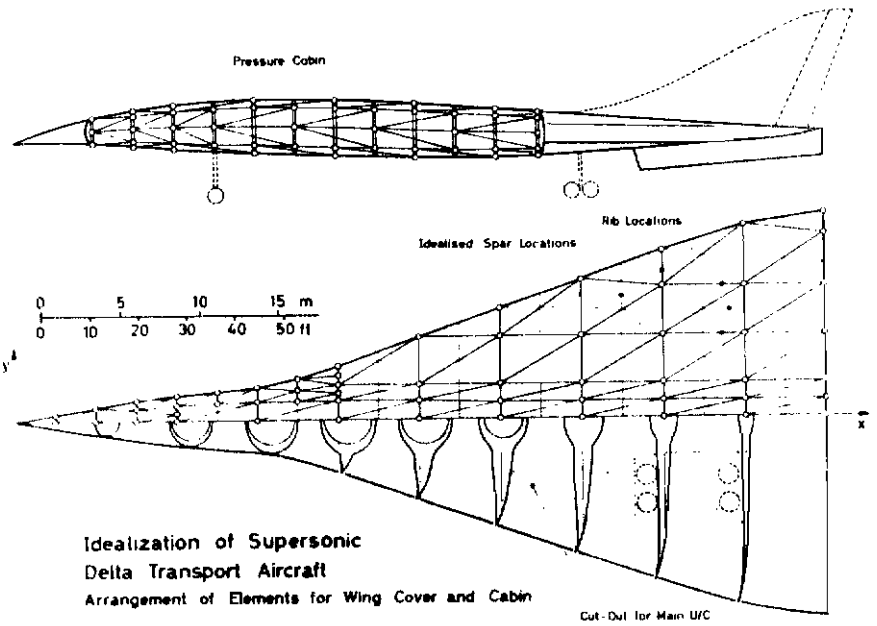

Idealization of Supersonic Delta Transport Aircraft

Arrangement of Elements for Wing Cover and Cabin

Fig. VI.3

The three symmetrical loading cases were considered (Fig.VI.5): Firstly, the non-airborne take-off-case, where a bump on the runway causes a magnified reaction on the main undercarriage, which is reacted intirely by the inertia of the fully-loaded aircraft. This appears to be the critical loading case for longitudinal bending with such slender configurations. Secondly, a manoeuvre case just after take-off, where the subsonic lift distribution appertains, and thirdly a manoeuvre case at supersonic speed, where 10% of the fuel may have been consumed, and lower allowable stresses are admissible due to kinetic heating and thermal loadings. The material properties assumed are meant to bear some relation to RR 58, the alloy actually employed in the Concorde, which initially has a strength about the same as 2024 alloy, but shows little deterioriation of properties with heat ageing, and similar ductility.

The assumed minimum sheet thickness of 0.040 in. represents a sandwich with 0.020 in.(25 swg) facings. Sheet thicknesses were increased as necessary during the iterations, in steps of 0.005 in. i.e. to 0.050, 0.060, 0.070 in. etc.. For the webs of the idealized spars, this procedure is not really correct, as each represents several spars and they need not all have the same web thickness. Each spar (and rib) element was assumed to have flanges of finite cross-sectional area, the lower limit of 0.1 in.^{2} for which represents that the necessary attachment angles. Steps of 0.01 in.^{2} were permitted. The asymmetry caused by the camber distribution has been accounted for by defining most of the lumped structural webs(at the 20 longitudinal stations) with SPARTA elements. With these belong 6-point triangles (TRIM6) and 3-point flanges (FLA3) for the covers and beams for the fuselage rings. The number of nodal points was now increased to 571 (from 162) and the unknowns to 1226, rather more than twice as many as before, since upper and lower surfaces now have to be defined.

The same loading cases were investigated as for the first wing, but the different geometry required adjustments of the lift and inertia data to obtain balance and the correct C.G. position. This aircraft was analysed using the above new elements with varying strains and ASKA in a more refined stage. A few exceptions using TRIM3 occurred at the nose and the edges of the wing. The coordinates for all corner and mid-points of the triangles were supplied in the programme. Their topological arrangement was defined via ASKA, which then computed the element stiffnesses k from the given coordinates for corner points. (All points were listed for convenience and regularity of numbering, superfluous ones are eliminated automatically by ASKA but results are presented for those originally specified). Where the ribs and beams represented by SPARTAs would intersect exactly at their mid-sections, they have been connected at three points (upper and lower surfaces and the point mid-way between). The wing has been analysed using the coordinates for the cambered version. Only the lower surface has to be removed locally to simulate an undercarriage cut-out. In this present calculation no provision has been made for a slit at the trailing edge for the inner edge of a control surface, but the sidewalls of the engine nacelles have been taken into account. One can argue that a slit at the trailing edge in the direction of flight simulates a control surface, as shear loads can be carried across a hinge line by a system of muttiple hinges, and the transfer of bending moment at discrete points by the actuating rods causes only a local redistribution of load. Obviously, no load can possibly be carried directly inboard from a control surface, hence we would introduce the slit.

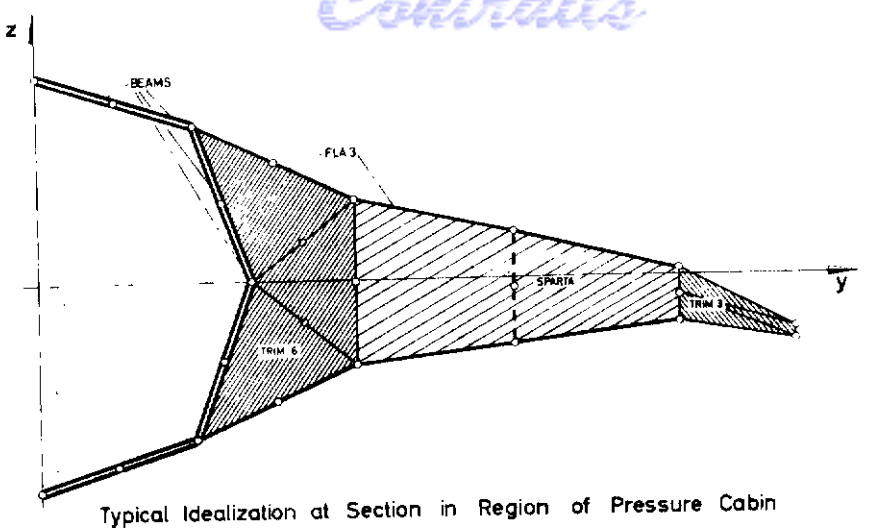

Typical Idealization at Section in Region of Pressure Cabin

Fig. VI.4

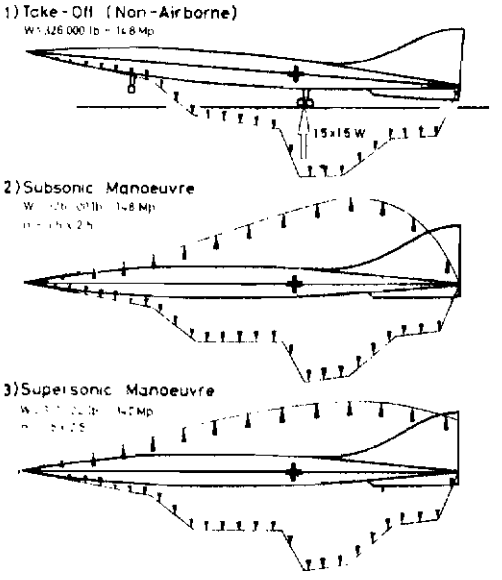

Allowable Stresses

Cases 1 and 2	σ_{max} = 45 000 lb/in² - 31,5 kp/mm²	
	τ_{max} = 25 000 lb/in² - 17,5 kp/mm²	
Case 3	σ_{max} = 36 000 lb/in² - 25 kp/mm²	
	τ_{max} = 20 000 lb/in² - 14 kp/mm²	

Loading Cases Fig.VI.5

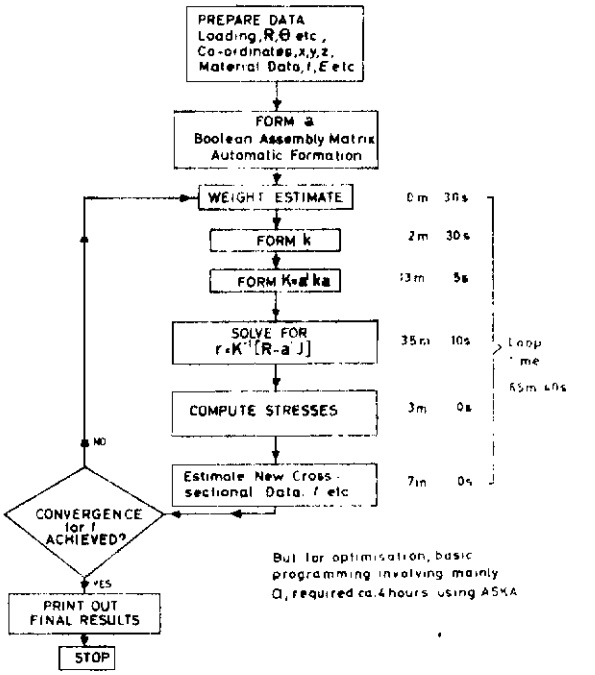

Supersonic Transport Aircraft
Analysis and Optimisation of
SIMPLIFIED FLOW DIAGRAM
1226 Unknowns

Fig.VI.6

In the calculation (by the Matrix Displacement method) the grid used was as in Fig.VI.3, but a small finite wing depth assumed at the otherwise sharp edges, as the rib and spar representation by very long triangular elements yielded a most exaggerated flexibility, particularly at the trailing edge, making the K matrix for the complete structure dangerously near-singular if computational accuracy was to be expected. The minimum sheet thicknesses and flange areas were inserted to obtain stiffnesses for the first calculation (0th iteration).

Fig.VI.6 shows a simplified flow diagram of the analysis and optimisation in conjunction with ASKA (see Appendix II), whereby the programming to describe the structure took about four hours. Actually, no thermal loading Θ or resulting initial stress matrix J was used, but the diagram indicates where they would be handled in the calculations. Results are presented in Figs.VI.7 and VI.8, the former showing the areas where skin thicknesses and spar web thicknesses had to be increased and their final values, together with the convergence of the 'theoretical structure weight' (see below) over six iterations. Envelopes of contours of maximum principal stress resulting from the three loading cases are in Fig.VI.8.

In these aircraft layouts the engines are slung underneath the wing, and the sidewalls of the nacelles are very stiff compared with the adjacent thin wing. It is possible that the heat problems with this powerplant arrangement demand sliding joints between their nacelle structure and the wing, or other connections not capable of fully effective load transfer, neither of which problems causes undue technical difficulty.

A question of the interrelation of the idealization and the optimisation arises when the spar flange cross-sectional area is not restricted or has a high upper limit. The structure with loading assumed applied at discrete nodal points might reduce to a grillage of beams with a thin sheet covering. Clearly, in the neighbourhood of a main undercarriage pickup, the bending moments must be carried by spar flanges since shear lag precludes anything else in the vicinity of concentrated loads. At other places, if the analysis yields large spar flanges, this may lead to acute shear lag problems on the scale of the analysis grid. We might well evolve concentrated spar booms in a structure idealized to apply the loading at discrete points where spars and ribs intersect.

One obtains from such an analysis what might be called a "theoretical structure weight' from the actual volume of the structural elements considered. On these aircraft, a sandwich covering of the thickness assumed represents an additional 6-7000 lb for core material, plus allowances for other stiffening and joints. We have knowledge of one modern aircraft with wings of medium aspect ratio, on which the actual wing structure weight was about 1.65 times what one would expect (i.e. from the weight of cover, spars, ribs, joints, leading and trailing edge, structure, etc.) due to detail brackets, cut-outs, and other secondary items. It is by no means certain that this undesirable ratio could be kept as low as 1.5 on a low aspect ratio wing with large, lightly-stressed area due to the fixed minimum allowable sheet thickness, and the factor of undefinability could even rise to 2.0 in., the in the absence of the utmost in stringent weight control.

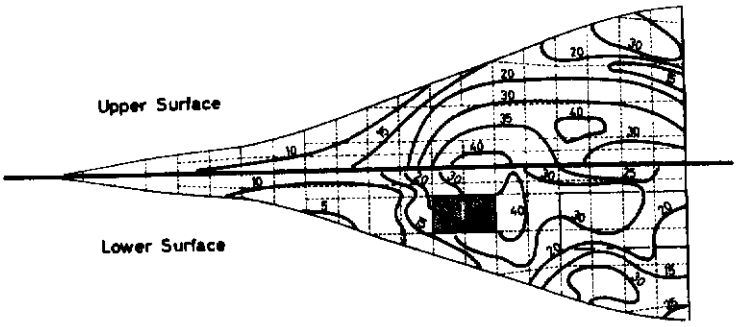

Supersonic Transport Aircraft

Optimised Wing (Three loading Cases)
Contours of Maximum Principal Stress in Covers(10^3lb/in^2)

Fig. VI.7

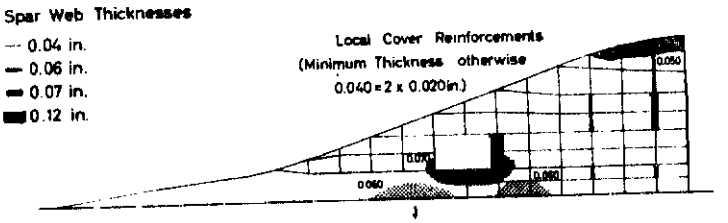

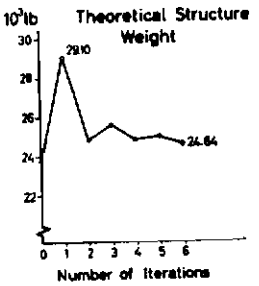

Supersonic Transport Aircraft

Optimised Wing (Three Loading Cases)

Fig. VI.8.

Appendix I

The Matrix Force Method for a Two-Cell Fuselage

With the exception of a brief mention in Chapter IV, in connexion with the calculation of plastic collapse loads, the Force method of analysis has not been discussed in the present work. Though at present overshadowed by the enormous and rapid developments in the Displacement method, the Force method still provides a useful tool for the analysis of structures which are amenable to a simple idealisation and where the degree of redundancy is considerably less than the number of unknowns required in the Displacement method. This usefulness is particularly marked if the computational facilities are limited. It would in any case be rash to conclude that the Force method has reached the end of its development and that the present relative positions are in any sense final.

A classic case where the Force method can be used to advantage is the fuselage structure of conventional aircraft, where the Wagner type of idealisation into end load-carrying flanges and shear carrying panels provides an adequate basis for calculation and design. An important element in the successful application of the Force method is the automatic generation of the self-equilibrating stress systems or redundancies. In Refs. 3 and 4 an extension was given for double-cell fuselages of the method for such automatic generation which was developed in Ref.2. We do not discuss this further here, but present the results of an application to a particular fuselage on which extensive measurements have also been made.

This is the two-cell version of the fuselage on which tests and calculations were reported previously[3,4]. It was made by adding a horizontal floor to the existing structure. The floor was of honeycomb sandwich construction, as was the outer shell, stiffened longitudinally with solid members bonded between the faces. Fig.A.1 shows the overall geometry and the constructional details. A large, asymmetric cut-out extended over three panel widths in both longitudinal and peripheral directions.

Comparisons between the computed stress distribution and the individual values measured by strain gauges are given in Figs. A.2 to A.8 for some representative loading cases. The agreement is, in general, very good, especially for the longitudinal direct stresses in the cover and floor. Stresses in the rings are also shown to be calculated with good accuracy, especially in the important region adjacent to the cut-out.

The calculations were based on an idealised outer cover with 20 effective flanges, a further 3 allowing for direct stresses in the floor. With 9 ring stations, the degree of primary redundancy was 148, which figure includes 8 Z-type redundancies associated with the two-cell cross-section. All primary self-equilibrating stress systems were generated automatically from the cross-sectional co-ordinates by the method described in Section 1.2 of Ref.3. These proved very well conditioned so that their improvement by the orthogonalisation process[2] was unnecessary. In all other respects,

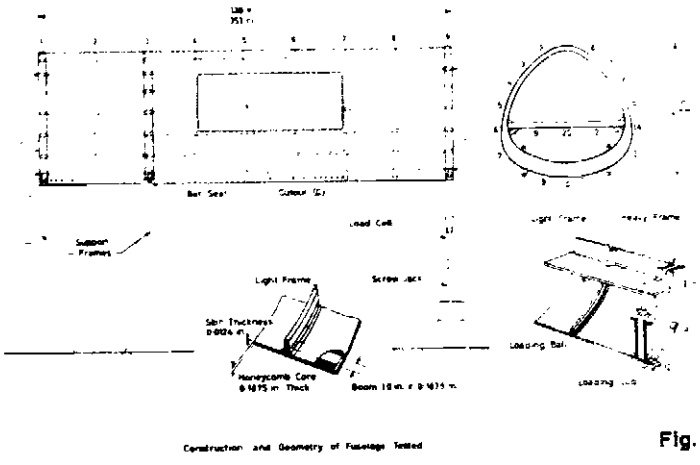

Construction and Geometry of Fuselage Tested

Fig. A.1

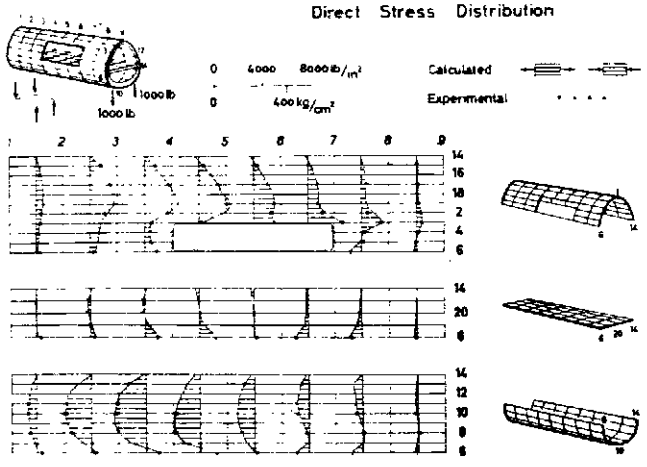

Fig. A.2

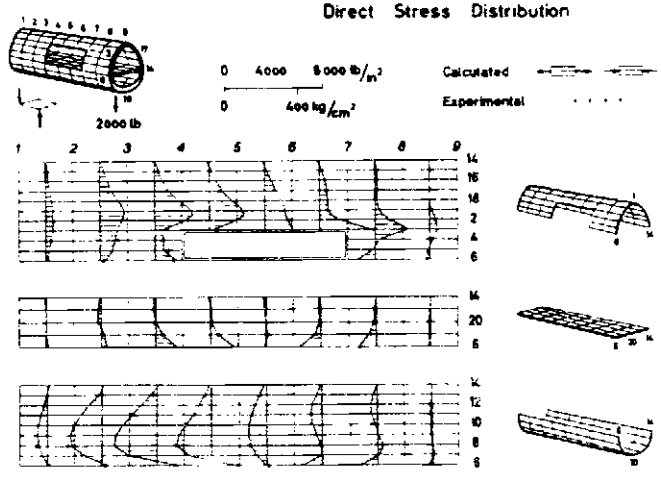

Fig. A.3

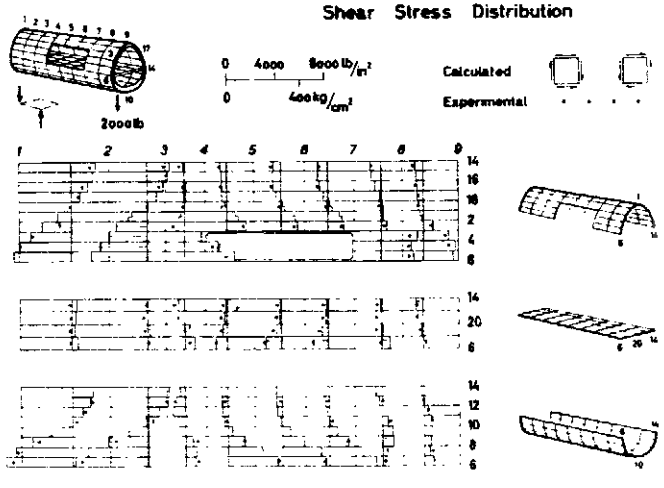

Fig. A.4

the calculations followed the standard pattern of Ref.2 and require no further comment.

By a coincidence, the line of attachment of the floor to the outer cover was one along which the direct stress in the single-cell fuselage, without cut-out, was zero. As a result the direct stresses in the floor were associated mainly with the effect of the large cut-out. Structurally, the shear carrying role of the floor was more significant, especially in providing a closed cell and a concomitant large increase in torsional stiffness over the length of the cut-out. This was reflected in a reduction of the stress perturbations in the region of the cut-out, as compared to the single-cell case. The most striking structural effect was the considerable increase in overall stiffness of the rings caused by the addition of the cross-members supporting the floor. This was shown in the theoretical analysis for the regularized fuselage, prior to the cut-out calculation, by the development of much higher direct stresses in the top of the cover (in the region of boom 1) than was achieved with the more flexible simply connected rings. Though masked somewhat by the influence of the cut-out, this is still noticeable in the distributions shown here.

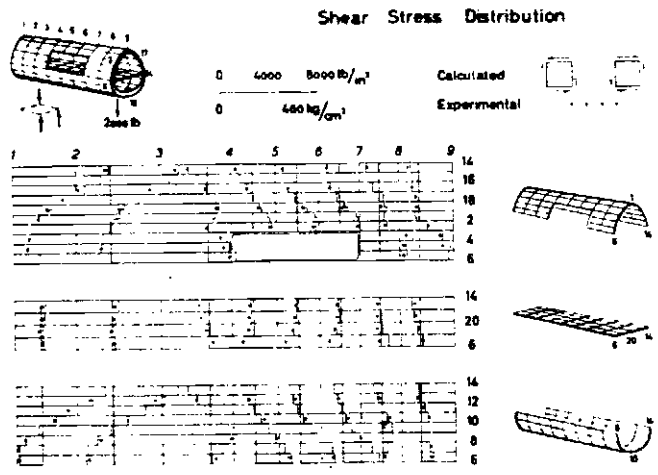

Fig. A.5

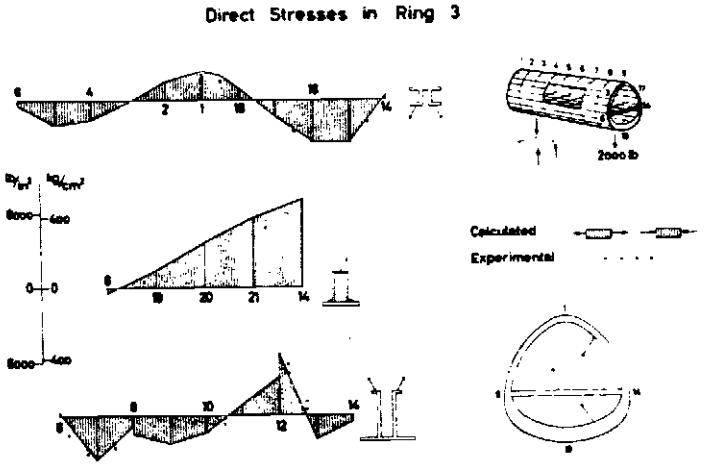

Fig. A.6

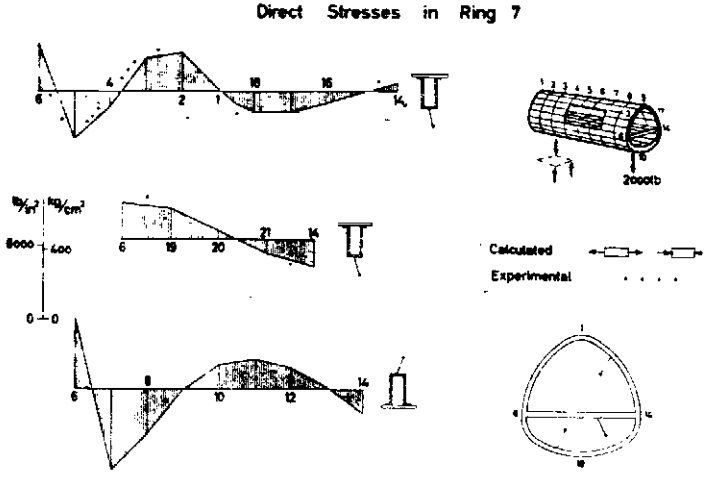

Fig. A.7

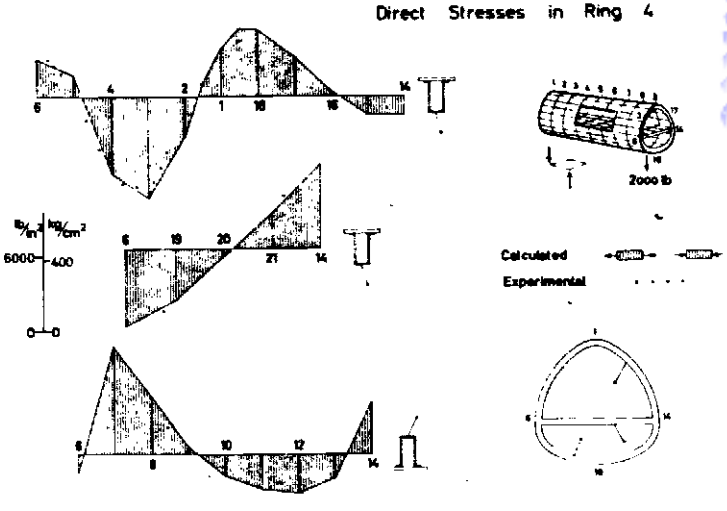

Fig. A.8

Appendix II

Software Developments at Institut für Statik und Dynamik (ISD), University of Stuttgart

In this Appendix, we present a brief description of two significant advances in software directly applicable to the Matrix analysis of complex structures and problems of mechanics.

ASKA[5], which stands for 'Automatic System for Kinematic Analysis' is a fully automatized system designed to facilitate the programming of complicated structures using the Matrix Displacement method. In particular, the accumulation of a large library of standard elements[3, 13-15] with accent on elements of general applicability and flexibility which can be connected to arbitrarily located nodal points within a general three-dimensional system has made this code a truly problem-oriented computer language.

The programming theory which has led to the present system depended on two main advances. The first was the development of Boolean and extended Boolean matrices as standard highly sophisticated operands within a matrix scheme[36] This led eventually to inclusion of these matrices in the matrix codes SELMA[37] and BEMAT[38] developed at ISD by the Systems Programming Group in close cooperation with the Applied Programming Group. The other big step forward was the development of a special ASKA language as a means of describing structures concisely. This language is by no means dependent upon the structural approach employed. In other words, it could be used just as successfully with a few minor alterations and extensions to set up problems for solution by the Matrix Force method.

Although it is possible, thanks to the high degree of automisation and standardization in ASKA, for an engineer to use the language without actually having a thorough grasp of the Matrix Displacement method, a broad knowledge of the basic theory is certainly desirable.

ASKA takes the major part of the work from the stress analyst and transforms the problem of the formation of the k and a matrices to that of defining the types of elements and their means of connection, taking full advantage of any repeated topological pattern. As it stands, one can use it for the solution of one-dimensional problems, e.g. a supported beam; two-dimensional problems, as in fuselages or shells; and three-dimensional problems, e.g. the analysis of a solid body. The language is quite powerful, as it can handle three-dimensional patterns tapering in all directions. The only limitations to the size of problem are, thanks to its generality, only those imposed by storage space and numerical accuracy. For those structures, typical of aircraft, which consist of several sub-structures, each with its own character (fuselage, wings, tailplane), the possibility exists of describing the sub-structures separately and joining them together through standard instructions. The assembly is, however, done prior to the solution, the complete structure being solved as one unit.

Broadly speaking, the user of ASKA defines an "advisory" list as to how he would like his points to be grouped. He also has to supply a list of elements stating their type, elastic properties, number and pattern of connection to the nodal points. A list of degrees of freedom to be suppressed

may also be provided, as well as a list of elements to be cut out. With this, the description of the structure is complete. Several such sub-structures can be defined following one another until the joining instructions are given and finally the end of the structure is announced. The steering programme is in normal matrix language with special orders added to the repertoire causing entry into the various ASKA subroutines, which use these lists to form the basic matrices automatically as well as perform any further computations required, and transfer control to the next instruction.

The ASKA language will accept the steering lists provided by the programmer in a "broad-minded" manner. It will revise, optimize and regroup, if necessary. It will also ensure the automatic elimination most of the degrees of freedom of the structure which are, by the nature or method of connection of the elements to the nodal points, found to be redundant. One should emphazise the importance of the basic knowledge of both structural theory as well as the manner in which ASKA functions. It is possible for an engineer to use this knowledge in order to shorten greatly the computation time and improve the accuracy of the solution, particularly in the case of a complex structure. Subsequent versions of ASKA will include further automatic optimization techniques to rearrange the structure lists and thereby achieve optimum conditions. To be careful, however, not to take control away from the user, has always been the philosophy in developing this system. A good theoretical background and a sound engineering instinct cannot be replaced by an automatic programme. To do that, in our opinion, is to misunderstand the purpose of automisation, which is aimed at saving man-power and reducing "donkey work", rather than as a replacement for human ingenuity.

Apart from the standard matrix operations encountered within a straight-forward solution of a structural problem by the Displacement method we have included many "satellite subroutines" which are, if required, assembled together with the basic ASKA and which can be used for various purposes. One can, for example, ask for information to be printed out in a clear manner, to indicate the final arrangement of the elements inside the machine; or the allowable degrees of freedom at each point.

Due to the relatively long computation times encountered in the solution of large structures, especially in the solution of non-linear problems, where an iteration procedure may be necessary a facility has been provided for interruption and resumption of the programme at any desired point. With the increasing importance of non-linear problems, including large displacements, plasticity, creep, etc., special provisions have also been made in ASKA to facilitate their computation. The diagonal supermatrix $\mathbf{k}$ for all the elements in the structure is computed as a result of one order. However, due to the enormous space which would be required for the assembly of the complete programme within the core store (including the full complement of subroutines necessary for the computation of all standard elements as well as the satellite subroutines) we have provided a method by which only those subroutines necessary for the computation of $\mathbf{k}$ for the element types actually used in the structure are assembled. The elements to be employed must therefore be stated explicity by the programmer.

The system makes internal use of the presence of zero submatrices, thus greatly reducing the computation times. One must stress, however, the importance of the initial description of the

structure provided, as this has a direct influence on the computation times and, therefore, should be given some initial thought. It is, on the whole, not difficult to achieve ab initio a near-optimum description. On the contrary, it will probably be the most logical and obvious way which will render the description itself as short as possible. It is only when one solves a particularly complex problem that such difficulties may arise.

The preparation and input of data provides a time-consuming problem. The guiding principle has been that only the most basic and necessary data should be called upon by ASKA. Effectively, ASKA requires only the coordinates of the nodal points and the basic geometrical properties of the elements. Alternatives have been provided for the programmer, who can, for example, supply data in the same sequence in which he has described his points and elements. The alternative is that he estimates the number of geometrical data required, and the machine will read them in, in the form of blocks of information and instruct him if his guess were correct. In either case, the machine will proceed to compute further.

ASKA is in principle a very flexible language. It is designed to accept the addition of new facilities as well as the extension of the element library to include new types. We appreciate also the role played by the UNIVAC 1107 soft- and hardware. The large fast backing stores have made it possible to organize and carry out the solution of such complex problems. The standard software of the 1107 was also one of the main reasons for the final elegance of the language developed. The basic matrix code used in conjunction with ASKA, since it is an A-package programme, is naturally SELMA. It has only been necessary to provide alternative subroutines to handle matrix operations involving large Boolean operands in order to speed up the calculations. For operations involving supermatrices like the formation of K and the solution of the system of equations etc., special subroutines have also been written to reduce computation times.

The foregoing description has concerned a problem-oriented structural language, which necessarily is based upon a matrix interpretive scheme. However, to keep pace with progress one needs a more sophisticated matrix code, and we have one in an advanced stage of development named ARGMAT, (39, 40, 41) being produced by the Systems Programming Group in collaboration with UNIVAC Division of the Sperry Rand Corporation.

ARGMAT is a self-adaptive matrix interpretive routine for the UNIVAC 1107 computer family. The interpreter in ARGMAT is designed to achieve a very complex data storage and retrieval function within the multi-level store of the machine in such a way that the least possible time is wasted by the central processors' waiting for data. Thus, the interpreter makes use of several modern programming techniques in an attempt to utilise fully the interrupt logic of the computer. It allows considerable generality in the structure of the data it handles without appreciably reducing the internal speed of the machine. The system is self-adaptive in the sense that it is able to generate its own source language for later processing when necessary, and also in the sense that is able to rearrange dynamically the data upon which it operates in such a way that it makes efficient use of the multi-level storage.

The basic elements of data handled by ARGMAT are matrices which may be Boolean, in single or multiple precision, real or complex, but the type of representation of a matrix may change

dynamically throughout a computation. ARGMAT also allows operations on matrices whose elements are matrices, i.e. , supermatrices. The interpreter is able to handle operations with supermatrices to any number of levels in a recursive manner. The data storage technique used to define and handle such matrices uses a threaded list. Each matrix has associated with it a title or 'header' describing the matrix by its dimensions, element precision and arithmetic type (real, double precision, complex or Boolean), its storage location (in core, drum, or FASTRAND) and whether it is a normal matrix or supermatrix. These headers are referenced by entries in a pick-up list which gives the address of the header in core, drum or mass storage. The pick-up list entries are referenced by address entries in the interpretive programme string. If the data referenced by a given header is a supermatrix, then its elements are not numbers but rather are addresses which refer to entries in the pick-up list. These elements are thus effectively the "names" of the supermatrices of the supermatrix; and the pick-up list entries referenced by them yield new headers which may refer to matrices with matrices as elements , and so on until numerical data is finally referenced. The threaded list technique generalises the data structure and its handling in ARGMAT and allows operations on very large matrices, since a matrix can be repeatedly subdivided into submatrices dynamically until the final matrices are small enough that they can be handled in core storage. In conjunction with the threaded list technique the interpreter uses dynamic storage allocation, i.e., a matrix may be called from a different set of physical drum or FASTRAND locations every time it is used.

If matrix instructions were interpreted one at a time, the central processor would spend most of its time waiting for data transferred into core. To avoid central processor waiting time, a matrix instruction look-ahead technique is employed by the interpreter. The effect of this high-level, three-instruction looking ahead is that, as the instant instruction n is being executed, the data for instruction $n+1$ are being read into core and the headers for instruction $n+2$ are also being read in.

Operations with supermatrices certainly present some difficulties but the recursive definition of an n -level supermatrix, plus the fact that matrix operations such as matrix addition, subtraction, multiplication and division ("inversion"), transposition, etc. are valid for matrices with matrices as elements leads to the solution; viz., a recursive generator for matrix interpretative instructions. This generator is written in such a way that if it is given an instruction to add supermatrices A and B it will generate a string of matrix interpretative instructions for the addition of their submatrices $a_1, b_1 ; a_2, b_2 ; \ldots ; a_n, b_n$. These generated instructions have the same format as those in the input programme string and thus make use of the basic features of the interpreter : dynamic storage allocation, look-ahead, and further recursion, if necessary. The matrix instruction generator is recursive since its ultimate output must be instructions referring to simple matrices, whereas its input may be instructions operating upon n -level supermatrices.

The generation process may appear to be time-consuming since it is recursive; however, this feature allows the user to build up and handle complex data structures in the same way he builds up the mathematical model of a mechanical structure or electrical circuit. A detail once handled need no longer required attention, even as a data name; for as the problem is defined or the physical system imagined, the generality and scope of the data structure keeps pace with the user's imagination. Any

programming system which allows the computer to act as an amplifier of human intellect with high gain cannot be criticised for using more computer time than some trivial programme which solves n simultaneous equations.

References

1) ARGYRIS, J.H. — Energy Theorems and Structural Analysis, Butterworths, London, 1960

2) ARGYRIS, J.H. KELSEY, S. — Modern Fuselage Analysis and the Elastic Aircraft, Butterworths, London, 1962

3) ARGYRIS, J.H. — Recent Advances in Matrix Methods of Structural Analysis, Progress in Aeronautical Sciences, Vol. 4, Pergamon Press, Oxford, London, New York, Paris, 1963

4) ARGYRIS, J.H. KELSEY, S. KAMEL, H. — Matrix Methods of Structural Analysis. A precis of recent developments. AGARDograph 72, Ed. de Veubeke, Pergamon Press, 1964

5) ARGYRIS, J.H. KAMEL, H. SØRENSEN, M. SCHMID, G. PRETSCH, H. — Automatic System for Kinematic Analysis (ASKA), Research Report to The Boeing Company, Airplane Division, February 1965 (to be published externally)

6) PRAGER, W. — Introduction to Plasticity, Addison-Wesley, 1959

7) HODGE, P.E. — Plastic Analysis of Structures, McGraw Hill, 1959

8) TIMOSHENKO, S. GOODIER, J.N. — Theory of Elasticity, McGraw Hill, 1951

9) HILL, R. — The Mathematical Theory of Plasticity, Oxford University Press, 1950

10) ARGYRIS, J.H. — Some Results on the Free-Free Oscillations of Aircraft Type Structures, Research Report to The Boeing Company, Airplane Division, November 1964; also read at the International Symposium of the IUTAM on the Mechanics of Linear Vibrations, Société Francaise des Mécaniciens, and British National Committee for Theoretical and Applied Mechanics, Paris, April 13-15, 1965, VI Session, Thursday, April 15, 1965; to be published by the Société Francaise des Mécaniciens, 1965.

11) ARGYRIS, J.H. — Three-Dimensional Anisotropic and Inhomogeneous Elastic Media, Matrix Analysis for Small and Large Displacements; Proceedings of the Eleventh International Congress of Applied Mechanics, Munich, September 1964; to be published by J. Springer, 1965.

12) ARGYRIS, J.H. — Matrix Analysis of Three-Dimensional Elastic Media, Small and Large Displacements, Journal of the AIAA, Vol. 3, No. 1, pp. 45-51, January 1965.

13) ARGYRIS, J.H. Three-Dimensional Anisotropic and Inhomogeneous Elastic Media; Matrix Analysis for Small and Large Displacements, Ingenieur Archiv, Vol. 34, No. 1, pp. 33-55 January 1965.

14) ARGYRIS, J.H. Elasto-Plastic Matrix Displacement Analysis of Three-Dimensional Continua, Journal of the Royal Aeronautical Society, Technical Note, Vol. 69, September 1965.

15) ARGYRIS, J.H. Triangular Elements with Linearly Varying Strain for the Matrix Displacement Method, Journal of the Royal Aeronautical Society, Technical Note, Vol. 69, October 1965.

16) ARGYRIS, J.H. Reinforced Fields of Triangular Elements with Linearly Varying Strain, Effect of Initial Strains, Journal of the Royal Aeronautical Society, Technical Note, Vol. 69, October 1965.

17) ARGYRIS, J.H. Matrix Displacement Analysis of Anisotropic Shells by Triangular Elements, Journal of the Royal Aeronautical Society, Technical Note, Vol. 69, November 1965.

18) ARGYRIS, J.H. Arbitrary Quadrilateral Spar Webs for the Matrix Displacement Method, Journal of the Royal Aeronautical Society, Technical Note, Vol. 69, December 1965.

19) SOBEY, A.J. a) The Estimation of Stresses around Unreinforced Holes in Infinite Elastic Sheets, R.A.E., Report Structures 283, October 1962.

b) Stress Concentration Factors for Rounded Rectangular Holes in Infinite Sheets, R.A.E., Report Structures 292, November 1962.

20) MORLEY, L.S.D. Skew Plates and Structures, Pergamon Press, Oxford, London, New York, Paris, 1963.

21) WITTRICK, W.H. Buckling of Oblique Plates with Clamped Edges under Uniform Compression, Aero. Quart. 4, 151, 1953.

Buckling of Oblique Plates with Clamped Edges under Uniform Compression, Aero. Quart. 5, 39, 1953.

22) CLOUGH, R.W. TOCHER, G.L. Analysis of Plate Bending using Triangular Elements, University of California, Berkeley, Report, 1962.

23) CLOUGH, R.W. The Finite Element Method in Structural Mechanics (Stress Analysis), John Wiley and Sons, Ltd., London, 1965.

24) HADLEY, G. Linear Programming, Addison Wesley, 1962.

25) DORN, W.S. GREENBERG, J.H. Linear Programming and Plastic Limit Analysis of Structures, Quarterly Appl. Maths., Vol. 15, 1957.

26) CHAN, A.S.L. On the Plastic Collapse of Structures, forthcoming Ph.D. Thesis, London University, 1966.

27) ARCHER, J.S. Consistent Mass Matrix for Distributed Mass Systems, Proc. ASCE, Journal of the Structural Division, 89, pp. 161-178, August 1963.

28) HURTY, W.C. Dynamic Analysis of Structural Systems Using Component Modes, AIAA Journal, Vol. 3, No. 4, pp. 678-685, 1965.

29) BIENZENO, C.B. Technische Dynamik, Second Edition, Vol. I, Chapter VII, 11, pp. 588-599, Springer Verlag, Berlin, 1953.

30) ARGYRIS, J.H. Matrix Analysis of Plates and Shells, Research Report to The Boeing Company, Airplane Division, October 1965. Also in abbreviated form: Matrix Analysis of Plates and Shells; Prolegomena to a General Theory, Ing. Archiv, Vol. 35, No. 2, 1966.

31) ARGYRIS, J.H. The Computer Shapes the Theory, Lecture to the Royal Aeronautical Society, May 18, 1965.

32) TABOREK, R.J.H. A Theoretical and Experimental Investigation on Aircraft Vibrations, M.Sc. (Eng. Thesis, University of London, 1962).

33) KARIAPPA, The Theoretical Prediction of the Free-Free Oscillations of a Delta Wing, Dr. Ing. Dissertation to be submitted to the Technische Hochschule Stuttgart, November 1965.

34) ARGYRIS, J.H. The Trondheim Lectures on the Matrix Theory of Structures, John Wiley's, New York, 1965.

35) RUSHTON, R.R. Electrical Analogue Solutions for the Deformation of Skew Plates, The Aeronautical Quarterly, pp. 169-180, May 1964.

36) ARGYRIS, J.H. Some Developments of Boolean Matrices, Research Report to The Boeing Company, Airplane Division, December 1964; to be published externally.